

N O T I C E

THIS DOCUMENT HAS BEEN REPRODUCED FROM
MICROFICHE. ALTHOUGH IT IS RECOGNIZED THAT
CERTAIN PORTIONS ARE ILLEGIBLE, IT IS BEING RELEASED
IN THE INTEREST OF MAKING AVAILABLE AS MUCH
INFORMATION AS POSSIBLE

507

(NASA-CR-163734) FUNDAMENTAL STUDIES IN
GEODYNAMICS Final Technical Report
(California Inst. of Tech.) 301 p
HC A14/MF A01

N81-11595

CSCL 08G

63/46

Unclass
29255



CALIFORNIA INSTITUTE OF TECHNOLOGY

PASADENA, CALIFORNIA



FINAL TECHNICAL REPORT

1 August 1979 - 31 July 1980

FUNDAMENTAL STUDIES IN GEODYNAMICS

NASA RESEARCH GRANT No. NSG-7610

FINAL TECHNICAL REPORT

Grant Number: NASA Research Grant No. NSG-7610

Name of Contractor: California Institute of Technology
Pasadena, California 91125

Principal Investigator: Don L. Anderson
Seismological Laboratory
California Institute of Technology
Pasadena, California 91125

NASA Technical Officer: J. A. Vitale - Code ETD-6
NASA
Washington, D. C. 20545

Title: Fundamental Studies in Geodynamics

Period of Grant: 1 August 1979 - 31 July 1980

Period of Report: 1 August 1979 - 31 July 1980

TABLE OF CONTENTS

	Page
Plate Motion Modelling	2
Rivera Plate Motions	2
Caribbean-South American Boundary.	3
Indian Plate Deformation	5
Pacific-North America	6
Seismicity and Subduction Processes.	9
Study of Slow Earthquakes.	10
Study of Free Oscillations	10
Figures	12
Appendices	34

- I. Present-Day Plate Motions: A Summary
- II. The Physics of Creep and Attenuation in the Mantle
- III. A Model of Dislocation-Controlled Rheology for the Mantle
- IV. A Global Geochemical Model for the Evolution of the Mantle
- V. Plate Tectonics on Venus
- VI. Hotspots, Basalts and the Evolution of the Mantle
- VII. The Early Evolution of the Mantle

Plate Motion Modelling

Plate motion modelling has evolved from global models to the study of motions of small plates, and to the investigation of possible plate deformation. Recent research under this grant has involved:

1. Verification of the relative motions of the Rivera plate with respect to its neighbors, i.e., North America, Cocos, and Pacific.
2. Reassessment of the interactions of the Caribbean and South American plates.
3. Interaction of Indian-Australian plate (the Indian plate undergoes deformation) with the Eurasian plate in Southeast Asia, in an attempt to place bounds on Asian deformation.
4. Detailed study of the Pacific-North America plate boundary.

The main technique used consists in assuming that the global plate motion model RM2 furnishes kinematic boundary conditions, and to use local geological and geophysical evidence for departure from ideal rigid plate tectonics. The bulk of this research was presented at the IGC meeting in Paris in July 1980, by Prof. Minster.

Rivera plate motions

The motions of the Rivera plate relative to its neighbors (Pacific, North America, Cocos) have been determined by inversion of data along the East Pacific Rise and the Rivera Fracture Zone (Minster and Jordan, 1979). All data used are from the oceanic environment. The resulting set of poles and 20 error ellipses are shown on Figure 1, and calculated

relative motions at selected points on Figure 2. Of interest is the model prediction of right lateral strike slip relative motion between Rivera and North America in a NW direction, at a rate of 1.3 cm/yr. The direction is compatible with offshore scarps near Tres Marias islands. This means that 1) very significant changes in the nature of plate interactions, from subduction (COCO-NOAM) to the South to strike-slip further north, and 2) this boundary may be the site of occasional strike-slip events.

Figure 3 shows a focal mechanism for the 1966 December 15 event ($m_b = 5.1$) in that region. Although the data are relatively few for such a small event, the solution is fairly well-constrained and is consistent with the predicted plate motions. Further confirmation will be obtained by studying the single largest earthquake in that region in the past 20 years (1976 February 9, $m_b = 5.5$).

Figure 4 (from Lowman, 1980) illustrates the three plate boundaries discussed next. They are 1) the Caribbean-South America boundary, described as right-lateral strike slip on this figure, 2) the Indian-Australian boundary, described as left-lateral strike-slip on Figure 4, and 3) the Pacific-North America boundary, with complications in the West North American continent shown on the map.

Caribbean-South America Boundary

The motions of the Caribbean plate were first described by Jordan (1975). We have reviewed these results in the light of the new models. Figure 5 is a simplified tectonic map of the northern portion of South America, shown in an oblique mercator projection about the RM2 CARB-SOAM

pole. The boundary appears as a fairly broad zone of continental deformation, with conjugate strike-slip faulting, and a significant component of shortening between the Curacao Ridge and the frontal thrust. However, the amount of shortening predicted by the model is somewhat less than that found by Jordan (1975). Again, rapid (5.4 cm/yr) left-lateral strike-slip motion is predicted between Central America and the Panama Basin, pointing to the Panama escarpment as a possible seismic gap.

The evidence for present-day plate deformation is shown on Figure 6a and 6b. This is a contour map of the logarithm of cumulative moment release (per degree square) in the period 1960-1980. Only shallow ($h < 70$ km) events with $m_b > 4$ have been used and smoothing was performed with a Gaussian filter of aperture $\sim 0.3^\circ$. Most of the activity is confined between the major thrusts confirming the interpretation of a diffuse plate boundary.

Direct evidence of subduction of the Caribbean plate under the Curacao ridge is found in the multichannel seismic data of Talwani et al. (1978) (Figure 7). The dip of seismic horizons thickening of sedimentary layers to the South indicate that slow subduction is probably currently taking place.

Another confirmation that RM2 provides the correct boundary conditions is shown on Figure 8 (from et al., 1978). Near Caracas, Venezuela, N-NW trending faults offset the large right-lateral EW fault systems (San Sebastian, El Pilar) in a right-lateral direction. Yet the complex multiple event of 1967 July 29 (the largest in recent history) shows a left-lateral focal mechanism. This is easily explained if the

regional maximum compressive stress is controlled by relative plate motions. Figure 8 shows that the compression axis for this focal mechanism is consistent with the RM2 prediction.

Thus, RM2 does not change the basic conclusions of Jordan (1975) and is consistent with additional evidence published since that study.

Indian Plate Deformation

Figure 9 depicts the geometry of the Indian-Australian plate motion relative to Eurasia in an oblique mercator projection about the (INDI-EURA) pole. The Australian plate was allowed to have a motion independent of the Indian plate so as to better satisfy data along the SE Indian Ridge (Minster and Jordan, 1978). The hypothetical boundary was arbitrarily assumed to coincide with the Ninetyeast ridge, in view of its high level of seismicity (Stein and Okal, 1978). Although the differential motion of the Indian and Australian portions is small (Figure 9), it is calculated to be of the order of 1 cm/yr SE-NW compression. This is consistent with compression axes determined by Stein and Okal (1978) shown on Figure 10.

In an attempt to refine the analysis, we investigated the possibility of interpreting the Java-Sumatra trench system as a convergent plate boundary between India (alternatively Australia) and Eurasia, keeping in mind possible significant relative motions between Southeast Asia and the Siberian platform. Figure 11 shows seismic slip vectors determined by Fitch (1972), plotted on an oblique mercator projection about the INDI-EURA pole. The observations are consistent with the general interpretation of an INDI-EURA convergent boundary, but

the scatter is too large to detect small discrepancies. Thus, although this permits us in principle to place bounds on the rates of plate deformation in the region, these bounds are not tight enough to be useful.

Pacific-North America

Figures 12a and 12b show a contour map of log cumulative moment along the Western North American plate boundary. It illustrates the diffuse and complex nature of the boundary, particularly in the Basin and Range province, and in Alaska. On the other hand, the plate margin appears to be simpler in the Gulf of California and along the Canadian coastline.

A simplified interpretive tectonic map of this area is shown on Figure 13, again in an oblique mercator projection about the PCFC-NOAM pole. Because of the complications associated with internal deformation of North America in the Basin and Range and Rio Grande Rift, the RM2 data set along this boundary (shown on Figure 14) did not include data inbetween 32'N and 50'N along the west coast of North America. Thus, it was hoped, no contamination of the model by complex tectonic deformations would occur.

On the other hand, comparison of Figures 13 and 14 shows the following.

- 1) Because of the paucity of tectonic information about northern Mexico, it is not easy to assess possible contamination of data in the Gulf of California by deformation to the East in the southern extension of the Basin and Range and Rio Grande regions.

2) Because of oblique subduction along the Queen Charlotte fault, earthquake slip vectors in that region may not be representative of true plate motion directions.

3) The active Denali fault system in Alaska may jeopardize the correct interpretation of slip vectors in the Eastern Aleutians and the Gulf of Alaska.

4) Known effects of the downgoing slab have been shown to bias fault plane solutions in the western Aleutians (Engdahl et al., 1977).

5) The plate boundary between Eurasia and North America is very uncertain, and there is no guarantee that subduction in the Kuriles is between Pacific and North America.

In view of these many uncertainties, one can legitimately question inferences based on the RM2 PCFC-NOAM rotation vector. To remove biases specifically associated with this plate boundary, we have performed a global plate motion inversion after removing the entire data subset just described, including the single rate datum between PCFC and NOAM at the mouth of the Gulf of California.

The resulting pole is shown on Figure 15 with the RM2 pole and their respective 2σ error ellipses. It is truly remarkable that the solutions are not resolvable from each other. The PCFC-NOAM motion determined from the rest of the world is practically identical to that determined from the plate boundary.

Figure 16 shows that the predicted direction of relative motion in central California is distinguishable from the azimuth of the San Andreas fault system at the 2σ level, whether or not PCFC-NOAM data are included. This in turn means that the San Andreas direction is not

representative of relative motion between PCFC and NOAM, but only of relative motion between the Pacific plate and the Great Valley region of California, or even between the Salinas block and the Great Valley.

Geologically and geodetically determined rates of slip along the San Andreas in central California yield a value of 3.7 cm/yr. If one accounts for auxiliary faults, this rate reaches up to 5.0 cm/yr. It is likely that the RM2 rate of 5.7 cm/yr is an upper bound. Figure 17 shows a plane geometry relative motion diagram between PCFC, NOAM and California (CALI) and Mojave (MOJA) blocks.

CALI-NOAM is obtained by differencing the RM2 PCFC-NOAM speed and the slip vector along the San Andreas fault. Since there is good evidence that this vector should have a non-zero component in a westerly direction (e.g., Zoback and Zoback, 1979) as shown on Figure 18, interpretation of Figure 17 leads to an upper bound of 5.0 cm/yr for the San Andreas fault system, in agreement with geological data. If we assume that the Garlock fault is the site of 0.7 cm/yr of left-lateral displacement, then a lower bound of 1.3 cm/yr for the San Andreas fault system is obtained to insure compression in the Transverse ranges. This lower bound is increased to 2.0 cm/yr if 0.7 cm/yr thrust displacement is allowed across the Garlock-White Wolf fault system. On the other hand, unless we have simultaneously a fairly high rate of slip on the San Andreas fault system, and a significant component of compression across the Garlock fault, the model predicts some amount of EW compression between the Mojave block and the stable part of NOAM, for which evidence is lacking.

The alternative is, of course, to assume that EW shortening takes

place between the San Andreas fault and the Pacific plate. Then the PCFC-CALI vector would trend in a more northerly direction than both the San Andreas fault and the PCFC-NOAM RM2 vector and EW Basin and Range extension is easily accommodated.

Thus, analysis of instantaneous relative motions on a regional basis, using the global model RM2 to provide kinematical boundary conditions leads us to the prediction of an EW component of shortening across the Salinas block.

Independent confirmation is provided by the orientations of compression axes of crustal events (Figure 19) and of fold axes (Figure 20) compiled respectively by Gawthrop (1978) and Burford (1967), which are consistent with a significant component of compression in a direction perpendicular to the San Andreas trend.

Quantitative estimates require the determination of bounds on azimuth and direction of Basin and Range opening. This work is underway.

Seismicity and Subduction Processes

We have studied correlations between coupling on the subduction-zone thrust plane, parameterized by regional maximum earthquake magnitudes, with other parameters of the subduction zone. We found that convergence rate and lithospheric age correlate with coupling. It was also determined that penetration depth correlates with lithospheric age and contact width with convergence rate, results compatible with work done by Isacks et al. (1968), Vlaar and Wortel (1976), and Wortel and Vlaar (1978). These correlations suggest that

large earthquake generation correlates with interface geometry or with age and rate in some other manner. This study was completed and the paper (Ruff, L., and H. Kanamori, Seismicity and the subduction process) is now in press in the Physics of the Earth and Planetary Interiors.

Study of Slow Earthquakes

Detailed analysis of IDA data was made to study a slow earthquake which occurred on December 18, 1978, in the Bouvet Islands region. Although the body-wave magnitude of this earthquake is very small ($m_b = 5.4$) it excited long-period Rayleigh waves with a very large amplitude. The seismic moment is determined to be 1.4×10^{28} dyne-cm, which is much larger than that for earthquakes with comparable body-wave magnitude. The mechanism of this event is consistent with the geometry of the transform fault in the Bouvet Islands region, and suggests that the plate motion there is somewhat slower than that on other older transform faults.

A similar analysis is currently being made for subduction-zone events.

Study of Free Oscillations

The earthquake that occurred in the Ecuador and Colombia border on December 12, 1979 is large enough to excite various long-period modes. Preliminary analysis identifies oS_2 , oS_3 , oS_4 and oS_0 modes very clearly. We have determined the mechanism of this event, and are preparing the data sets to be used for more extensive analyses of the

free oscillations. This type of study provides information intermediate in period to body waves and longer duration plate motions.

RIVERA PLATE

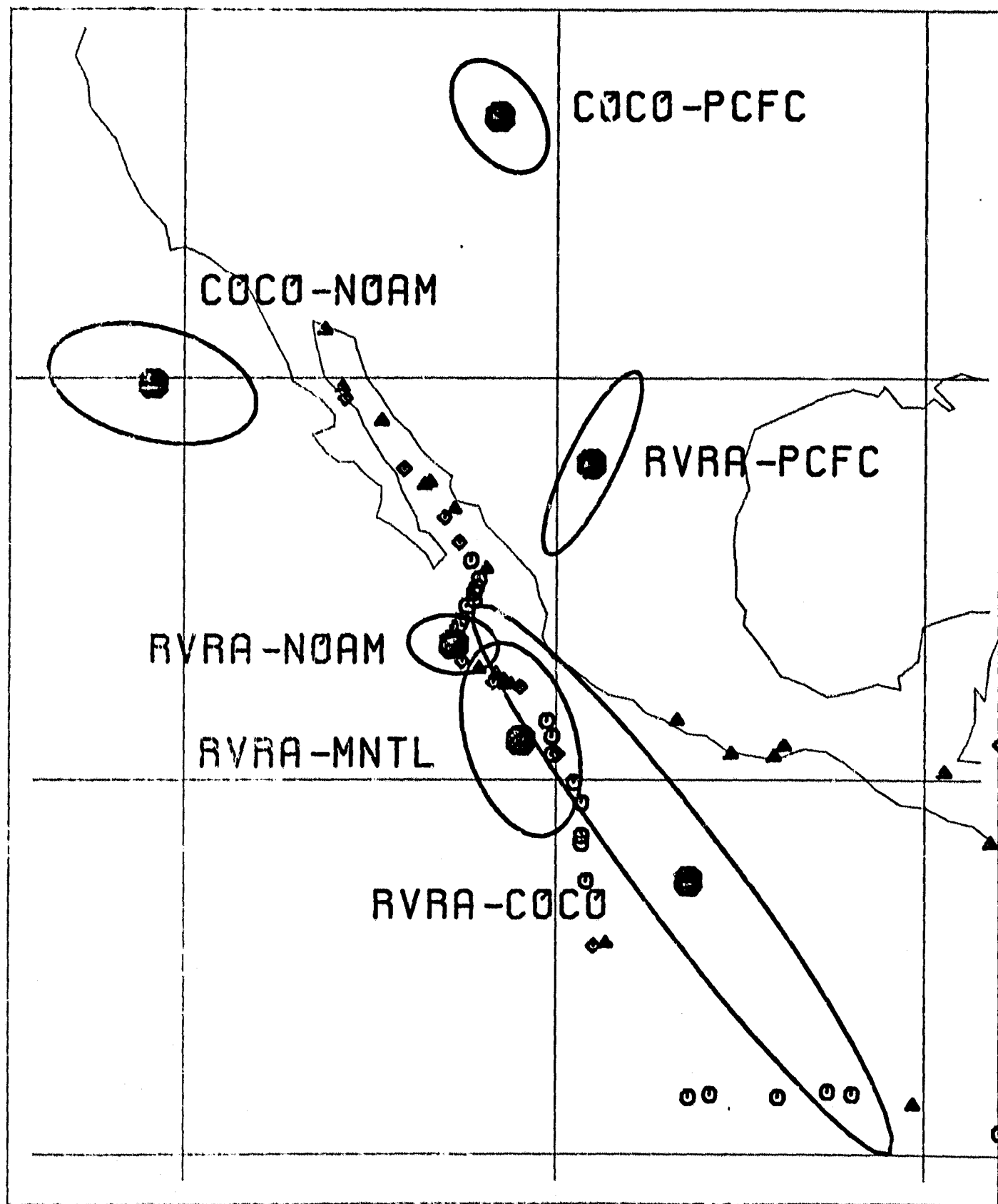
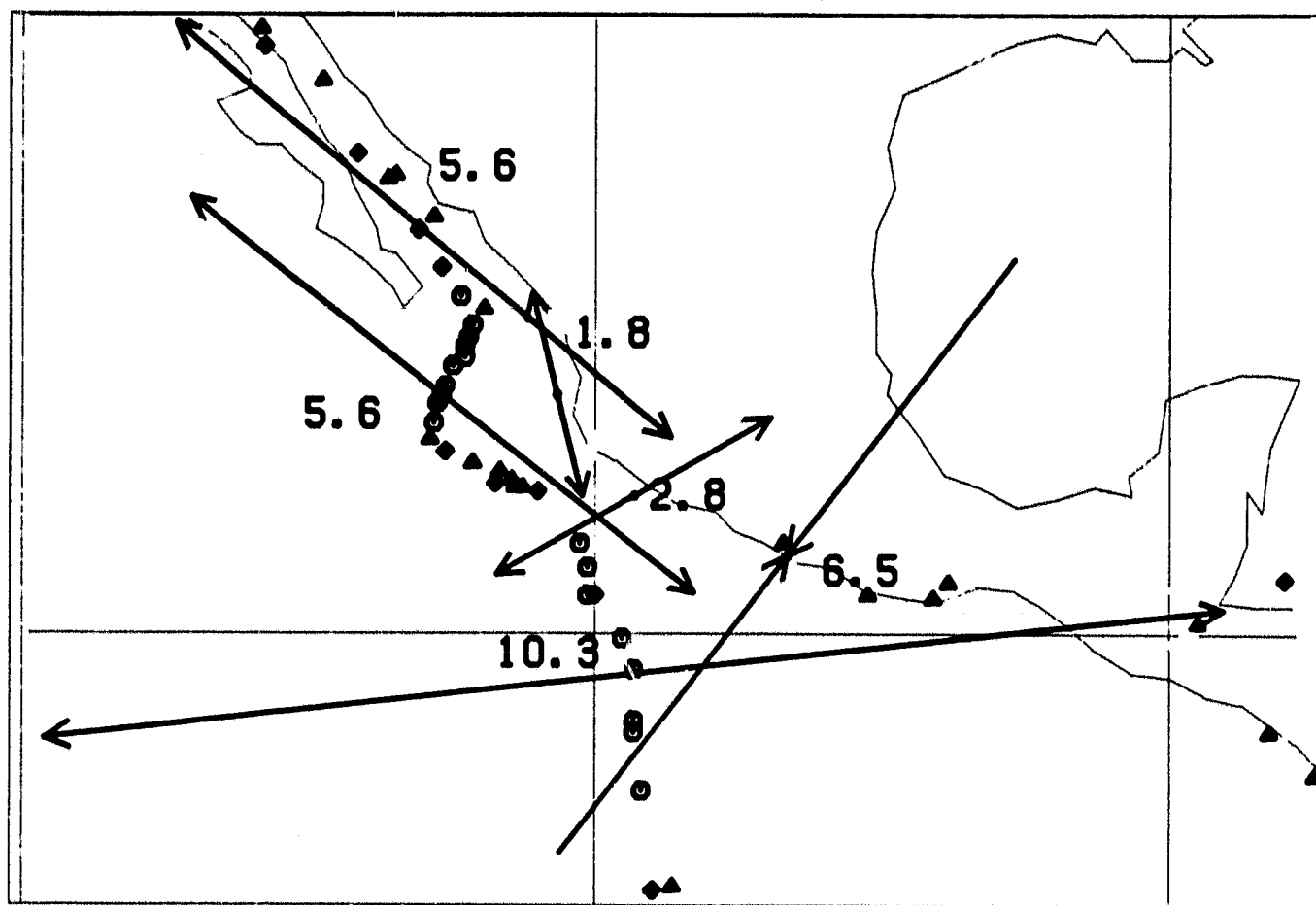


Figure 1

RIVERA PLATE, RELATIVE VELOCITIES



Figure

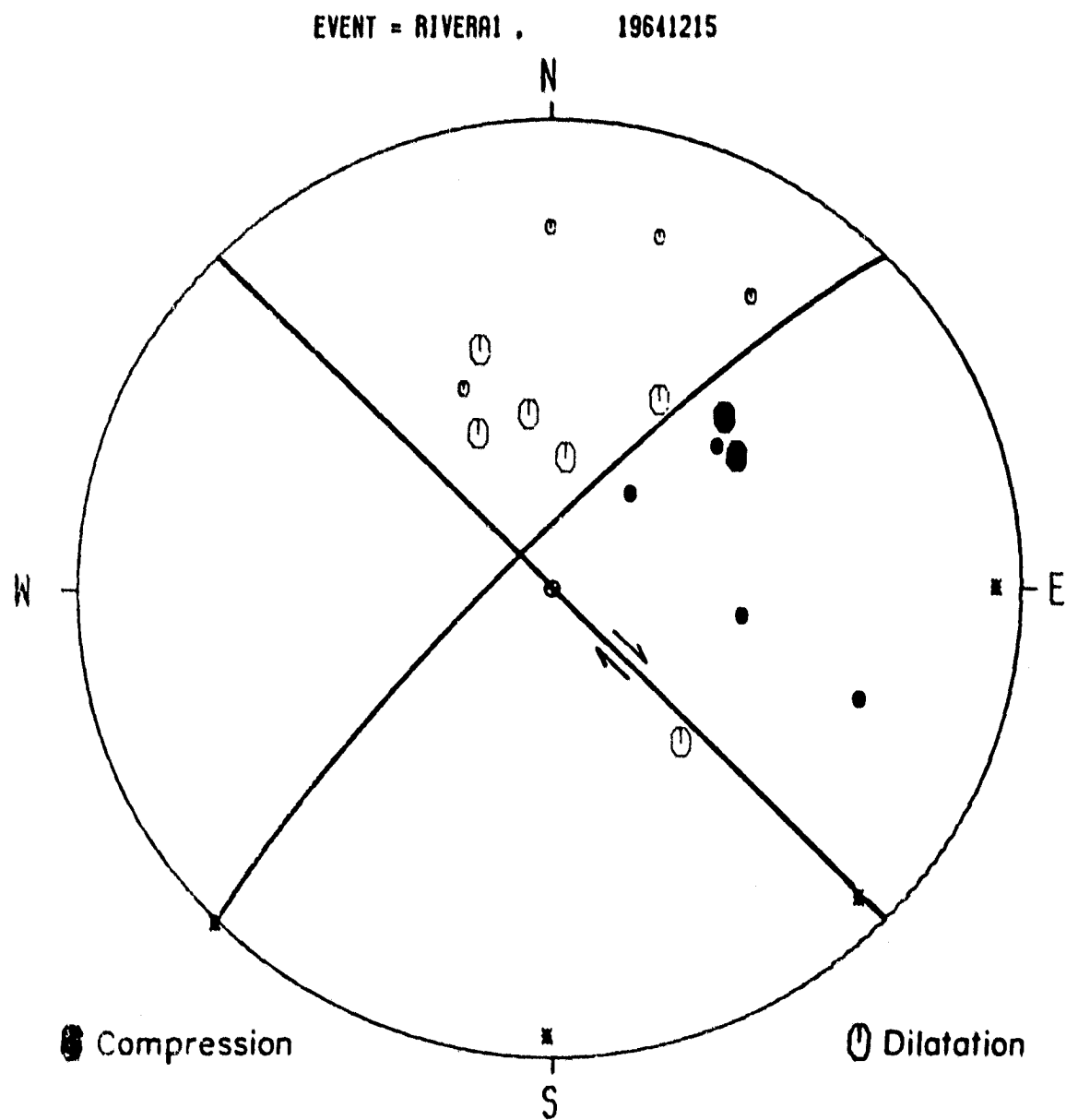


Figure 3

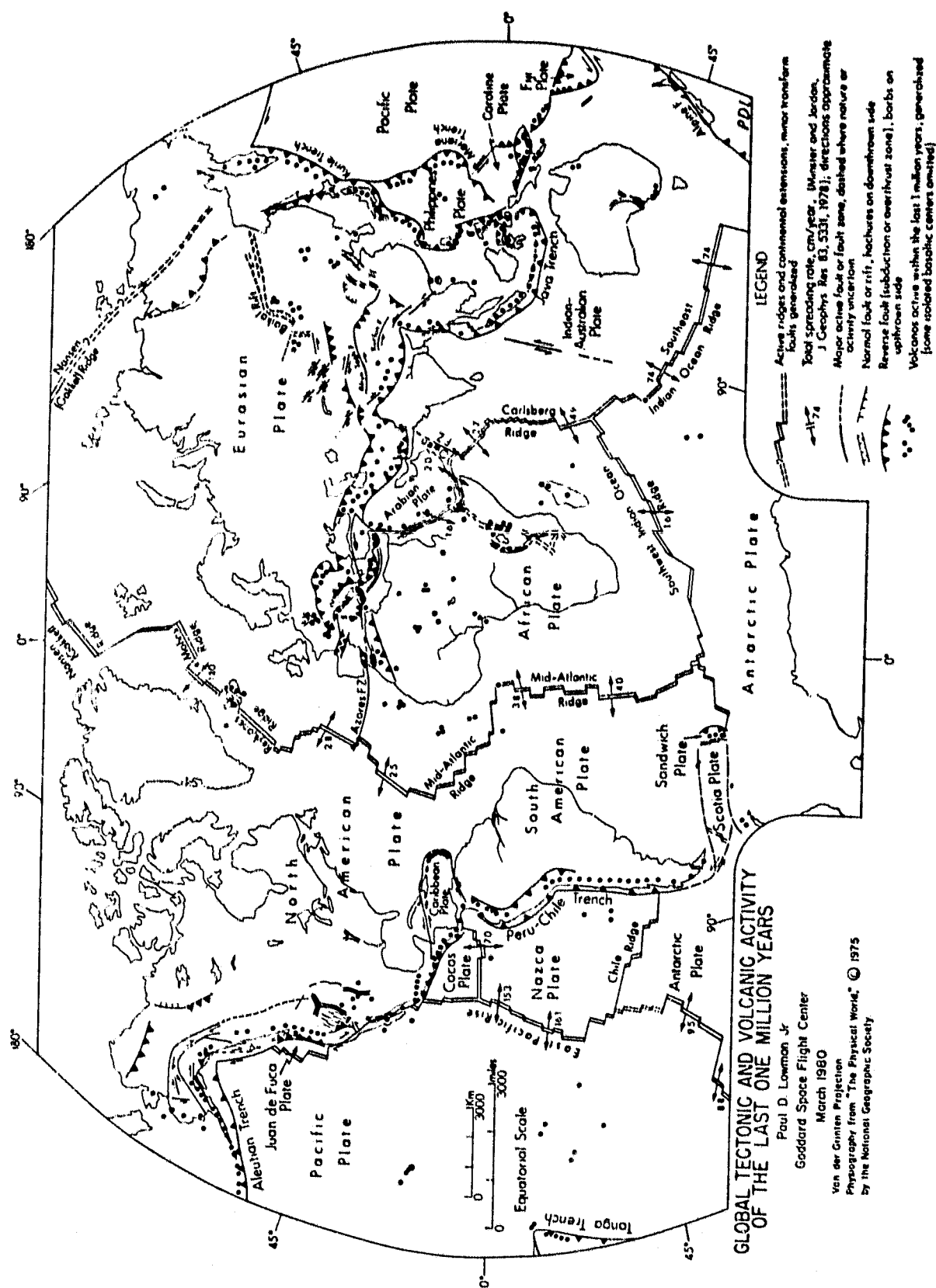


Figure 4

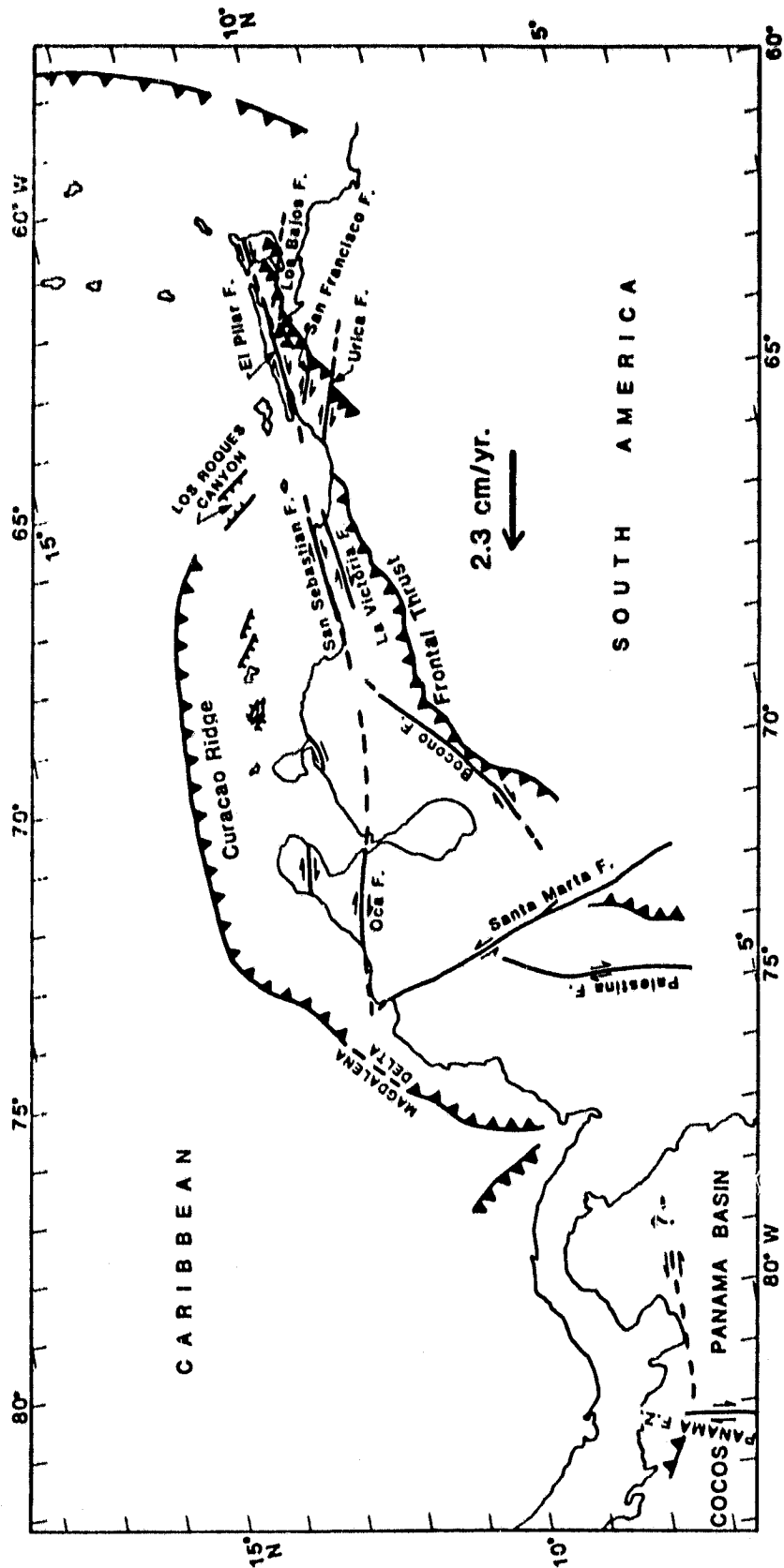


Figure 5

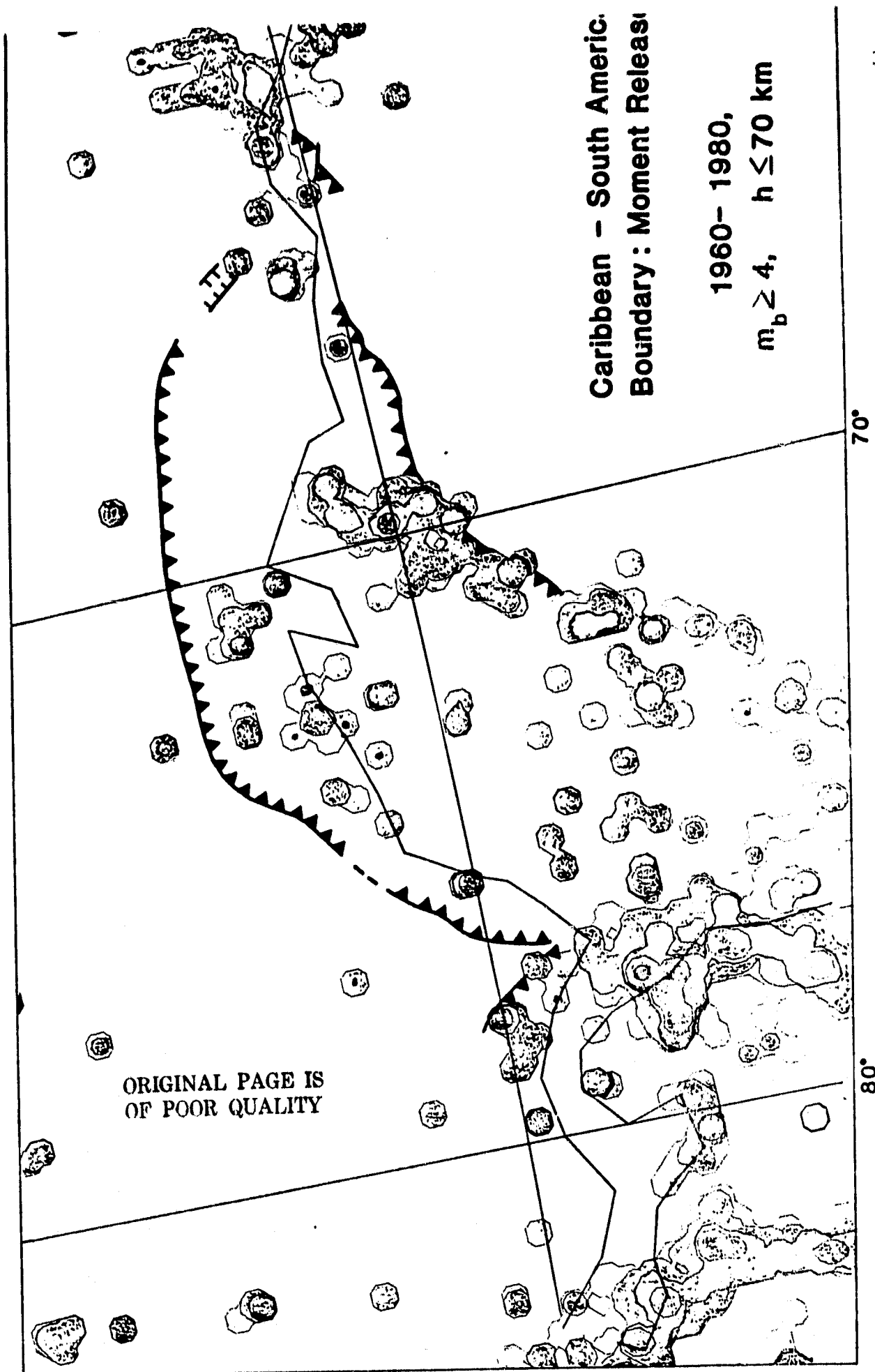


Figure 6a

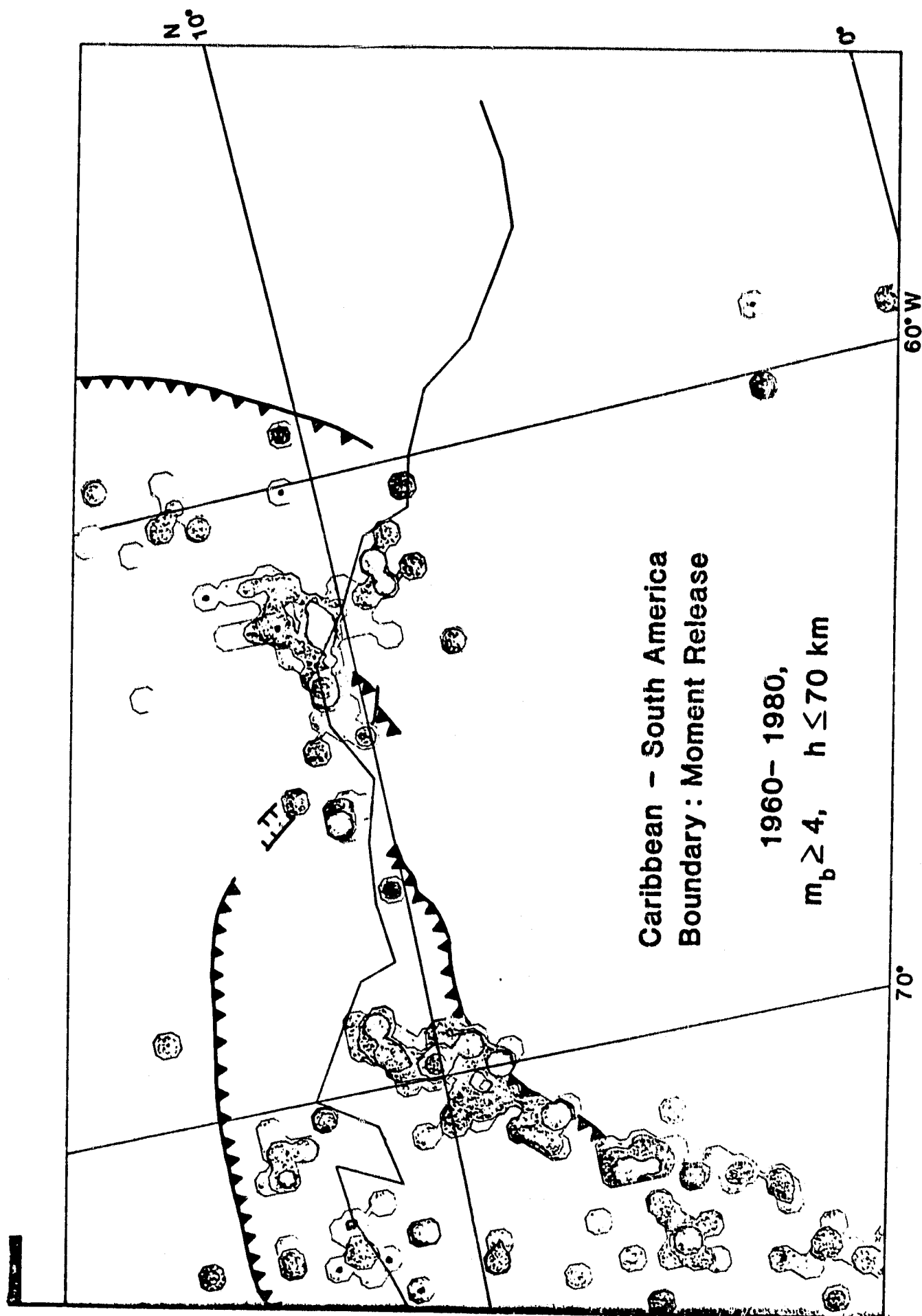


Figure 6b

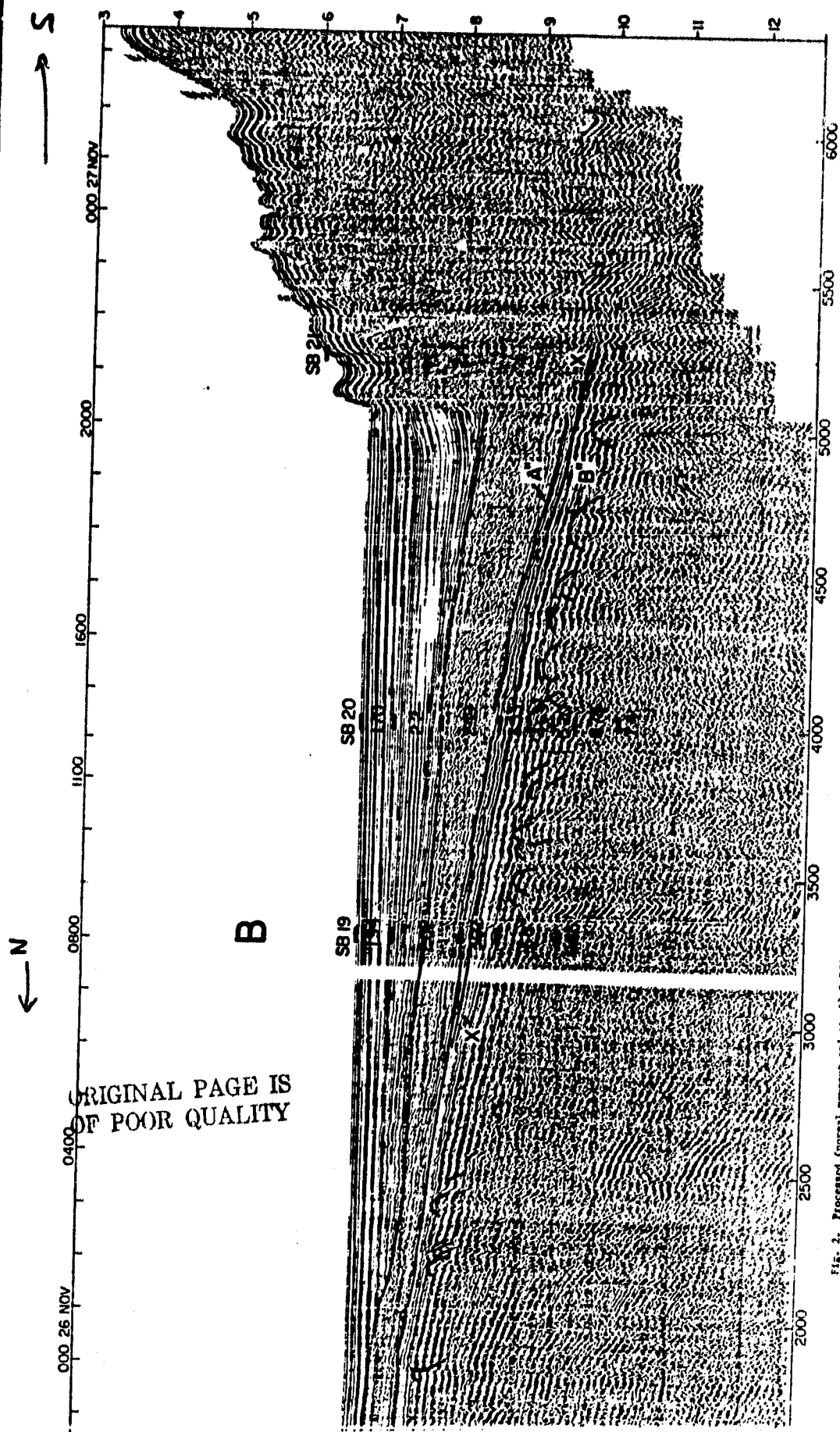


Fig. 2. Processed (normal movement and at-a-2) L-DGO MCS line 8 from the Venezuelan Basin to the Curacao Ridge is shown as a time section. Vertical exaggeration at the sea bottom is approximately 17.5 to 1. The location of the line is shown in Figure 1. Hour marks are given along the top of the figure. CDP numbers are given along the bottom of the figure. SNIR, etc., indicate sonobuoy refraction results plotted as time sections.

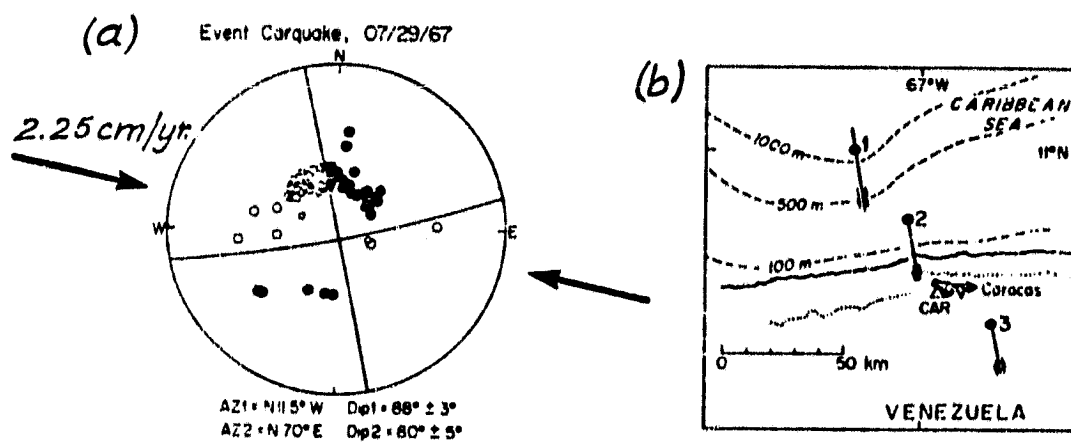


Figure 8

OBLIQUE MERCATOR/ INDI-EURA POLE

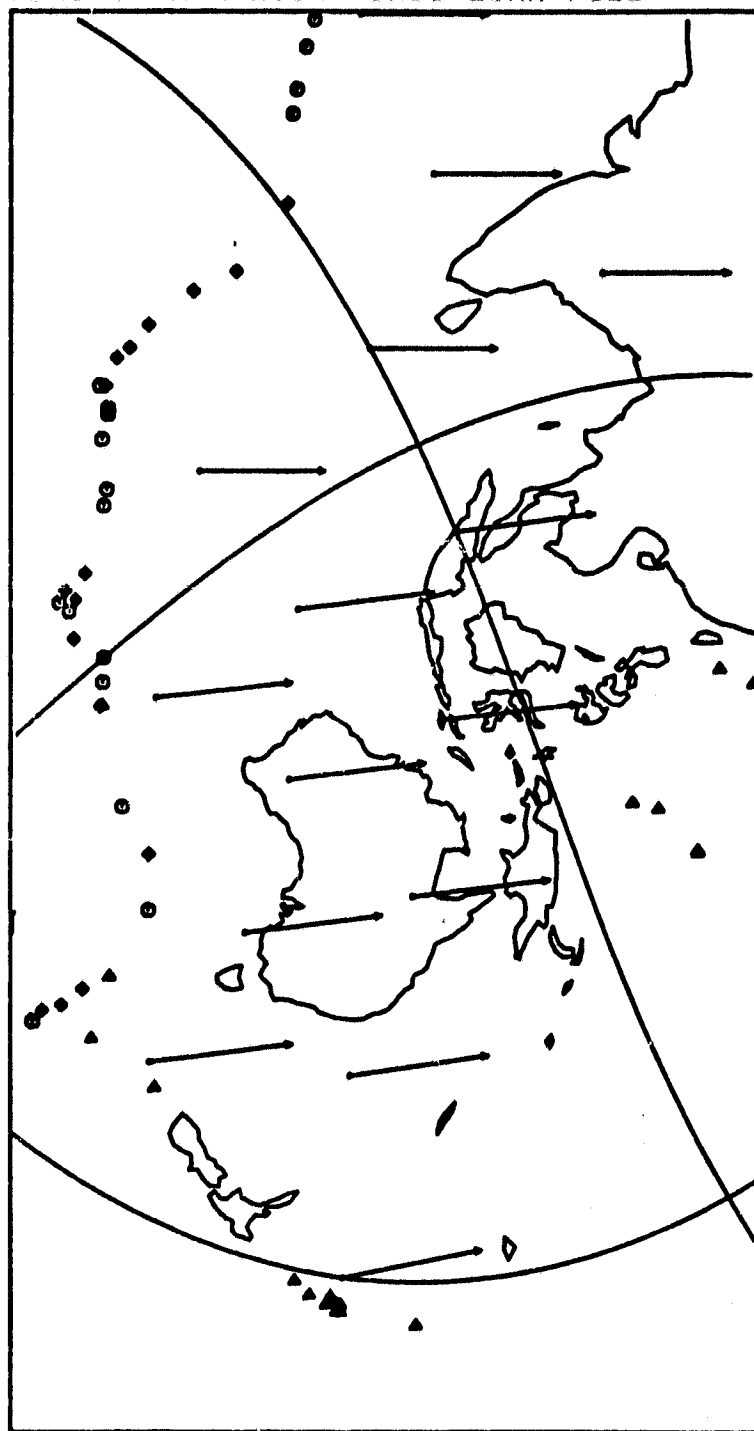


Figure 9

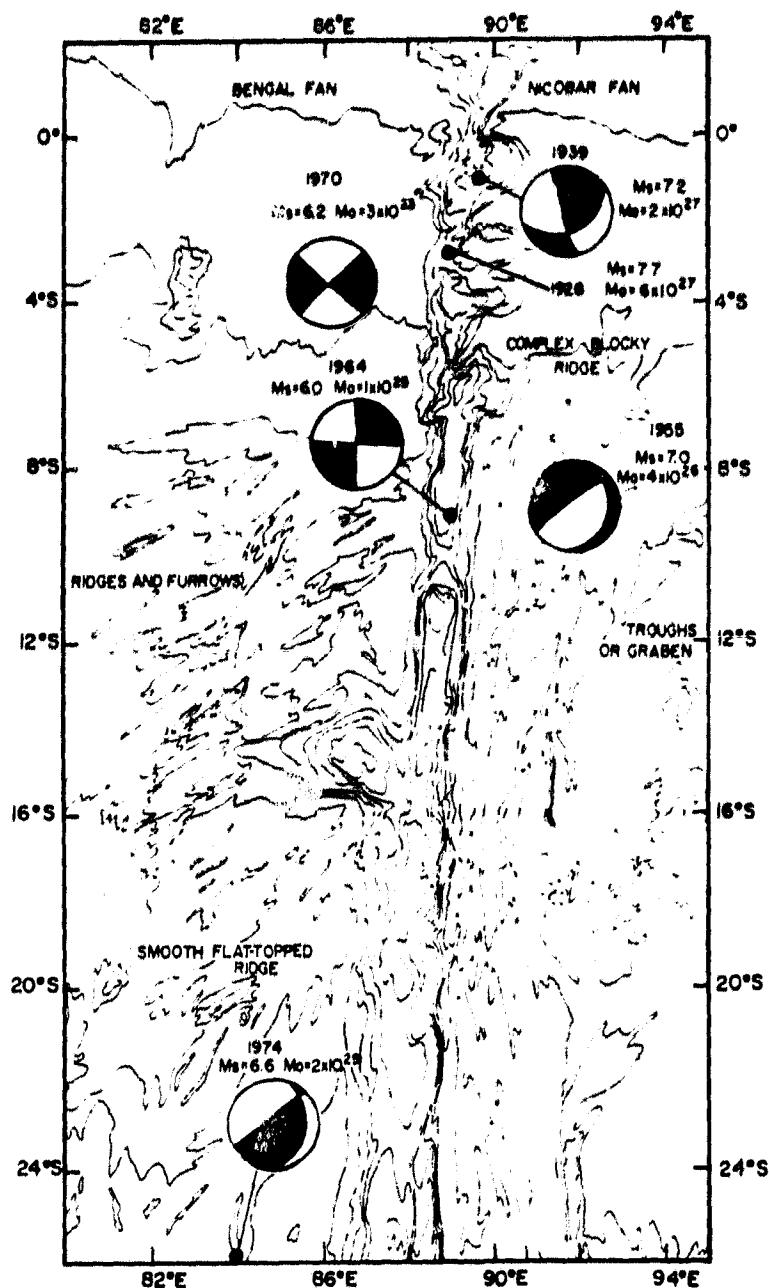


Figure 10

Fig. 12. Focal mechanism, magnitudes, and moments for major earthquakes near the Ninetyeast Ridge. The mechanism of the 1928 event could not be reliably determined. Note that the 1939 and 1964 events on the ridge show strike slip motion, the 1955 event is a normal fault, and the 1974 event is a thrust fault. The moments of the 1928 and 1939 earthquakes are much greater than any of the more recent events.

Acknowledgments. We thank Bob Geller, Yoshio Fukao, Hiroo Kanamori, Bernard Minster, and Tom Jordan for advice and assistance. R. L. Fisher supplied us with the bathymetric maps. Kazuya Fujita, Rob Cockerham, and Norman Sleep read the manuscript and made many valuable suggestions. We also thank the staff of many observatories around the world who provided us with seismograms and bulletins. Seth Stein was supported by a fellowship from the Fannie and John Hertz Foundation. This research was also supported by NSF grants EAR 76-14262 and EAR 77-13641. Contribution 2966, Division of Geological and Planetary

Sciences, California Institute of Technology, Pasadena, California 91125.

References

- Allen, C. R., P. St. Amand, C. F. Richter, and J. N. Nordquist, Relationship between seismicity and geologic structure in the southern California region, *Bull. Seismol. Soc. Amer.*, **55**, 753-797, 1965.
- Bowin, C. O., Origin of the Ninetyeast ridge from studies near the equator, *J. Geophys. Res.*, **78**, 6029-6043, 1973.

OBLIQUE MERCATOR/ INDI-EURA POLE

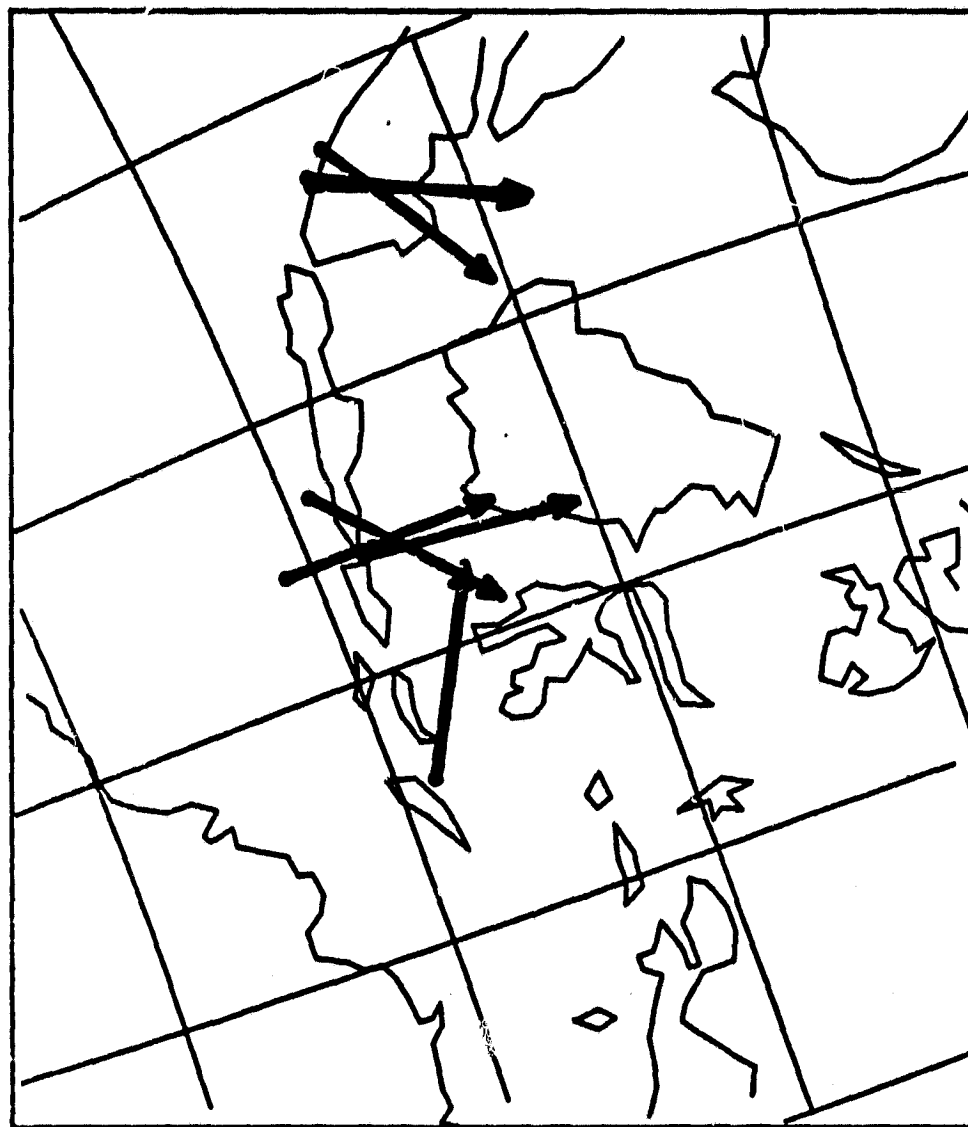


Figure 11

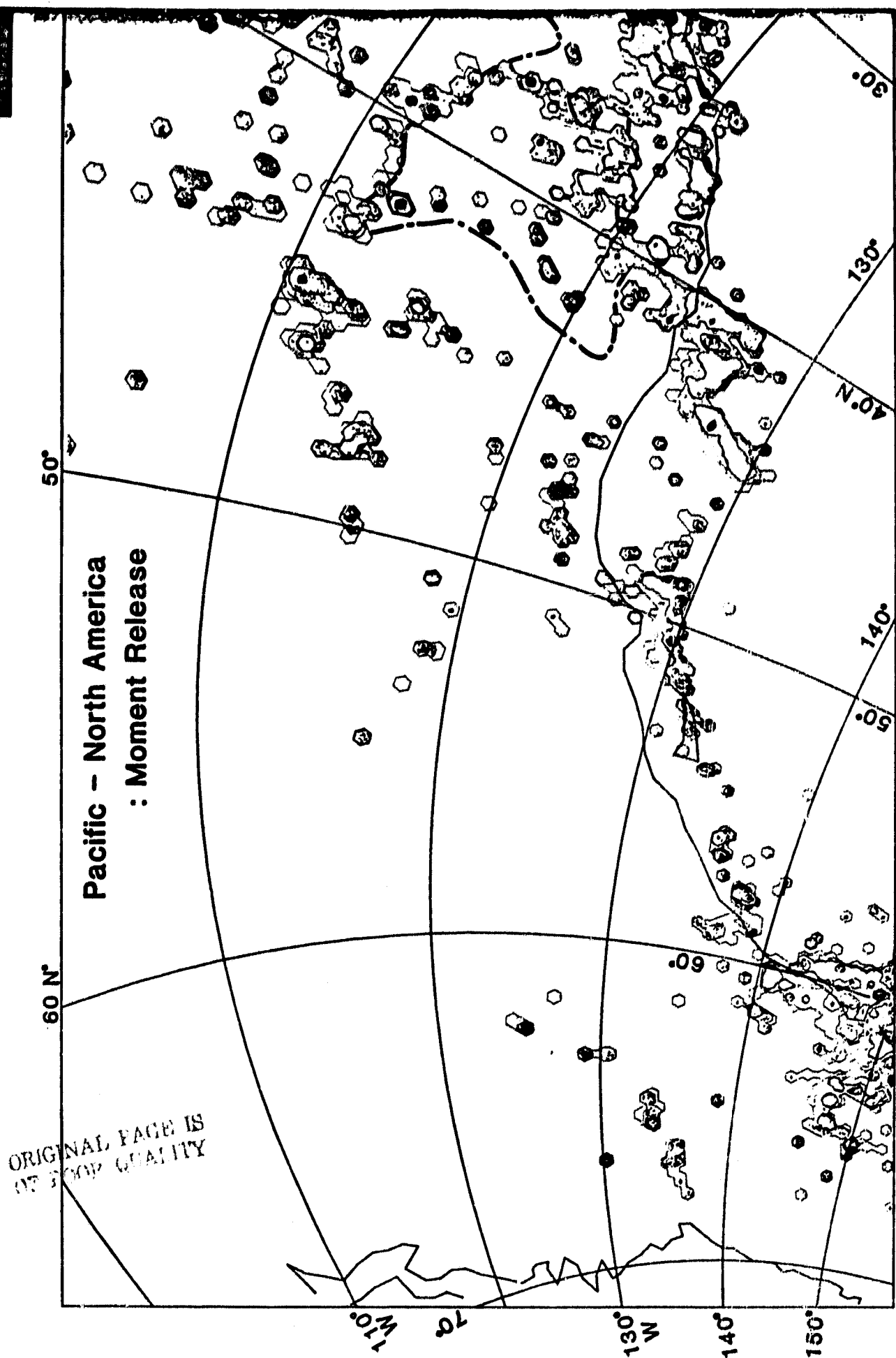


Figure 12a

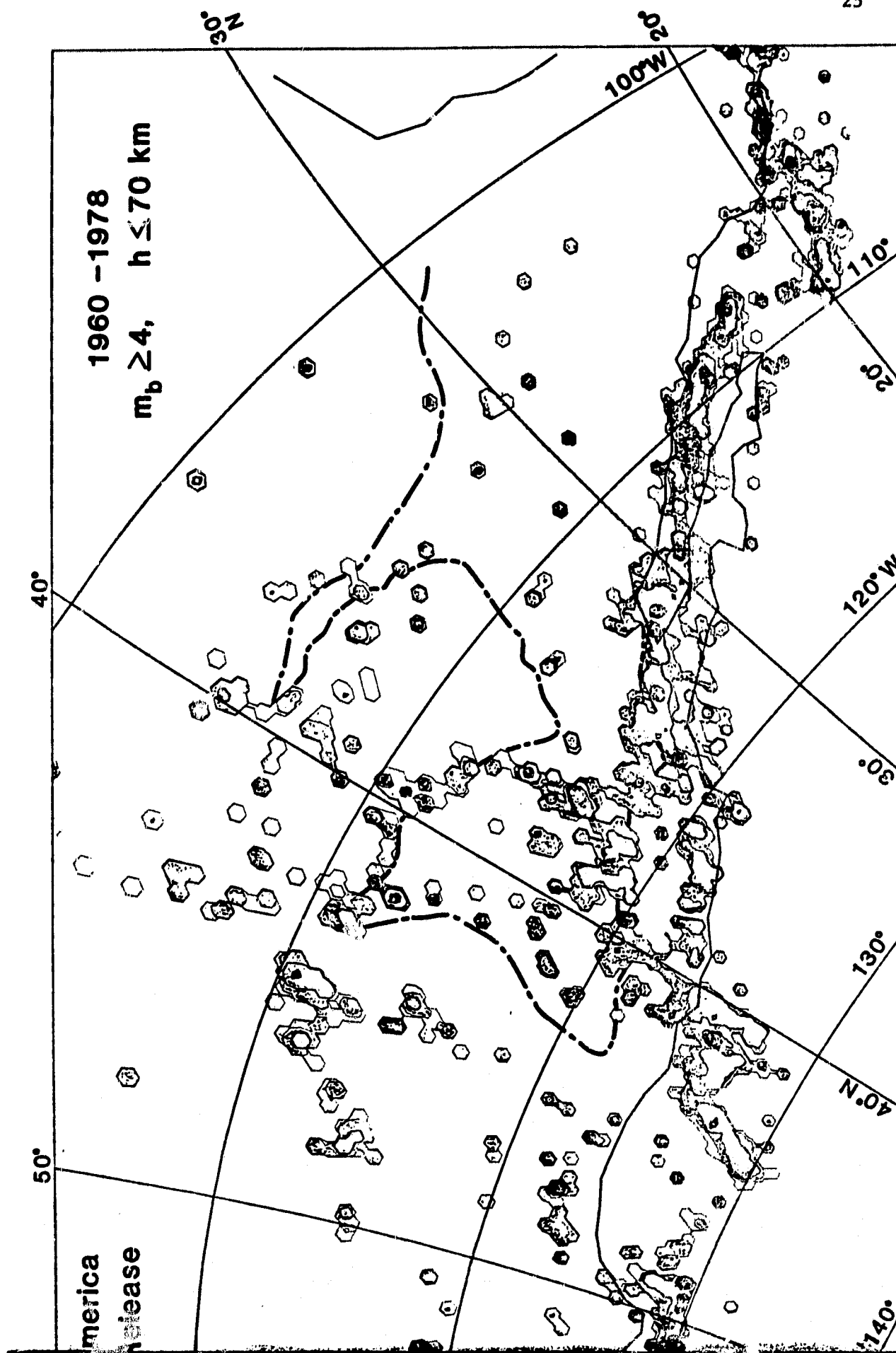


Figure 12b

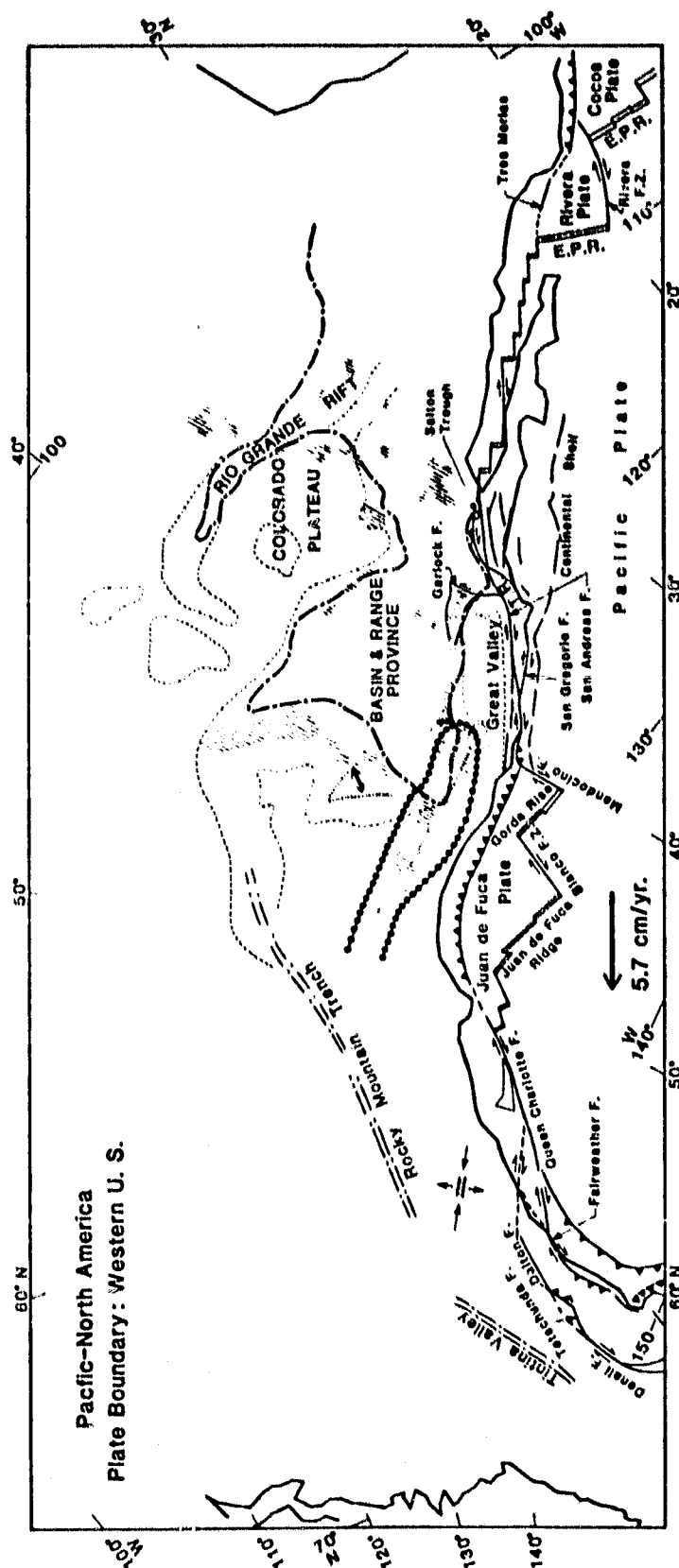


Figure 13

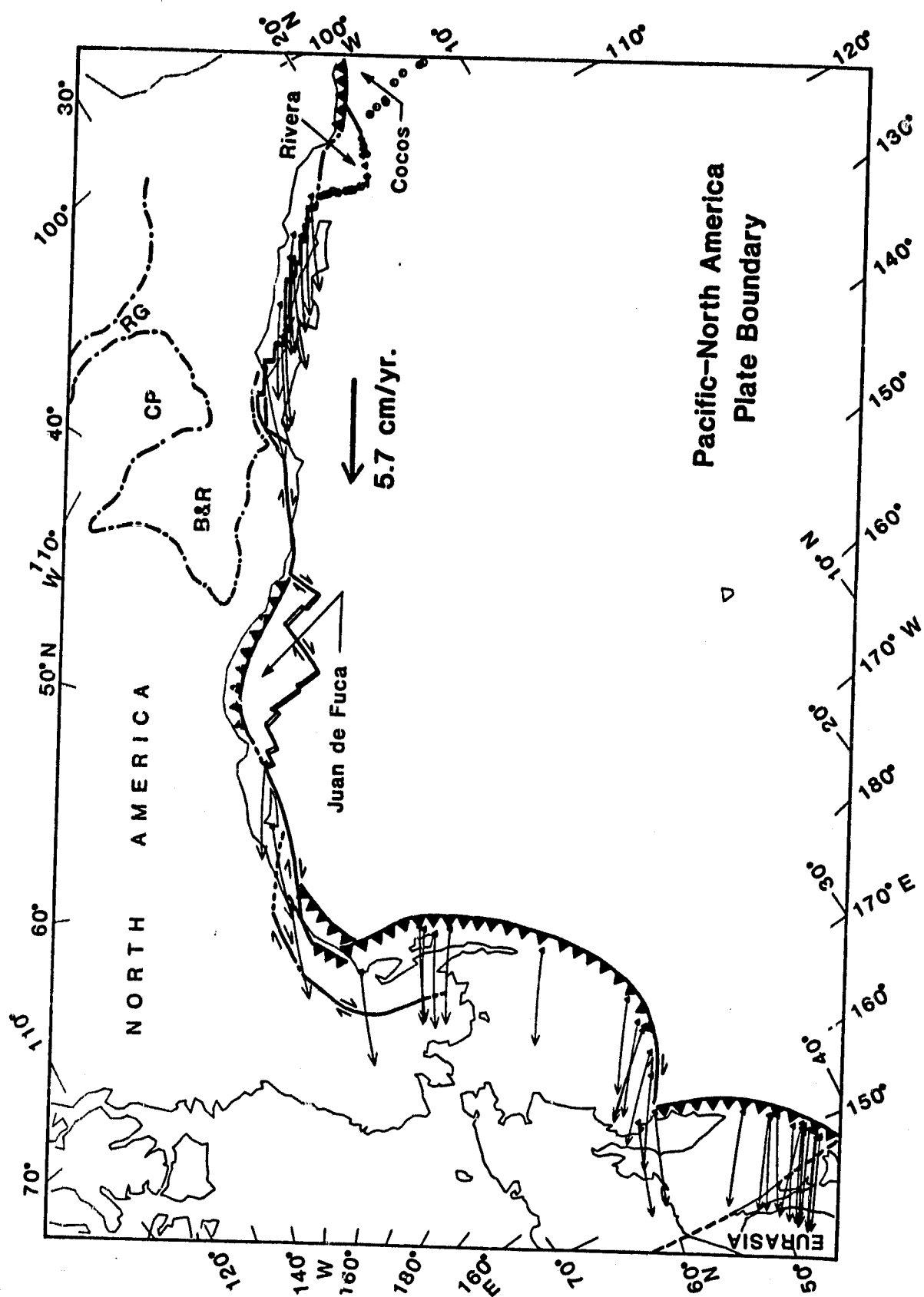


Figure 14

PCFC - NOAM POLE

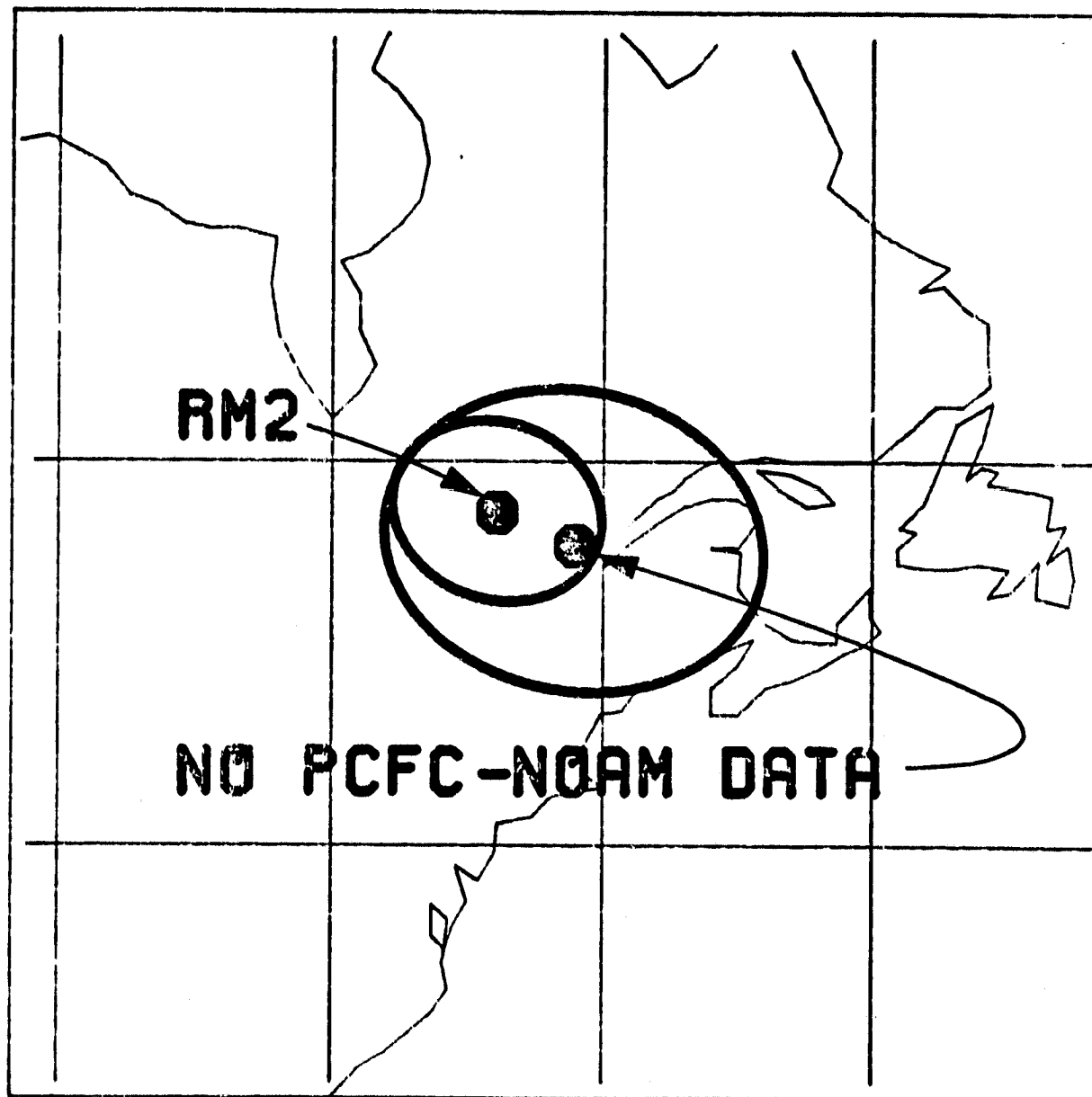
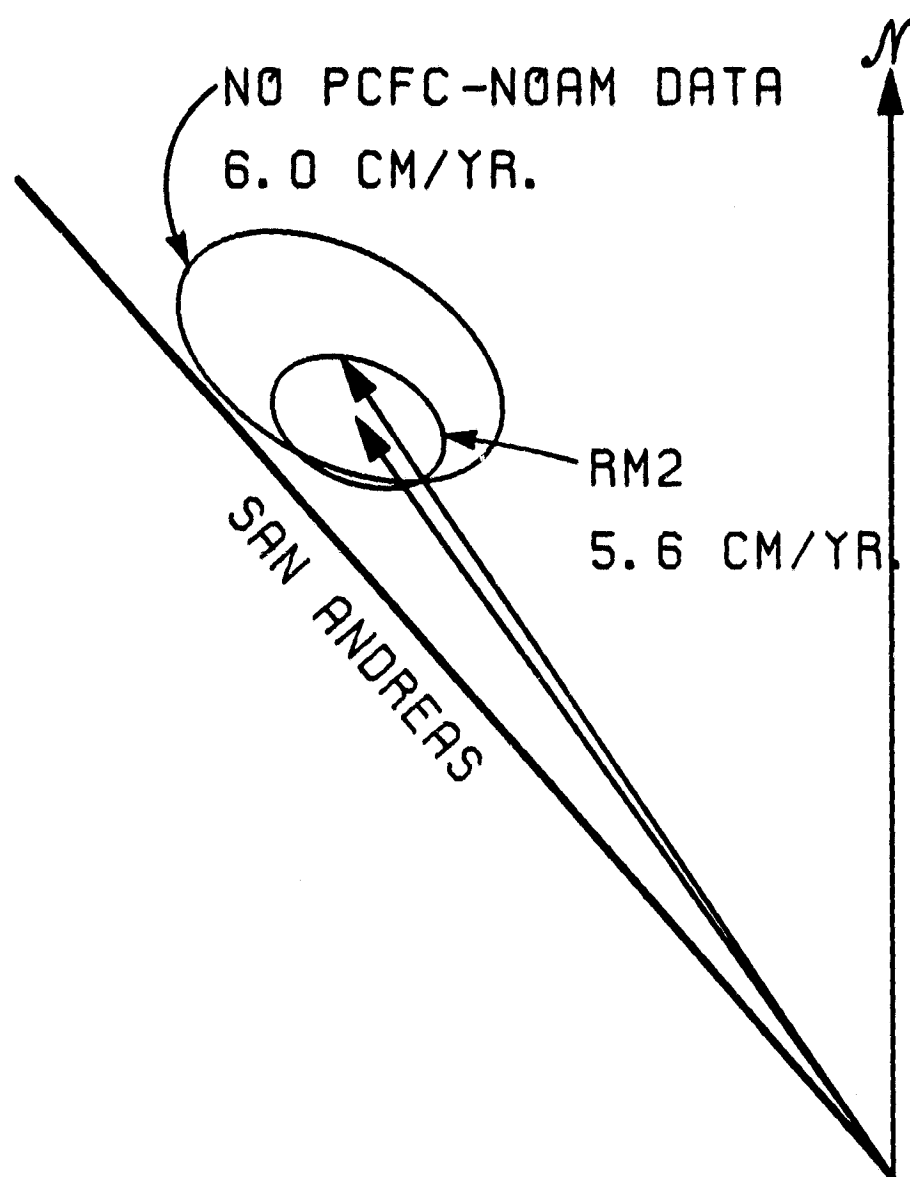


Figure 15



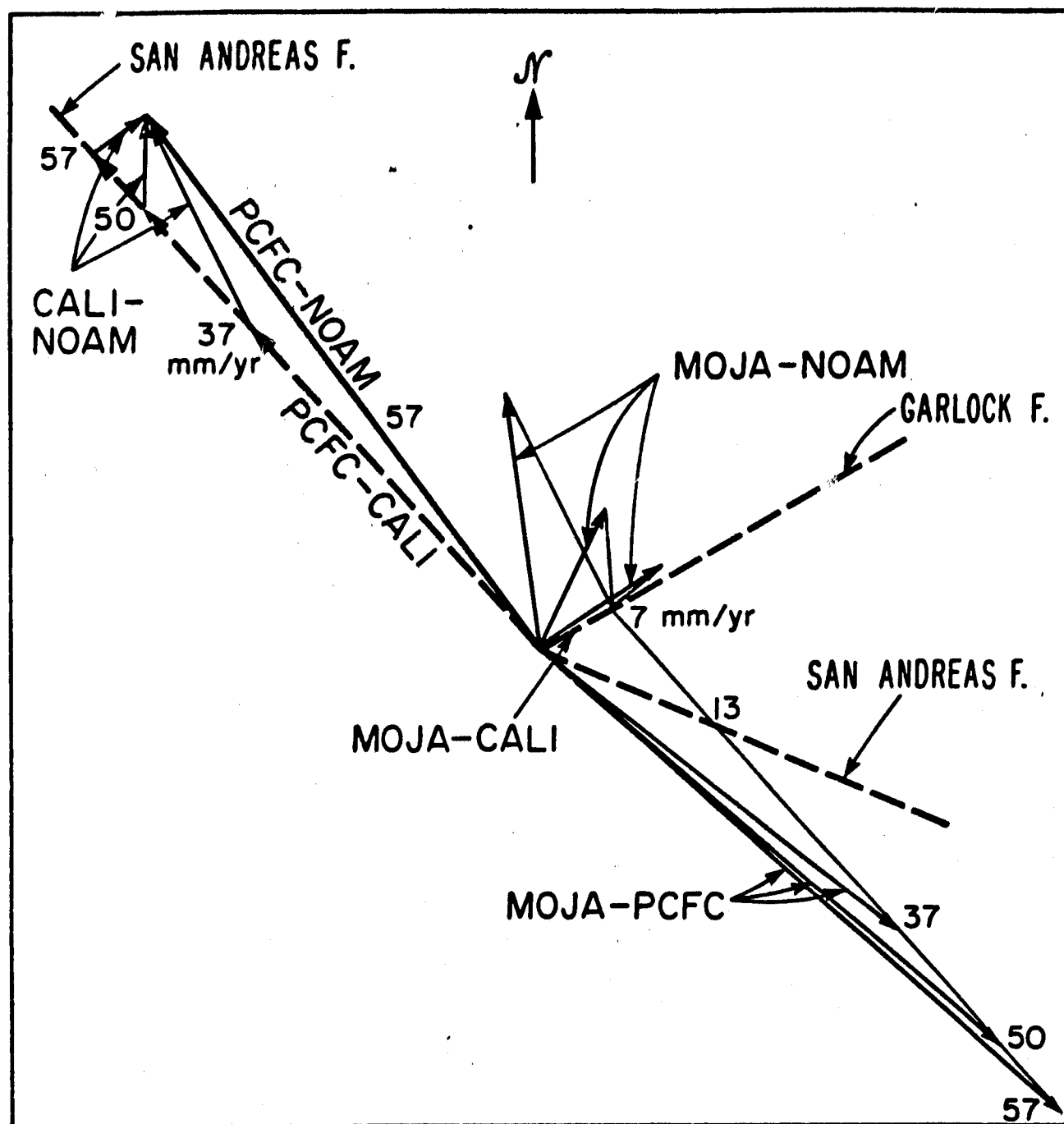


Figure 17

ZOBACK AND ZOBACK: STRENGTH OF THE CRUST

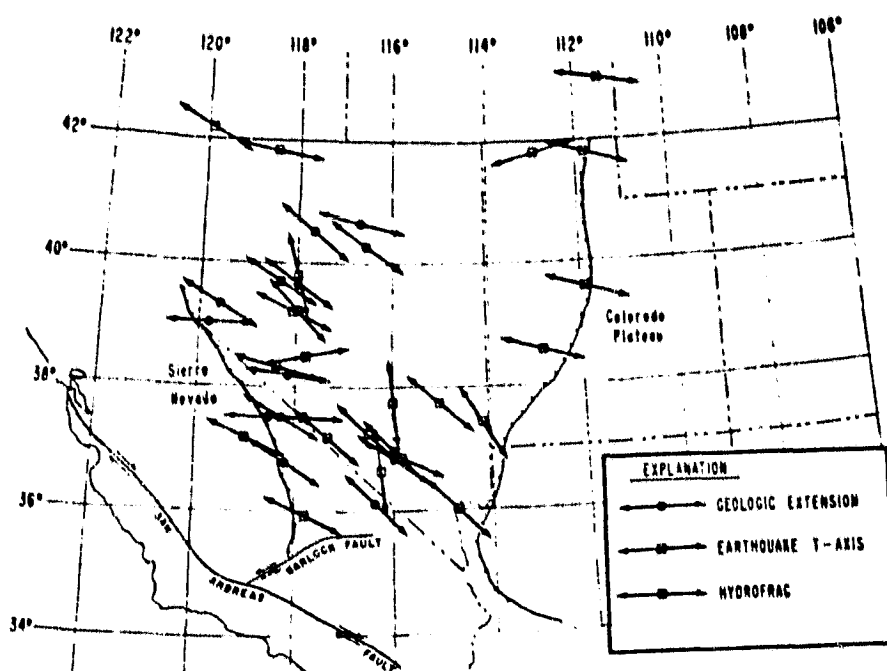


Fig. 1. Extension directions and least principal stress orientations for the northern Basin and Range province.

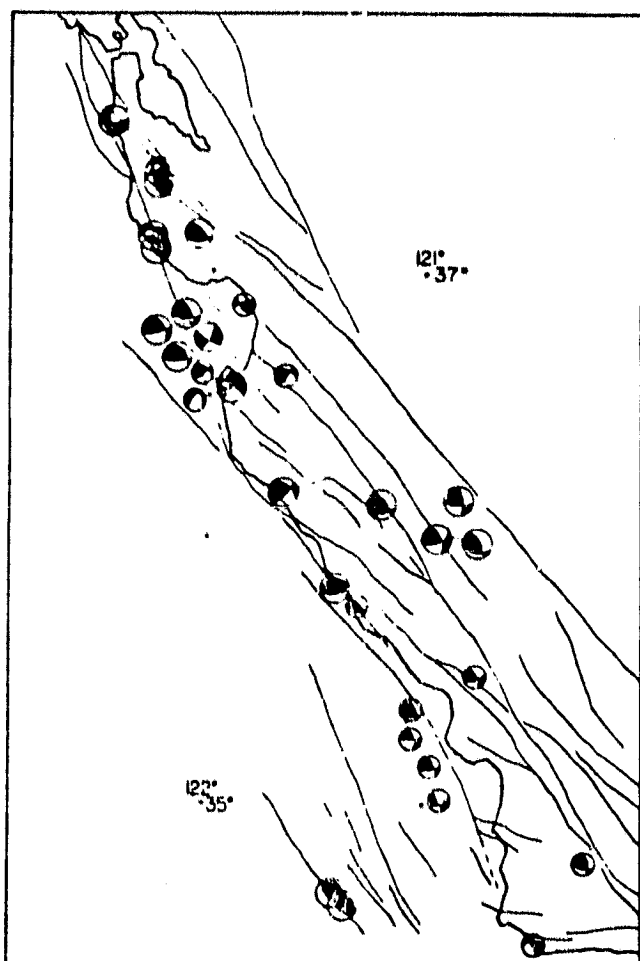


FIGURE 8. Focal mechanisms of earthquakes. Shaded area indicates compressional quadrant in lower hemisphere plot. Large mechanism plots are better determined than the smaller mechanism plots.

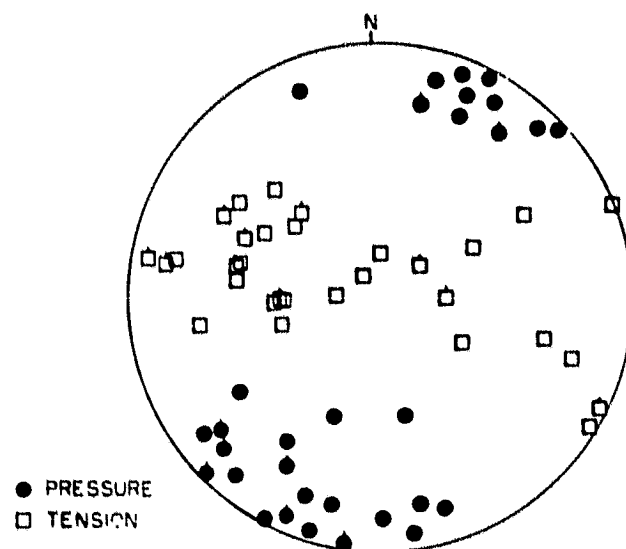


FIGURE 9. Pressure and tension axis plot. Small area of pressure axis on focal sphere indicates that compression dominates the local tectonics. Tick marks indicate the event occurred south of 35° 30' near the Transverse Range province.

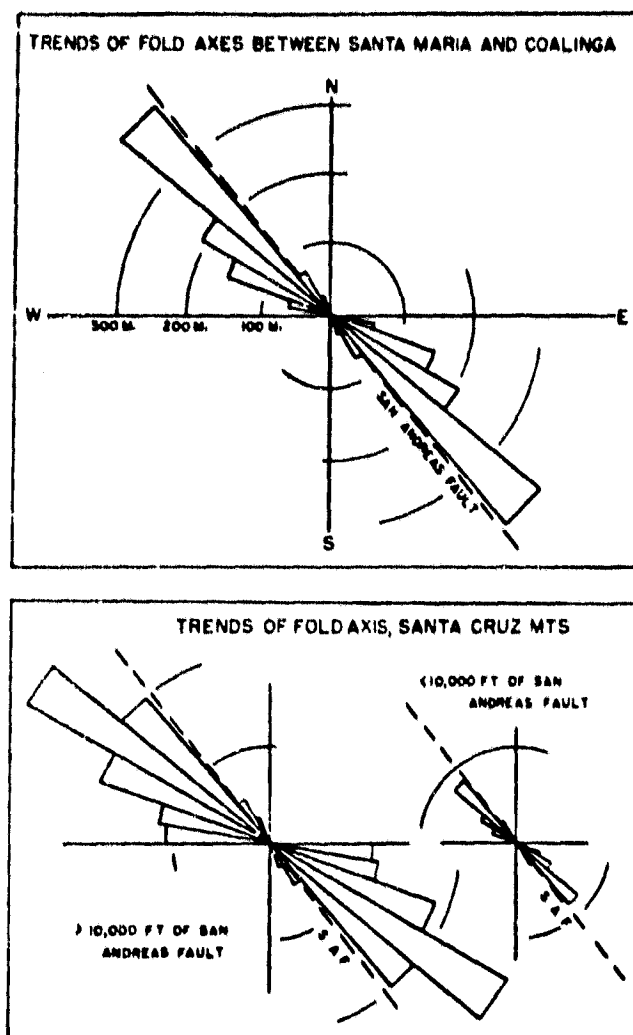


FIGURE 10. Fold axis plot indicating the lengths of folds in the Coast Ranges with a particular trend (from Burford, 1967).

APPENDIX I

PRESENT-DAY PLATE MOTIONS: A SUMMARY

J. Bernard Minster

Thomas H. Jordan

Annales de Géophysique (Coulomb volume).

PRESENT-DAY PLATE MOTIONS: A SUMMARY

J. Bernard Minster

**Seismological Laboratory, California Institute
of Technology, Pasadena, California 91125**

Thomas H. Jordan

**Geological Research Division, Scripps Institution
of Oceanography, La Jolla, California 92093**

January, 1979

Revised, February, 1980

Annales de Géophysique (Coulomb volume)

Abstract

We review the progress in modeling instantaneous plate kinematics, with an emphasis on recently developed models of present-day plate motions derived by the systematic inversion of globally distributed data sets. The 11-plate model RM2 (Minster and Jordan, 1978) is described, and the relative and absolute velocity fields associated with this model are summarized in a series of maps.

Modeling Plate Kinematics

In the several years following Wilson's (1965a) outline of the basic kinematical concepts, plate tectonics was transformed from a bold new hypothesis to an established theory. Many new ideas promulgated during this critical period were synthesized in a book by Coulomb (1969, 1972); ten years later these ideas continue to guide research in solid earth science.

One of the most spectacular successes of the plate theory was the early solution of the instantaneous kinematical problem, namely: in the present geological epoch, where are the plate boundaries and what are the plate motions? Wilson (1965a) recognized that the three kinematical boundary types - divergent, convergent and transform - correspond to three classes of deformation zones - spreading oceanic ridges, active mountains and island arcs, and major shear faults - "connected into a continuous network of mobile belts about the earth which divide the surface into several large rigid plates." McKenzie and Parker (1967) and Morgan (1968) introduced the geocentric angular velocity vector as a description of instantaneous plate motion and began to determine these vectors by fitting sea-floor spreading rates, strikes of transform faults and azimuths of earthquake slip vectors. This pioneering work culminated in Le Pichon's (1968) masterful synthesis of plate movements past and present, in which he produced a model for the instantaneous relative velocities of six major plates: Africa, America, Antarctica, Eurasia, India and Pacific.

Since 1968 the kinematical models have been considerably refined by numerous special studies of specific geographical regions. Among these

are McKenzie and Sclater's (1971) treatise on plate tectonics in the Indian Ocean, Pitman and Talwani's (1972) analysis of sea-floor spreading in the North Atlantic, the study by Molnar et al. (1975) of the South Pacific, Hey's (1974) modeling of plate interactions in the East Pacific, and Jordan's (1975) study of the Caribbean.

The numerical algorithms for computing the angular velocities have also been improved. In the original papers by McKenzie and Parker (1967) and Morgan (1968) pole positions were constructed by graphical methods. These methods were automated by Le Pichon (1968) to handle large data sets; he minimized the root-mean-square difference between the observed and computed azimuths of relative motion by searching over a grid of possible pole positions. McKenzie and Sclater (1971) discussed various fitting criteria and devised fitting algorithms based on matrix solutions to the minimization problem. As they noted, the problem is complicated by the fact that, although the relative velocity vector at any point on a plate boundary is a linear functional of the angular velocity vector, the unit vector describing the azimuth of relative motion is not. In practice this nonlinearity poses no difficulties for most geometries and can be accommodated by the iterative solution of suitably linearized equations.

The instantaneous kinematic problem for the global plate mosaic was attacked using iterative, nonlinear least-squares inversion methods by Chase (1972) and Minster et al. (1974). Since all angular velocity vectors describing the relative motions among M plates are uniquely specified by $3(M-1)$ parameters, to determine a global model from, say,

N data (rates and/or azimuths at arbitrary boundary points) requires the solution of an $N \times 3(M-1)$ system of equations, where N is typically an order of magnitude or more greater than M. In this formulation the compatibility conditions (e.g., triple-junction closure) are automatically satisfied. Because the problem is over-determined an exact solution to this system generally does not exist, and the particular approximate solution chosen depends on the fitting criterion satisfied. Minster et al. (1974) advocated the minimization of a fitting function which is the sum of the squares of the differences between the observed and computed data, each normalized by an estimate of the standard observational error. If the data are assumed to have errors which are normally distributed, this choice yields the classical maximum likelihood estimate of the model perturbation, and the linear theory can be used to estimate uncertainties in the model induced by uncertainties in the data. The theory also allows the computation of what Minster et al. (1974) have termed "data importances", quantities which are indicative of the information distribution among the data and which are useful in assessing a model's fit to the data set.

Our experience in applying this algorithm to the plate kinematic problem has demonstrated to us its effectiveness. Although the algorithm involves the linearization of a nonlinear problem, convergence to a good solution is generally rapid, and no difficulties with spurious local minima have been encountered. The uncertainties in the model parameters derived from the linear theory have proven to be effective measures of the model errors caused by random observational errors, although, of

course, they do not account for data bias.

Two recent, independent studies by Chase (1978) and Minster and Jordan (1978) have presented global kinematical models derived by the inversion of improved data sets. The wealth of new data in the ocean basins is impressive: every major oceanic ridge is now well populated with both azimuths and rates of relative motion (Figure 1), and the uncertainties in the angular velocity vectors have been much reduced. Although some significant differences between Chase's solution and ours are revealed by a detailed comparison, most are ascribable to slight differences in data selection and interpretation. Clearly the models can be refined, but we anticipate that any future modifications will be minor.

occurs, then the azimuth residuals (observed-computed) for transforms characterized by left-lateral faulting should be systematically more positive than those for right-lateral transforms. In fact, sinistral transform faults show slightly more negative residuals than dextral transform faults, opposite to that expected from the leaky transform hypothesis. The difference is not statistically significant, however, and the RM2 fit to the transform fault data appears to be unbiased. Therefore, there is no evidence in our results to indicate that leaky transforming commonly occurs.

A complete and convenient description of the instantaneous relative motions among M plates is given by the geohedron, the set of $3(M-2)$ angular velocity vectors for plate pairs sharing common boundaries (McKenzie and Parker, 1974). The 27 relative velocity vectors of the RM2 geohedron are listed in Table 1 in both spherical and cartesian coordinate systems. The poles and their associated 95% confidence regions are depicted in Figures 2-4. Also shown are the best-fitting poles (BFP's) for individual plate boundaries determined by separate inversion of data sets for specific plate pairs, wherever possible (Minster and Jordan, 1978, Table 3). The differences between RM2 and the BFP set result from the $2M-5$ vector compatibility conditions implicit in the simultaneous inversion scheme. In most cases these differences are small, and RM2 provides a nearly optimal fit to localized data subsets. Significant differences do exist, however, for AFRC-NOAM, INDI-PCFC, INDI-ANTA and INDI-AFRC. The discrepancy for AFRC-NOAM involves RM2's misfit to transform azimuths in the FAMOUS area, discussed above. The discrepancies between RM2 and

detailed history of plate motions as well as the spatial scale lengths over which the primary bathymetric data are averaged. Complications arise in regions such as the central North Atlantic where an apparent reorientation of the motions has occurred in the last several million years (Macdonald, 1977; Fox et al., 1979). Here two trends are superposed, an older trend of about S80°E represented by the mean azimuths of major transform faults (e.g., Oceanographer and Atlantis) and a younger, nearly east-west trend of smaller, more recent faults (e.g., Transforms A and B in the FAMOUS area and en echelon faults within the Oceanographer F.Z.). In this case we used the younger trends in the RM2 data set, although, surprisingly, they were not fit by the model; RM2 instead predicts azimuths compatible with the mean trends of the major transforms. (This misfit is indicative of internal inconsistencies in the data pertaining to the relative motions about the Azores triple junction not readily associated with the time-averaging problem; see Minster and Jordan, 1978, pp. 5341-5343, for further discussion.) In most cases, however, complications of this sort are not apparent, and the large-scale trends of transforms are probably representative of plate motions during the last several million years. This hypothesis is supported by the good agreement between transform fault azimuths and the slip vectors of transform fault earthquakes, which truly do measure "instantaneous" motions.

The RM2 data set has also been examined for systematic discrepancies between observed transform fault azimuths and model-predicted directions. One possible source for such discrepancies could be widespread "leaky" transform faulting in the sense of Menard and Atwater (1969). If this

Relative Motions: Model RM2

The model designated Relative Motion 2 (RM2) resulted from the simultaneous inversion of 110 spreading rates, 78 transform fault azimuths and 142 earthquake slip vectors (Minster and Jordan, 1978); in many cases the angular velocity vectors have been significantly improved with respect to our previous model RM1 (Minster et al., 1974). RM2 represents the instantaneous relative motions among 11 major plates: Africa (AFRC), Antarctica (ANTA), Arabia (ARAB), Caribbean (CARB), Cocos (COCO), Eurasia (EURA), India (INDI), Nazca (NAZC), North America (NOAM), Pacific (PCFC) and South America (SOAM).

In compiling the RM2 data set, shown in Figure 1, the data from intra-continental environments such as the Alpine belt and complex tectonic regions such as the western Pacific were generally excluded, because these areas exhibit complexities not easily described by rigid plate kinematics, and the assumptions fundamental to a simple plate model may not apply. Hence the details of Mediterranean, Asian and Indonesian tectonics are not represented by this instantaneous kinematical model.

Of course, no kinematical model based on geological data is really "instantaneous"; in particular, the spreading rate estimates and transform fault azimuths average in some way the motions over substantial time intervals. For a spreading rate datum the pertinent time interval is simply the age of the magnetic anomaly used to obtain the rate. We generally employed anomalies 2 and 2', so that the mean averaging interval for the RM2 rate data is less than 3 My. The relevant averaging intervals for the transform fault azimuths are more uncertain, however, and depend upon the

the BFP's for the INDI poles are thought to be diagnostic of internal deformation within the Indian plate (Minster and Jordan, 1978), although we concede that the problem could result from other, unrecognized sources of data bias.

Absolute Motions

Nothing within the axiomatic framework of plate tectonics points to a natural, absolute reference frame in which to describe plate motions. The need to choose such a frame arises only when one enlarges the class of observations to be explained beyond the manifestations of plate-plate interactions or when one attempts to model the dynamics of plate motions. A particular frame of interest in discussions of plate dynamics is one fixed with respect to the average position of the deep mantle, assumed to be rigid or at least to have typical internal motions much slower than the motions of the plates; we refer to this frame as the mean mesospheric frame.

Wilson (1963, 1965b) proposed that various island chains and aseismic ridges are generated by the motions of the crust over hotspots fixed in the mantle. Morgan (1971, 1972a,b) expanded this concept and presented a model of 15 plates moving in a slowly changing frame defined by a score of hotspots, each of which he associated with an upwelling convective plume. In a test of the Wilson-Morgan hypothesis Minster et al. (1974) used RML to construct a model designated Absolute Motion 1 (AML) by fitting the observed azimuths of twenty hotspot traces. They found no cause to reject the Wilson-Morgan hypothesis and concluded that these hotspots showed no significant relative motions in the last 10 My, although their ability to resolve such motions was admittedly limited. Other studies have concluded that, averaged over longer time intervals (>40 My), some hotspots have relative speeds of the order of 1 cm/yr (Morgan, 1972b; Burke et al., 1973; Molnar and Atwater, 1973; Molnar and Francheteau, 1975). Nevertheless, these relative speeds appear to be much smaller than the typical absolute

speeds of the faster plates, upon which the hotspot traces are best developed, so that the concept of a hotspot reference frame remains useful for the short time scales used to derive instantaneous motions. Furthermore, if the directions of hotspot migration are nearly random, this reference frame may be a very good approximation to the mean mesospheric frame. Chase (1978) and Minster and Jordan (1978) have derived absolute motion models based on hotspot data and compatible with their revised estimates of relative motions.

The models based on the Wilson-Morgan hypothesis have been compared with other proposed criteria for fixing plate velocities in the mean mesospheric frame. One is to require that the lithosphere as a whole possess no net rotation with respect to this frame, a criterion discussed and applied by Minster et al. (1974), Lliboutry (1974) and Solomon and Sleep (1974). The no-net-rotation model is one member of a more general class of mechanical models obtained by balancing a system of forces acting on the plates (Solomon and Sleep, 1974; Solomon et al., 1975; Gordon et al., 1978). Another class of absolute motion models is obtained by fixing a particular plate with respect to the mean mesospheric frame, such as the Antarctic (Knopoff and Leeds, 1972), African (Burke and Wilson, 1972) or Caribbean (Jordan, 1975) plates. Tullis (1972) suggested that downgoing slabs act as anchors in the mantle and thus specify an absolute reference frame. This concept was discussed by Kaula (1975), who proposed a general boundary velocity minimization criterion, and Jordan (1975), who used the idea to rationalize his conclusion that the Caribbean plate is essentially fixed with respect to the mean mesospheric frame.

In Table 2 and Figures 5 and 6 we present the absolute motion model designated AM1-2. This model was derived from RM2 by fitting the azimuths of nine hotspot traces and the rates from five (Minster and Jordan, 1978). The data set was restricted to include only those constraints on hotspot migration pertinent to the last 10 My. This time span is really the minimum interval for which good hotspot data can be obtained, although it exceeds by over a factor of three the mean averaging interval for the relative motion data. Consequently, the data set is dominated by information from the rapidly moving plates in the Pacific Ocean; no Atlantic or Indian Ocean hotspot traces were employed.

The AM1-2 velocity field depicted in Figures 5 and 6 shows a number of interesting features which are common to most proposed absolute velocity models. The contrast between fast moving oceanic plates and slower moving continent bearing plates, noted by Minster et al. (1974), is striking, although the rapid motion of INDI, which has the same proportion of continental area as ANTA, prevents an exact dichotomy. The four fastest plates (PCFC, COCO, NAZC, INDI) are also the only plates being subducted along a significant fraction of their boundaries, a correlation noted by Jordan and Minster (1974) and discussed in detail by Forsyth and Uyeda (1975). As Aggarwal (1978) has shown, an even better correlation between plate geometry and absolute velocities is obtained if the percentage length of ridge is included in the analysis. There is a general increase of absolute velocities away from the spin axis, which is reflected in the distribution of global seismicity (Solomon et al., 1975). Systematic attempts to relate these correlations to plate mechanics have been made by Solomon et al. (1975), Forsyth and Uyeda (1975) and Chapple and Tullis (1977), but similar patterns do not seem to apply to Tertiary times (Solomon et al., 1977; Jurdy, 1978), so

caution must be exercised in attributing to them any dynamical significance.

When examining the absolute velocity field in Figures 5 and 6, it should be kept in mind that AM1-2 is associated with much larger uncertainties than RM2, because the resolution of the hotspot data is intrinsically limited and because caveats must be attached to the Wilson-Morgan hypothesis. The relative errors in the directions of absolute motion are generally small for points on the fast moving plates, but they can exceed 100% for points on the slowest plates, particularly EURA and ANTA. In these cases, the directions are not usefully constrained by the data used to derive AM1-2. A more complete discussion of these uncertainties is given by Minster and Jordan (1978).

The large uncertainties associated with AM1-2 should also be kept in mind when comparing this model with other estimates of absolute motions. Models based on some of the alternate hypotheses discussed above can be constructed from Table 2 by vector addition. A detailed comparison (Minster and Jordan, 1978, pp. 5348-5349) yields the following conclusions: the no-net-rotation model and the model obtained by fixing AFRC do not provide adequate fits to the hotspot data, whereas any of the three plates CARB, EURA or ANTA could be stationary with respect to the hotspot frame.

Discussion

Plate tectonics is the unifying model which ties surface geology to planetary evolution. As noted by Deffeyes (1970) a useful and simple measure of global tectonic activity is the rate of production and destruction of lithosphere associated with plate motions. This calculation requires only minimal information about plate geometry (Deffeyes, 1970; Chase, 1972). Table 3 gives the area budget for the RM2 plate set; in the computation we have assumed symmetric spreading at ridges, unilateral lithosphere destruction at trenches, and that the area loss is shared equally by both plates in a continental collision. Clearly, the net growth of some plates (e.g., ANTA, AFRC, SOAM AND NOAM) and the net shrinking of others (e.g., PCFC, INDI, NAZC, COCO) observed at the present time must be satisfied by any successful dynamical model, a point emphasized in the work of Hager and O'Connell (1978).

There are conspicuous instances where the ideal rigid plate model fails to describe adequately the complexities of tectonic interactions. These may include continental collisions (e.g., Molnar and Tapponnier, 1975), zones of incipient rifting (e.g., Courtillot, 1979), and regions of deformation along continental margins (e.g., Jordan, 1975). In these complex areas the rigid plate model has only limited utility, but it does provide the kinematical boundary conditions which must be satisfied by local models of deformation.

Acknowledgments:

Part of this research was supported by the National Aeronautics and Space Administration under contract NSG-7610, and by the National Science Foundation under grant EAR 78-12962. Contribution Number 3223, Division of Geological and Planetary Sciences, California Institute of Technology, Pasadena, California 91125.

BIBLIOGRAPHY

- Aggarwal, Y. P., 1978, Scaling laws for global plate motions: Consequences for the driving mechanism, interplate stresses and mantle viscosity, Trans. Amer. Geophys. Union, 59, 1202.
- Burke, K., and J. T. Wilson, 1972, Is the African plate stationary?, Nature, 239, 387-390.
- Burke, K., W. S. F. Kidd, and J. T. Wilson, 1973, Relative and latitudinal motion of Atlantic hotspots, Nature, 245, 133-137.
- Chapple, W. M. and T. E. Tullis, 1977, Evaluation of the forces that drive the plates, J. Geophys. Res., 82, 1967-1984.
- Chase, C. G., 1972, The n-plate problem of plate tectonics, Geophys. J. Roy. Astr. Soc., 29, 117.
- Chase, C. G., 1978, Plate kinematics: The Americas, East Africa, and the rest of the world, Earth Planet. Sci. Lett., 37, 353-368.
- Coulomb, J., 1969, L'expansion des fonds océaniques et la dérive des continents, Presses Universitaires de France, Paris.
- Coulomb, J., 1972, Sea floor spreading and continental drift, D. Reidel Publ. Co. Dordrecht, Holland.
- Courtillot, V., 1979, Opening of the Gulf of Aden and Afar by progressive tearing. preprint.
- Deffeyes, K. S., 1970, The axial valley: A steady-state feature of the Terrain, in The megatectonics of continents and oceans, edited by H. Johnson and B. L. Smith, Rutgers Univ. Press, New Brunswick, N.J., pp 194-222.
- Forsyth, D. W., and S. Uyeda, 1975, On the relative importance of driving forces of plate motion, Geophys. J. Roy. Astron. Soc., 43, 163-200.

- Fox, P. J., F. W. Schroeder, R. M. Moody, W. C. Pitman, and P. J. Hoose, 1979, The bathymetry of the Oceanographer fracture zone and the Mid-Atlantic Ridge at 35°N with implications for central north Atlantic plate motion, submitted to Deep Sea Res.
- Gordon, R. G., A. Cox, and C. E. Harter, 1978, Absolute motion of an individual plate estimated from its ridge and trench boundaries, Nature, 274, 752-755.
- Hager, B. H., and R. J. O'Connell, 1978, Subduction zone dip angles and flow driven by plate motion, Tectonophysics 50, 111-133.
- Hey, R. N., 1974, Tectonic evolution of the Cocos-Nazca Rise, Ph.D. thesis, Princeton Univ., Princeton, N.J.
- Jordan, T. H., 1975, The present-day motions of the Caribbean plate, J. Geophys. Res., 80, 4433-4439.
- Jordan, T. H., and J. B. Minster, 1974, Plate motions with respect to the mantle (abstract), EOS Trans. AGU, 55, 557.
- Jurdy, D. M., 1978, An alternate model for early Tertiary absolute plate motions, Geology, 6, 469-472.
- Kaula, W. M., 1975, Absolute plate motions by boundary velocity minimizations, J. Geophys. Res., 80, 244-248.
- Le Pichon, X., 1968, Sea-floor spreading and continental drift, J. Geophys. Res., 73, 3661-3697.
- Lliboutry, L., 1974, Plate movement relative to rigid lower mantle, Nature, 250, 298-300.
- Macdonald, K. C., 1977, Near-bottom magnetic anomalies, asymmetric spreading, oblique spreading, and tectonics of the Mid-Atlantic Ridge near lat. 37°N, Geol. Soc. Amer. Bull., 88, 541-555.
- McKenzie, D. P., and R. L. Parker, 1967, The North Pacific: An example of tectonics on a sphere, Nature, 216, 1276-1280.

- McKenzie, D. P., and R. L. Parker, 1974, Plate tectonics in ω space, Earth Planet. Sci. Lett., 22, 285-293.
- McKenzie, D. P., and J. G. Sclater, 1971, The evolution of the Indian Ocean since the late Cretaceous, Geophys. J. Roy. Astron. Soc., 25, 437-528.
- Menard, H. W., and T. Atwater, 1969, Origin of fracture-zone topography, Nature, 22, 1037-1040.
- Minster, J. B., T. H. Jordan, P. Molnar, and E. Haines, 1974, Numerical modelling of instantaneous plate tectonics, Geophys. J. Roy. Astron. Soc., 36, 541-576.
- Minster, J. B. and T. H. Jordan, 1978, Present-Day Plate Motions, J. Geophys. Res., 83, 5331-5354.
- Molnar, P., and T. Atwater, 1973, Relative motion of hot spots in the mantle, Nature, 246, 288-291.
- Molnar, P., and J. Francheteau, 1975, The relative motion of 'hot spots' in the Atlantic and Indian oceans during the Cenozoic, Geophys. J. Roy. Astron. Soc., 43, 763-774.
- Molnar, P., and P. Tapponnier, 1975, Cenozoic tectonics of Asia: Effects of a continental collision, Science, 189, 419-426.
- Molnar, P., T. Atwater, J. Mammerickx, and S. M. Smith, 1975, Magnetic anomalies, bathymetry, and the tectonic evolution of the South Pacific since the late Cretaceous, Geophys. J. Roy. Astron. Soc., 40, 383-420.
- Morgan, J. W., 1968, Rises, trenches, great faults, and crustal blocks, J. Geophys. Res., 73, 1959-1982.
- Morgan, W. J., 1971, Convection plumes in the lower mantle, Nature, 230, 42-43.
- Morgan, W. J., 1972a, Deep mantle convection plumes and plate motions, Am. Ass. Petrol. Geol. Bull., 56, 203-213.

- Morgan, W. J., 1972b, Plate motions and deep mantle convection, Geol. Soc. Amer. Mem., 132, 7-22.
- Pitman, W. C., and M. Talwani, 1972, Sea-floor spreading in the North Atlantic, Geol. Soc. Amer. Bull., 83, 619-646.
- Solomon, S. C., and N. H. Sleep, 1974, Some simple physical models for absolute plate motions, J. Geophys. Res., 79, 2557-2567.
- Solomon, S. C., N. H. Sleep, and R. M. Richardson, 1975, On the forces driving plate tectonics: Inferences from absolute plate velocities and intraplate stress, Geophys. J. Roy. Astron. Soc., 42, 769-802.
- Solomon, S. C., N. H. Sleep, and D. M. Jurdy, 1977, Mechanical models for absolute plate motions in the early Tertiary, J. Geophys. Res., 82, 203-212.
- Tullis, T. E., 1972, Evidence that lithospheric slabs act as anchors (abstract), Trans. Amer. Geophys. Union, 53, 522.
- Wilson, J. T., 1963, A possible origin of the Hawaiian Islands, Can. J. Phys., 41, 863-870.
- Wilson, J. T., 1965a, A new class of faults and their bearing on continental drift, Nature, 207, 343-347.
- Wilson, J. T., 1965b, Evidence from ocean islands suggesting movement in the Earth, R. Soc. Lond. Phil. Trans., 258, 145-165.

TABLE CAPTIONS

Table 1: First plate named moves counterclockwise with respect to the second. Cartesian coordinates defined with respect to spin axis and Greenwich meridian.

Table 2: Plates move counterclockwise about poles. Cartesian coordinates defined with respect to spin axis and Greenwich meridian.

TABLE 1: RM2 GEOHEDRON

RELATIVE ROTATION VECTORS

Plate Pair	θ °N	ϕ °E	ω deg/My	ω_x deg/My	ω_y deg/My	ω_z deg/My
AFRC-ANTA	9.45	-41.70	0.149	0.1095	-0.0976	0.0244
AFRC-EURA	25.23	-21.18	0.104	0.0874	-0.0339	0.0442
AFRC-NOAM	80.43	56.36	0.258	0.0238	0.0357	0.2546
AFRC-SOAM	66.56	-37.29	0.356	0.1126	-0.0858	0.3266
ANTA-PCFC	64.67	-80.23	0.964	0.0700	-0.4065	0.8712
ANTA-SOAM	87.69	75.21	0.302	0.0031	0.0118	0.3021
ARAB-AFRC	30.82	6.43	0.260	0.2222	0.0250	0.1334
ARAB-EURA	29.82	-1.64	0.357	0.3097	-0.0088	0.1776
CARB-SOAM	73.51	60.84	0.202	0.0280	0.0502	0.1940
COCO-CARB	23.60	-115.55	1.543	-0.6098	-1.2757	0.6179
COCO-NAZC	5.63	-124.40	0.972	-0.5463	-0.7978	0.0953
COCO-NOAM	29.80	-121.28	1.489	-0.6707	-1.1041	0.7399
COCO-PCFC	38.72	-107.39	2.208	-0.5150	-1.6438	1.3810
EURA-NOAM	65.85	132.44	0.231	-0.0637	0.0696	0.2104
EURA-PCFC	60.64	-78.92	0.977	0.0921	-0.4701	0.8515
INDI-AFRC	17.27	46.02	0.644	0.4271	0.4426	0.1912
INDI-ANTA	18.67	32.74	0.673	0.5366	0.3450	0.2156
INDI-ARAB	7.08	63.86	0.469	0.2049	0.4175	0.0577
INDI-EURA	19.71	38.46	0.698	0.5146	0.4087	0.2353
INDI-PCFC	60.71	-5.79	1.246	0.6066	-0.0615	1.0868
NAZC-ANTA	43.21	-95.02	0.605	-0.0386	-0.4396	0.4145
NAZC-CARB	47.30	-97.57	0.711	-0.0635	-0.4779	0.5226
NAZC-PCFC	56.64	-87.88	1.539	0.0314	-0.8460	1.2857
NAZC-SOAM	59.08	-94.75	0.835	-0.0355	-0.4278	0.7166
NOAM-CARB	-33.83	-70.48	0.219	0.0609	-0.1717	-0.1220
NOAM-PCFC	48.77	-73.91	0.852	0.1557	-0.5398	0.6411
NOAM-SOAM	25.57	-53.82	0.167	0.0888	-0.1215	0.0720

TABLE 2: MODEL AM1-2

ABSOLUTE ROTATION VECTORS

Plate	θ °N	ϕ °E	ω deg/My	ω_x deg/My	ω_y deg/My	ω_z deg/My
AFRC	18.76	-21.76	0.139	0.1221	-0.0487	0.0446
ANTA	21.85	75.55	0.054	0.0126	0.0488	0.0202
ARAB	27.29	- 3.94	0.388	0.3443	-0.0237	0.1781
CARB	-42.80	66.75	0.129	0.0375	0.0872	-0.0879
COCO	21.89	-115.71	1.422	-0.5724	-1.1885	0.5300
EURA	0.70	-23.19	0.038	0.0347	-0.0148	0.0005
INDI	19.23	35.64	0.716	0.5492	0.3938	0.2358
NAZC	47.99	-93.81	0.585	-0.0261	-0.3907	0.4347
NOAM	-58.31	-40.67	0.247	0.0983	-0.0844	-0.2099
PCFC	-61.66	97.19	0.967	-0.0574	0.4553	-0.8510
SOAM	-82.28	75.65	0.285	0.0095	0.0370	-0.2819
Net Rotation	-51.09	65.44	0.251	0.0655	0.1434	-0.1953

TABLE 3

AREA BUDGET FOR RM2

Plate Name	Area Created (km ² /yr)	Area Destroyed (km ² /yr)	Net Growth (km ² /yr)	Relative Area Change(10 ⁻⁹ yr ⁻¹)
AFRC	0.322	0.025	0.297	3.76
ANTA	0.575	0.026	0.549	9.31
ARAB	0.024	0.048	-0.024	-4.92
CARB	0.001	0.009	-0.008	-2.08
COCO	0.174	0.211	-0.037	-12.86
EURA	0.060	0.117	-0.057	-0.83
INDI	0.339	0.693	-0.354	-5.90
NAZC	0.439	0.505	-0.066	-4.43
NOAM	0.107	0.017	0.090	1.51
PCFC	0.690	1.207	-0.517	-4.79
SOAM	<u>0.157</u>	<u>0.030</u>	<u>0.127</u>	3.09
TOTALS	2.888	2.888	0.	

FIGURE CAPTIONS

Figure 1: Relative velocities from RM2 at selected points along plate boundaries. Mercator projection; latitude and longitude marks every 30°. Numbers are rates in cm/yr. The RM2 data is used to outline major plate boundaries. Circles are rate data, lozenges and triangles are transform fault and slip vector azimuth data respectively. Velocity vectors are drawn symmetrically about point of calculation in direction of relative motion with length proportional to rate.

Figure 2: Poles for model RM2, with their 95% confidence ellipses. RM1 and best fitting poles, where available, are shown for comparison.

Figure 3: Poles for model RM2, with their 95% confidence ellipses. RM1 and best fitting poles, where available, are shown for comparison.

Figure 4: Poles for model RM2, with their 95% confidence ellipses. RM1 and best fitting poles, where available, are shown for comparison.

Figure 5: Absolute motions at selected points from model AM1-2. Conventions are similar to figure 1. Stars are absolute poles, about which plate rotation is counterclockwise. Asterisks are antipoles.

Figure 6: Absolute velocity field from AM1-2. Vectors drawn along small circles about absolute poles with exaggeration factor 2.22×10^7 , so that 1 cm/yr is mapped into 2 geocentric degrees at 90° from pole. Orthographic projections, centered at a) $0^\circ\text{N}, 0^\circ\text{E}$; b) $0^\circ\text{N}, 90^\circ\text{E}$; c) $0^\circ\text{N}, 180^\circ\text{E}$; d) $0^\circ\text{N}, 90^\circ\text{W}$; e) North pole; f) South pole.

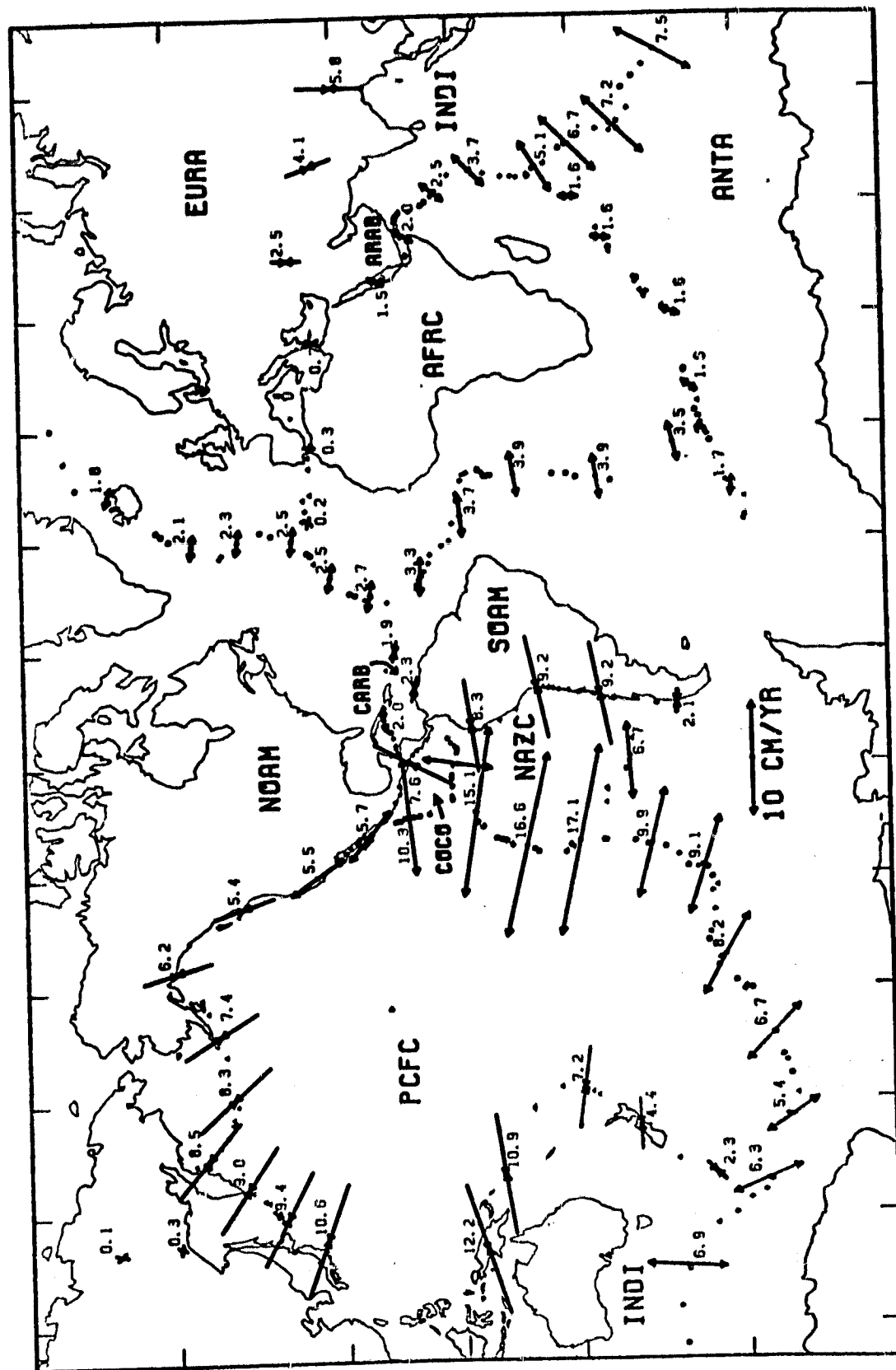


Fig. 1

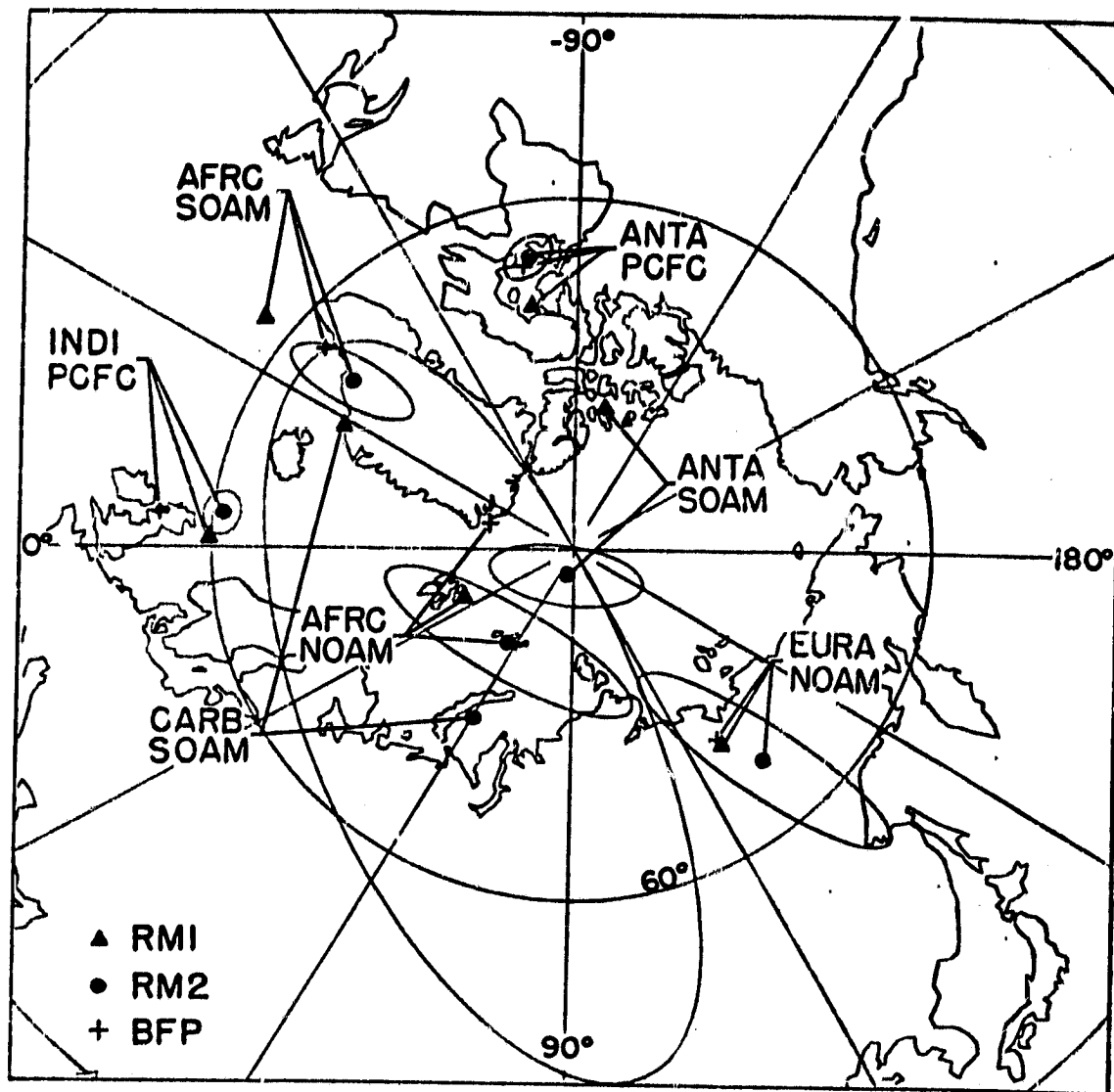
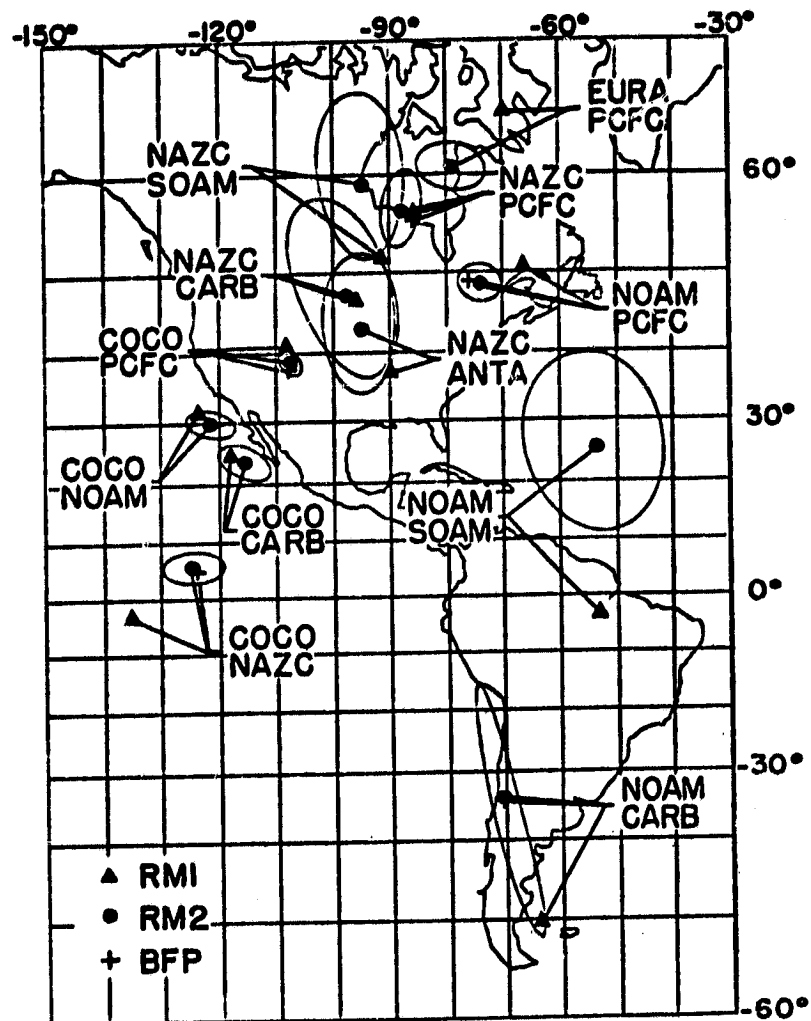


Fig. 2



ORIGINAL PAGE IS
OF POOR QUALITY

Fig. 3

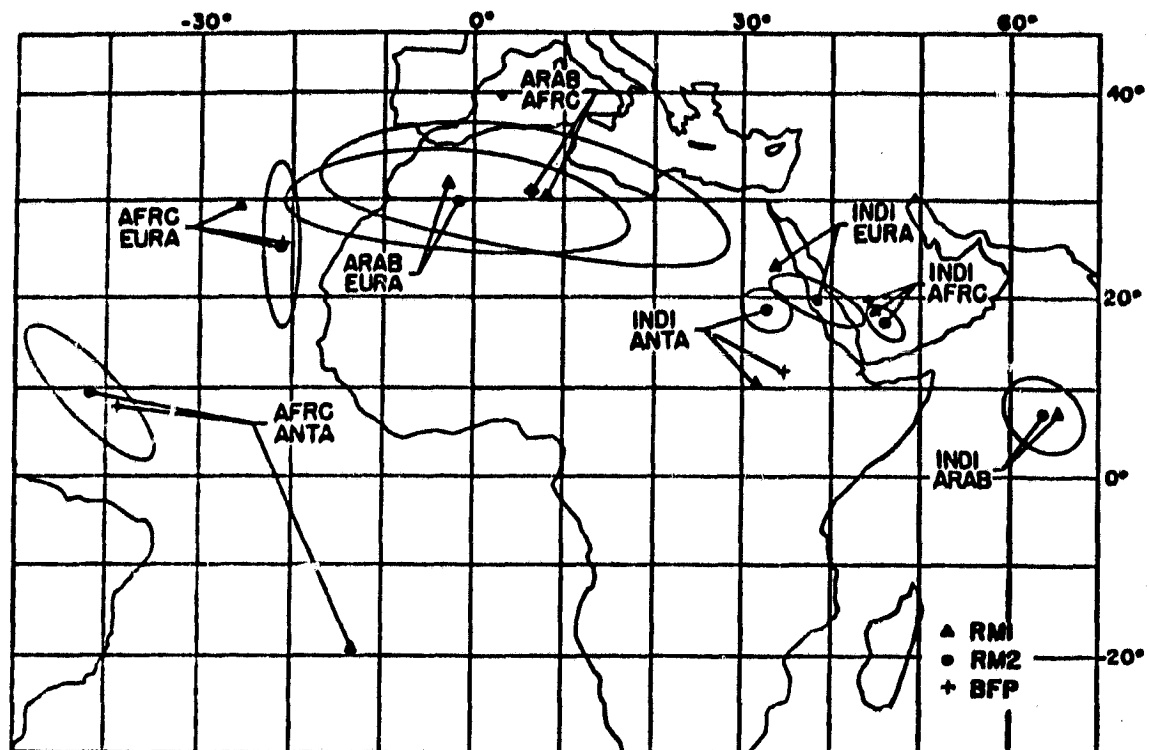


Fig. 4

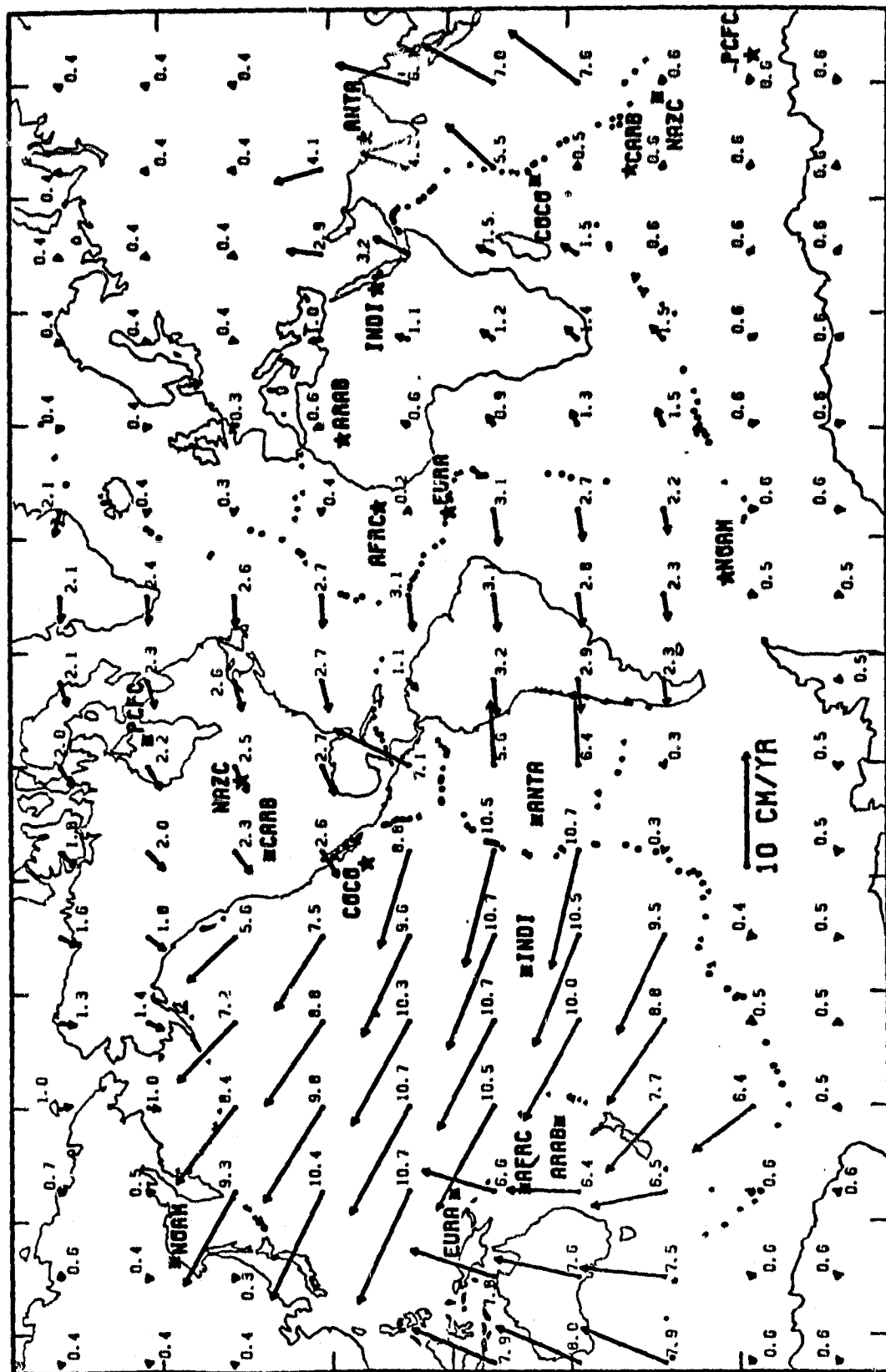


Fig 5

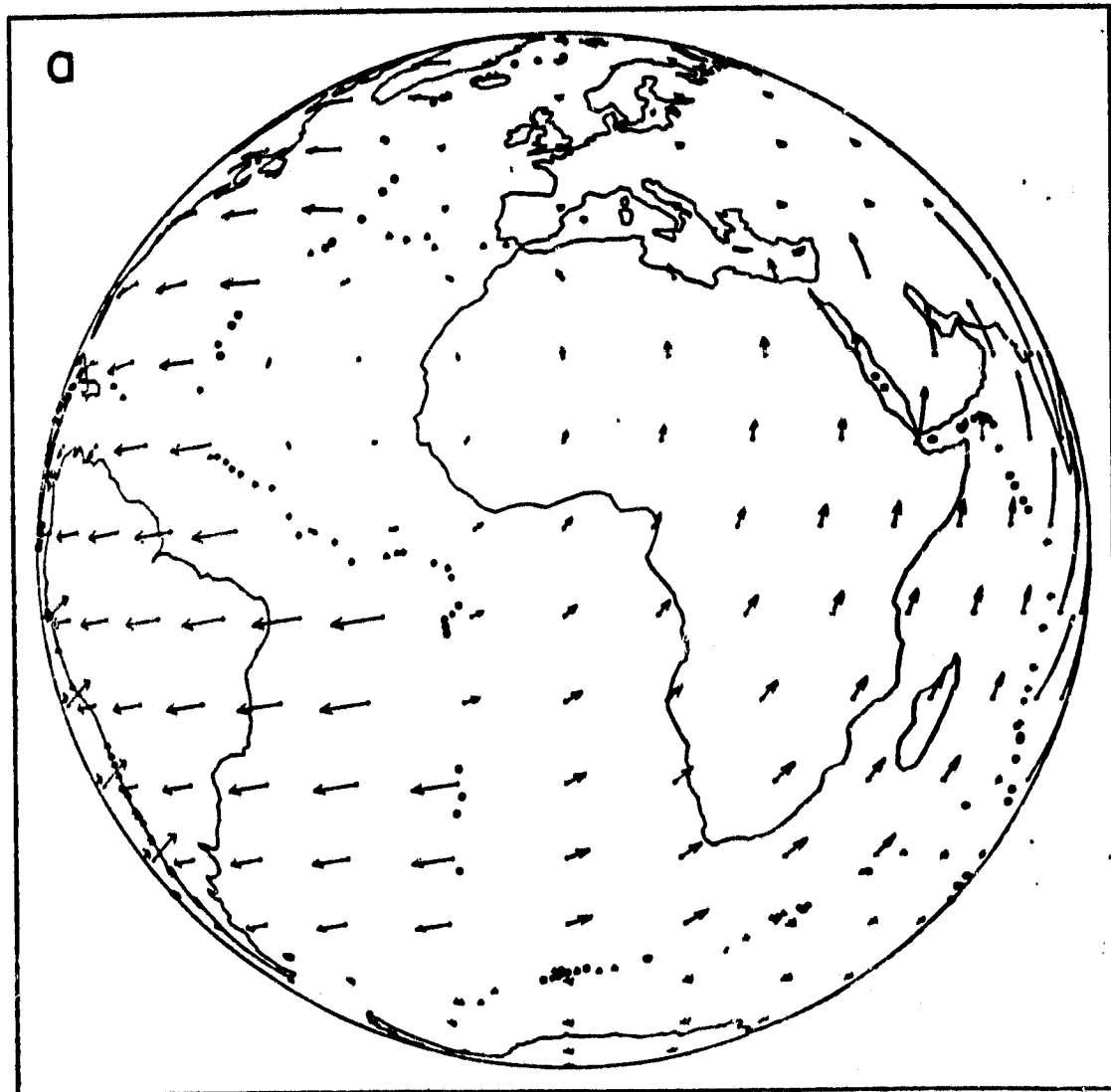


Fig. 6a

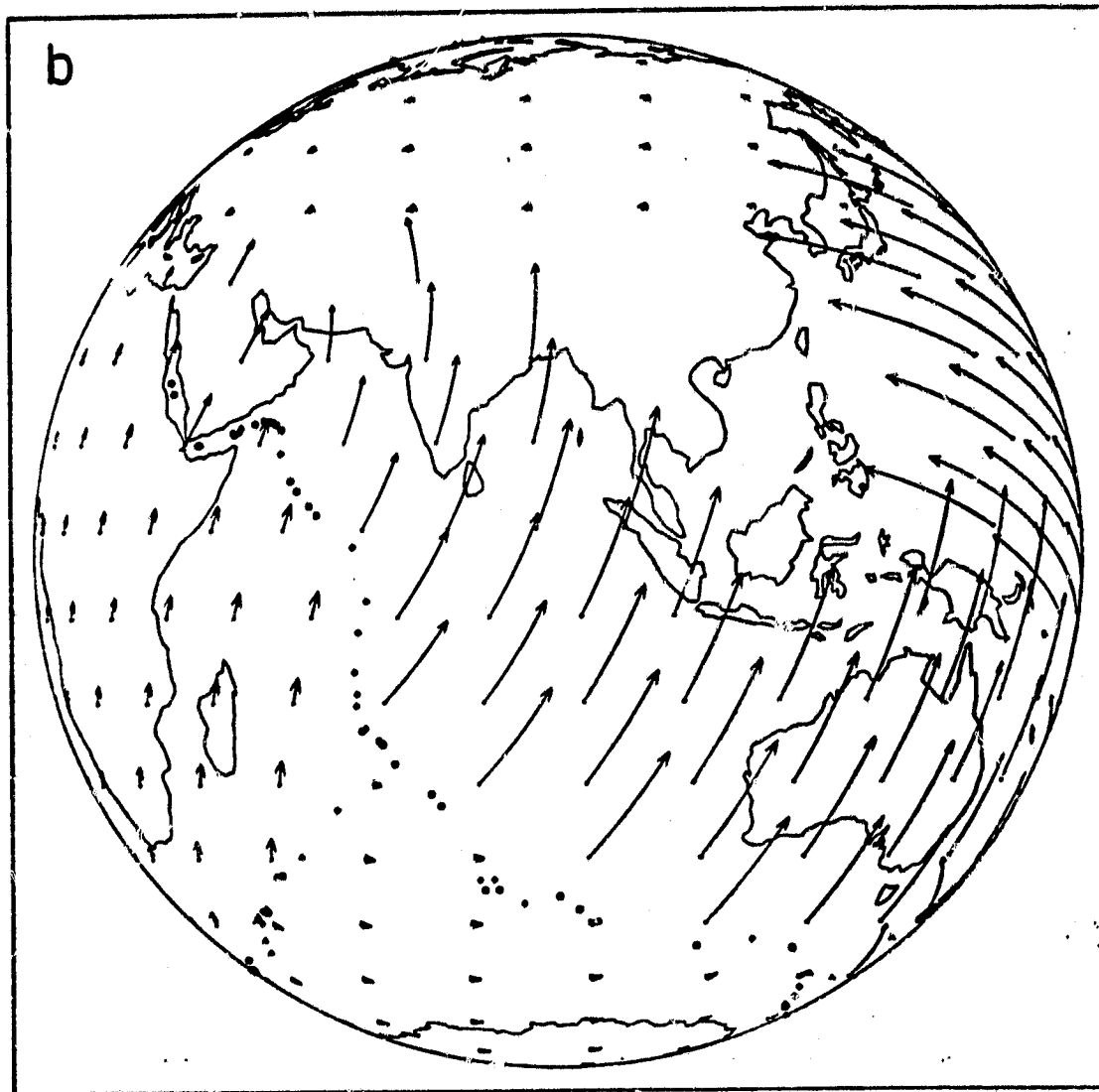


Fig. 6b

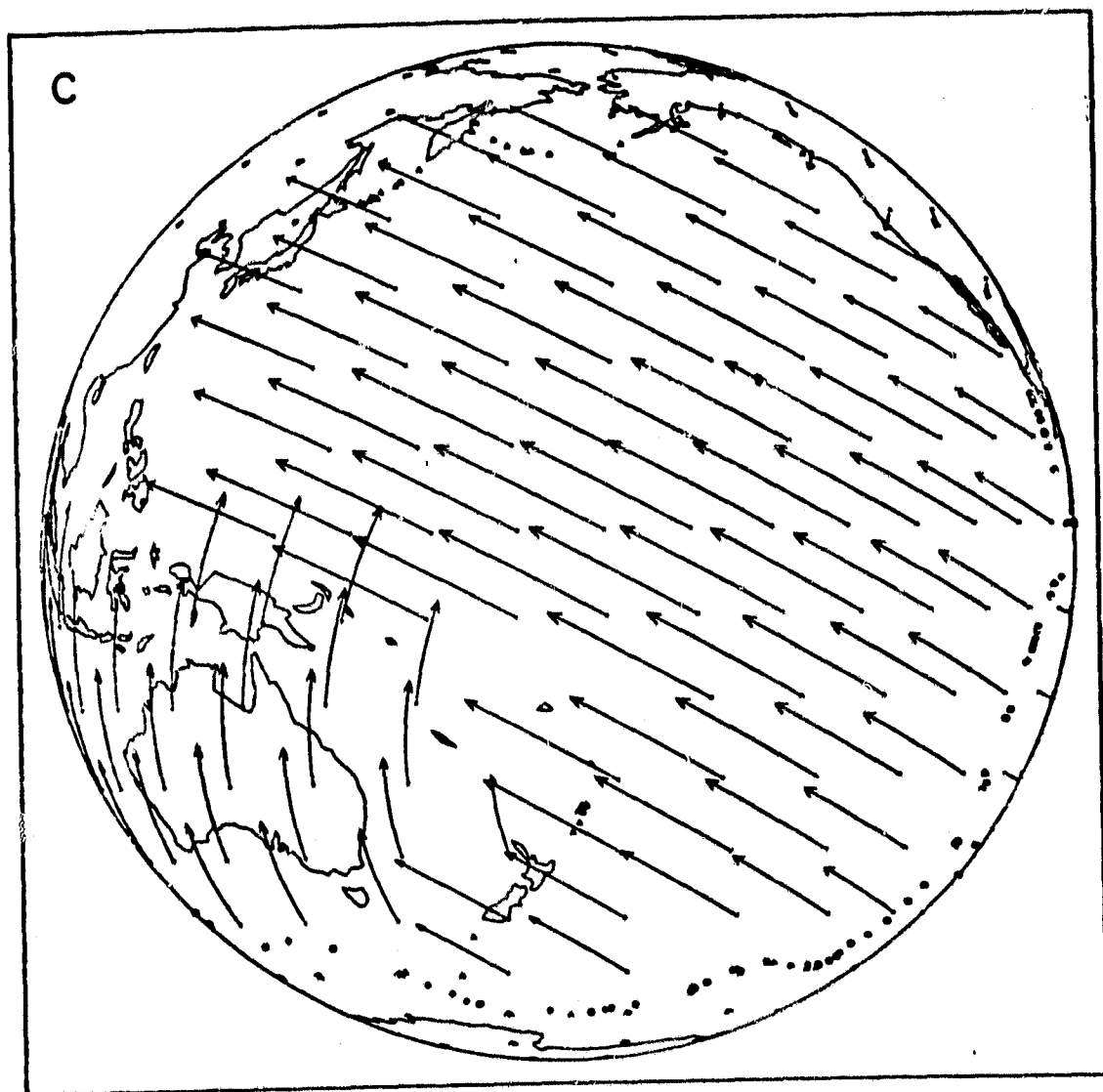


Fig. 6c

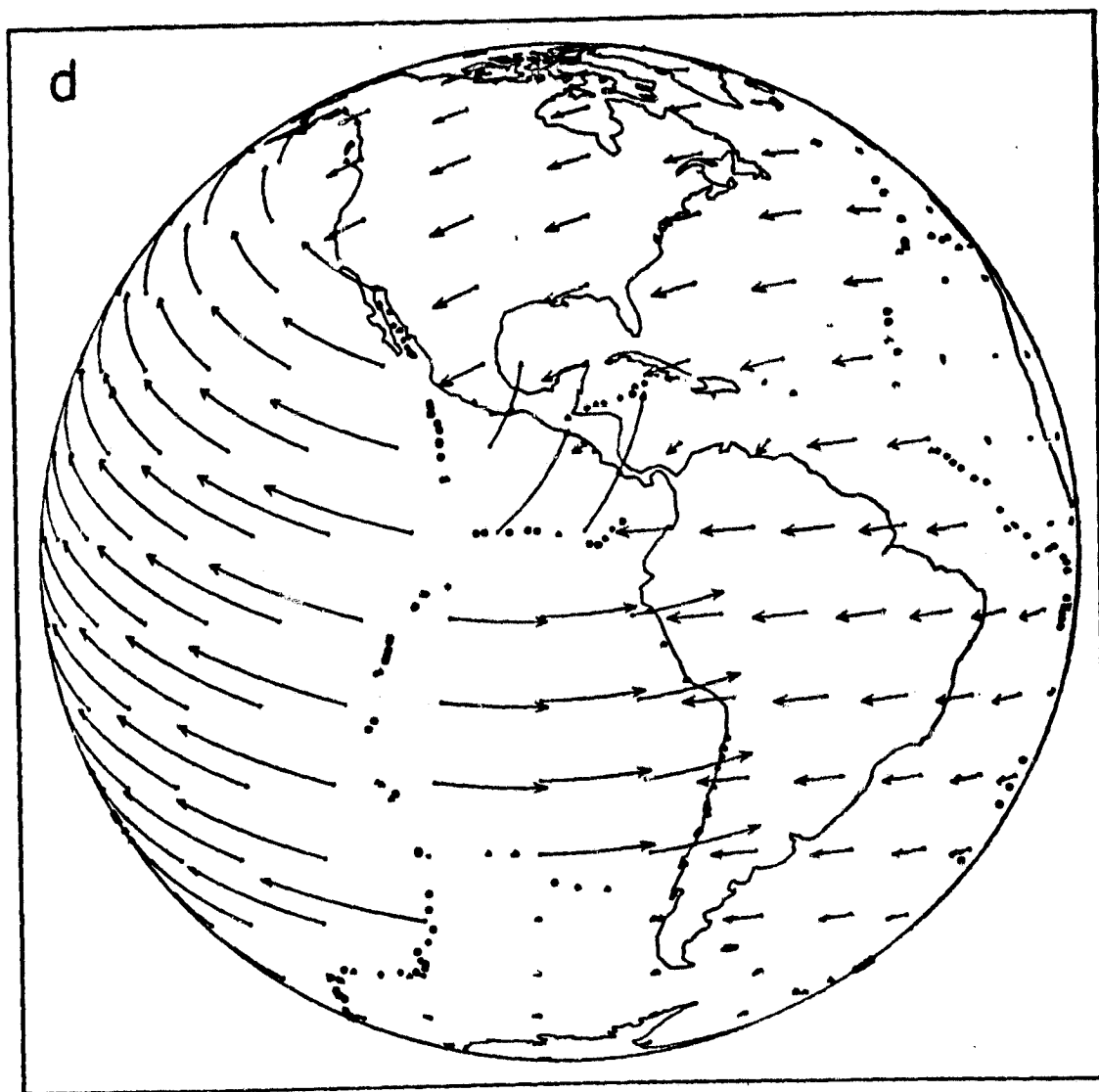


Fig. 6d

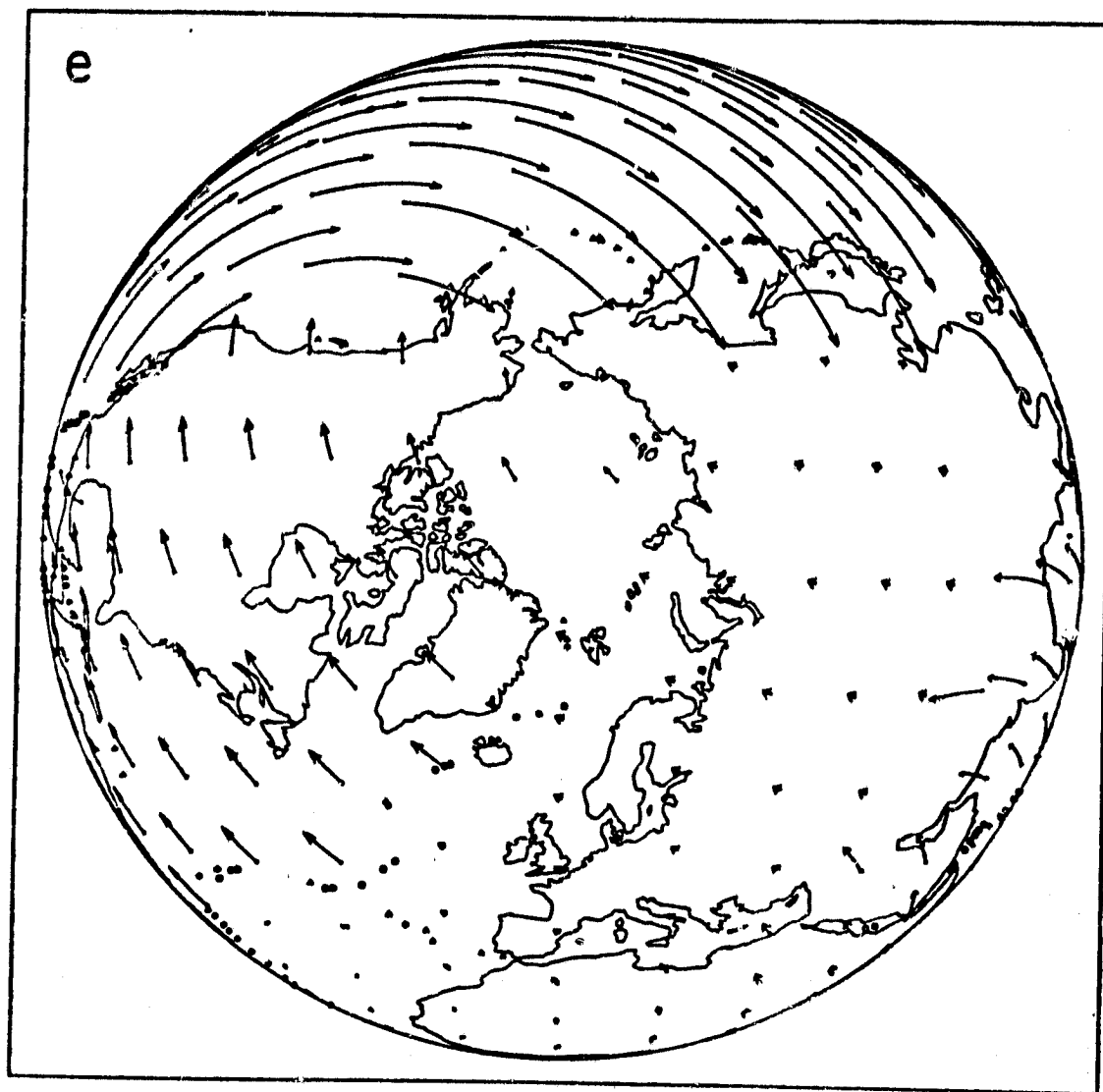


Fig. 6c

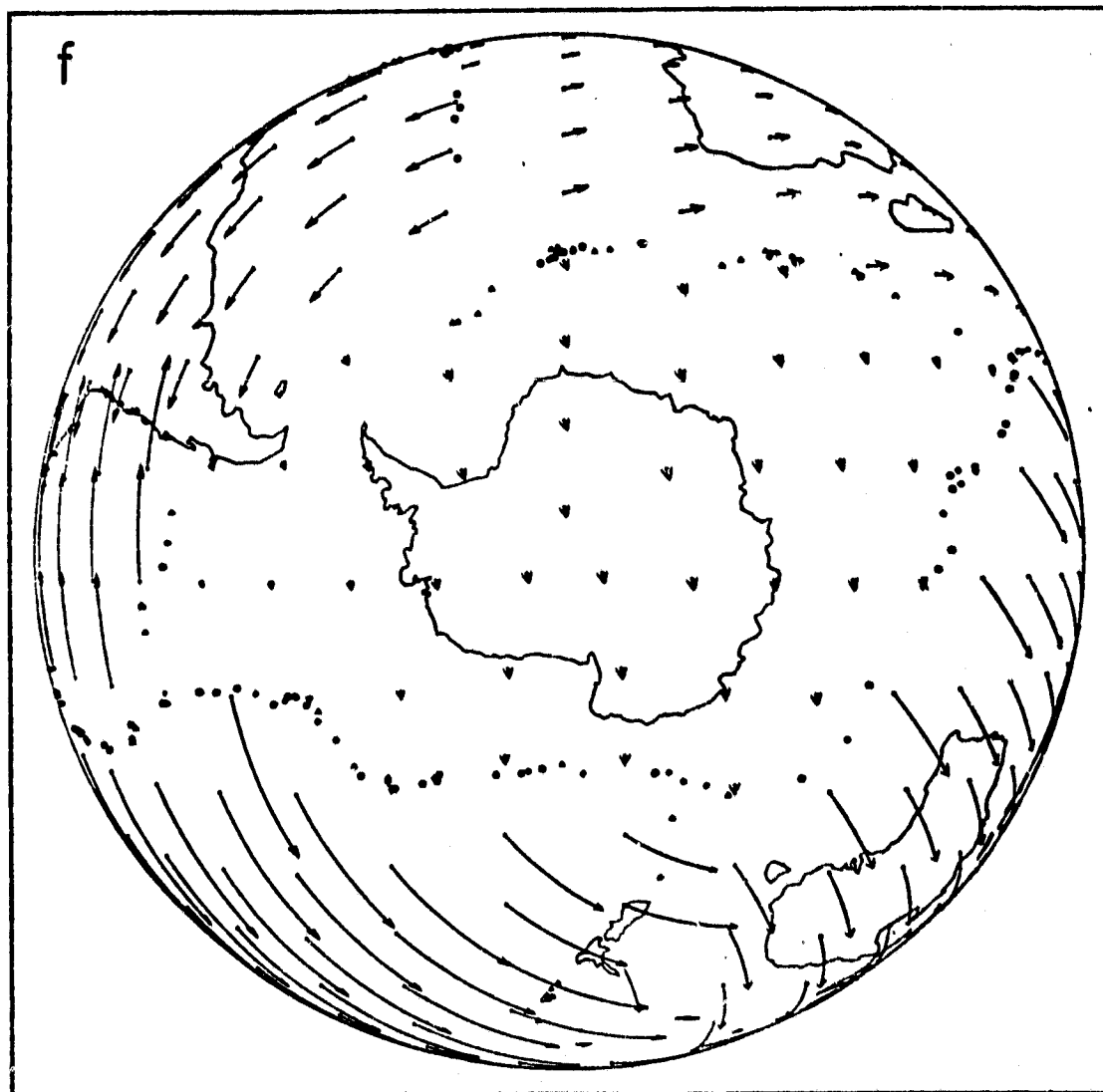


Fig. 6f

APPENDIX II

THE PHYSICS OF CREEP AND ATTENUATION IN THE MANTLE

Don L. Anderson

J. Bernard Minster

Journal of Geophysical Research, submitted.

Revised April 29, 1980

The Physics of Creep and Attenuation in the Mantle

Don L. Anderson

and

J. Bernard Minster

Seismological Laboratory, California Institute
of Technology, Pasadena, California 91125

Abstract

Dislocations contribute to both seismic wave attenuation and steady-state creep in the mantle. The two phenomena involve quite different strains and characteristic times but they can both be understood with simple dislocation models. The most satisfactory model for creep involves the glide of dislocations across subgrains but rate limited by the climb of jogged dislocations in the walls of a polygonized network. The jog formation energy contributes to the apparent activation energy for creep, making it substantially larger than the activation energy for self-diffusion. The theory leads to either a σ^2 or σ^3 law for creep rate, depending on the length of the dislocations relative to the equilibrium spacing of thermal jogs.

Attenuation in the mantle at seismic frequencies is probably caused by the glide of dislocations in the subgrains. Kink and impurity drag can both contribute to the glide time constant. The kink-formation, or Peierls barrier, model for dislocation glide appears to be a low-temperature, high-frequency mechanism most appropriate for pure systems. A small amount of impurity drag brings the dislocation glide characteristic time into the seismic band at upper mantle temperatures.

The attenuation and creep behavior of the mantle are related through the dislocation structure. Discussion of the various possible mechanisms is facilitated by casting them and the geophysical data in terms of a pre-exponential characteristic time and an activation energy. The relaxation strength is an additional parameter that can be used to identify the attenuation mechanism. Mobile dislocations in subgrains, rather than cell-walls, have the appropriate characteristics to explain the damping of seismic waves in the upper mantle. The grain boundary peak may be responsible for attenuation in the lithosphere.

I. Introduction

The high temperature creep of most crystalline solids is controlled by dislocation climb or glide plus climb [Weertmann, 1968]. For a wide variety of metallic, ionic and polar crystals the activation energies for creep and self-diffusion are essentially identical, indicating that the motions of dislocations are rate-limited by self-diffusion. Furthermore, in the stress range of about 10^{-2} to 10^{-5} G, where G is the shear modulus, the stress exponent of the creep rate is about 3, consistent with dislocation climb or the glide of jogged dislocations. Both of these mechanisms of steady-state creep require self-diffusion. The third-power creep law is satisfied by olivine in the stress range of several hundred bars to several kilobars [Kohlstedt and Goetze, 1974, Goetze and Kohlstedt, 1973, Kohlstedt et al., 1976].

The laboratory creep law for olivine is commonly assumed to hold for the much lower stresses and strain rates appropriate for the mantle and this has been the basis for the calculation of many viscosity profiles for the mantle. It has also been assumed that the activation energy of creep, 125 kcal/mole, represents the diffusional activation energy for the slowest moving species. It has recently been found, however, that the activation energies for diffusion of oxygen and silicon in olivine are only about 90 kcal/mole [Reddy et al., 1980, Jaoul et al., 1979]. In addition, at low-stresses the stress exponent may be closer to two than to three.

The mechanism of attenuation in crystalline solids also appears to be an activated process. Dislocation damping is a high-temperature mechanism that is rate-limited by the diffusion of point defects. The glide of dislocations does not necessarily require self-diffusion and can therefore operate on a much shorter time scale than climb. The purpose of this paper is to investigate the role of dislocations in both creep and attenuation.

II.a. Activated processes

Thermally activated relaxation processes, including those that are controlled by diffusion, are functions of a characteristic relaxation time that can be written

$$\tau = \tau_0 \exp(E^*/RT) \quad (1)$$

where τ_0 , the pre-exponential, is the relaxation time at infinite temperature and E^* is the effective activation energy. For simple point defect mechanisms τ_0^{-1} is close to the Debye frequency, $\sim 10^{13} \text{ sec}^{-1}$. For mechanisms involving dislocations or dislocation-point defect interactions τ_0 depends on other parameters, such as dislocation lengths, Burgers vectors, kink and jog separations, Peierls stress, interstitial concentrations, etc.

The activation energy, depending on the mechanism, is a composite of activation energies relating to self-diffusion, kink or jog formation, Peierls energy, bonding energy of point defects to the dislocation, core-diffusion and so on. E^* for creep of metals is often just the self-diffusion activation energy, E_{SD} .

Non-elastic processes in geophysics are commonly expressed in terms of viscosity, for long-term phenomena, and Q for oscillatory and short-term phenomena. It is convenient to express these in terms of the characteristic time. For creep

$$\tau = \sigma / G \dot{\epsilon} = \eta / G \quad (2)$$

where σ , G , $\dot{\epsilon}$ and η are the deviatoric stress, rigidity, strain rate and viscosity, respectively. Thus, the characteristic time can be simply computed from creep theories and experiments.

Relaxation theories of attenuation can be described by

$$Q^{-1} = 2Q_0^{-1} \omega\tau / (1 + \omega^2\tau^2) \quad (3)$$

where ω is the frequency, Q^{-1} is the standard measure of attenuation and Q_0^{-1} is the peak value of attenuation at $\omega\tau = 1$. In the mantle, where Q is low, we infer that the characteristic relaxation time is close to $1/\omega$, the reciprocal of the measurement frequency. High values of Q indicate that $\omega \gg 1/\tau$ or $\omega \ll 1/\tau$. In these cases $Q \sim \omega$ or ω^{-1} . When Q is slowly varying we are probably in the midst of an absorption band which is conveniently explained as the result of a distribution of relaxation times [Liu et al., 1977; Anderson et al., 1977; Minster, 1980].

Since Q is small in the higher temperature regions of the mantle it is likely that at seismic periods the mantle is on the low-temperature side of an absorption band. Thus

$$Q^{-1} = 2Q_0^{-1}/\omega\tau = (2Q_0^{-1}/\omega\tau_0) \exp(-E^*/RT) \quad (4)$$

in regions of rapidly varying attenuation. In this paper we use the seismic data to estimate the relaxation time in the upper mantle and its variation with depth. Details of the attenuation in the midst of an absorption band, and the effect of a spectrum of relaxation times are discussed in a companion paper (Minster and Anderson, 1980). The High Temperature Background (HTB) is a dominant mechanism of attenuation in crystalline solids at high-temperature and low-frequency. This usually satisfies a $Q \sim \omega$ or $Q \sim \omega^a$ relation. The latter has been interpreted by Anderson and Minster (1978) in terms of a distribution of relaxation times. The former is valid for all relaxation mechanisms when the measurement frequency is sufficiently high. In the following $\hat{\tau}_0$ will be used for the pre-exponential creep, or Maxwell, relaxation time and τ_0 will be used for the attenuation, or Q , characteristic time.

II.b. Activation energies for climb and glide

The creep of ductile materials such as metals is rate limited by self-diffusion. This is the case for either pure diffusional creep or dislocation climb. In these circumstances the activation energy for creep is the same as that for self-diffusion. In olivine the activation energy for creep is appreciably higher than that for self-diffusion of O^{2-} or Si^{4+} . This suggests that creep may be controlled by kink or jog formation [Gueguen, 1979].

The activation energy for creep when dislocation climb is due to nucleation and lateral drift of jogs is $(1/2)(E_{SD}^* + E_{CD}^* + 2E_j^*)$ or $(1/2)(E_{SD}^* + E_{CD}^* + 4E_j^*)$ depending on whether the dislocations are longer or shorter than the equilibrium jog spacing. Here E_{SD}^* , E_{CD}^* and E_j^* are the activation energies for self-diffusion, core-diffusion and jog formation, respectively [Hirth and Lothe, 1968].

E_{SD}^* is 90 kcal/mole for both oxygen and silicon diffusion [Reddy et al., 1980, Jaoul et al., 1979]. The jog formation energy is somewhat greater than kink formation energy [Hirth and Lothe, 1968]. The activation energy controlling high-temperature deformation of olivine has been estimated by Goetze and Kohlstedt [1973] to be 135 kcal/mole from the climb of dislocation loops in olivine and 122-128 kcal/mole by Ashby and Verrall [1978] and Goetze [1978] from creep data on olivine.

In the absence of interstitial defects near the dislocation the activation energy for glide is E_k^* if the kink density is high and $2E_k^*$ when the dislocation length is shorter than the equilibrium distance between kinks. E_k^* is the kink formation energy which Stocker and Ashby [1973] estimate to be 26 kcal/mole. The activation energy for glide is therefore 52 kcal/mole if the kink spacing is large or if double kink formation is required for glide. If point defects must diffuse with the dislocation line then their diffusivity may be rate limiting. The activation energy for Mg-Fe interdiffusion in olivine is about 58 kcal/mole for 0.9 mole fraction Mg, decreasing to 50 kcal/mole for pure forsterite [Misener, 1974]. Dislocation glide in olivine will therefore have an activation energy of the order of 50-60 kcal/mole unless there are slower moving species in the vicinity of the dislocation. Olivine in contact with pyroxene is likely to have excess silicon interstitials as a dominant point defect [Stocker, 1978]. The activation energy in this case may be due to drag of silicon interstitials, about 90 kcal/mole. There is also a small term representing the binding energy of interstitials to the dislocation. This is ordinarily a few kcal/mole [Van Bueren, 1961] but data are lacking for silicates. The kink and jog formation energies in silicates are also highly uncertain and the above estimates for olivine are approximate.

The activation energy for dislocation core diffusion should be similar to that for surface diffusion. This, for metals, is usually about 1/2 to 2/3 of the lattice diffusion value. If this rule applies to olivine the core diffusion activation energy would be about 50 to 60 kcal/mole. The hot-pressing experiments of Schwenn and Goetze [1978] yield a value of 85 kcal/mole, close to that for lattice diffusion of O^{2-} and Si^{4+} . The dislocation mobility experiments of Goetze and Kohlstedt [1974] also suggest that the activation energies for lattice and core diffusion are similar. The actual values determined in

their experiments may be interpreted as the sum of the diffusion and jog formation energies. A high value for the core and surface activation energies is expected from the heat of vaporization, which is much higher for silicates than for metals.

If we adopt $E_{SD}^* = E_{CD}^* = 90$ kcal/mole and $E_{creep}^* = 125$ kcal/mole then the implied jog formation energy is 35 kcal/mole. This is much greater than is typical of metals. This is also expected since the kink and jog formation energies are proportional to Gb^3 which is much greater for silicates than for metals.

Because of the high values for core diffusion and jog formation we expect relatively high values for the creep activation energy for silicates and a non-correspondance with the self-diffusional activation energy, except for Coble and Nabarro-Herring creep which will dominate for very small grain sizes and low-stresses.

A summary of the physical properties of olivine is assembled in Table 1. These will be used in subsequent calculations.

II.c. Geophysical constraints on the activation parameters

Some of the activation parameters for creep and attenuation can be estimated directly from the geophysical data. The characteristic time scales of relaxation processes in the mantle depend on temperature, through the activation energy, and the pressure, through the activation volume. Stress has an indirect effect on relaxation times since it controls such parameters as dislocation density and subgrain size. The characteristic frequency of atomic processes and processes involving dislocation motions are typically 10^{-13} to 10^{-10} seconds. The characteristic relaxation time for creep in the upper mantle, the ratio of viscosity to rigidity, is about 10^{10} seconds. For temperatures of 1500-1600 K, appropriate for the upper mantle, the required activation energy is 145-170 kcal/mole. This can be compared with the activation energy for creep of olivine 125-165 kcal/mole [Goetze, 1978, Jaoul et al., 1979] and similar values inferred for the climb of dislocations in olivine [Goetze, 1978, Kohlstedt et al., 1976].

Judging from the attenuation of surface waves [Anderson and Archambeau, 1964, Anderson and Hart, 1978] the characteristic time controlling the attenuation of seismic waves in the upper mantle is of order of 10^2 seconds. This implies an activation energy in the range 90-100 kcal/mole for the above τ_0 . This is close to the activation energy found for diffusion of O^{2-} and Si^{4+} in olivine [Reddy et al., 1980; Jaoul et al., 1979]. A higher value for τ_0 gives a smaller value for E^* .

The trade-off between τ_0 and E^* is shown in Figure 1. The curves to the right cover a range of upper mantle temperatures and viscosities. The curves to the left represent the seismic band. Theories of creep and attenuation predict $\tau_0 - E^*$ pairs. Those which fall in the areas shown are geophysically

plausible mechanisms. Low values of τ_0 require low values for E^* . As we will show, the characteristic pre-exponential times are not the same for creep and attenuation.

It is not simple to estimate the pre-exponential characteristic time appropriate for attenuation in the mantle. High-temperature background damping processes in metals give τ_0 in the range of 10^{-12} - 10^{-14} seconds [Nowick and Berry, 1972]. Lower temperature peaks give characteristic times one or two orders of magnitude higher [Woïrgard, 1976]. Theoretically, the times scale as the diffusivity which is typically three orders of magnitude lower in silicates than in metals. On the other hand, subgrain sizes and dislocation lengths in the mantle can be expected to be one or two orders of magnitude greater than typical laboratory grain sizes in metals. Since $\tau_0 \sim \ell^2/D$ the characteristic time for the mantle may therefore be of the order of 10^{-6} to 10^{-8} seconds. There is very limited data on silicates. For sintered forsterite with grain size of 5×10^{-4} cm Jackson [1969] obtained 4×10^{-13} sec for a relatively low-temperature relaxation peak. His temperatures were not high enough to resolve the HTB peak but one can calculate from his data that $\tau_0 \ll 10^{-7}$ seconds. The subgrain size in olivine at 10 bars, a reasonable mantle stress, is of the order of 10^{-1} cm [Durham et al., 1977]. The mantle relaxation times can therefore be estimated from the forsterite data as about 10^{-8} sec. This implies an activation energy of 58-74 kcal/mole if the upper mantle seismic absorption band is centered at 100 seconds.

Although τ is proportional to ℓ^2 for most attenuation and creep mechanisms there are other factors which affect the characteristic times. Steady-state creep is controlled by self-diffusion of the slowest moving species. This affects both D_0 and E^* . E^* for creep, which also includes the

energy of jog formation, is therefore greater than E^* for attenuation which need not involve self-diffusion. For a polygonized network the climb of dislocations in cell walls is rate-limiting but the characteristic time for creep involves both the motion of the long mobile dislocations in the cells and the shorter dislocations in the walls. For attenuation, the separate population of dislocations would give rise to widely separated internal friction peaks. A wide separation of characteristic times can therefore be obtained from a single dislocated solid.

Although there is a large uncertainty in the τ_0 appropriate for attenuation in the mantle the range of inferred activation energies is consistent with diffusion control. The lower end of the range is consistent with activation energies found at high temperatures, low frequencies and low strains in Al_2O_3 and Mg_2SiO_4 [Jackson, 1969]. These in turn are comparable to those appropriate for interstitial drag (Mg-Fe) or double-kink formation.

II.d. Estimates of τ_0 and E^* for olivine

The characteristic relaxation time for creep of olivine can be obtained from high-temperature laboratory experiments. The relatively low stress, <2 kbar, creep data satisfies

$$\dot{\epsilon} = A\sigma^n \exp\left(-E/RT\right) \quad (5)$$

Using the Kohlstedt-Goetze data with $n = 3$ and $E = 125$ kcal/mole and the relation

$$\hat{\tau}_0 = \sigma G / \dot{\epsilon}_0 \quad (6)$$

we obtain $\hat{\tau}_0 = 3 \times 10^{-9}$ to 3×10^{-11} sec for the stress range 1 - 10 bars. The low-stress data has a σ^2 trend. In this case $\hat{\tau}_0$ is 10^{-9} to 10^{-10} sec. A summary of $\hat{\tau}_0$ values consistent with the olivine creep data is given in Table 2. A range of activation energies is given.

From the rigidity and viscosity the relaxation time of the upper mantle is $10^{10 \pm 1}$ seconds. Using an activation energy of 125 kcal/mole and a range of upper mantle temperatures from 1100 to 1300°C the inferred value for τ_0 is 10^{-6} to 10^{-10} seconds. This is consistent with the laboratory creep data for differential stresses in the range of a fraction of a bar to about 5 bars. The mantle $\hat{\tau}_0$ values also overlap the lower values for $\hat{\tau}_0$ determined from dislocation mechanisms rate limited by silicon diffusion.

The effect of pressure can be estimated from the observation that both viscosity and Q do not vary by more than 2 orders of magnitude in the mantle [Anderson and Hart, 1978, Peltier, 1979]. This constrains the activation volume to be between 4 and 9 cm³/mole. Since the activation volume of oxygen, the largest major ion in the mantle, is about 11 cm³/mole and decreases with pressure and since the effective activation volume depends on all diffusing ions for coupled diffusion, the result from the mantle is consistent with diffusional control for both dislocation creep and attenuation.

A crude estimate of the activation energy controlling attenuation can be obtained from the observation that Q can vary by about an order of magnitude over relatively short distances both laterally and vertically in the upper mantle. Using 200° C as a reasonable difference in temperature the inferred activation energy is about 52 kcal/mole. This, in turn, requires a τ_0 of about 10^{-5} - 10^{-6} seconds for the attenuation mechanism.

These results support previous conclusions that both creep and attenuation in the mantle are activated processes that are controlled by diffusion. They are also consistent with numerous studies on a variety of materials that high temperature creep and internal friction are controlled by the diffusive motion of dislocations. The large modulus defect implied by the upper mantle low-velocity, low- Q zone is also consistent with a dislocation relaxation mechanism [Gueguen and Mercier, 1972; Anderson and Minster, 1980]. Point defect internal friction peaks are generally relatively sharp, occur at low temperatures and do not exhibit the low Q 's and large velocity dispersion that characterize the mantle and the high temperature internal friction peaks.

III. Calculation of creep of olivine

The climb velocity of a dislocation, when both self-diffusion and jog formation are important is [Hirth and Lothe, 1968]

$$v = (4\pi D_{SD} \sigma b^2 / kT) \exp(\Delta E - \Delta E_j) / 2RT \quad (7)$$

We use $D_{SD} = D_{Si} = (D_{Si})_0 \exp(-E_{Si}/RT)$ since Si^{4+} appears to be the slowest moving species. We assume that the material contains cells or subgrains of diameter L . The creep equation is [Gittus, 1976]

$$\dot{\epsilon} = K \sigma^3 D \Omega^{1/3} / G^2 kT \quad (8)$$

where $\sigma = Gb/L$ has been taken as the effective stress operating on the mobile dislocations of length L . The parameter K is the ratio of cell diameter to the average dislocation length, including mobile and cell-wall dislocations. This parameter has not been measured in olivine but the ratio of average mobile dislocation length to cell diameter is about 15 [Durham et al., 1977]. This means that the Gittus parameter $K > 15$. Gittus also assumes that each subgrain contains only one mobile dislocation. Equation (8) still applies if there are more dislocations per subgrain but the K parameter would have a different value. The strain rate increases with an increase in mobile dislocation density but decreases with a decrease in length of the dislocations. K is therefore a slowly varying function of the mobile dislocation density in the subgrains. ΔE in equation (7) is $E_{SD} - E_{CD}$.

The calculated creep curves are given in Fig. 2 using D_0 for silicon and K of 29 and 15. A K of 29 fits the data. There is a direct trade-off

between D_0 and K . If oxygen proves to be the slowest moving species then, with current estimates of its diffusivity, the compatible K is 8.

The subgrain structure of stressed olivine, a characteristic it shares with other crystalline materials, also affects the attenuation. If we assume that only the free dislocations contribute to the high temperature attenuation, their lengths are

$$L = K(Gb/\sigma) \quad (9)$$

The relaxation time then depends inversely on stress squared and, with $K = 10$, the characteristic times are 10^2 greater than they would be for a uniform Frank network. Note that the characteristic time for creep is proportional to K^{-6} , i.e. very much shorter than the case for a uniform network.

Steady-state creep data for olivine for stresses between several hundred bars and several kilobars is well fit by a dislocation climb model where the strain rate is proportional to the third power of the stress [Goetze, 1978]. At lower stresses the data deviates from this relationship and approaches a stress-squared dependency. The stress-squared dependency at low stresses is suggested by data of Kohlstedt and Goetze [1974], Durham et al. [1979] and Berckhomer et al [1979].

The dislocation climb velocity for the case where the equilibrium jog spacing is greater than the average dislocation length is [Hirth and Lothe, 1968].

$$V = \frac{4\pi \ell D_{SD} \Omega b \sigma}{a^2 b kT \ln(z/b)} \exp(\Delta E^* - 4E_J^*)/2RT \quad (10)$$

where z is the mean free path of a core vacancy along the dislocation line ($\sim 1.4a$), a is the height of a thermal jog at high temperature, ℓ is the dislocation length, D_{SD} is the pre-exponential self-diffusion coefficient (approximately equal to the diffusivity of the slowest moving species), Ω is the atomic volume, b is the Burgers vector, σ is the stress, ΔE is the difference in activation energy between self-diffusion and core diffusion. Setting $a \sim b \sim \Omega^{1/3}$ and writing $\dot{\epsilon} = \rho Vb$, we have

$$\dot{\epsilon} \sim 4\pi D_{SD} b \sigma^2 / kTG \quad (11)$$

We have used the relation $Gb/\ell = \sigma$ where G is the rigidity. Equation (11) has the required stress dependency and an effective activation energy which is substantially greater than the self-diffusion activation energy.

IV.a. Attenuation

The actual physical mechanism of attenuation in the mantle is uncertain but it is likely to be a relaxation process involving a distribution of relaxation times (e.g., Minster, 1980). Many of the attenuation mechanisms that have been identified in solids occur at relatively low temperatures and high frequencies and can therefore be eliminated from consideration. These include point defect and dislocation resonance mechanisms which typically give absorption peaks at kilohertz and megahertz frequencies at temperatures below about half the melting point. The so-called grain boundary and cold-work peak and the "high temperature background" occur at lower frequencies and higher temperatures. These mechanisms involve the stress induced diffusion of dislocations. The Bordoni peak occurs at relatively low temperature in metals but may be a higher temperature peak in silicates.

Even in the laboratory it is often difficult to identify the mechanism of a given absorption peak. The effects of amplitude, frequency, temperature, irradiation, annealing, deformation and impurity content must be studied before the mechanism can be identified with certainty. This information is not available for the mantle or even for the silicates which may be components of the mantle. Nevertheless, there is some information which helps constrain the possible mechanism of attenuation in the mantle.

1. The frequency dependence of Q is weak over most of the seismic band. At frequencies greater than about 1 Hz Q appears to increase linearly with frequency [Kanamori and Anderson, 1977, Minster, 1978, Sipkin and Jordan, 1979]. This is consistent with the behavior expected on the low-temperature side of a relaxation band. A weak frequency dependence is best accomplished by invoking a distribution of relaxation times. A distribution of dislocation

lengths, grain sizes and activation energies may be involved.

2. Although it has not been specifically studied, there has been no evidence brought forward to suggest that seismic attenuation is amplitude or stress dependent. Laboratory measurements of attenuation are independent of amplitude at strains less than 10^{-6} . Strains associated with seismic waves are generally much less than this.

3. The radial and lateral variations of Q are our best clues to the effects of temperature and pressure. The lower Q regions of the mantle seem to be in those areas where the temperatures are highest. This suggests that most of the upper mantle is on the low-temperature side of an absorption band or in the band itself. At a depth of 100 km the temperature of the continental lithosphere is about 200 K less than under oceans. Q is roughly 7 times larger under continent. This implies an activation energy of about 50 kcal/mole.

4. The variation of Q with depth in the mantle covers a range of less than two orders of magnitude. This means that the effects of temperature and pressure are relatively modest or that they tend to compensate each other.

5. Losses in shear are more important than losses in compression. This is consistent with stress induced motion of defects rather than a thermo-elastic mechanism or other mechanisms involving bulk dissipation.

IV.b. Dislocation damping

The general expression for the characteristic time of stress induced diffusion of a dislocation line is

$$\tau = (kTL^2/D_0Gb^3) \exp(E^*/RT) \quad (12)$$

In the bowed string approximation for climb L is the dislocation length, D_0 is the pre-exponential self-diffusion coefficient and E^* is the activation energy for self-diffusion. If the climb is rate-limited by core diffusion (CD) then [Woirgard, 1976]

$$L^2 = \ell^4/\lambda b \quad (13)$$

where ℓ is the dislocation length, $\lambda = b \exp(E_j/RT)$ is the jog separation and D_0 and E^* refer to core diffusion. The effective activation energy is therefore the sum of the core diffusion and jog formation energies. If $D_0(\text{CD}) = 10^3 D_0(\text{SD})$ and $\ell = 10^3 b$ the τ_0 for core-diffusion is 10^3 times that for self-diffusion. At modest temperature, however, $\tau(\text{CD}) < \tau(\text{SD})$ if $E_{\text{CD}} < E_{\text{SD}}$. In general, relaxation peaks with high activation energies occur at higher temperature and lower frequency than those with lower activation energies. The presence of point defects, kinks or jogs along the dislocation line changes the characteristic time.

An estimate of the relaxation time for climb can be obtained from the values in Table 1. We first assume that the dislocation length is the same as the subgrain size, which in turn is related to the tectonic stress (Durham et al., 1977

$$L = 15 Gb/\sigma \quad (14)$$

Using D_{S1} and σ between 1 and 10 bars we obtain τ_0 of $1 - 10^{-2}$ seconds. Neither the self-diffusion nor the core-diffusion characteristic times can be brought into the upper mantle seismic band with the appropriate activation energy (Table 1 and Figure 1). The actual mobile dislocation lengths in olivine are about 15 times smaller than the subgrain size. This reduces τ_0 to 4×10^{-3} to 4×10^{-5} seconds. With an activation energy of 90 kcal/mole the relaxation time at upper mantle temperatures is 10^8 to 10^6 seconds, still well outside the seismic band but straddling the Chandler period. Dislocation climb in subgrains is therefore unlikely to contribute to seismic attenuation but may contribute to damping of the Chandler wobble.

The dislocation lengths in cell walls are an order of magnitude smaller than in the cells. This makes a further reduction in τ_0 to about 10^{-5} to 10^{-7} sec. This gives relaxation times just outside the seismic band at mantle temperatures and $E^* = 90$ kcal/mole but the relaxation strength is very small because of the limited bow-out possible for small dislocations.

Therefore, it appears that dislocation climb can be ruled out as a mechanism for attenuation in the mantle. We therefore turn our attention to dislocation glide.

In general dislocations glide much faster than they climb and the relaxation time is therefore much reduced. Glide is rate limited by lattice (Peierls) stresses or by point defects.

For a gliding dislocation, rate limited by the diffusion of interstitial defects [Schoeck, 1963]

$$L^2 = C_i \ell^2 \quad (15)$$

where C_i is the concentration of interstitials along the dislocation line at sufficiently high temperature

$$C_1 = C_D \exp (-E_B/RT) \quad (16)$$

and C_D is the bulk concentration of interstitial point defects or impurity atoms and E_B is the binding energy of the point defects to the dislocation line. The diffusivity is that appropriate for the diffusion of the impurity or interstitial ions.

Using $D_0 = 10^{-3} \text{ cm}^2/\text{sec}$ and $C_D \sim C_1 = 10^{-3}$ we obtain τ_0 of 10^{-6} to 10^{-8} seconds for typical dislocation lengths appropriate for mantle stresses of 1 to 10 bars. These, combined with activation energies appropriate for diffusion of cations in silicates give relaxation times in the seismic band at upper mantle temperatures. The impurity content refers to that in the subgrains. Most impurities in the mantle are probably at grain boundaries and therefore the grain interiors are relatively pure. The above estimate for C_D is therefore not unreasonable.

IV.c. Relaxation strength

The relaxation strength, or maximum value for Q_0^{-1} , is given by

$$2 Q_0^{-1} = (1/6\sqrt{5}) \rho_m l^2$$

for a collection of randomly oriented gliding dislocations (Minster and Anderson, 1980). In the subgrains $\rho_m = 1/l^2$ for a rectangular grid of dislocations and the relaxation strength is about 7.5% or a Q of about 26. The same relationship holds for a Frank network in the cell walls but because of the small volume in the walls the average relaxation strength is very small for the wall contribution to the attenuation.

The relaxation strength is proportional to the area swept out by the gliding dislocations and gives the difference between the high-frequency or low-temperature modulus and the relaxed modulus. Gueguen and Mercier (1972) and Anderson and Minster (1980) pointed out that the velocity and attenuation in the upper mantle low-velocity zone could be explained by dislocation relaxation.

IV.d. Examples of dislocation mechanisms of attenuation

The Koster peak occurs in cold-worked metals containing interstitial impurities, some of which have concentrated along the dislocations. It occurs at high temperature and low frequency and usually gives a τ_0 of 10^{-13} to 10^{-14} seconds for metals with O, N or H interstitials. It is believed to be caused by an interaction between dislocations and interstitial point defects in the neighborhood of the dislocation [Schoeck, 1963]. With reasonable choices of parameters it can explain attenuation in the mantle.

The grain boundary peak (GBP) occurs in metals at about one-half the melting temperature at 1 Hz. Actually, a series of peaks are often observed between about 0.3 and 0.6 T_m . The activation energies range from about 0.5-1.0 of the self-diffusion activation energy and are higher for the high temperature peaks. An increase in solute concentration increases the magnitude of the higher temperature peak [Nowick and Berry, 1972]. These peaks are all superimposed on an even stronger high-temperature background which dominates at very high temperature. In synthetic forsterite a strong peak occurs at about 0.25-0.5 Hz at 1000°C [Jackson, 1968] with an activation energy of 57 kcal/mole. At upper mantle temperatures this absorption would shift to about 10^{-2} seconds and therefore would not be important at seismic frequencies. In addition the peak is much less pronounced in natural olivine and the HTB gives greater absorption than the GBP at temperatures greater than about 1500° C. The GBP may be responsible for attenuation in the lithosphere.

The Bordoni Peak was first identified in deformed ("cold worked") metals at low temperature. It is unlikely to be important at mantle temperatures and seismic frequencies but it would be useful to know its properties for mantle minerals since it contains information about the Peierls energy.

The Hirth and Lothe [1968] theory for the characteristic relaxation time gives

$$\tau = \frac{b^2 kT}{2E_k D_k} \exp(2E_k/RT) \quad (17)$$

With nominal values for olivine the relaxation time at mantle temperatures is 10^{-7} seconds. Thus, this is a high frequency, low temperature mechanism.

The controlling activation energy is $2E_k$ or about 52 kcal/mole for olivine. This combination of τ_0 and E^* make it unlikely that the Peierls' energy alone controls attenuation in the mantle. It may be a responsible for the "grain boundary" peak in olivine for which Jackson [1968] obtained τ_0 of 10^{-13} sec and E^* of 57 kcal/mole. The value for E_k , however, is uncertain.

V. Discussion

Values of $\hat{\tau}_0$ of order 10^{-7} to 10^{-12} seconds for the upper mantle are implied by relaxation times of $10^9 - 10^{10}$ seconds at temperatures of 1400-1600 K and an activation energy of 125 ± 5 kcal/mole. These values are consistent with both laboratory creep data and creep in a polygonized network model of olivine if the stresses are less than about 10 bars. This applies to both the σ^3 and σ^2 laws. If kilobar level stresses existed in the upper mantle then the inferred viscosity and relaxation times would be at least 6 orders of magnitude lower than observed. On the other hand, there is no contradiction with kilobar level stresses being maintained in the lithosphere for 10^6 years if temperatures are less than about 900 K. Kilobar level stresses also shift the absorption band to much higher frequencies.

The same dislocations contribute to phenomena with quite different time scales. The climb of jogged dislocations is rate-limited by self-diffusion and jog-nucleation. In silicates, and other materials with high Peierls energy, the activation energy for creep can be appreciably greater than for self-diffusion. At finite temperature the creep rate will therefore be slower, and the characteristic time longer, than for materials rate-limited by self-diffusion alone. The effective activation energy for creep is either E_j or $2E_j$ greater than for self-diffusion, depending on whether the dislocation length is smaller or larger than the equilibrium spacing of thermal jogs. These two situations lead to a $\dot{\epsilon}^3$ or $\dot{\epsilon}^2$ creep law. If the activation energy for core-diffusion is less than for self-diffusion the effective activation energy is reduced by one-half the difference of the two. This is a relatively small effect and appears to be negligible for olivine.

On the other hand, the glide of dislocations is controlled by a much smaller activation energy and is therefore much faster than climb at finite temperature. This is the case whether glide is controlled by kink nucleation or diffusion of interstitials. Both creep and attenuation depend on dislocation length and therefore tectonic stress. They are both also exponentially dependent on temperature although the controlling activation energies are different. In principle, the viscosity of the mantle can be estimated from the Q.

C-2

VI. Directions for future research

There is now abundant data on the high-temperature creep of olivine. The various creep theories can be tested with this data and relatively confident extrapolations can be made to lower strain rates. There is no inconsistency between the laboratory and geophysical data. The major uncertainty is the stress dependence and activation energy at low stresses and the microstructure at low stresses. The Gittus theory satisfies the laboratory and geophysical data. The assumption that there is only one mobile dislocation per grain and that this traverses the grain by glide alone may need modification. The theory also assumes that cell-walls of all orientation behave the same. Nevertheless, the Gittus theory seems closer to reality than theories involving climb alone in Frank networks.

The calculation of relaxation times and relaxation strengths for glide in the subgrains is straight forward and appears capable of explaining the seismic attenuation data. The laboratory data for checking the theory is basically non-existent for silicates. Low frequency, small strain experiments on deformed and annealed single and polycrystals at a variety of temperatures is required. The effect of impurity content must also be studied in both olivine and peridotite. In principal, seismic data can be used to infer temperature, dislocation density, stress and subgrain impurity content. This paper has hopefully made the case for a new generation of geophysical experiments.

Acknowledgements

This research was supported by the Earth Sciences Section, National Science Foundation Grant No. EAR77-14675 and the National Aeronautics and Space Administration Grant No. NSG-7610, Contribution Number 3411, Division of Geological and Planetary Sciences, California Institute of Technology, Pasadena, California 91125.

Table 1
Material Properties for Olivine

Property	Symbol	Value	Units
Burger's vector	b	6×10^{-8}	cm
Oxygen ion volume	Ω	1×10^{-23}	cm ³
Shear modulus	G	8×10^{11}	dy/cm ²
Silicon diffusivity ⁽¹⁾			
pre-exponential	D_{Si}	1.5×10^{-6}	cm ² /sec
activation energy	E_{Si}	90	kcal/mole
Oxygen diffusivity ⁽²⁾			
pre-exponential	D_{ox}	3.5×10^{-3}	cm ² /sec
activation energy	E_{ox}	89	kcal/mole
Mg-Fe diffusivity ⁽³⁾			
pre-exponential	D_{Mg}	3.4×10^{-3}	cm ² /sec
activation energy	E_{Mg}	47	kcal/mole
Subgrain size †			
Dislocation length	K'	15	--
Kink energy ⁽⁴⁾	E_k	26	kcal/mole
Jog energy ⁽⁵⁾	E_j	35	kcal/mole

(1) Jaoul et al., 1979

(2) Reddy et al., 1980

(3) Misener, 1974

(4) Stocker and Ashby, 1973

(5) From creep data

Table 2

Summary of Experimental $\hat{\tau}_0$ Values
 Consistent with Kohlstedt-Goetze Creep Data

	<u>σ^3-law</u>	<u>Stress</u>	
		1 bar	10 bar
E* (kcal/mole)	120	3×10^{-8} sec.	3×10^{-10} sec.
	125	0.7×10^{-8}	0.7×10^{-10}
	135	0.35×10^{-9}	0.35×10^{-11}
	<u>σ^2-law</u>		
	120	3×10^{-11}	3×10^{-12}
	125	0.7×10^{-11}	0.7×10^{-12}
	135	0.35×10^{-12}	0.35×10^{-13}

125 kcal/mole is experimental activation energy

References

- Anderson, D. L. and C. Archambeau, The anelasticity of the Earth, J. Geophys. Res., 69, 2071-1964.
- Anderson, D. L., H. Kanamori, R. Hart and H. Liu, The Earth as a seismic absorption band, Science, 196, 1104-1106, 1977
- Anderson, D. L. and B. Minster, The frequency dependence of Q in the Earth and implications for mantle rheology and Chandler Wobble, Geophys. J. R. Astron. Soc.,
- Anderson, D. L. and R. Hart, Q of the Earth, J. Geophys. Res., 83, 5869-5882, 1978.
- Anderson, D. L., and B. Minster, Seismic velocity, attenuation and rheology of the upper mantle, Annales de Géophysique, (in press), 1980.
- Ashby, M. and R. Verrall, Micromechanisms of flow and fracture and their relevance to the rheology of the upper mantle, Phil. Trans. R. Soc. Lond. A, 288, 59-95, 1977.
- Berckhemer, H., F. Auer and J. Drisler, High-temperature anelasticity and elasticity of mantle peridotite, Phys. Earth Planet. Interiors, 20, 48-59, 1979.
- Celli, V., M. Kabler, T. Ninomiya and R. Thomson, Theory of dislocation mobility in semiconductors, Phys. Rev., 131, 58-72, 1963.
- Durham, W., C. Goetze and B. Blake, Plastic flow of oriented single crystals of olivine 2. observations and interpretations of the dislocation structures, J. Geophys. Res., 82, 5755-5770, 1977.
- Gittus, J. H., Theoretical equation for steady-state dislocation creep effects of jog-drag and cell formation, Phil. Mag., 34, 401-411, 1976.
- Goetze, C. and D. Kohlstedt, Laboratory study of dislocation climb and diffusion in olivine, J. Geophys. Res., 78, 5961-5971, 1973.

- Goetze, C., The mechanisms of creep in olivine, Phil. Trans. R. Soc. Land. A. 288, 99-119, 1978.
- Gueguen, Y., High temperature olivine creep: evidence for control by edge dislocations, Geophys. Res. Lett., 6, 357-360, 1979.
- Gueguen, Y., and J. M. Mercier, High Attenuation and the low-velocity zone, Phys. Earth Planet. Int., 7, 39-46, 1973.
- Hirth, J. and J. Lothe, Theory of dislocations, McGraw-Hill, New York, p. 780, 1968.
- Jackson, D., Grain boundary relaxation and the attenuation of seismic waves, Thesis, M.I.T., Cambridge, Mass., 1969.
- Jaoul, O., C. Froidevaux and M. Poumellec, Atomic diffusion of ^{18}O and ^{30}Si in forsterite: implications for the high temperature creep mechanisms ICG abstracts, Internat. Un. of Geodesy and Geophysics, XVII, General Assembly, Canberra, Australia, 1979.
- Kanamori, H. and D. L. Anderson, Importance of physical dispersion in surface-wave and free-oscillation problems; a review, Rev. Geophys. Space Phys., 15, 105-112, 1977.
- Kohlstedt, D. and C. Goetze, Low-stress high-temperature creep in olivine single crystals, J. Geophys. Res., 79, 2045-2051, 1974.
- Kohlstedt, D., C. Goetze and W. Durham, Experimental deformation of single crystal olivine with application to flow in the mantle, in The Physics and Chemistry of Minerals and Rocks (ed. S. K. Runcorn) p. 35-49, Wiley, London, 1976.
- Liu, H., D. L. Anderson and H. Kanamori, Velocity dispersion due to anelasticity; implications for seismology and mantle composition, Geophys. J. R. Astron. Soc., 47, 41-58, 1976.

- Minster, J., Transient and impulse responses of a one-dimensional linearly attenuating medium - II. A parametric study. Geophys. J. R. Astron. Soc., 52, 503-524, 1978.
- Minster, J. B., Anelasticity and attenuation, in A. Dziewonski and E. Boschi, eds., Proc. Enrico Fermi Intern. Sch. Phys. Academic Press (in press) 1980.
- Minster, J. B., and D. L. Anderson, A model of dislocation controlled rheology for the mantle, submitted to Phil. Trans. Roy. Soc., London, 1980.
- Misener, D. V., Cationic diffusion in olivine to 1400°C and 35 kbar, Carnegie Inst. Washington Publ. 634, 117-129, 1974.
- Nowick, A., and B. Berry, Anelastic relaxation in crystalline solids, Academic Press, New York, p. 677, 1972.
- Peltier, W., Mantle convection and viscosity, in A. Dziewonski and E. Boschi, eds., Proc. Enrico Fermi Intern. Sch. Phys., Academic Press (in press) 1980.
- Reddy, K. P. R., S. M. Oh, L. D. Major, Jr., and A. R. Cooper, Oxygen diffusion in forsterite, J. Geophys. Res., 85, 322-326, 1980.
- Schoeck, G. Friccion interna debido a la interaccion entra dislocaciones y atomos solutos, Acta Metall. 11, 617-622, 1963.
- Schwenn, M. and C. Goetze, Creep of olivine during hot-pressing, Tectonophysics, 48, 41-60, 1978.
- Sipkin, S. and T. Jordan, Frequency dependence of Q_{ScS} , Bull. Seismol. Soc. Amer., 69, 1055-1079, 1979.
- Stocker, R., Influence of oxygen pressure on defect concentrations in olivine with a fixed cationic ratio, Phys. Earth Planet. Interiors, 17, 118-129, 1978.
- Stocker, R. and M. Ashby, On the rheology of the upper mantle, Rev. Geophys. Space Phys., 11, 391-426, 1973.

Van Bueren, H., Imperfections in crystals, North-Holland, Amsterdam, p. 676, 1960.

Weertmann, J., Internal friction of metal single crystals, J. Appl. Phys., 26
202-210, 1955.

Weertmann, J., Dislocation climb theory of steady-state creep, Trans. Am. Soc.
Met., 61, 681-694, 1968.

Woirgard, J., Modèle pour Les pics de frottement interne observés a haute
température sur Les monocristaux, Phil. Mag., 33, 623-637, 1976.

Figure Caption

Figure 1. Pre-exponential τ_0 vs. activation energy combinations that satisfy the seismic data (left) and rebound data (right) for a range of upper mantle temperatures.

Figure 2. Creep in polygonized olivine for several values of K. data from Kohlstedt et al. (1976).

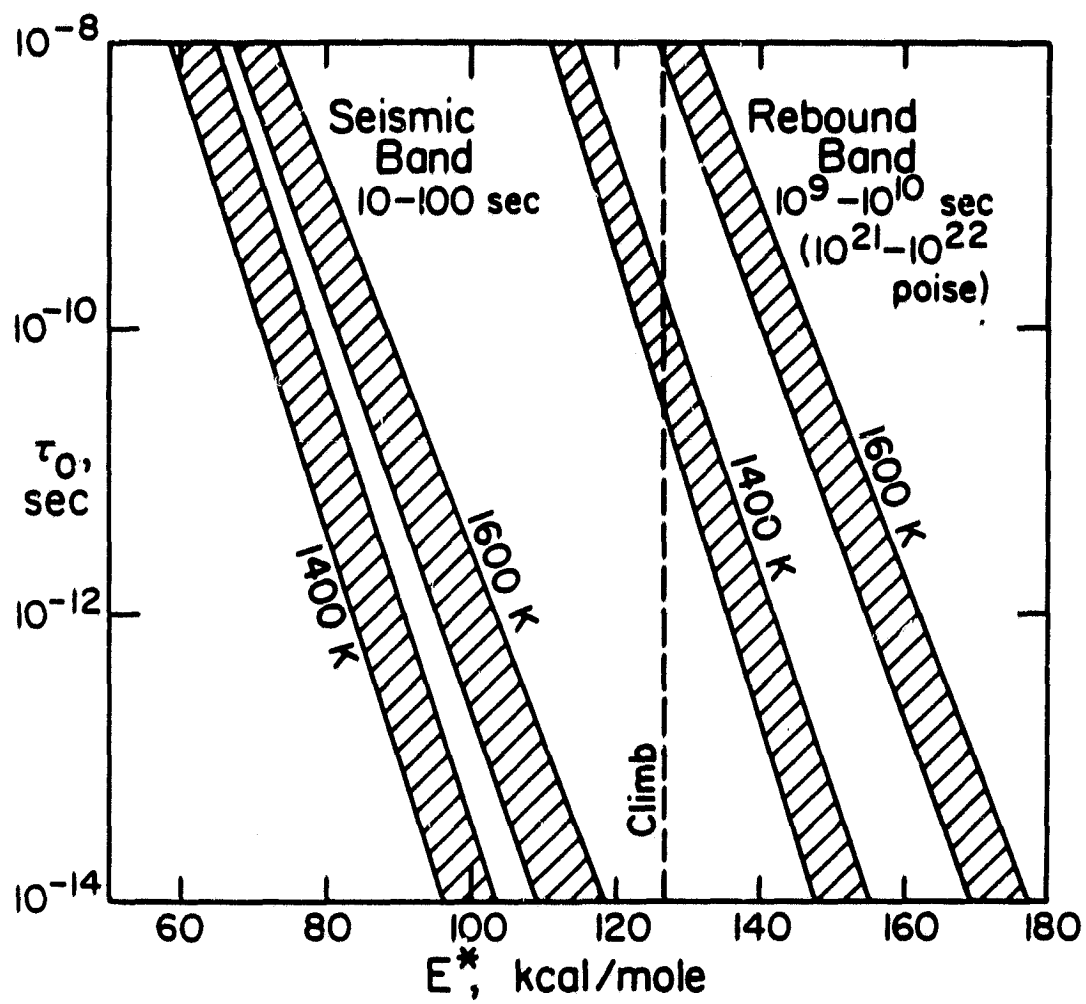


Fig. 1

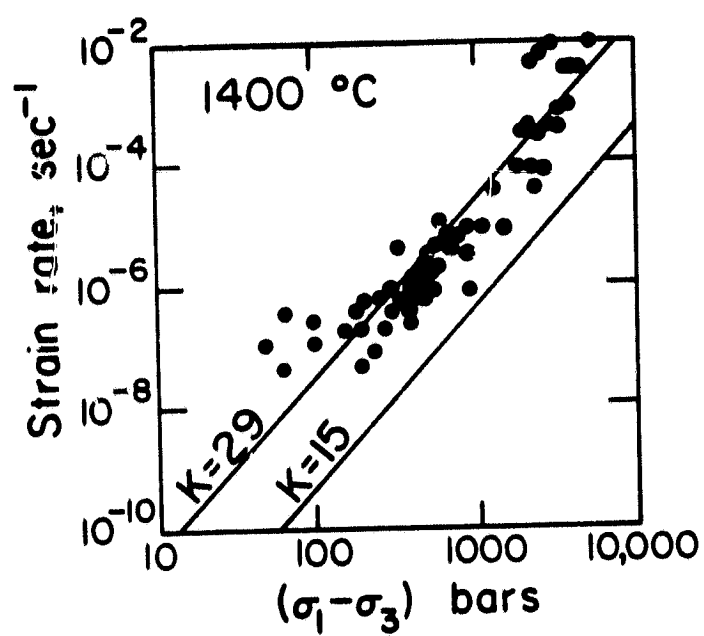


Fig.2

APPENDIX III

A MODEL OF DISLOCATION-CONTROLLED RHEOLOGY
FOR THE MANTLE

J. Bernard Minster

Don L. Anderson

Philosophical Transactions of the Royal Society of London (in press).

A model of dislocation-controlled rheology

for the mantle

(Running title: Dislocation-controlled mantle rheology)

by

J. Bernard Minster

Don L. Anderson

April 7, 1980

Revised May 27, 1980

**Submitted to Philosophical Transactions of the Royal Society
of London.**

**Contribution Number 3416, Division of Geological and Planetary
Sciences, California Institute of Technology, Pasadena,
California 91125**

Contents

	<u>Page</u>
Introduction	1
I <u>Scaling laws</u>	2
II <u>Diffusion-controlled dislocation damping</u>	5
1) Retardation spectrum	5
2) Relaxation strength	8
a) Case of a distribution of activation energies	9
b) Case of a broad distribution of lengths	10
3) Creep function	11
a) Short time regime	11
b) Transitional regime	12
c) Long time regime	13
4) Attenuation properties	13
a) Long periods	14
b) Absorption band	15
c) High frequencies	16
III <u>Steady state rheology</u>	16
1) An idealized microstructural model	16
2) Creep mechanisms	18
IV <u>Applications and discussion</u>	24
1) Constraints on creep models	24
a) Self-diffusion	25
b) Creep activation energy	26
c) Microstructural constants	28
d) Maxwell times	29
2) Comparison of creep models	30
a) Diffusional creep	30
b) Intracell recovery creep	30
c) Pile-up model	31
d) Cell-wall recovery under applied stress	31
e) Cell-wall recovery under self-stress	31
f) Cell-wall recovery controlled by double jog	32
nucleation and core diffusion	33
g) σ_T^2 creep law	33
3) Creep in the mantle	37
4) Constraints on attenuation	37
a) Peierls barrier model of the Bordoni peak	38
b) Glide controlled by kink diffusion	39
c) Glide of jogged screw dislocations	39
d) Dragging of point defects	40
5) Absorption band in the mantle	43
6) High temperature background attenuation (HTB)	46
V <u>Conclusions</u>	47

Abstract

The dislocation microstructure of mantle materials can account simultaneously for long term steady-state creep, and for stress wave attenuation at seismic frequencies. The hypothesis that a single microstructural model explains the rheology for characteristic times ranging from 1 to 10^{10} seconds can be used to restrict the class of permissible rheological models for the mantle. We review steady-state dislocation damping models in order of increasing complexity, and reject those which do not satisfy laboratory data or geophysical constraints.

This elimination procedure leads us to consider an organized microstructure, in which most dislocations are found inside subgrain walls. The cells contain relatively few dislocation links. These are free to bow under small, i.e. seismic, stresses. The time constant of this mechanism is controlled either by the diffusion of kinks or of point defects bound to the dislocation line. The glide of intragrain dislocations explains the magnitude and frequency range of seismic attenuation. Steady state creep is governed by recovery through climb and annihilation in cell walls. Under conditions of jog undersaturation, climb is controlled by jog formation in addition to self diffusion, and the model requires a higher creep activation energy than for self-diffusion, in agreement with observations on olivine. Quantitative agreement with laboratory data is achieved if the density of cell wall dislocations is one to two orders of magnitude higher than the density of intracell dislocations. Self-diffusion is probably controlled by silicon diffusion at low pressure and by oxygen diffusion at high pressure. The long term tectonic stress is the dominant factor which determines scale lengths; as a result, the total strength of the relaxation associated with bowing of intracell dislocation links is fixed by the geometry and is of the order of 10%. This limits the width of

the seismic absorption band to 2-3 decades in frequency for each mantle mineral. The actual position of the seismic absorption band is determined primarily as a result of a tradeoff between temperature, pressure and tectonic stress.

This model provides a physical framework within which Q and viscosity are related via the dislocation microstructure.

Glossary of Symbols

α	exponent for frequency dependent Q
b	Burgers vector
β_d	geometrical constant
c_j	jog concentration
C	normalization constant
d	climb distance for annihilation
D, D_0	diffusivity and preexponential diffusion constant
D_{oQ}	diffusion constant for attenuation
D_{os}	diffusion constant for self-diffusion
$D(\tau)$	retardation spectrum
$\gamma(\omega)$	attenuation coefficient
Δ	relaxation strength
$E_m^* \leq E^* \leq E_M^*$	activation energy and range
E_Q^*	activation energy for attenuation
E_s^*	activation energy for self-diffusion
E_j	jog formation energy
E_k	kink formation energy
ΔE^*	difference between bulk and core diffusion activation energy
$\epsilon, \dot{\epsilon}$	strain and strain rate
$J(t)$	compliance response
J_u	unrelaxed compliance
J_r	relaxed compliance
δJ	compliance defect
K, K_m, K_s	microstructural scaling constants

k	Boltzmann constant
$k(\omega)$	complex wave number
$\ell, \bar{\ell}$	dislocation link length, and average
L, \bar{L}	subgrain size, and average
ℓ_c	critical length for multiplication
λ	scale length for dislocation drag mechanism
λ_v	scale length for vacancy diffusion
Λ	mean free path of dislocations
μ	rigidity
n_w	number of lattice spacings between cell wall dislocations
ω	frequency
Ω	atomic volume
Ω_v	vacancy volume
$p(\ell), p(E^*)$	probability distributions
P	pressure
$\Psi(t)$	creep function
$Q(\omega)$	quality factor
R	gas constant
R_c	radius of curvature of dislocation line
r_w	dislocation spacing in cell walls
r_1, r_2	inner and outer cutoff radii for vacancy diffusion
ρ	total (smeared) dislocation density
ρ_m	density of mobile dislocations
ρ_w	density of dislocations composing cell boundaries

σ_s	seismic (transient) stress
σ_T	tectonic (steady state) stress
T	temperature
t_μ	time for multiplication
τ	retardation time
τ_0	preexponential retardation time
τ_m, τ_M	limits of retardation spectrum
$\hat{\tau}$	Maxwell time
V, V_D	dislocation migration (drift) velocity
$V_p(\omega)$	phase velocity
V_u, V_r	unrelaxed and relaxed phase velocities
V^*	activation volume
\bar{z}	mean free path of vacancy along dislocation core

Subscript index

NH	Nabarro-Herring diffusion
IG	intragrain recovery mechanism
pu	dislocation pile-up mechanism
cw	cell-wall recovery mechanism
sq	σ^2 creep law

INTRODUCTION

It is probable that steady-state creep in the mantle is controlled by dislocation climb (Weertman, 1970, 1972; Goetze and Brace, 1972; Green and Radcliffe, 1972; Goetze and Kohlstedt, 1973) and is therefore limited by the slow process of self-diffusion and, possibly, jog nucleation. On the other hand, dislocation motion at short times and under very low stress is probably due to glide and is rate limited by faster diffusional processes involving small point defects or kinks (e.g., Simpson and Sosin, 1972). This has led Gueguen and Mercier (1973), and Anderson and Minster (1980a) to propose diffusion-controlled dislocation bowing as an attenuation mechanism for seismic waves in the mantle. There is therefore a possible close connection between seismic attenuation and viscosity via the dislocation structure of the mantle.

In this paper we develop a simplified physical model which allows us to bridge the vastly different time scales and strains involved in steady state creep and anelastic behavior. The fundamental assumption is that the microstructure of mantle grains is controlled by long-term processes and is therefore statistically time invariant, and that mobile dislocation links are free to bow by glide under small transient stresses. The long-term, large strain deformation is controlled by climb, and therefore by self-diffusion and jog formation. The small anelastic strain associated with bowing of mobile dislocation links leads to stress relaxation and consequently to attenuation of stress waves. Although greatly simplified, the formalism is quite general and can accommodate a distribution of grain sizes, dislocation link lengths and activation energies. The detailed analysis will be carried out for a physically plausible and geophysically interesting family of such distributions. The necessary scaling relations are given in section I.

We then develop a formal theory of attenuation by diffusion-controlled dislocation bowing, and provide the necessary results to analyze absorption bands with a mild frequency dependence of Q . In section III, we present a sequence of creep models of increasing complexity, and recast all results in terms of Maxwell characteristic times. This permits us to test the various models against quantitative observational constraints as well as to impose the necessary constraints for self consistency. This is done in section IV for creep models as well as attenuation models. We show that quantitative agreement with laboratory data and geophysical observations can be achieved simultaneously for both aspects of the rheology if the microstructure presents a fairly high degree of organization. The preferred creep model is a generalization of Gittus' (1976a) model. The width of the absorption band is probably associated with a distribution of activation energies and/or dislocation link lengths.

I. SCALING LAWS

Although there is abundant evidence that mantle minerals contain many dislocations (e.g., Raleigh and Kirby, 1970; Green and Radcliffe, 1972; Goetze and Kohlstedt, 1973), the actual microstructure under mantle conditions is uncertain. Plausible assumptions can be made, however, since the bulk of mantle material has remained under quasi-constant low stress ($1-10^2$ bars) over long times ($>10^6$ years). In view of the high temperatures and pressures, we can assume that the dislocation microstructure of mantle minerals in situ is that pertinent to high temperature steady state creep.

The substructural characteristics associated with high temperature steady state creep have been observed for a wide variety of materials. Summaries of

the most significant properties show that they are remarkably similar from material to material (e.g., Mukherjee et al., 1969; Poirier, 1976; Takeuchi and Argon, 1976a; Durham et al., 1977). By comparison with laboratory results, and in view of the supporting theories of Gittus (1976a,b), we shall assume that most dislocations in the mantle are associated with cell walls of subgrains, and that the subgrains contain only a few dislocations, with no tangles nor pile-ups. We shall further assume that these few free dislocations may be strongly pinned at isolated points, and that the segments between pinners can bow-out under low stress. Under larger stress multiplication may take place, either by glide (Frank-Read sources) or climb (Bardeen-Herring sources).

The problem of superposing a low level transient (seismic) stress on a much larger steady (tectonic) stress is quite complex. Because of the very different time scales involved, the problems can be decoupled to first order and we shall assume that the transient is actually superposed on a static, "equilibrium" configuration of internal stress.

Further specification and simplification of the model can be achieved by use of empirical scaling laws; namely (e.g., Mukherjee et al. 1969; Takeuchi and Argon, 1976a);

- 1) The average subgrain size is inversely proportion to the (tectonic) stress

$$\bar{L}/b \propto \mu/\sigma_T \quad (1)$$

where b is the Burgers vector and μ the rigidity.

- 2) The dislocation density within subgrains is proportional to the square of stress

$$b^2 \rho_m \propto (\sigma_T/\mu)^2 \quad (2)$$

Here we have identified intragrain dislocations with the mobile dislocations, of density ρ_m . Comparison of these two scaling laws leads to

$$b^2 \rho_m \sim K_m^2 (b/\bar{L})^2 \quad (3)$$

The observations of Durham et al. (1977) on laboratory deformed olivine lead to a proportionality constant K_m of the order of 10, although this value is quite uncertain. Since the volume of subgrains is proportional to \bar{L}^3 , this implies that the length of dislocation line per cell is proportional to the cell dimension \bar{L} . We may assume that this statistical scaling law holds locally in the sense that it holds in a neighborhood which is very large compared with the cell size but very small compared with the averaging length of a seismic wave.

If ρ is the total dislocation density, then we may write

$$\rho = \rho_m + \rho_w \quad (4)$$

where ρ_w is the density of dislocations composing cell walls. For materials which show a strong degree of organization, ρ_w may be over an order of magnitude greater than ρ_m (e.g., Takeuchi and Argon, (1976a), and thus is a good approximation to the "smeared" dislocation density, in the sense of Holt (1970) and Gittus (1976a,b). On the basis of theoretical and observational consideration, these authors argue that a relation similar to (3) holds for the smeared density, in the form

$$b^2 \rho \sim K^2 (b/\bar{L})^2 \quad (5)$$

Observations on metals point to values of K ranging from 10 to 20, but higher values may be expected theoretically for materials with a higher Peierls energy (Gittus, 1976 a,b). Consistency between the three equations (3)-(5) requires that ρ_m and ρ_w scale with grain size, and hence with stress in a

similar way. Further, ρ_w is an order of magnitude larger than ρ_m if K is only three times greater than K_m .

Although most of the preceding considerations are based on observational evidence on metals, the observations of Durham and Goetze (1977) and Durham *et al.* (1977) indicate olivine is no exception. Of course, detailed description of the microstructure involves many complications, so that the present model must be taken as an idealization. Our purpose is to test some of its consequences.

II. DIFFUSION-CONTROLLED DISLOCATION DAMPING

1) Retardation spectrum

The most commonly — and most successfully — used model of dislocation damping is the classical Koehler-Granato-Lücke model (Koehler, 1952; Granato and Lücke, 1956). This is a string model for a dislocation strongly pinned at both ends, and we use it as a starting point. A recent treatment of the problem at low frequency, where inertial effects can be neglected, is given by Simpson and Sosin (1972).

We may write the force balance equation for the string model of the dislocation line in the form:

$$\sigma_s b - \mu b^2 / 2R_c - V kT / \lambda D = 0 \quad (6)$$

Here σ_s is the applied (seismic) stress, R_c the radius of curvature, and V the migration velocity (fig. 1). λ and D are a scale length and a diffusion coefficient which are characteristic of the particular viscous drag mechanism considered. Since we treat the problem as the superposition of a transient (seismic) stress on an equilibrium state, R_c and V take the values which correspond to equilibrium with σ_s . For small bow-out (6) reduces to a diffusion equation, and solutions have been derived by Friedel *et al.* (1955), Weertmann (1955), Schoeck (1963), and numerous subsequent authors.

For a link of length ℓ , strongly pinned at both ends, the anelastic strain due to bow-out is given by

$$\epsilon(t) = \epsilon(\infty) [1 - \exp(-t/\tau)] \quad (7)$$

which is the classical result for a standard linear solid where the retardation time is

$$\tau = 2\ell^2 kT / \pi^2 \mu b^2 \lambda D \quad (8)$$

If we introduce the steady-state drift velocity V_D of an infinite dislocation line under the applied stress σ_s ,

$$\tau = \frac{1}{\pi^2} \frac{\sigma_s}{\mu} \frac{\ell^2}{b V_D} \quad (9)$$

which is also of the general form

$$\left. \begin{aligned} \tau &= \tau_0 \exp[E_Q^*/RT] \\ \tau_0 &= A(T) \ell^2 / D_{oQ} \end{aligned} \right\} \quad (10)$$

Here E_Q^* is the activation energy for this attenuation mechanism, and D_{oQ} is the preexponential diffusivity factor for the controlling diffusing species.

A distribution of retardation times can be achieved through a spectrum of preexponential factors τ_0 and/or a spectrum of activation energies E_Q^* . It is well known (e.g., Nowick and Berry, 1972) that a localized distribution of retardation times, with a spectrum decaying rapidly away from a dominant value, can be replaced for most purposes by an effective, single mechanism. In such

cases, the essential characteristics of the medium do not differ drastically from those of a standard linear solid.

It is more useful, for our purposes, to allow for the possibility that a broad spectrum of retardation times is available. We have suggested previously (Anderson and Minster, 1980a, Minster and Anderson, 1980) a normalized density of the form

$$D(\tau) = \frac{\alpha}{\tau_M^\alpha - \tau_m^\alpha} \frac{1}{\tau^{1-\alpha}} H(\tau - \tau_m) H(\tau_M - \tau) \quad (11)$$

Among the many possible physical models which entail the distribution (11) we shall consider two extreme cases:

- 1) A distribution of lengths with probability density

$$p(\ell) = C_\ell \ell^{2\alpha-4} \quad ; \quad \ell_m < \ell < \ell_M \quad (12)$$

where C_ℓ is the normalization factor.

- 2) A distribution of activation energies with probability density

$$p(E_Q^*) = C_E \exp [\alpha E_Q^*] \quad ; \quad E_m^* < E_Q^* < E_M^* \quad (13)$$

where C_E is again a normalization factor.

The general case clearly consists of a simultaneous distribution of lengths and activation energies. In his discussion of the problem, Macdonald (1963) also considers juxtaposed intervals in τ with different values of α .

As we shall see shortly, the nonlocal character of the absorption band associated with the spectrum (11) is only significant for small values of α . The richest variety of rheological behavior is observed in the range

$\alpha \in [-1,1]$; in the remainder of this paper, we confine our attention to this range. Note, however, that the limit $\alpha \rightarrow 0$ must be taken with some care, and results for this case will be given separately.

The cutoffs τ_m and τ_M are taken here as phenomenological parameters to be constrained by the physical model. Since the actual behavior of the spectrum outside the range $[\tau_m, \tau_M]$ is immaterial for our purposes, as long as $D(\tau)$ decays rapidly away from this range, we have assumed sharp cutoffs. Localized spectra can be conveniently simulated by taking a narrow range, $\tau_m \sim \tau_M$, irrespective of α .

Let J_u be the unrelaxed compliance of the material, and δJ be the compliance defect. The compliance response is then

$$J(t) = J_u + \delta J \psi(t) = J_u [1 + \Delta \psi(t)] \quad (14)$$

Here $\psi(t)$ is the normalized creep function and Δ the relaxation strength. The medium is anelastic, that is, undergoes time dependent, but linear and recoverable strain response to an applied stress (Nowick and Berry, 1972; Minster, 1979). The complete anelastic behavior of the material under low stress can be described in terms of Δ and ψ .

2) Relaxation strength

The compliance defect δJ depends on the total area swept by mobile dislocations as they bow out, as $t \rightarrow \infty$. The calculation is a classical one (e.g., Friedel et al., 1955) and yields

$$\Delta = \beta_d \frac{\rho_m}{\bar{\ell}} \int_0^\infty \ell^3 p(\ell) d\ell \quad (15)$$

Here ρ_m is the density of mobile dislocations, $p(\ell)$ the density function of the link length distribution, and $\bar{\ell}$ the average link length. β_d is a geometrical

factor which depends on the orientation and geometrical arrangement of the dislocations. For edge dislocations which may only glide, and are all optimally oriented $\beta_d \approx 1/6$. If they are randomly oriented β_d drops to $1/6\sqrt{5}$. If they are allowed to bow by climb as well as glide, $\beta_d \approx \sqrt{7/6\sqrt{15}}$.

Actually, the averaging should only take place over the possible orientations of the glide planes (Friedel et al., 1955; Simpson and Sosin, 1972). For our purposes, approximate estimates are sufficient. Evaluation of (15) leads to the following results:

a) Case of a distribution of activation energies

$$\Delta \sim \beta_d \rho_m \bar{\ell}^2 \quad (16)$$

It may be noted that this result is the correct one whenever the distribution of lengths is highly localized. Whenever the separation of mobile dislocations is comparable to the length $\bar{\ell}$ (e.g., Frank network), the relaxation strength is about 6% for glide, and 11% if climb is permitted as well.

b) Case of a broad distribution of lengths, $\ell_m \ll \ell_M$

We find in that case if α is small

$$\bar{\ell} \sim \frac{3-2\alpha}{2-2\alpha} \ell_m \quad (17)$$

and we may distinguish three cases, according to the sign of α :

$$\alpha < 0 \quad \Delta \approx -4 \frac{(1-\alpha)^3}{\alpha(3-2\alpha)^2} \beta_d \rho_m \bar{\ell}^2 \quad (18)$$

$$\alpha = 0 \quad \Delta \approx \frac{8}{9} \ln \frac{\ell_M}{\ell_m} \beta_d \rho_m \bar{\ell}^2 \quad (19)$$

$$\alpha > 0 \quad \Delta \approx \frac{4}{\alpha} \frac{(1-\alpha)^3}{(3-2\alpha)^2} \left(\frac{\ell_M}{\ell_m} \right)^{2\alpha} \beta_d \rho_m \bar{\ell}^2 \quad (20)$$

Comparison with (12) and (17) indicates that the relaxation strength is dominated by the more numerous shorter links if α is small, and that it increases rapidly with α . This is in agreement with expectations since an increase in α leads to relatively more abundant long dislocations. Note that in equations (16)-(20) we can use the scaling law (3) in the form

$$\rho_m \bar{\ell}^2 = \left(\frac{K_m \bar{\ell}}{\bar{L}} \right)^2 \quad (21)$$

which illustrates more precisely the effect of the microstructure. If the link length scales linearly with subgrain size, then a spread in the distribution of lengths tends to increase Δ toward values greater than the 10% predicted by (16). If the link length $\bar{\ell}$ does not increase with \bar{L} , then the material tends to be underpopulated in mobile dislocations and the modulus defect is rather small.

3) Creep function

The normalized creep function is given by

$$\psi(t) = \int_0^\infty (1 - e^{-t/\tau}) D(\tau) d\tau \quad (22)$$

With the density (11), evaluation of the integral yields

$$\psi(t) = 1 - \frac{\alpha t^\alpha}{\tau_M^\alpha - \tau_m^\alpha} \left[\Gamma\left(-\alpha, \frac{t}{\tau_M}\right) - \Gamma\left(-\alpha, \frac{t}{\tau_m}\right) \right] \quad (23)$$

where Γ is the incomplete gamma function. This expression possesses a proper limit as $\alpha \rightarrow 0$, which can be expressed in terms of exponential integral functions:

$$\psi_{\alpha \rightarrow 0}(t) = 1 - \frac{1}{\ln(\tau_M/\tau_m)} \left[\text{Ei} \left(-\frac{t}{\tau_m} \right) - \text{Ei} \left(-\frac{t}{\tau_M} \right) \right] \quad (24)$$

In the limit of a narrow spectrum ($\tau_m \sim \tau_M$), we get the case of a standard linear solid, which does not require elaboration. In the case of a broad spectrum ($\tau_m \ll \tau_M$), the creep history is best characterized in terms of three successive regimes.

a) Short time $t \ll \tau_m$

For such short times, none of the dislocation segments has relaxed.

We find

$$\alpha < 0 : \quad \psi(t) \sim \frac{-\alpha}{1-\alpha} \frac{t}{\tau_m} \quad (25)$$

$$\alpha = 0 : \quad \psi(t) \sim \frac{1}{\ln(\tau_M/\tau_m)} \frac{t}{\tau_m} \quad (26)$$

$$\alpha > 0 : \quad \psi(t) \sim \frac{\alpha}{1-\alpha} \left(\frac{\tau_m}{\tau_M} \right)^\alpha \frac{t}{\tau_m} \quad (27)$$

This linear time dependence implies Newtonian behavior for small time. It is of interest that the normalized creep function ψ depends on the width of the spectrum in (26) and (27), but does not in (25), for which the density of long retardation times is much smaller. If we consider the combination $\Delta\psi$, this remains true in the case of a distribution of activation energies (eq. 16). On the other hand, combination of eqs. (18-20), and (25-27) show that irrespective of α , $\Delta\psi$ depends only on ℓ_m for small times if the spectrum is due to a length distribution. This last result could have been anticipated since only the shorter links can react on this time scale.

b) Transitional Regime $\tau_m \ll t \ll \tau_M$

During this interval, more and more dislocation links reach their final

equilibrium position. As a result we expect this regime to be one of strain hardening. The dominant terms are, according to the sign of α :

$$\alpha < 0 : \psi(t) \sim 1 - \Gamma(1-\alpha) \left(\frac{t}{\tau_m} \right)^\alpha \quad (28)$$

$$\alpha = 0 : \psi(t) \sim \frac{1}{\ln(\tau_M/\tau_m)} \left[C + \ln \frac{t}{\tau_m} \right] \quad (29)$$

where C is Euler's constant

$$\alpha > 0 : \psi(t) \sim \left(\frac{\tau_m}{\tau_M} \right)^\alpha \left(\frac{t}{\tau_m} \right)^\alpha \quad (30)$$

These are reminiscent of various transient rheologies which have been observed on many materials. Once more, we note that $\Delta\psi$ is independent of the width of the spectrum if (18)-(20) are used, as opposed to (16). And again we note the influence of α on the rheology. For α negative, strain hardening is very rapid and the anelastic strain rapidly approaches an equilibrium value. For α positive, the higher density of slow retardation mechanisms is felt for times much longer than τ_m and anelastic strain continues to grow as a power law. The intermediate value $\alpha = 0$ yields a logarithmic creep law.

c) "Long time" regime $\tau_m \ll \tau_M \ll t$

For such long times, all links have relaxed to their equilibrium, bowed position. The normalized creep function is exponentially close to unity in all cases. This stage is reached when all dislocation segments have reached the same equilibrium radius of curvature. This radius may be smaller than $0.5 \ell_M$, however, for high enough applied stress. In that case, an equilibrium configuration is never reached because the longer links begin to multiply and this gives rise to unbounded plastic strain. We shall return to this point later.

4) Attenuation properties

In the frequency domain, the anelastic properties described above give rise to an absorption band with fairly simple properties. The basic concepts are found in Liu et al. (1976), and have been recently reviewed by Kanamori and Anderson (1977) and Minster (1979). Let V_u be the unrelaxed high-frequency wave velocity; the complex wave number is then given by

$$k^2(\omega) = \frac{\omega^2}{V_u^2} \left[1 + \frac{\alpha\Delta}{\tau_M^\alpha - \tau_m^\alpha} \int_{\tau_m}^{\tau_M} \frac{d\tau}{\tau^{1-\alpha}(1+i\omega\tau)} \right] \quad (31)$$

which may be represented in terms of hypergeometric functions. As shown by O'Connell and Budiansky (1978) an unequivocal and convenient definition of the quality factor is

$$Q(\omega) = - \operatorname{Re} [k^2(\omega)] / \operatorname{Im} [k^2(\omega)] \quad (32)$$

Although no simple analytical form can be derived for $Q(\omega)$, asymptotic expressions can be obtained fairly easily in the various regimes already mentioned. In the limit of a very narrow spectrum, the absorption band reduces to the classical Debye peak. For a broad spectrum, we consider three frequency bands.

a) Long periods $\omega\tau_m \ll \omega\tau_M \ll 1$

$$\alpha < 0 : Q(\omega) \sim - \frac{1+\alpha}{\alpha} \frac{1+\Delta}{\Delta} \left(\frac{\tau_M}{\tau_m} \right)^\alpha (\omega\tau_M)^{-1} \quad (33)$$

$$\alpha = 0 : Q(\omega) \sim \left[\frac{1+\Delta}{\Delta} \ln \frac{\tau_M}{\tau_m} - 1 \right] (\omega\tau_M)^{-1} \quad (34)$$

$$\alpha > 0 : Q(\omega) \sim \frac{1+\alpha}{\alpha} \frac{1+\Delta}{\Delta} (\omega\tau_M)^{-1} \quad (35)$$

$Q(\omega)$ is found to increase linearly with period, the classical behavior of the long period side of an absorption band. For monochromatic waves at such periods, all dislocation links bow out to equilibrium and the medium exhibits relaxed elastic behavior, with phase velocity

$$v_r \sim v_u / \sqrt{1+\Delta} \quad (36)$$

b) Absorption band $\omega\tau_m \ll 1 \ll \omega\tau_M$

Asymptotic approximations are more laborious to derive in this case. We find

$$\alpha < 0 : \quad Q(\omega) \sim \cotan \frac{\alpha\pi}{2} - \frac{1+\Delta}{\Delta} \frac{\cos \alpha\pi/2}{\alpha\pi/2} (\omega\tau_m)^\alpha \quad (37)$$

$$\alpha = 0 : \quad Q(\omega) \sim \frac{1+\Delta}{\Delta} \frac{2}{\pi} \ln \frac{\tau_M}{\tau_m} - \frac{2}{\pi} \ln \omega\tau_M \quad (38)$$

$$\alpha > 0 : \quad Q(\omega) \sim \cotan \frac{\alpha\pi}{2} + \frac{1}{\Delta} \frac{\cos \alpha\pi/2}{\alpha\pi/2} (\omega\tau_M)^\alpha \quad (39)$$

Depending on the sign of α , $Q(\omega)$ decreases or increases as ω^α . With $\alpha = 0$ Q is quasi-independent of frequency; this assumption is often used in seismology (e.g., Liu et al., 1976; Anderson et al., 1976; Minster, 1978a,b). A mild frequency dependence such as predicted by (39) has also been suggested by various authors (e.g., Jeffreys, 1970; Jeffreys and Crampin, 1970; Macdonald, 1961, 1963; Anderson and Minster, 1980a,b; Strick, 1970).

It is interesting to note that there is little generality to be gained by letting α take values outside the range $[-1,1]$. A power law dependence of $Q(\omega)$ on ω still holds, but $Q(\omega)$ cannot vary faster than ω or ω^{-1} within the framework of linear models such as the present one. Thus, a sharp drop of the relaxation spectrum is difficult to distinguish from a simple cut-off insofar as the absorption band is concerned.

The physical dispersion is obtained from the definition

$$k(\omega) = \frac{\omega}{V_p(\omega)} - i\gamma(\omega) \quad (40)$$

where $V_p(\omega)$ is the phase velocity and $\gamma(\omega)$ the attenuation coefficient.

Asymptotic results are conveniently derived only if $Q(\omega) \gg 1$, i.e., in the low loss approximation. We have then

$$\alpha < 0 : \quad V_p(\omega) \sim V_u \left[1 - \frac{\Delta}{2} + \frac{1}{2} \cotan \frac{\alpha\pi}{2} Q^{-1}(\omega) \right] \quad (41)$$

$$\alpha = 0 : \quad V_p(\omega) \sim V_u \left[1 + (\pi \ell n \omega \tau_M)^{-1} Q^{-1}(\omega) \right] \quad (42)$$

$$\alpha > 0 : \quad V_p(\omega) \sim V_u \left[1 - \frac{1}{2} \cotan \frac{\alpha\pi}{2} Q^{-1}(\omega) \right] \quad (43)$$

Thus, for $\alpha \neq 0$, the phase velocity varies as a power of frequency, whereas $\alpha = 0$ yields the classical logarithmic dispersion.

c) High Frequencies $1 \ll \omega\tau_m \ll \omega\tau_M$

At high frequencies, none of the dislocation links reach their relaxed equilibrium configuration. Little anelastic strain takes place, and we have the following limiting behavior:

$$\alpha < 0 : \quad Q(\omega) \sim - \frac{1-\alpha}{\alpha\Delta} \omega\tau_m \quad (44)$$

$$\alpha = 0 : \quad Q(\omega) \sim \frac{\ell n(\tau_M/\tau_m)}{\Delta} \omega\tau_m \quad (45)$$

$$\alpha > 0 : \quad Q(\omega) \sim \frac{1-\alpha}{\alpha\Delta} \left(\frac{\tau_M}{\tau_m} \right)^\alpha \omega\tau_m \quad (46)$$

Once again, comparison with (17)-(20) shows that these limits are independent of the distribution of lengths when such a distribution controls the absorption band. This is consistent with our discussion of $\psi(t)$ for short times. On the other

hand, the width of the band enters (45) and (46) explicitly when one considers a distribution of activation energies instead. The linear increase of Q with frequency is characteristic of the high frequency side of an absorption band, $V_p(\omega)$ asymptotically approaches V_u in that limit.

These properties are summarized on figure 2 which depicts three absorption bands with $\alpha = -0.25, 0$, and 0.25 respectively, as well as the associated dispersive characteristics of the medium.

The so-called high temperature background internal friction in crystalline solids possesses the general characteristics derived above for intermediate and high frequencies (e.g., Minster, 1979). There is therefore a suggestion that laboratory frequencies are on the high frequency-low temperature side of an absorption band of the type discussed here. A similar relationship appears to hold in the upper mantle at seismic frequencies (Anderson and Minster, 1980b). Since an investigation of attenuation as a function of temperature depends critically on the activation energy, we defer discussion of these aspects until a specific physical model is discussed.

III. STEADY STATE RHEOLOGY

1) An idealized microstructural model.

For a given applied (tectonic) stress σ_T the equilibrium radius of curvature of the dislocation lines is obtained by solving (6) in the static limit

$$R_c = \mu b / 2\sigma_T \quad (47)$$

Links with lengths $\ell > \ell_c = 2R_c$ bow beyond a semi-circle and thereafter multiply, either through a Frank-Read mechanism, if glide only is permitted, or a Bardeen-Herring mechanism for glide plus climb. A crude estimate of the time required

for multiplication is obtained by considering the mid-point of the link, and assuming that the link is a circular arc at all times during bowing out; then

$$t_{\mu}(\ell) = \int_0^{\ell/2} v^{-1}(x) dx \quad (48)$$

where $V(x)$ is obtained by solving (6) for this geometry. The solution takes the form

$$t_{\mu}(\ell) = \frac{\ell_c}{2v_D} f(\ell/\ell_c) \quad (49)$$

where

$$f(x) = \frac{x}{2} + \ln \sqrt{\frac{2(x-1)}{x}} + \frac{1}{\sqrt{x^2-1}} \tan^{-1} \sqrt{\frac{x+1}{x-1}} \quad (50)$$

Figure 3 is a graphical comparison of the relaxation time (9) and the multiplication time (49) under the same applied stress $\sigma = \sigma_S = \sigma_T$. It illustrates the region of validity of the anelastic theory developed in the previous section. For sufficiently large stress, ℓ_c is shorter than some or all of the mobile links. These links multiply on a time scale $t_{\mu}(\ell)$ and we have non-recoverable plastic strain. The function $f(x)$ has a minimum for $x = 1.66$; thus links with $\ell = 1.66 \ell_c$ are the first to multiply. It is reasonable to expect that they will dominate the distribution of lengths in the long run since they are associated with the most efficient yielding process. According to this argument, we expect

$$\bar{\ell} \sim 1.66 \mu b / \sigma_T \sim \rho_m^{-1/2} \quad (51)$$

The remarkable agreement with the observations of Durham et al. (1977) is undoubtedly fortuitous, but nevertheless gives some credence to this simple

argument. It is noteworthy that this only differs slightly from the results of Takeuchi and Argon (1976b), which involve much more sophisticated modeling techniques.

Observations of subgrain dimensions in olivine compiled by Durham et al. (1977) are well fit by a relation of the form

$$\bar{L} \sim K_s \frac{\mu b}{\sigma_T} \quad (52)$$

with K_s in the range 15 to 50. When combined with (51) and (3), this yields a constant K_m in the range 9 to 30. Under mantle conditions we may speculate that the material has been annealed over a very long period of time, so that intragrain dislocation density may be somewhat lower than in laboratory samples, and the degree of organization higher. These factors conspire to decrease the estimate of K_m , so that $K_m \sim 10$ may be an appropriate value, especially in view of the uncertainties involved. Thus emerges a microstructural model involving subgrains of dimension $\bar{L} \sim 20 \ell_c$ containing rather few mobile dislocations of mean length $\bar{\ell} \sim 2\ell_c$. All lengths scale inversely with the long term tectonic stress σ_T . If most dislocations are to be found in cell walls so that ρ_w in equation (4) is indeed over an order of magnitude greater than ρ_m , then we must take the constant K in equation (5) to be greater than 30. We now explore the consequences of this highly idealized and simplified microstructure for various creep mechanisms.

2) Creep mechanisms.

A convenient method of comparison of rheological mechanisms is through their characteristic times. For steady state creep we consider the Maxwell time

$$\tau = \sigma_T / \mu \dot{\epsilon} \quad (53)$$

where $\dot{\epsilon}$ is the strain rate. Reviews of possible creep mechanisms are provided by Weertmann (1970), Stocker and Ashby (1973) and Poirier (1976). For our purposes we shall compare three basic mechanisms: diffusional creep, dislocation creep controlled by intragrain recovery, and dislocation creep controlled by cell wall recovery.

For diffusional creep we use the Nabarro-Herring creep equation in the form

$$\dot{\epsilon}_{NH} = C_{NH} \frac{D_S}{L^2} \frac{\sigma_T \Omega}{kT} \quad (54)$$

so that

$$\dot{\epsilon}_{NH} = C_{NH} \left(\frac{\mu}{\sigma_T} \right)^2 \frac{kTb^2 \exp [E_S^*/RT]}{\mu D_{OS} \Omega} \quad (55)$$

Here we have assumed the cell walls to be efficient sources and sinks of vacancies. D_{OS} and E_S^* are the preexponential diffusivity and activation energy for self diffusion, and Ω is the atomic volume. C_{NH} is a constant of order 20 (Stocker and Ashby, 1973). This equation is easily generalized to include Coble creep.

For dislocation creep models we invoke the simple form of Orowan's equation discussed by Poirier (1976). At steady state, the hardening rate is exactly balanced by the recovery rate and the strain rate is expressed by

$$\dot{\epsilon} = \rho_m b \frac{\Lambda}{d} V \quad (56)$$

Here Λ is the mean free path of the dislocation; d is the distance covered at the rate controlling speed V . Most models assume that $V = V_c$, the climb velocity, and d is the distance covered by climb.

Takeuchi and Argon (1976b) have proposed a model where glide and climb are equally difficult, due to the drag of a Cottrell atmosphere by edge segments. In that case the mean free path Λ is about equal to the critical length $\bar{\ell}$ and so is d . An upper bound to the creep rate, and thus a lower bound to the Maxwell time is obtained by taking $V = V_c$, and we may use (e.g., Hirth and Lothe, 1968)

$$V_c = 2\pi \frac{\sigma_T \Omega_v}{kT} \frac{D_{os} \exp [-E_s^*/RT]}{\lambda_v} \quad (57)$$

Here Ω_v is the volume of a vacancy, and λ_v is a scale length associated with vacancy diffusion, of the form

$$\lambda_v \sim b \ln(r_2/r_1) \quad (58)$$

where r_1 and r_2 are inner and outer cutoff radii (e.g., Hirth and Lothe, 1968; Takeuchi and Argon, 1976b; Poirier, 1976). Typical values of the ratio r_2/r_1 for intragrain processes are of the order of 10^4 , and the Maxwell time is found to be

$$\hat{\tau}_{IG} = C_{IG} \left(\frac{\mu}{\sigma_T} \right)^2 \frac{kT b^2 \exp [E_s^*/RT]}{\mu D_{os} \Omega_v} \quad (59)$$

which is of the same form as (55), but where the constant C_{IG} is now of order unity. This mechanism is thus more efficient than the generalized Nabarro-Herring diffusion. The estimate (59) may be decreased further by $\frac{d}{\Lambda} \sim \frac{\bar{\ell}}{\Lambda}$ if glide is somewhat easier than climb and the mean free path of intracell dislocations is longer than $\bar{\ell}$. But in that case we rapidly reach the point where many, if not most dislocations actually collide with cell walls. Then a more appropriate model is one where recovery in subgrain boundaries plays a specific role. Such models have been reviewed by Weertman (1972) and by Poirier (1976), and a brief

discussion is given by Minster and Anderson (1980). For Weertman's (1972) model with dislocation pile-ups, the Maxwell time $\hat{\tau}_{pu}$ is given by (59) where the proportionality constant is replaced by

$$C_{pu} = 1/0.006K_s^3 \quad (60)$$

Alternative models have been proposed which yield a stronger stress dependence of the creep rate. However, as noted by Weertman (1972) and Poirier (1976) they usually stem from ad-hoc modifications of the σ^3 creep law which arise naturally under minimal assumptions. A model which involves explicitly the microstructural constant K is that of Gittus (1976a). The following is a simplified treatment of it, adapted for our purposes.

The mean free path of mobile dislocations is bounded from above by the subgrain size \bar{L} . In the limiting case where recovery takes place exclusively by climb in cell walls, we actually take $\Lambda = \bar{L}$. The mean separation between dislocations in cell walls is $r_w = \bar{L}/K^2$, and Gittus (1976a) gives the following expression for the steady-state creep rate

$$\dot{\epsilon} = - \frac{dr_w}{d\epsilon} / \frac{dr_w}{d\epsilon} = - v_c / (dr_w/d\epsilon)$$

This is equivalent to (56) if one notes that for each length \bar{L} of dislocation entering the cell walls after sweeping the cell cross section, annihilation required to keep a constant density in the wall takes place by climb over a distance

$$d = \delta r_w \approx r_w^2 / \bar{L} \sim \bar{L} / K^2 \quad (61)$$

In addition, climb in the cell walls may take place under conditions of jog under-saturation in vacancies (e.g., Friedel, 1964; Hirth and Lothe, 1968); In that case, (58) must be replaced by (e.g., Poirier, 1976)

$$\lambda_v \sim 2\pi b c_j^{-1} = 2\pi b \exp [E_j/RT] \quad (62)$$

where c_j is the jog concentration along the dislocation line and E_j is the jog formation energy. The Maxwell time is found to be

$$\hat{\tau}_{cw} = C_{cw} \left(\frac{\mu}{\sigma_T} \right)^2 \frac{kT b^2 \exp [(E_s^* + E_j)/RT]}{\mu D_{os} \Omega_v} \quad (63)$$

where $C_{cw} \sim 3/K^4$. Cell wall recovery is therefore a more efficient mechanism, and is a high temperature mechanism since it possesses a higher effective activation energy.

In the cell wall model of Gittus (1976a) the force causing climb is associated with the self stress of the boundary network. Climb takes place so as to shorten the total dislocation length of the boundary and thus reduce the energy of the boundary. In this case, σ_T must be replaced in (57) by $\mu b/2r_w$. This mechanism is the more efficient one when

$$b/2r_w > \sigma_T/\mu \quad (64)$$

This constraint is satisfied for $K^2 > 2K_s$. In that case, the estimate (63) for the Maxwell time remains valid, with a new value of the constant

$$C_{cw} \sim 2K_s^3/K^6 K_m^2 \quad (65)$$

The expression (57) for the climb velocity must be modified somewhat when the contribution of core diffusion is taken into account and when the wall dislocations are straight, with few geometrical jogs. In that case, the appropriate expression is (e.g., Hirth and Lothe, 1968, p. 528)

$$V_c = 4\pi \frac{\sigma_T \Omega_v}{kT} \frac{D_{os} \exp [-(E_s^* + E_j - \Delta E^*/2)/RT]}{b \ln (\bar{z}/b)} \quad (66)$$

Here, ΔE^* is the difference between the activation energies for bulk diffusion and core diffusion, and \bar{z} is the mean free path of vacancies along the dislocation line

$$\bar{z} \sim b \sqrt{2} \exp [\Delta E^*/2RT] \quad (67)$$

Expression (66) holds when jog spacing is larger than \bar{z} , that is when $E_j > \Delta E^*/2$; in other words, it assumes undersaturation. It is easy to see that use of (66) yields again a Maxwell time of the form (63), although the activation energy is somewhat smaller. The constant C_{cw} is not very different from (65):

$$C_{cw} \sim \frac{1}{2\pi} \ln(\bar{z}/b) K_s^3 / K_m^6 K_m^2 \quad (68)$$

All the mechanisms considered so far (eqs. 55, 59, 63) lead to Maxwell times proportional to σ_T^{-2} ; in other words the creep rate, $\dot{\epsilon}$, varies as σ_T^3 in each case, and the main sources of variation among these models lie in the different constants and activation energies. A significantly different behavior obtains when the Gittus cell wall model is adopted and climb is controlled by double jog nucleation. Indeed, in this model, the dislocation segments in the cell wall networks have a length r_w which may be shorter than thermal jog separation. In that case the climb velocity (66) must be multiplied by $r_w c_j / b$ (Hirth and Lothe, 1968, p. 528), and σ_T^2 dependence of the creep rate results (Minster and Anderson, 1980). Note that this circumstance implies a high activation energy, and that $\hat{\tau}$ is only proportional to σ_T^{-1} . One might therefore expect this mechanism to dominate at high temperatures and low stresses, but this in turn would imply high thermal jog densities and longer dislocation segments, which might lead to a contradiction. Thus the existence of a domain in (T, σ_T) space where this mechanism dominates depends on whether the inequality $r_w < b c_j^{-1}$ can be satisfied without violating microstructural scaling laws.

This can be written

$$K^2 > K_s \frac{\mu}{\sigma_T} e^{-E_J/RT} \quad (69)$$

which places a lower bound on the stress and/or an upper bound on the temperature if the other parameters are known. In that case we have

$$\left. \begin{aligned} \hat{\tau}_{sq} &= \hat{\tau}_{cw} \frac{K^2}{K_s} \exp [E_J/RT] \\ C_{sq} &= \frac{K^2}{K_s} C_{cw} \end{aligned} \right\} \quad (70)$$

For applications to the earth, we must correct the Maxwell time expression given above for the effect of confining pressure. This correction term is unfortunately quite uncertain. We shall assume that, for practical purposes, the only effect is to increase the effective activation energy by PV^* , where P is the pressure and V^* is an activation volume. In the absence of a simple and reliable theory for V^* when core diffusion takes place, it seems unjustified to attempt a more sophisticated treatment.

IV. APPLICATIONS AND DISCUSSION:

In view of the models presented above, attenuation and creep properties may be closely connected via the dislocation microstructure. We shall use the hypothesis that a single microstructural model explains both aspects of the rheology to place constraints on the model parameters.

1) Constraints on creep models

The most stringent and useful constraints we can place on the various creep models outlined above is that they should satisfy laboratory data on olivine. These data have been summarized by Kohlstedt and Goetze (1974), Durham *et al.* (1977) and Goetze (1978). The range of stresses for which experimental data

are available is 10^2 - $5 \cdot 10^4$ bars, but the class of models which we consider here is probably only applicable for stresses smaller than 2 kbars (Goetze, 1978; Kohlstedt, 1979). Furthermore, since we are interested in large regions of the mantle where the tectonic stress is probably only a few bars, we must assume that extrapolation of laboratory trends to low stresses is possible, using the scaling laws described earlier.

Based on the general aspect of the microstructure, and on some observations on dislocation glide, Durham et al. (1977), and Goetze (1978) suggest that Takeuchi and Argon's (1976b) creep model (e.g., eq. 59) may be appropriate for laboratory deformed olivine, in the range ~ 100 -2000 bars. The comparison is qualitative, however, and no numerical comparison was given. We have already shown (Anderson and Mieser, (1980b), that a straightforward application of Gittus' (1976a) creep model could explain observations quantitatively. In this paper, we consider a more general class of models and compare them systematically against various observational constraints, starting with direct estimates of some physical parameters.

a) Self diffusion: When multi-species coupled diffusion takes place, self diffusion is largely controlled by the bulk diffusion of the slowest moving species (e.g., Stocker and Ashby, 1973). In silicates, this has long been thought to be oxygen (e.g., Ashby and Verrall, 1978; Sammis et al., 1977). A recent estimate of the diffusivity of oxygen in forsterite is (Reddy et al., 1980)

$$D(O) = 3.5 \cdot 10^{-3} \exp[-89000/RT] \text{ cm}^2/\text{sec}$$

Recently, however, a lower diffusivity has been found for silicon (Jaoul et al., 1979; Pommellec et al., 1980)

$$D(Si) = 1.5 \cdot 10^{-6} \exp[-90000/RT] \text{ cm}^2/\text{sec}$$

In this paper we shall consider either alternative to be possible and present results for both cases. In Mg_2SiO_4 , the appropriate atomic volume Ω appearing in (55) is $\frac{1}{4}$ the molecular volume ($7.2 \text{ cm}^3/\text{mole}$) if oxygen is the controlling species, and the total molecular volume ($28.8 \text{ cm}^3/\text{mole}$) if silicon is the controlling species (Stocker and Ashby, 1973).

Undoubtedly a similar distinction should be made about the vacancy volume Ω_v in the dislocation creep models. Such differences are rather trivial, however, compared with uncertainties in the other parameters. We shall make the simple choice

$$\left. \begin{aligned} E_s^* &= 90 \text{ kcal/mole} \\ D_{os} &= \begin{cases} 3.5 \cdot 10^{-3} \text{ cm}^2/\text{sec} & (\text{oxygen}) \\ 1.5 \cdot 10^{-6} \text{ cm}^2/\text{sec} & (\text{silicon}) \end{cases} \\ \Omega_v &\approx b^3 \\ b &\sim 7 \cdot 10^{-8} \text{ cm} \quad (\text{Stocker and Ashby, 1973}) \end{aligned} \right\} \quad (71)$$

b) Creep activation energy: The various models of dislocation creep which we have at our disposal entail activation energies which result from combinations of poorly known quantities, such as jog formation energy, etc... . On the other hand, the creep activation energy for olivine at high temperature has been estimated from laboratory observations. Recent interpretations of experimental data converge to $125 \pm 3 \text{ kcal/mole}$ (Kohlstedt and Goetze, 1974; Durham and Goetze, 1977; Ashby and Verrall, 1978; Goetze, 1978).

Our approach is to assume that the creep activation energy is $E_c^* = 125 \text{ kcal/mole}$ and to consider the variation of unknown quantities subject to this constraint. Thus for cell-wall climb under applied stress (eq. 63) we have

$$E_s^* + E_j = 125 \quad ; \quad E_j = 35 \text{ kcal/mole} \quad (72)$$

For cell-wall climb under self-stress, and core diffusion (eq. 65).

$$E_j - \Delta E^*/2 = 35 \text{ kcal/mole} \quad (73)$$

Here ΔE^* is the difference between the activation energy for bulk diffusion and that for core diffusion. For metals, ΔE^* is $1/3 E_s^*$ to $1/2 E_s^*$ in many cases (e.g., Hirth and Lothe, 1968). On the other hand, we have argued (Anderson and Minster, 1980b) that ΔE^* may be close to zero for olivine since activation energies for hot pressing experiments (Schwenn and Goetze, 1978) and dislocation loop mobility (Goetze and Kohlstedt, 1975) do not yield activation energies much lower than E_s^* and E_c^* , respectively.

For our purposes, we shall consider the entire range $0 \leq \Delta E^* \leq 1/2 E_s^*$. In the case of the σ^2 creep law (eq. 70), the constraint (73) must be rewritten as

$$2E_j - \Delta E^*/2 = 35 \text{ kcal/mole} \quad (74)$$

Equations (73) and (74) lead to the following respective ranges for the jog formation energy E_j :

$$35 < E_j < 58 \text{ kcal/mole} \quad (75)$$

$$17 < E_j < 29 \text{ kcal/mole} \quad (76)$$

These ranges indicate much higher values than for metals (e.g., Friedel, 1964), an acceptable conclusion in view of the greater cell sizes, and the higher Peierls energies involved in silicates. These values may also be compared with the estimate of 26 kcal/mole for the kink energy suggested by Stocker and Ashby (1973); jog energies should indeed be greater than kink energies (Hirth and Lothe, 1968).

The ranges (75) and (76) involve much smaller values than the geometrical estimates of order $0.1 \mu b^3 \sim 100$ to 300 kcal/mole (Friedel, 1964). Geometrical estimates are admittedly very uncertain (Hirth and Lothe, 1968), even in the case of the simplest metallic crystal structures. In the absence of a suitable theory for silicates, we hypothesize that the discrepancy between E_c^* and E_s^* is an empirical measure of the jog formation energy, subject to the constraint equations (73) or (74) if core diffusion takes place.

c) Microstructural constants. The scaling constants K_s and K_m can be estimated directly from the observations of Durham et al. (1977). Again these estimates are subject to fairly large uncertainties, and there is no guarantee that they can be used for extrapolation to mantle conditions. We take $K_s = 15$ and $K_m = 10$; these values lie in the lower range of observations, and we have already argued that they may be appropriate. The constant K will be treated as a model parameter in our discussion. Domains of validity of the various creep models can be summarized as follows:

- For cell-wall climb under self stress instead of applied stress (eq.64)

$$K^2 > 2K_s \quad (77)$$

- For σ^2 creep law to be permissible (eq. 69)

$$K^2 > K_s \frac{\mu}{\sigma_T} \exp [-E_j/RT] \quad (78)$$

- An additional constraint must be placed on K for cell-wall recovery models with climb under jog undersaturation in vacancies. It places an upper bound on dislocation separation in the walls: $\frac{r_w}{b} = n_w < n_c$, where n_c is a critical number of lattice spacings of the order of $\exp [E_j/RT]$, which is large in the present applications. It is commonly assumed that saturation occurs if the separation is of the order of $10^{1/4} b$ -- e.g., in subgrains -- (Friedel, 1964).

We shall assume, rather arbitrarily, that n_c is at least a factor of 10 smaller ($n_c < 1000$), although this concept is not very clear. If the transmission electron micrographs presented by Durham et al. (1977) are assumed to be typical, then n_w appears to be of the order of a few hundreds for applied stresses of a few hundred bars. The constraint can be written

$$K^2 > K_s \left(\frac{\mu}{\sigma_T} \right) \frac{1}{n_c} \quad (79)$$

If it fails to be satisfied, then saturation may take place and the climb velocity is of the form (57); jog formation is not a controlling process. On the other hand, as we mentioned earlier, for straight cell wall dislocations, with few geometrical jogs, thermal jog pair nucleation is important and the saturation condition is simply (e.g., Hirth and Lothe, 1968)

$$E_j > \Delta E^* / 2 \quad (80)$$

This is always satisfied under constraint (73), and under constraint (74) it implies $\Delta E^* < 70$ kcal/mole.

d) Maxwell times: As shown by Goetze (1978), creep data on olivine at stresses greater than about 2 kbars are well fitted by a Dorn creep law. Below 2 kbars a power law creep appears to give a reasonable interpretation. Figure 4 shows the creep data of olivine collected for a variety of published sources by Kohlstedt and Goetze (1974), and supplemented with the creep observations of Durham and Goetze (1977) on olivine single crystals with odd orientations (their figure 4). All data have been reduced to a common temperature of 1673°K using an activation energy of $E_c^* = 125$ kcal/mole.

The observations of creep rate below 2 kbars can support either a $\dot{\epsilon} \propto \sigma^3$ or a $\dot{\epsilon} \propto \sigma^2$ interpretation, and the scatter does not allow us to restrict the number of acceptable models on that basis alone. The bulk of the data, and

detailed observations on individual samples by Durham and Goetze tend to support the higher exponent, but the lower stress observations seem to indicate a less sensitive stress dependence of the creep rate. As indicated on the figure, this can result in several orders of magnitude variations in the extrapolated creep rate at 10 bars, in addition to the intrinsic scatter.

Each data point in figure 4 was converted into a preexponential Maxwell time $\hat{\tau}_0$, using a rigidity of 650 kbars. The resulting stress dependence is shown on figure 5, together with the σ^{-2} and σ^{-1} extrapolations to low stress, corresponding to the alternate interpretations of figure 4. Rough ranges for $\hat{\tau}_0$ at 10 bars are:

$$\left. \begin{array}{l} \text{- For } \sigma^3 \text{ creep laws } \hat{\tau}_0 (10 \text{ bars}) \sim 10^{-11} \text{ to } 5 \cdot 10^{-10} \text{ seconds} \\ \text{- For } \sigma^2 \text{ creep } \hat{\tau}_0 (10 \text{ bars}) \sim 2 \cdot 10^{-13} \text{ to } 10^{-11} \text{ seconds} \end{array} \right\} \quad (81)$$

We use these ranges as observational constraints to compare the various models discussed in the previous section.

2) Comparison of creep models

A convenient procedure to compare the various models is to compute the predicted Maxwell time preexponential factor calculated at a fixed temperature (1673°K) and stress (10 bars).

a) Diffusional creep (eq. 55):

According to the preceding discussion, we do not have any free parameter left in this model. If oxygen diffusion is rate controlling, we find $\hat{\tau}_0 (1673, 10) \approx 3.7 \cdot 10^{-3}$ sec, and if silicon diffusion is rate controlling, we find $\hat{\tau}_0 \approx 2.1$ sec. These values are many orders of magnitudes too large and we can eliminate this possibility. In addition, the predicted activation energy is 90 kcal/mole, which is much smaller than the observed value.

b) Intracell recovery creep (eq. 59):

In that case, we find

$$\hat{\tau}_0 \sim 6.2 \cdot 10^{-6} \text{ sec for oxygen diffusion}$$

$$\hat{\tau}_0 \sim 1.4 \cdot 10^{-2} \text{ sec for silicon diffusion}$$

These estimates are still much too large to satisfy laboratory observations, and the predicted activation energy of 90 is too small. We may therefore eliminate this model as well.

c) File-up model (eq. 60):

If oxygen controls self-diffusion, constraint (81) requires $130 \leq K_g \leq 470$ in that case. This range becomes $1700 \leq K_g \leq 6200$ if silicon is rate controlling. These values are much larger than the observed range. Furthermore, the predicted activation energy is 90 kcal/mole. We must therefore turn to a more flexible model.

d) Cell-wall recovery under applied stress (eq. 63):

We now have the parameters K and E_j at our disposal. As pointed out earlier, a jog formation energy of 35 kcal/mole would reconcile the activation energy with the observed value. If oxygen is the controlling species for bulk diffusion, then at 10 bars and 1673°K, $\hat{\tau}_0 \sim 1.84 \cdot 10^{-5}/K^4$; when combined with the constraints (81), this results in $14 < K < 37$. If silicon is the controlling species, we get $96 < K < 256$. Thus, if silicon controls self diffusion, the data require a very pronounced concentration of the dislocation population in the cell walls, ρ_w being two to three orders of magnitudes greater than ρ_m . If oxygen controls self diffusion, then ρ_w is only required to be one order of magnitude or less greater than ρ_m .

In either case, however, K is too large to satisfy constraint (77). In other words, the model is self invalidating if the concept of cell-wall climb under self stress can be applied.

e) Cell-wall recovery under self stress (eq. 64- 65):

Testing this modeling hypothesis proceeds in the same fashion as above. We must postulate a jog formation energy of $E_j = 35$ kcal/mole to reconcile the activation energies. If oxygen controls self diffusion, then at 10 bars and

1673°K, $\hat{\tau}_0 \sim 4.14 \cdot 10^{-4}/K^6$; The observational constraints (81) yield in that case $9 \leq K \leq 19$. If silicon is the controlling species, we get $35 \leq K \leq 68$.

Thus if oxygen is the controlling species, the data imply a rather low range for K. In fact, it would be legitimate to argue that the microstructure would be so poorly defined that an intracell recovery model should really be considered. We have already seen, however, that this model does not appear to be successful.

The hypothesis that silicon-controlled self diffusion limits the recovery rate by climb in cell walls under self stress is a more attractive one. The density of cell wall dislocations ρ_w is predicted to be one order of magnitude or more greater than the density of intracell, mobile dislocations ρ_m , in accordance with the premises of this model. This model cannot be rejected by our testing procedure.

f) Cell wall recovery controlled by double jog nucleation and core diffusion (eqs. 66-68):

This model is a generalization of the previous one. We have now the extra parameter ΔE^* at our disposal. If we let ΔE^* vary from zero to $1/2 E_s^*$, the corresponding variation of K, as implied by the constraints (81), is shown on figure 6. The results are shown under the alternate hypotheses that oxygen or silicon controls self diffusion.

Once more, the results for oxygen tend to conflict with the premises of the microstructural model, whereas the results for silicon yield a self consistent picture, except possibly at very low stresses of the order of one bar, for which dislocation spacing in cell walls is large even with sizable values of K. This model is thus an acceptable alternative to the previous one, especially if further experiments should indicate a low activation energy for core diffusion, and a concomitantly high jog formation energy.

The presently available data, although rather limited and indirect, tend to point to low values of ΔE^* (Anderson and Minster, 1980b); in that case the approximate range is $40 < K < 80$, pointing to a sharply defined microstructure.

g) σ_T^2 creep law (eq. 70):

This law applies to a cell-wall model where cell wall dislocation segments are shorter than the thermal jog separation. This leads to the constraint (78), and interpretation of the observations in terms of this rheology leads to the second set of bounds on $\hat{\tau}_0$ (1673,10) in (81). If oxygen diffusion controls the self diffusion rate, then this model is unacceptable and must be rejected, as can be seen on figure 7; It does not satisfy (78) for admissible core diffusion activation energies. If silicon is the controlling species, then once more a range of satisfactory values of K is obtained. The model is generally associated with quite low values of E_j , however, and is also incompatible with our conjecture that ΔE^* is small. We must therefore consider it to be less satisfactory than the previous ones.

3) Creep in the mantle

The systematic comparison of available models which we just performed does not yield a unique acceptable model for low-stress, high-temperature creep. However, two general models satisfy all of our criteria in a self consistent fashion. Both involve cell wall recovery under self stress, both assume that silicon controls self diffusion, and both can be accommodated by the same microstructure, with $40 \leq K \leq 70$; either model constitutes a generalization of the creep model originally developed by Gittus (1976a). Their only major difference is that core diffusion is ignored in one case, and accounted for in the other. Note that both models do not quite coincide for $\Delta E^* = 0$, due to various approximations made in estimating the climb velocity (e.g., Hirth and Lothe, 1968).

In order to assess the applicability of our model to mantle rheology, we have calculated the Maxwell times for a range of applied stress from 1 to 1000 bars, as a function of temperature, and for preexponential factors compatible with laboratory observations. For simplicity we have chosen $\hat{\tau}_0 \sim 7 \cdot 10^{-11}$ sec at 10 bars, noting however that laboratory evidence can allow for values about five times larger or smaller. This in turn corresponds to $K \sim 50$, which means that the total length of dislocations in cell walls is 25 times greater than the total length of intracell dislocations.

The results are displayed on figure 8. Also shown is a box outlining a plausible range of mantle environments for comparison only (temperatures from 1000°C to 1800°C; viscosity from 10^{19} to 10^{24} poises). Thus the model can easily accommodate geophysical observations in a quantitative sense. This calculation ignores the effect of confining pressure, however, and this brings a new complication to the problem.

In a multispecies diffusion situation, the total activation volume for diffusion of the i^{th} species is (e.g., Stocker and Ashby, 1973)

$$V_i^* = \frac{\alpha V_A + \beta V_B + \gamma V_C + \delta V_D + \dots}{\alpha + \beta + \gamma + \delta + \dots} + V_m^i \quad (82)$$

where $\alpha, \beta \dots$ are stoichiometric coefficients; $V_A, V_B \dots$ are atomic volumes of individual species; V_m^i is the activation volume for motion of the i^{th} species, which we assume to be close to an atomic volume. For Mg_2SiO_4 , this leads to $11 \text{ cm}^3/\text{mole}$ for oxygen, and about $4 \text{ cm}^3/\text{mole}$ for silicon. The preferred ranges of values of Sammis *et al.* (1977) for the mantle decrease from 11 to $\sim 6 \text{ cm}^3/\text{mole}$ for the upper mantle, and from 6 to $3 \text{ cm}^3/\text{mole}$ for the lower mantle. They point out that this bounds the total variation of viscosity across the transition region (300-1000 km) to be less than two orders of magnitude. This argument was used in reverse by Anderson and Minster (1980a), based on the modeling work of

Peltier (1980), to argue for an effective activation volume between 4 and 9 cm³/mole.

If we ignore for the moment the pressure dependence of the activation volume, the estimates for silicon and oxygen given above have an interesting and potentially important implication. Should silicon be the controlling species, then the pressure correction to the effective creep activation energy is about 0.1 P kcal/mole, where P is in kilobars; this correction is about 0.27 P kcal/mole if oxygen is the controlling species. If we now fix the microstructural model, the Maxwell time preexponential factors under both hypotheses are practically in the ratio of the diffusivities. At zero pressure this ratio is essentially independent of temperature because the activation energies are almost identical. According to our systematic evaluation of creep models, oxygen diffusion is then too rapid to satisfy the laboratory observations, and silicon diffusion appears to be rate controlling. The effect of pressure may reverse these roles, as shown on figure 9. We calculated Maxwell times, for a fixed load of 10 bars, ($\hat{\tau}_0 = 7 \cdot 10^{-11}$ for silicon diffusion), under the alternate hypotheses that silicon or oxygen are the controlling species, and for confining pressures up to 300 kbars. Because of the larger activation volume assumed for oxygen diffusion, we find that oxygen becomes the slower species at high pressure for a fixed temperature. As an indication of mantle conditions, we considered a geotherm with a linear temperature gradient of 0.3 °C/km, and a temperature of 1700°K at 400 km depth, and plotted the corresponding trajectory on figure 9. The switch over from silicon controlled diffusion takes place at a pressure between 100 and 200 kbar (300 to 600 km depth).

Activation volumes are expected to decrease with increasing pressure based on an elastic continuum model (e.g., O'Connell, 1977; Sammis *et al.*, 1977).

In applying (82), it is clear that the activation volume for silicon diffusion is controlled in turn by the much larger atomic volume of oxygen. As a result,

it can be expected that both estimates of the activation volume might decrease at depth in about the same proportion. This will have two consequences:

- 1) The switch over from silicon controlled diffusion to oxygen controlled diffusion will happen at greater pressure and thus greater depth, and
- 2) The smaller activation volume in the lower mantle will tend to limit the variations of apparent viscosity with depth (Sammis et al., 1977).

These comparisons are very crude, and the results can vary considerably with model parameters. We have ignored chemical variations, changes in lattice structure with pressure, effects of water content on the activation energy... etc. Our microscopic models are probably not yet precise enough to support such sophistication. However, some general inferences can be made, which are robust with respect to the variations in interpretive models. For example, at mantle temperatures, very low effective viscosities (as low as 10^{15} poises) would be observed under loads of 1 kilobar. Thus the model precludes the persistence of such loads for times longer than the corresponding Maxwell time ($\sim 10^3$ sec). Loads of the order of 100 bars might explain the low apparent viscosities inferred by Nur and Mavko (1974) on the basis of post seismic rebound data. On the other hand, persistent loads of the order of 10^3 bars can be sustained by a cold lithosphere over geological times (e.g., Anderson and Minster, 1980a; Minster and Anderson, 1980). Reinterpretation of isostatic rebound data in terms of a phenomenological power-law flow compatible with our models was performed by Crough (1977). His analysis is a particularly striking illustration of the tradeoffs between temperature, confining pressure, and applied load of the kind shown in figures 8 and 9. His results, for an applied load of 10 bars, yield Maxwell times of $3.5 \cdot 10^8$ sec for the Canadian shield and $1.7 \cdot 10^7$ sec for Bonneville. As seen on figure 9, this is in good quantitative agreement with the predictions from the microscopic model.

4) Constraints on attenuation

For the purposes of discussing attenuation, we may recast equation (9) in a form comparable to the expressions for the Maxwell time by introducing the critical length ℓ_c (e.g., Figure 3):

$$\tau = C_Q \left(\frac{\mu}{\sigma_T} \right)^2 \frac{kT \exp[E_Q^* / kT]}{\mu D_{oQ} \lambda} \quad (83)$$

$$C_Q = \frac{2}{\pi^2} \left(\frac{\ell}{\ell_c} \right)^2 \quad (84)$$

where ℓ_c is the critical length associated with the long term background ("tectonic") stress σ_T . The most interesting implication of this formalism is, of course, that in order to insure consistency with the argument leading to (51), we must now postulate a very narrow distribution of lengths, clustered about the value $\bar{\ell} = 1.66 \ell_c$. This has several important consequences.

The first and most straightforward is that the relaxation strength is given by (16), and if the scaling law (51) holds, Δ is of the order of 10% and is independent of stress.

The second consequence is that the absorption band itself depends rather strongly on the background tectonic stress. It shifts to high frequency with increasing stress and to low frequency with decreasing stress. Comparison of (83) with the Maxwell time yields in fact

$$\tau \sim \frac{C_Q}{C_{cw}} \frac{b}{\lambda} \frac{D_{os}}{D_{oQ}} \exp \left[(E_Q^* - E_C^*) / RT \right] \hat{\tau}_{cw} \quad (85)$$

Thus, given microscopic models for creep and attenuation - in particular, given the diffusivities and activation energies -, we have a formal connection between steady state creep, attenuation and tectonic stress, through the microstructure. This opens the possibility of formalizing the empirical correlations studied for example by Anderson (1966), Meissner and Vetter (1979) and Berckhemmer et al. (1979) within the framework of a physical model.

The third major consequence of requiring the microstructure to be compatible with the creep model is that a distribution of lengths is no longer available. Thus eq. (12) cannot be at the source of a broad absorption band. To get a spread of preexponential factors, we must turn to either a distribution of D_{oQ} or of λ . The alternative, of course, is to rely on a distribution of activation energies to broaden the absorption band. In that case, the width and intensity of the band depends mainly on temperature, but its position along the frequency or temperature axis depends on the tectonic stress σ_T .

Numerous authors have considered diffusion controlled dislocation damping as a possible mechanism for anelastic attenuation at low frequencies. A fairly recent treatment is that of Simpson and Sosin (1972). Some of the main alternatives are listed below.

a) Peterls barrier model of the Bordoni peak

A Peterls barrier model of the Bordoni peak gives a relaxation time of the correct form. If we use the simplified theory of Hirth and Lothe (1968, p. 500), the activation energy is $2E_k$, where E_k is the kink formation energy, estimated to be ~ 26 kcal/mole by Stocker and Ashby (1973). The preexponential diffusivity is $D_{oQ} \sim v b^2$ where v is an atomic frequency of the order of 10^{13} sec^{-1} , so that $D_{oQ} \sim 10^{-2} \text{ to } 10^{-2} \text{ cm}^2/\text{sec}$. The scale length λ is found to be $\lambda \sim c_Q \bar{\epsilon} (\mu/\sigma_T)^2 (\sigma_i/\mu)$, where σ_i denotes the internal stress. For intragrain processes, with few dislocations, σ_i is expected to be controlled mainly by the line tension (Gittus, 1976a), and thus to be comparable to σ_T . λ is therefore of order $\bar{\epsilon}\mu/\sigma_T$ and τ_0 is of the order of $10^{-15} \text{ to } 10^{-16}$ seconds, and is practically independent of σ_T . We have therefore a high frequency, low temperature mechanism, which does not operate in the seismic band and in the mantle. A more detailed review of the Bordoni peak is given by Nowick and Berry (1972).

b) Glide controlled by kink diffusion

Glide controlled by kink diffusion (Hirth and Lothe, 1968, p 497) might be appropriate in view of the high Peierl energy of olivine (e.g. Gueguen, 1979). For an initially straight segment of length $\bar{\ell}$, bowing out by kink pair generation and diffusion we have

$$\lambda \sim \frac{2 b \bar{\ell}}{\bar{\ell} + b \exp [E_k/RT]} \quad (86)$$

$$D_Q \sim v b^2 \exp [-E_k/RT] \quad (87)$$

Two circumstances may arise, depending on which term dominates the denominator of (86).

Let us assume, for the sake of argument, that $E_k = 26 \text{ kcal/mole}$ (Stocker and Ashby, 1973), and that $\sigma_T = 10 \text{ bars}$. Then, for temperatures lower than the transition temperature $T_t \approx 1120^\circ \text{K}$ we have $\lambda \sim 2 \bar{\ell} \exp [-E_k/RT]$. The effective activation energy is then $E_Q^* \sim 2 E_k \sim 52 \text{ kcal/mole}$, and we have $\tau_0 \sim 10^{-12} \text{ sec}$. Above T_t , we have $\lambda \sim 2b$, $E_Q^* \sim 26 \text{ kcal/mole}$, and $\tau_0 \sim 10^{-7}$. In either case this yields an absorption bank at much higher frequency than the seismic band. It must be recognized, however, that the kink formation energy is very uncertain, and that the transition temperature is very sensitive to both E_k and σ_T , as shown in Table 1. Thus, for $\sigma_T = 10 \text{ bars}$ and $E_k = 35 \text{ kcal/mole}$, we find $\tau_0 \sim 5 \cdot 10^{-12} \text{ sec}$, $E_Q^* \sim 70 \text{ kcal/mole}$, and the absorption band approaches 1 Hz near 1500°K and longer periods at lower temperatures. This mechanism is therefore a potential candidate, particularly in regions where the stress is fairly high and the temperature fairly low, such as in the lithosphere.

c) Glide of jogged screw dislocations

Yet another alternative is provided by the glide of jogged screw dislocations, where the jogs can only move by the production or absorption of point defects (Hirth and Lothe, 1968, p 535). In that case the diffusivity D_{oQ} is that for self diffusion D_{os} , which in turn is related to the diffusion of oxygen or

silicon according to our discussion of creep. For small stresses we have $\lambda = 4\pi b/c_j$ where c_j is the jog concentration. Two cases arise; either the jogs are geometrical, and λ is of order b to within one or two orders of magnitude, E_Q^* is then $\sim E_s^* = 90$ kcal/mole; or the dislocation segments lie in Peierls valleys and we must consider thermal jogs (Gittus, 1976a). In the latter case λ is $4\pi b$ and the activation energy is $E_Q^* \sim E_s^* + E_j \geq 125$ kcal/mole in accordance with the creep model. In either case, it is easy to verify that the retardation time is many orders of magnitude longer than the seismic periods. For example, under an applied stress of 10 bars, we get $\tau \approx 10^{13}$ sec at 1600°K if silicon controls self diffusion and thermal jogs are the dragging defects. On that basis, Anderson and Minster (1980b) rejected this mechanism as a candidate for seismic attenuation. For the case of geometrical jogs, a lower bound for τ is obtained by taking $\lambda = 4\pi b$ and using the diffusivity of oxygen. Then $\tau \sim 5 \cdot 10^5$ sec at 1600°K and 10 bars. Using silicon diffusivity and/or, taking the effect of pressure into account can easily increase this value by several orders of magnitude. We may conclude that this mechanism might be a candidate for the attenuation of the Chandler wobble, although it is not clear that the anelastic theory of section II still applies when the retardation times become comparable to the Maxwell time for steady state creep.

d) Dragging of point defects

Dragging of an atmosphere of point defects bound to the dislocation is a more versatile and successful model. Original applications to internal friction are due to Weertman (1955), and Friedel et al. (1955). A specific model was proposed by Schoeck (1963) to explain the cold work peak in b.c.c. metals. Further improvements and modifications were subsequently proposed by Barrand and Leak (1964), Gibala (1967), Ino and Sugeno (1967), and more recently by Miner et al. (1976). Covalent crystals were considered by Southgate and Mendelson (1965). Dragging of a Cottrell atmosphere is an essential ingredient of Takeuchi and Argon's (1976) model for steady state

creep. Binding of these defects to the dislocation line is usually assumed to be elastic, although electrical interaction probably is important in ionic crystals at high temperature (Eshelby et al. 1958; Brown, 1961; Menezes and Nix, 1974 a,b).

This class of models has been demonstrably successful in the case of simple crystal structures. We propose to extend it to mantle materials. The point defects which contribute to drag may include self interstitials, impurity interstitials, or substitutional atoms with a slightly different ionic radius if the binding mechanism to dislocations is elastic in nature.

Defects associated with a local charge imbalance (Smyth and Stocker, 1975; Stocker and Smyth, 1978; Stocker 1978) might be involved if electrical interaction is important. Let E_B be the binding energy of the point defect to the dislocation and c_L the bulk (lattice) concentration of defects away from dislocations. Then a very simple model of equilibrium between bound and unbound defects is obtained under the assumption that Fermi-Dirac statistics are applicable (Hirth and Lothe, 1968). The high temperature approximation yields a mean distance between defects along the core (e.g. Miner et al. 1976)

$$\lambda \sim \frac{b}{c_L} \exp [-E_B/kT] \quad (88)$$

where binding energy is of the order of a few kcal/mole for many metals (e.g. Nowick and Berry, 1972). But the analysis leading to (88) assumes implicitly a high level of purity of the material. This might be appropriate for intragrain environments if most impurities eventually migrate to grain boundaries as we have argued before (Anderson and Minster, 1980b). On the other hand, if the binding energy is only 1 e.v., then the exponential is of order 10^{-3} at mantle temperatures, and is thus of the same order or smaller than c_L . The high temperature approximation (88) is no longer valid in that case and we must consider the case where a very large fraction

of core sites are occupied by a dragging point defect. The scale length λ is then comparable to b , and this limit yields an upperbound for τ .

Under these circumstances both D_{oQ} and E_Q^* are effective quantities for the diffusion of defects bound to the dislocation core. At sufficiently high temperatures, where (86) holds, E_Q^* would be augmented by the binding energy. In the absence of a good theory we shall ignore such complications for the present. Diffusivity data which are potentially relevant include the cationic diffusion parameters in oxides, silicates and aluminates compiled by Ahrens and Schubert (1975), and a larger data set for metal oxides compiled by Kofstad (1972). If we restrict our attention to measurements which involve a broad range of high temperatures, typical preexponential diffusivities are in the range $10^{-3} - 10^{-2} \text{ cm}^2/\text{sec}$, although order of magnitude fluctuations are not uncommon. For a tectonic stress of 10 bars, this implies a preexponential retardation time $\tau_o \sim 10^{-6}$ to 10^{-5} seconds. If $\lambda > b$ this estimate should be lower. If we choose $\tau_o = 10^{-6}$ seconds, then in order to bring the absorption band into the seismic range (1 sec to 10^3 sec) at 1600°K , we require $45 \lesssim E_Q^* \lesssim 65$ kcal/mole. An increase of λ to $10^3 b$ changes this requirement to $65 \lesssim E_Q^* \lesssim 90$ kcal/mole. These values must be lowered if we choose a lower reference temperature, or if a lower tectonic stress is assumed. The permissible range encompasses the scatter of activation energies listed by Ahrens and Schubert (1975). It includes the range of estimates of 47-58 kcal/mole for interdiffusion of Mg^{++} and Fe^{++} in olivine (Misener, 1974).

Unfortunately, there is little experimental evidence available to further constrain the class of acceptable models. Jackson (1969) found $\tau_o \sim 4 \cdot 10^{-13}$ sec and $E^* \sim 57$ kcal/mole for an absorption peak near 1 Hz in fine grained olivine. He interpreted it as a grain boundary peak. However, we are interested in larger grain sizes, and higher temperatures, and therefore in the high temperature background attenuation seen in Jackson's data, for which estimation

of the relaxation parameters is difficult (Anderson and Minster, 1980).

Berckhemmer et al. (1979) used linearity to interpret transient creep superposed on a steady state regime, in natural peridotites, in terms of attenuation $Q(\omega)$. However, the transient stress and steady state load used were both in the $1 - 10^2$ bars range; it is not clear whether the superposition of transient and steady state creep can be handled as we have in our model, since the time scales and stress ranges tend not to be so clearly separated. The authors report an apparent activation energy of 30 kcal/mole for $Q(\omega)$, which they interpret as αE_s^* with $\alpha \sim 0.3$ (e.g. Anderson and Minster, 1980a). If instead we choose to interpret this number as E_Q^* , it falls on the low activation energy side of the bulk of cationic diffusion data. This however would be inconsistent with the observed frequency dependence, i.e. $(\omega\tau)^\alpha$ variation of Q in these experiments.

Although we do not have enough experimental constraints at our disposal to propose a better specified model and then test it against geophysical data, we can still use seismological observations to limit the range of permissible models.

5) Absorption band in the mantle

The model affords a large enough number of parameters (including tectonic stress σ_T), which may all vary with position, that there can be no doubt that all available geophysical observations could be explained by it. For purposes of illustration we shall only consider here the tradeoffs between temperature, pressure, and tectonic stress and consider other parameters to be fixed. In particular, we assume a low purity for mantle material, so that $\lambda \sim b$ and $\tau_0 \sim 10^{-6}$ sec at $\sigma_T = 10$ bars and $T \sim 1500^\circ\text{K}$.

At any given point in the mantle, the width of the band is then only controlled by the spectrum of activation energies. Since the strength Δ is fixed to $\sim 10\%$ in this model, the intensity of the absorption band (in the

case $\alpha = 0$, eq. 37) is given by

$$Q_m \sim \frac{2}{\pi \Delta} \frac{\delta E^*}{RT} \quad (89)$$

where δE^* is the range of activation energies. Several authors have argued that a low value of Q_m is required by seismic observations, at least in the regions of the mantle where the absorption band coincides with the seismic band. A value $Q_m \sim 25$ is in good agreement with the seismic data (Solomon, 1972; Anderson and Hart, 1978). Sipkin and Jordan (1979) report a $Q(\text{ScS}) \sim 170$ for periods of 10 sec to 1000 sec. If ScS should spend only one fourth of its travel time in the low Q regions of the earth, then $Q_m \lesssim 40$. Equation (89) allows us to place a limit on the range of activation energies: at mantle temperatures $\delta E^* \lesssim Q_m/2$ (kcal/mole). A range $45 \lesssim E^* \lesssim 60$ kcal/mole is therefore consistent with this constraint and with the laboratory data on cationic diffusion. Note that this yields an absorption band which is only about two decades wide at mantle temperatures. One consequence is that the value of α in (11) is rather immaterial, so that we will choose $\alpha = 0$.

For a temperature of 1500°K the range of retardation times is 3-500 seconds, which lies within the seismic band. An increase of temperature shifts the absorption band to higher frequencies; an increase in pressure has the opposite effect and so does a decrease in tectonic stress. Based on their observation that $Q(\text{ScS})$ increases with frequency in the range 0.1-1 Hz, Sipkin and Jordan (1979) suggest an effective cutoff τ_m for the mantle absorption band averaged by ScS near one second. Comparable conclusions have been reached by other investigators (e.g. Kanamori and Anderson, 1977; Minster, 1978b; Lundquist, 1979). In terms of our model, a high value for $Q(\text{ScS})$ in the 1 Hz band means that this frequency does not lie within the frequency band for an extensive range of depths. The much lower values of $Q(\text{ScS})$ reported by Sipkin and Jordan in the 10-1000 sec band suggest in fact that the absorption band

remains at periods longer than 1 second in spite of increasing temperature with depth.

This may be due to either a decrease in tectonic stress at depth, or to the effect of pressure if the activation volume is large enough. For example a change of one order of magnitude in σ_T shifts the band by two decades in frequency. With an activation energy of ~ 50 kcal/mole and at mantle temperatures, a similar shift is achieved by a temperature change of about 400°C . Thus it may be expected that the stress-temperature tradeoff is most important in regions with a high geothermal gradient and a simultaneous decrease of stress with depth, such as the upper mantle (e.g. Schubert *et al.* 1976). On the other hand, if dynamical transition zones (boundary layers) mark the bottom of convection cells in the mantle (Jeanloz and Richter, 1979) then both temperature and stress increases would tend to combine and cause a rapid shift of the absorption band toward higher frequencies. This might provide a physical interpretation for a low Q zone of the sort hypothesized by Anderson and Hart (1978) at the base of the mantle.

Discussion of the effect of pressure is predicated on the adoption of an activation volume V_Q^* , for which we have no data. For purposes of discussion, let us consider again a geotherm with a linear 0.3°K/km gradient and a temperature of 1700°K at 400 km depth. For a pressure independent activation volume V_Q^* , and at constant tectonic stress σ_T , the effect of pressure will overcome the effect of temperature if

$$\frac{d}{dP} \left[\frac{E_Q^* + PV_Q^*}{RT} \right] \geq 0 \quad (90)$$

or

$$V_Q^* \gtrsim 2.5 \cdot 10^{-2} E_Q^* \quad (91)$$

where V_Q^* is in cm^3/mole and E_Q^* is in kcal/mole. Thus, with a spectrum of activation

energies between 45 and 60 kcal/mole, and the geotherm described above, the absorption band shifts to longer period with increasing depth if $V_Q^* \gtrsim 1.1 \text{ cm}^3/\text{mole}$. In order to illustrate this phenomenon we show in Figure 10 the absorption band and associated dispersion, for a fixed stress $\sigma_T = 10$ bars, at depths of 100, 200..., 500km, for which the assumed temperatures are shown on the figure. V_Q^* was fixed at $4 \text{ cm}^3/\text{mole}$, a value large enough to illustrate the initial shift of the band to high frequency with rapidly increasing temperature, followed by a progressive shift toward longer periods, due to increased pressure.

More complicated scenarios can of course be envisaged, with a spectrum of activation volumes, phase transitions, etc... Some of these refinements have been considered by Lundquist (1979, 1980). They go well beyond our present purposes.

6) High temperature background attenuation (HTB)

We have suggested before (e.g. Anderson and Minster, 1980) that the dominant mechanism of attenuation in the mantle corresponds to the HTB in laboratory experiments. A description of its properties is found in Nowick and Berry (1972). An important, unanswered, question is whether the HTB is anelastic or viscoelastic in nature. The work of Friedel et al. (1955), and more recently the analysis of Woignard (1976) clearly indicate the possibility of a broad, high temperature anelastic peak. Figure 11 shows our model at zero pressure and at frequencies comparable to laboratory experiments. It points to a testable aspect of the model, namely, the development of a peak, at sufficiently low frequency and/or high temperature. Observation of such a peak, in well annealed material deformed under low stress to steady state would not only either provide support for our model or infirm it, but it would yield needed direct estimates of the model parameters.

V. CONCLUSIONS

The main conclusion of this work is that a dislocation microstructure model is capable of simultaneously explaining steady state creep and attenuation in the mantle. Our preferred model involves a sharply organized microstructure, where most dislocations are found in cell walls. Steady state creep is controlled by recovery through climb in the cell walls. Good quantitative agreement with laboratory observations of creep in olivine is obtained if silicon controls self diffusion. However, because of the larger activation volume of oxygen, we expect that oxygen diffusion will become the controlling factor at sufficient depth. We hypothesize that the discrepancy between oxygen or silicon diffusion activation energies and the observed activation energy for creep is a measure of jog formation energy, which is then somewhat greater than 35 kcal/mole, depending on the efficiency of core diffusion.

Attenuation of seismic waves takes place through bowing of the few intracell dislocations, controlled either by kink diffusion (particularly at high frequency) or by the dragging of an atmosphere of point defects bound to the dislocations. Due to the paucity of laboratory observations, the success of this model is judged on more qualitative and circumstantial evidence.

The microstructure depends on the long term tectonic stress, which exerts a strong influence on both creep and attenuation properties. Within the framework of this model, stress, viscosity and Q are related, so that estimating one of these parameters provides constraints on the others. The scaling laws do not favor a wide spread of length scales, so that the relaxation strength is fixed in this model, and is of the order of 10%. A broad absorption band can be achieved with a spectrum of activation energies, but seismological requirements as to the intensity of attenuation in the band limit its width to 2 or 3 decades. The main parameters controlling the position of the low Q

band are temperature, pressure, and tectonic stress. The absorption band coincides with the seismic band in the upper mantle, but shifts to longer periods at greater depths due to the combined effects of increased pressure and possibly lowering the shear stress. It must be noted, however, that sharp shifts to shorter periods are expected in hypothetical boundary layers, due to larger temperature gradients and higher stresses. In the bulk of the mantle, however, seismic frequencies appear to be on the high frequency - low temperature side of the absorption band. The absorption band can also be expected to be broadened in the mantle because of the distributions in D_0 , E^* , $\bar{\epsilon}$ and μ expected for a polymineralic aggregate and the anisotropy of the grains. Each mineral has its own physical properties but, at least in the upper mantle, the total breadth of the band is constrained by the minimum allowable damping.

Our models adopt a very simple view of dislocations in complex crystal structures pertinent to silicates. We have ignored the complications associated with partial dislocations, and the differences between dislocations with different Burgers vectors. A more detailed discussion is provided, for example, by Gueguen (1979) (see also the comment by Poirier at the end of Goetze's (1978) paper). The dislocation model proposed here may be viewed as a possible alternative to grain boundary mechanisms described for example by O'Connell and Budiansky (1977). Its validity must be ultimately tested against further experimental data.

Acknowledgments:

This research was supported by the Earth Sciences Section National Science Foundation Grant No. EAR77-14675, and National Aeronautics and Space Administration Grant No. NSG-7610.

TABLE 1: Transition temperature T_t

σ_T E_k kcal/mole	1 bar	10 bars	100 bars
25	540°K	1080°K	1350°K
35	1250°K	1510°K	1885°K
45	1620°K	1940°K	2420°K

References:

- Ahrens, T. J. and G. Schubert 1975 Gabbro-eclogite reaction rate and its geophysical significance, Rev. Geophys. Space Phys. 13, 383-400.
- Anderson, D. L. 1966 Earth's viscosity, Science 151, no. 3708, 321-322.
- Anderson, D. L., H. Kanamori, R. S. Hart and H. P. Liu 1976 The Earth as a seismic absorption band, Science 196, 1104-1106.
- Anderson, D. L. and R. S. Hart 1978 Attenuation models of the earth, Phys. Earth Planet. Int. 16, 289-306.
- Anderson, D. L. and J. B. Minster 1980a Seismic velocity, attenuation and rheology of the upper mantle, Ann. Geophys., Prof. J. Coulomb Symposium, (in press).
- Anderson, D. L. and J. B. Minster 1980b The physics of creep and attenuation in the mantle, (submitted).
- Ashby, M. F. and R. A. Verall 1978 Micromechanisms in flow and fracture, and their relevance to the rheology of the upper mantle, Phil. Trans. R. Soc. London A 288, 59-95.
- Barrand, P. and C. M. Leak 1964 Precipitation and the deformation damping peak in iron alloys, Acta Metall. 12, 1147-1152.
- Berckhemmer, H., F. Auer and J. Drisler 1979 High-temperature anelasticity and elasticity of mantle peridotite, Phys. Earth Planet. Int. 20, 48-59.
- Brown, L. M. 1961 Mobile charged dislocations in ionic crystals, Phys. Stat. Solidi 1, 585-599.
- Crough, S. T. 1977 Isostatic rebound and power-law flow in the asthenosphere, Geophys. J. R. Astr. Soc. 50, 723-738.
- Durham, W. B. and C. Goetze 1977 Plastic flow of oriented single crystals of olivine, 1, mechanical data, J. Geophys. Res. 82, 5737-5754.

Durham, W. B., C. Goetze and B. Blake 1977 Plastic flow of oriented single crystals of olivine, 2, observations and interpretations of the dislocation structures, J. Geophys. Res. **82**, 5755-5770.

Eshelby, J. D., C. W. A. Newey, P. L. Pratt and A. B. Lidiard 1958 Charged dislocations and the strength of ionic crystals, Phil. Mag. **3**, 75-89.

Friedel, J. 1964 Dislocations, pp. 491. New York: Pergamon Press.

Friedel, J., D. Boulanger and C. Crussard 1955 Constantes élastiques et frottement intérieur de l'aluminium polygonisé, Acta Metall. **3**, 380-391.

Gibala, R. 1967 On the mechanism of the Koster relaxation peak, Acta Metall. **15**, 428-430.

Gittus, J. H. 1976a Theoretical equation for steady-state dislocation creep effects of jog drag and cell formation, Phil. Mag. **34**, 401-411.

Gittus, J. H. 1976b Theoretical value of the ratio (k) of cell diameter to dislocation spacing for a material undergoing dislocation creep, Phil. Mag. **35**, 293-300.

Goetze, C. 1978 The mechanisms of creep in olivine, Phil. Trans. R. Soc. London **288**, 99-119.

Goetze, C. and W. F. Brace 1972 Laboratory observations of high temperature rheology of rocks, Tectonophysics **12**, 583-600.

Goetze, C. and D. L. Kohlstedt 1973 Laboratory study of dislocation climb and diffusion in olivine, J. Geophys. Res. **78**, 5961-5971.

Granato, A. and K. Lucke 1956 Theory of mechanical damping due to dislocations, J. Appl. Phys. **27**, 583-593.

Green, H. W. and S. V. Radcliffe 1972 Dislocation mechanisms in olivine and flow in the upper mantle, Earth and Planet. Sci. Lett. **15**, 239-247.

Gueguen, Y. 1979 High temperature olivine creep: evidence for control by edge dislocations, Geophys. Res. Lett. **6**, 357-360.

Gueguen, Y. and J. M. Mercier 1973 High attenuation and the low-velocity zone, Phys. Earth Planet. Int. 7, 39-46.

Hirth, J. and J. Lothe 1968 Theory of dislocations, pp. 780, New York: McGraw-Hill

Holt, D. L. 1970 Dislocation cell formation in metals, J. Appl. Phys. 41, 3197-3201.

Ino, H. and T. Sugeno 1967 The cold-work damping peak in Alpha-iron, Acta Metall. 15, 1197-1205.

Jackson, D. 1969 Grain boundary relaxation and the attenuation of seismic waves, Ph.D. Thesis, M.I.T., Cambridge, Mass.

Jaoul, O., C. Froideveaux and M. Poumellec 1979 Atomic diffusion of ^{18}O and ^{30}Si in forsterite: implication for the high temperature creep mechanism, (abstract) IUGG XVII General Assembly, Canberra, Australia.

Jeanloz, R. and F. M. Richter 1979 Convection, composition, and the thermal state of the lower mantle, J. Geophys. Res. 89, 5497-5504.

Jeffreys, Sir Harold 1970 The Earth, 5th ed. London: Cambridge University Press.

Jeffreys, H. and S. Crampin 1970 On the modified Lomnitz law of damping, Mon. Not. R. astr. Soc. 147, 295-301.

Kanamori, H. and D. L. Anderson 1977 Importance of physical dispersion in surface-wave and free-oscillation problems, Review, Rev. Geophys. Space Phys. 15, 105-112.

Koehler, J. S. 1952 Imperfections in nearly perfect crystals. New York: Wiley.

Kofstad, P. 1972 Nonstoichiometry, diffusion, and electrical conductivity in binary metal oxides, pp. 382. New York: Wiley-Interscience.

Kohlstedt, D. L. and G. Goetze 1974 Low-stress high-temperature creep in olivine single crystals, J. Geophys. Res. 79, 2045-2051.

Kohlstedt, D. L. 1979 Creep behavior of mantle materials (abstract), IUGG XVII General Assembly, Canberra, Australia.

Liu, H. P., D. L. Anderson and H. Kanamori 1976 Velocity dispersion due to anelasticity; implications for seismology and mantle composition, Geophys. J. R. Astr. Soc. 47, 41-58.

Lundquist, G. M. 1979 The frequency dependence of Q, Ph.D. Thesis, CIRES, University of Colorado, Boulder, Colorado.

Lundquist, G. M. 1980 Constraints on the absorption band model of Q, J. Geophys. Res. (submitted).

Macdonald, J. R. 1961 Theory and application of a superposition model of internal friction and creep, J. Appl. Phys. 3, 2385-2398.

Macdonald, J. R. 1963 Transient and temperature response of a distributed thermally activated system, J. Appl. Phys. 34, 538-552.

Meissner, R. and U. Vetter 1979 Relationship between the seismic quality factor Q and the effective viscosity, J. Geophys. Res. 45, 147-158.

Menezes, R. A. and W. D. Nix 1974a High temperature dislocation mobility in LiF, part I. Charged dislocations in ionic crystals, Mat. Sci. and Eng., 16, 57-66.

Menezes, R. A. and W. D. Nix 1974b High temperature dislocation mobility in LiF, part II. Glide mobility of dislocations at high temperatures, Mat. Sci. and Eng. 16, 67-73.

Miner, R. E., R. Gibala and F. A. Hultgren 1976 An application of the Schoeck theory to the cold-work internal friction peak in iron, Acta Metall. 24, 233-239.

Minster, J. B. 1978a Transient and impulse responses of a one-dimensional linearly attenuating medium - I. Analytical results, Geophys. J. R. Astr. Soc. 52, 479-501.

Minster, J. B. 1978b Transient and impulse responses of a one-dimensional linearly attenuating medium - II. A parametric study. Geophys. J. R. Astr. Soc., 52, 503-524.

Minster, J. B. 1980 Anelasticity and attenuation A. Dziewonski and E. Boschi, (eds.) Proc. Enrico Fermi Intern. Sch. Phys., New York: Academic Press (in press).

Minster, J. B. and D. L. Anderson 1980 Dislocations and nonelastic processes in the mantle, J. Geophys. Res. (in press).

Misener, D. V. 1974 Cationic diffusion in olivine to 1400°C and 35 kbar, Carnegie Inst. Washington Publ., 634, 117-129.

Mukherjee, A. K., J. E. Bird and J. E. Dorn 1969 Experimental correlations for high-temperature creep, A.S.M. Trans., 62, 155-179.

Nowick, A. and B. Berry 1972 Anelastic relaxation in crystalline solids, pp. 677 New York: Academic Press.

Nur, A. and G. Mavko 1974 Postseismic viscoelastic rebound, Science, 183, 204-206.

O'Connell, R. J. 1977 On the scale of mantle convection, Tectonophysics, 38, 119-136.

O'Connell, R. J. and B. Budiansky 1977 Viscoelastic properties of fluid-saturated cracked solids, J. Geophys. Res., 82, 5719-5736.

O'Connell, R. J. and B. Budiansky 1978 Measures of dissipation in viscoelastic media, Geophys. Res. Lett., 5, 5-8.

Peltier, W. R. 1980 Mantle convection and viscosity A. Dziewonski and E. Boschi (eds.) Proc. Enrico Fermi Intern. Sch. Phys., Academic Press, (in press).

Poirier, J. P. 1976 Plasticité à haute température des solides cristallins, Eyrolles, Paris.

Poumellec, M., O. Jaoul, C. Froidevaux and A. Havette 1980 Silicon diffusion in forsterite: A new constraint for understanding mantle deformation, (preprint).

Raleigh, C. B. and S. H. Kirby 1970 Creep in the upper mantle, Mineral. Soc. Amer. Spec. Paper, 3, 113-121.

Reddy, K. P. R., S. M. Oh, L. D. Major, Jr., and A. R. Cooper 1980 Oxygen diffusion in forsterite, J. Geophys. Res., 85, 322-326.

Sammis, C. G., J. C. Smith, G. Schubert and D. A. Yuen 1977 Viscosity-depth profile of the earth's mantle: effects of polymorphic phase transitions, J. Geophys. Res., 82, 3747-3761.

Schoeck, G. 1963 Fricción interna debido a la interacción entre dislocaciones y átomos solutos, Acta Metall., 11, 617-622.

Schubert, G., C. Froidevaux and D. A. Yuen 1976 Oceanic lithosphere and asthenosphere: thermal and mechanical structure, J. Geophys. Res., 81, 3525-3540.

Schwenn, M. and C. Goetze 1978 Creep of olivine during hot-pressing, Tectonophysics, 48, 41-60.

Simpson, H. M. and A. Sosin 1972 Contribution of defect dragging to dislocation damping, I, theory, Phys. Rev. B, 5, 1382-1393.

Sipkin, S. and T. Jordan 1979 Frequency dependence of Q_{ScS} Bull. Seismol. Soc. Amer., 69, 1055-1079.

Smyth, D. M. and R. L. Stocker 1975 Point defects and non-stoichiometry in forsterite, Phys. Earth Planet. Int., 10, 183-192.

Solomon, S. C. 1972 On Q and seismic discrimination, Geophys. J. R. Astr. Soc., 31, 163-177.

Southgate, P. D. and K. S. Mendelson 1965 High-temperature dislocation damping in covalent crystals, J. Appl. Phys., 36, 2685-2692.

Stocker, R. L. 1978 Influence of oxygen pressure on defect concentrations in olivine with a fixed cationic ratio, Phys. Earth Planet. Int., 17, 118-129.

Stocker, R. L. and M. F. Ashby 1973 On the rheology of the upper mantle, Rev. Geophys. Space Phys., 11, 391-497.

Stocker, R. L. and D. M. Smyth 1978 Effect of enstatite activity and oxygen partial pressure on the point-defect chemistry of olivine, Phys. Earth Planet. Int., 16, 145-156.

Takeuchi, S. and A. S. Argon 1976a Steady-state creep of single-phase crystalline matter at high temperature, J. Mater. Sci., 11, 1542-1566.

Takeuchi, S. and A. S. Argon 1976b Steady-state creep of alloys due to viscous motion of dislocations, Acta. Metall., 24, 883-890.

Weertman, J. 1955 Internal friction of metal single crystals, J. Appl. Phys., 26, 202-210.

Weertman, J. 1970 The creep strength of the Earth's mantle, Rev. Geophys. Space Phys., 8, 145-168.

Weertman, J. 1972 High temperature creep produced by dislocation motion, J. E. Dorn Memorial Symposium (Cleveland, Ohio).

Woirgard, J. 1976 Modèle pour les pics de frottement interne observés à haute température sur les monocristaux, Phil. Mag., 33, 623-637.

Figure Captions

- Fig. 1: Sketch of a bowing dislocation of length l strongly pinned at both ends. V is the migration velocity, R_c the radius of curvature.
- Fig. 2: Three examples of absorption band and associated dispersion characteristics, for $\alpha = 0.25$, 0 , and 0.25 respectively. $\tau_n = 1$ sec, $\tau_M = 10^4$ sec. Relaxation spectra have been adjusted so as to yield identical high frequency behavior.
- Fig. 3: Comparison of relaxation time τ and multiplication time t_μ as function of dislocation length normalized to critical length.
- Fig. 4: Steady state creep rate observations in olivine compiled by Kohlstedt and Goetze (1974) (circles) supplemented by observations of Durham and Goetze (1977) (triangles), as a function of applied stress. Data for stresses greater than 2000 bars are shown with smaller symbols.
- Fig. 5: Same data as figure 4, converted to Maxwell times, assuming a rigidity $\mu = 650$ kbars.
- Fig. 6: Structural parameter K as a function of difference between bulk diffusion and core diffusion, for cell wall recovery model controlled by double jog nucleation. Also indicated is the jog formation energy which yields a creep activation energy of 125 kcal/mole (eq. 73), and on the left, the dislocation separation in the cell walls, for various values of the applied stress. Shaded areas indicate range of K values which bracket laboratory data shown on figure 5. Forbidden area for this model (eq. 77) is also indicated.

- Fig. 7: Same as figure 6, for σ^2 creep law. Jog formation energy calculated by equation (74). Forbidden area corresponds to eq. (78).
- Fig. 8: Temperature dependence of Maxwell time for several values of applied load, for a creep model which satisfies laboratory observations with a σ^3 interpretation.
- Fig. 9: Effect of confining pressure on Maxwell times. At pressures greater than 200 kbars, oxygen diffusion becomes slower and controls self diffusion. Simple thermal model of the mantle is shown, and compared with Crough's (1977) estimates for isostatic rebound.
- Fig. 10: Hypothesized mantle absorption band for $\Delta = 10\%$, $\sigma_T = 10$ bars, $45 \leq E_Q^* \leq 60$ kcal/mole, $V_Q^* = 4$ cm³/mole, calculated at pressures of 100 to 500 kbars, for which indicated temperatures were assumed. Also shown are the dispersive properties associated with the absorption band.
- Fig. 11: Temperature dependence of absorption band of fig. 10, for three frequencies appropriate for laboratory, indicating possible interpretation in term of high temperature background attenuation.

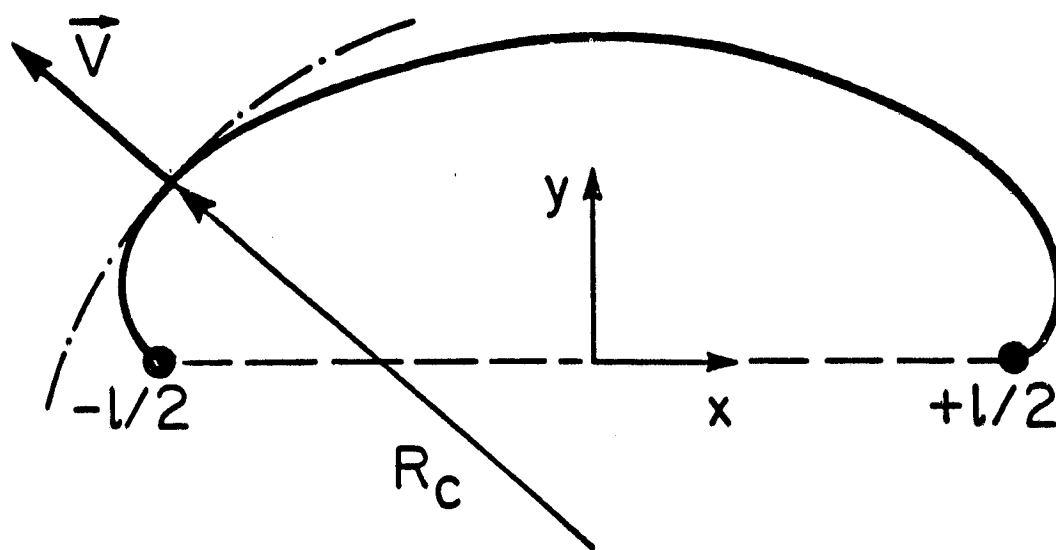


Fig. 1

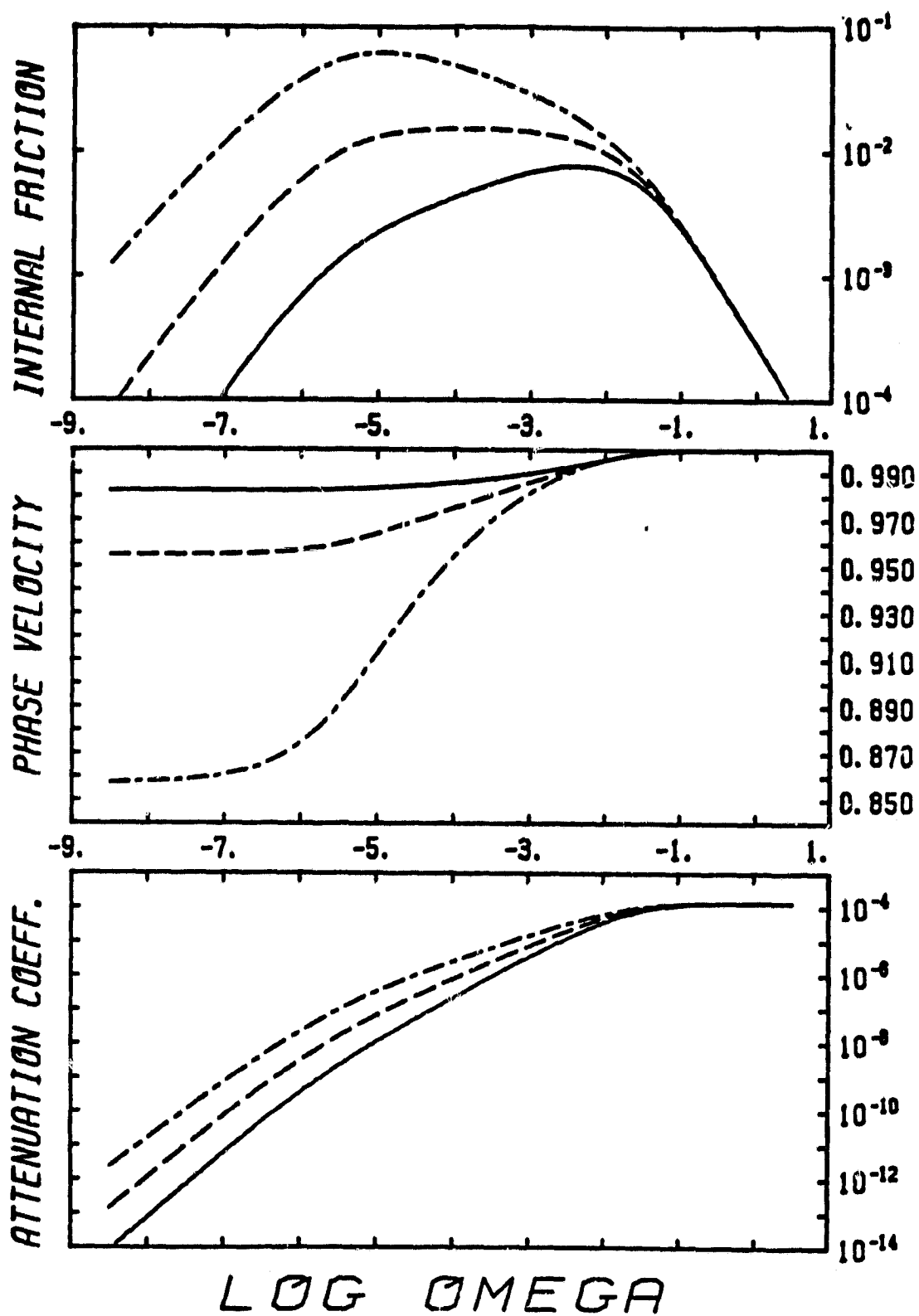


Fig. 2

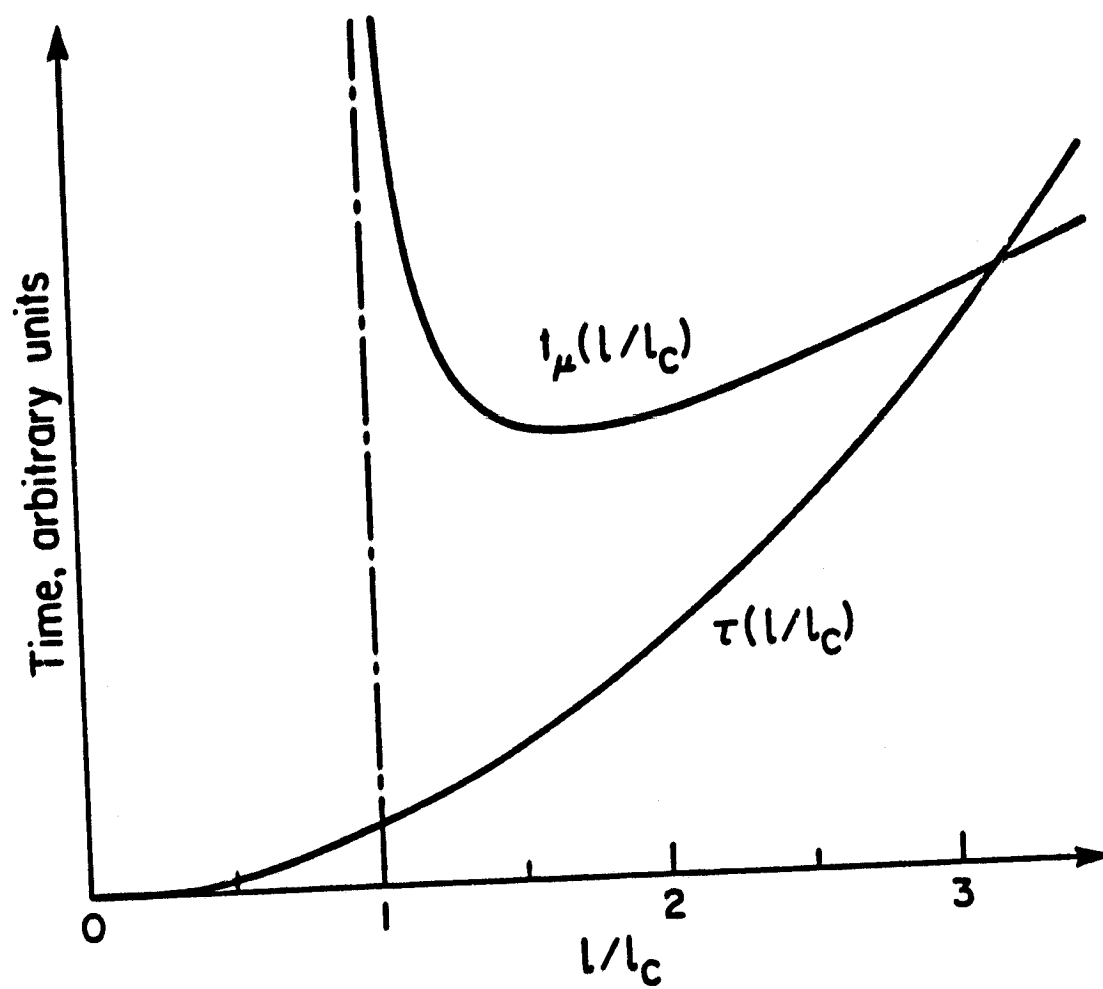


Fig. 3

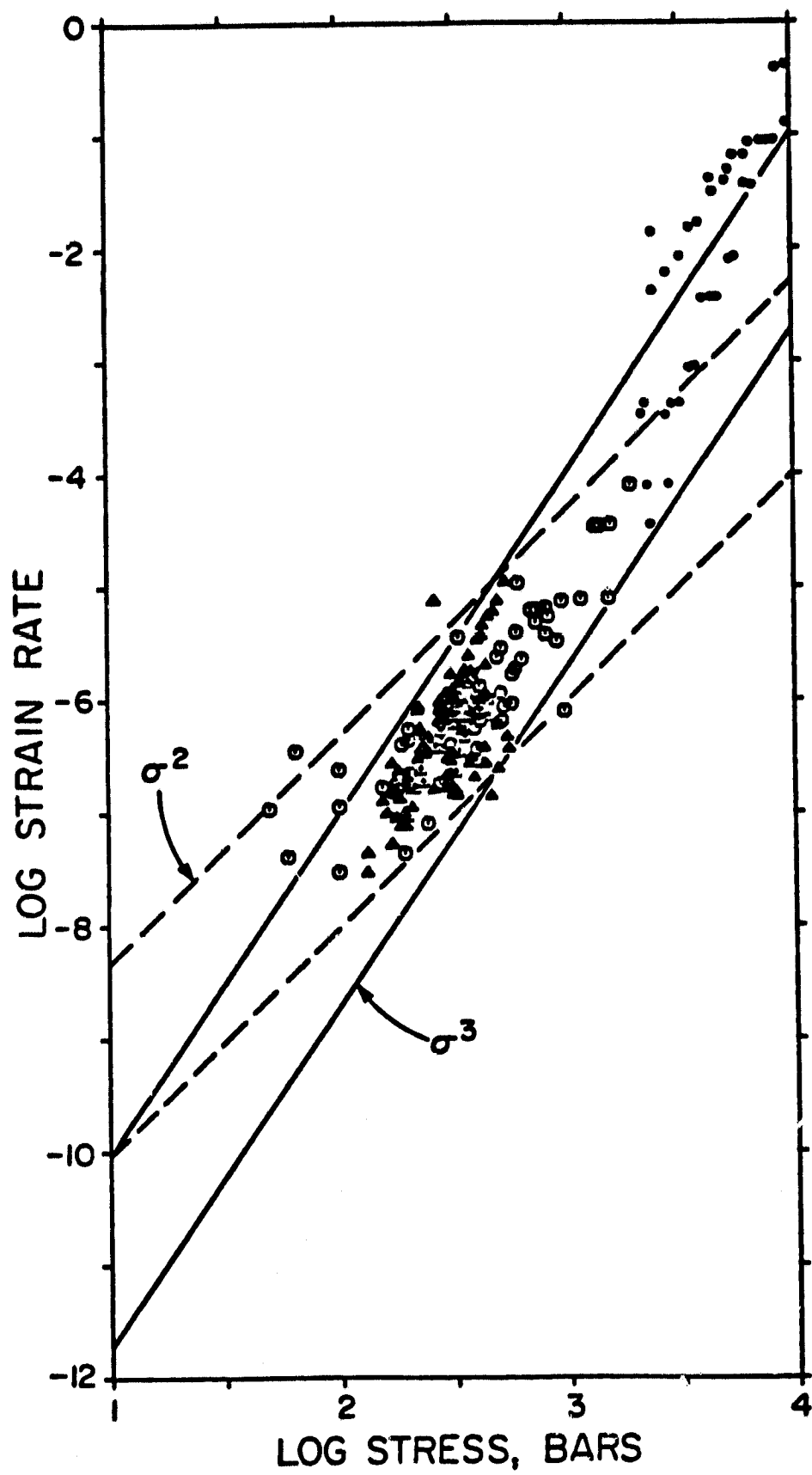


Fig. 4

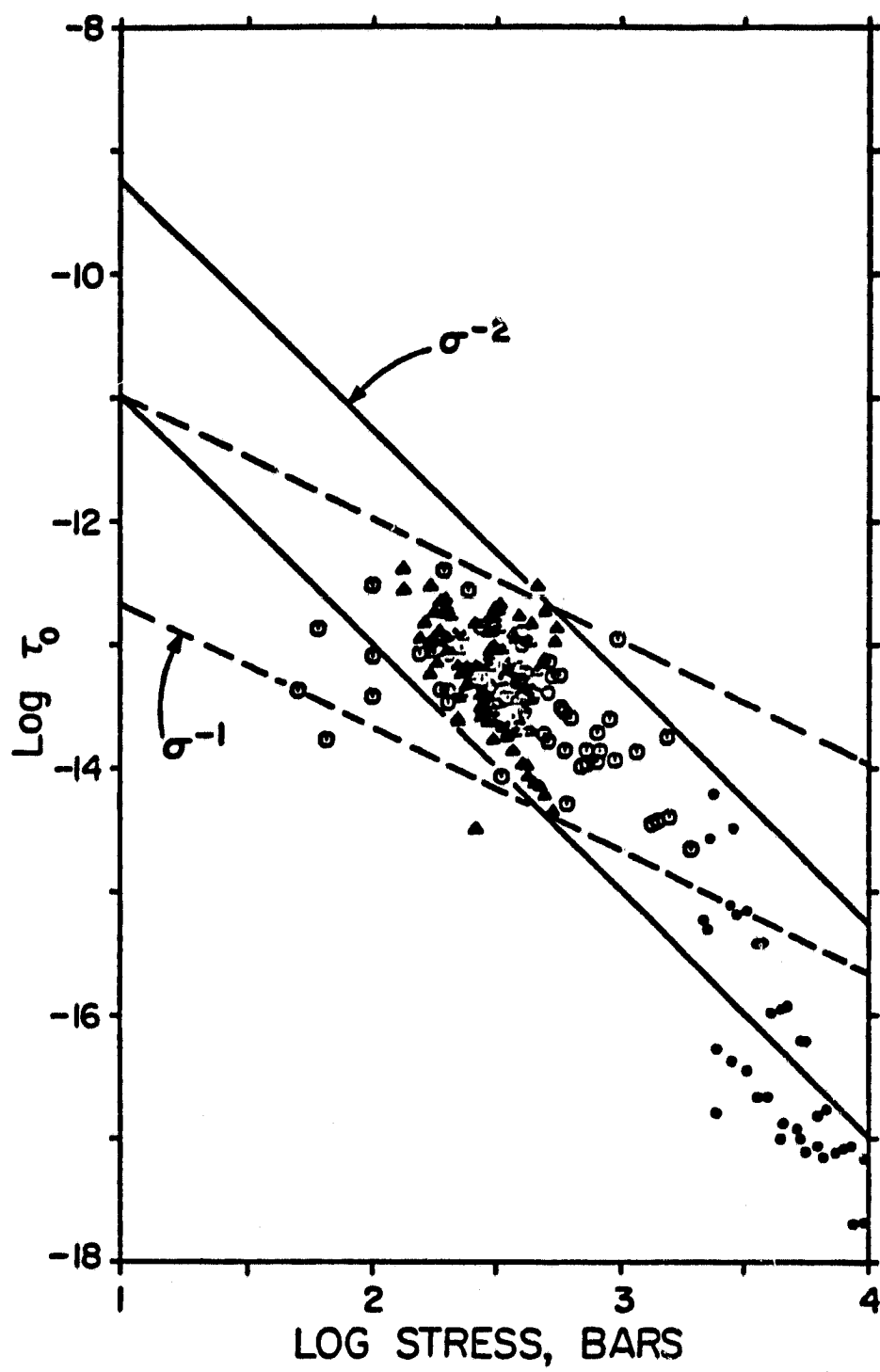


Fig. 5

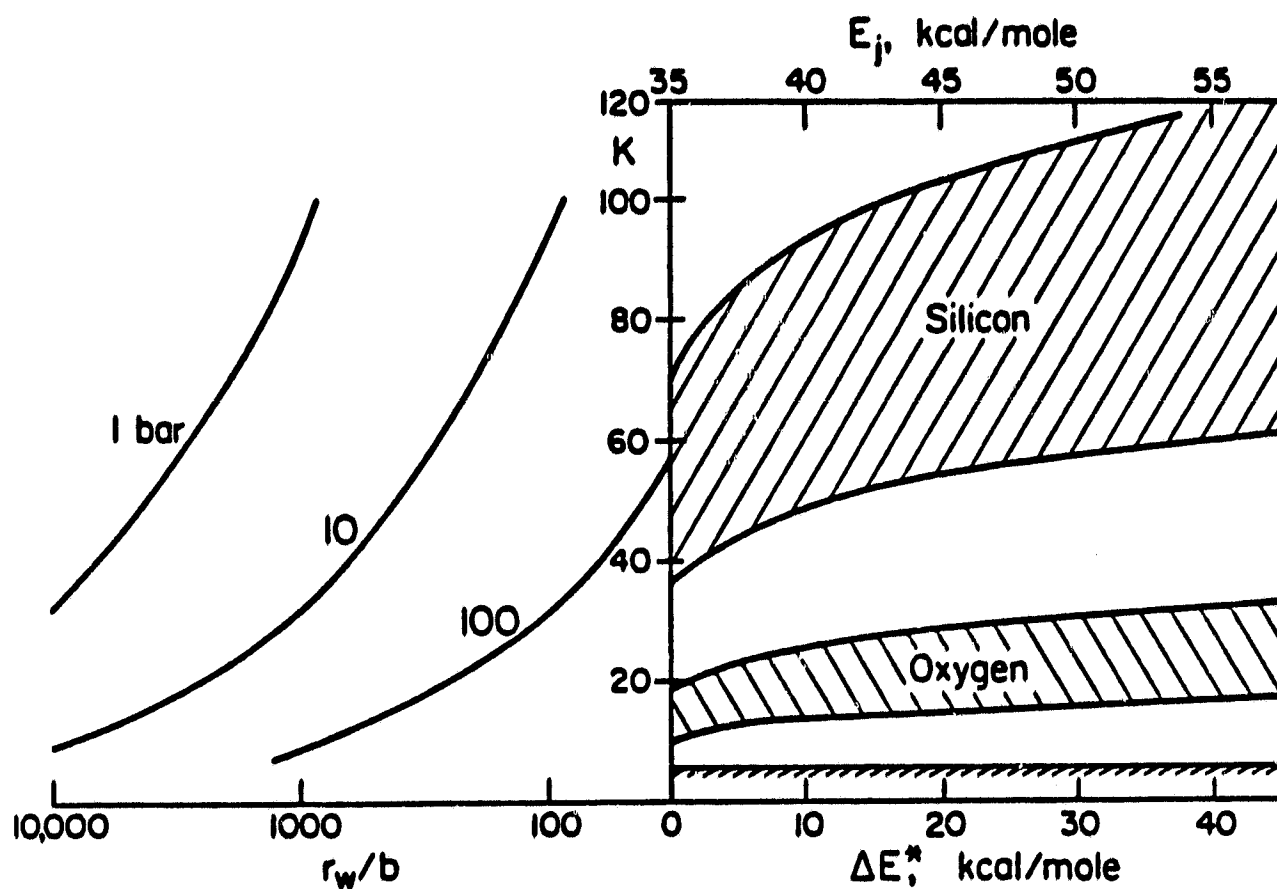


Fig. 6

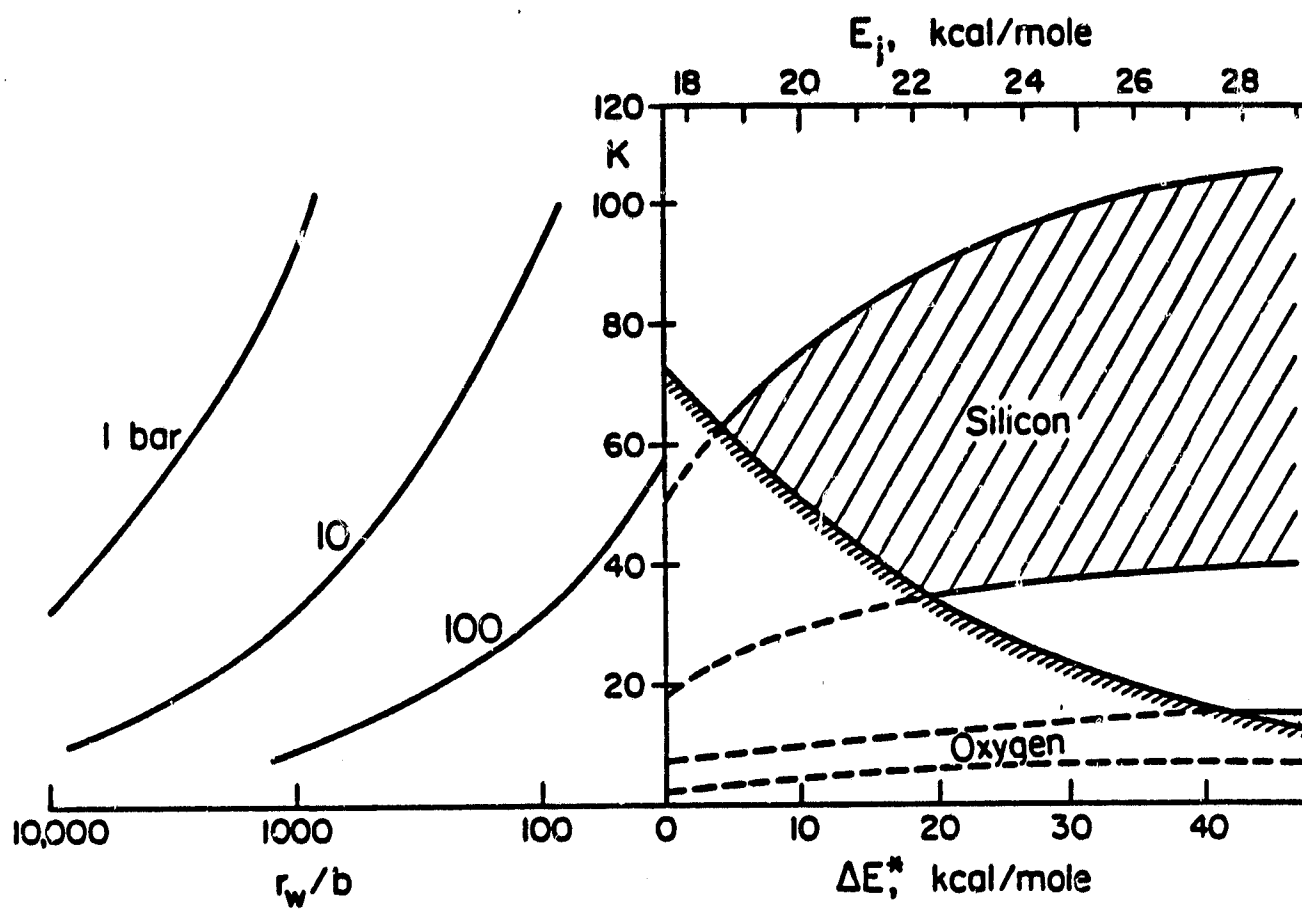


Fig. 7

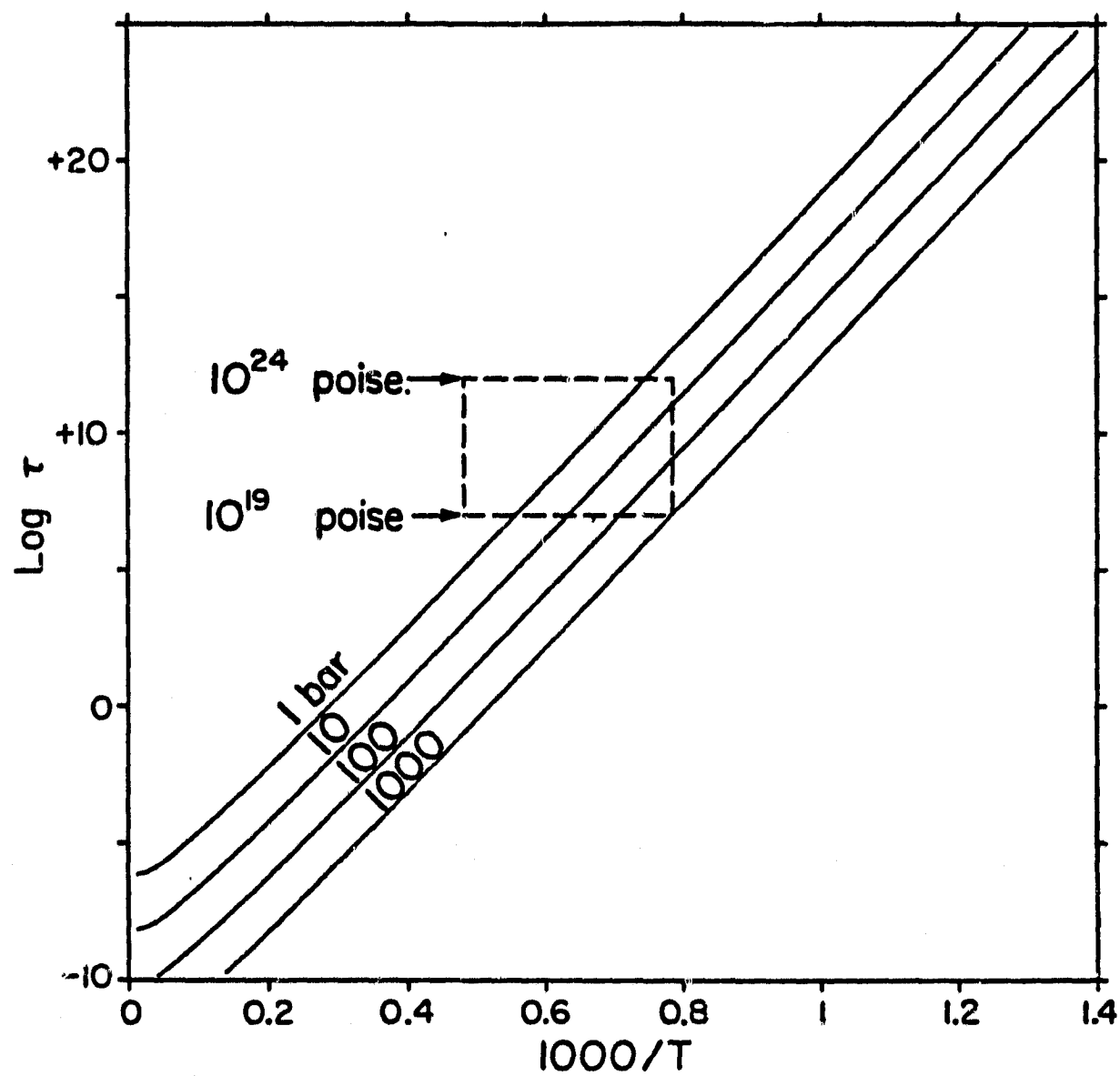


Fig. 8

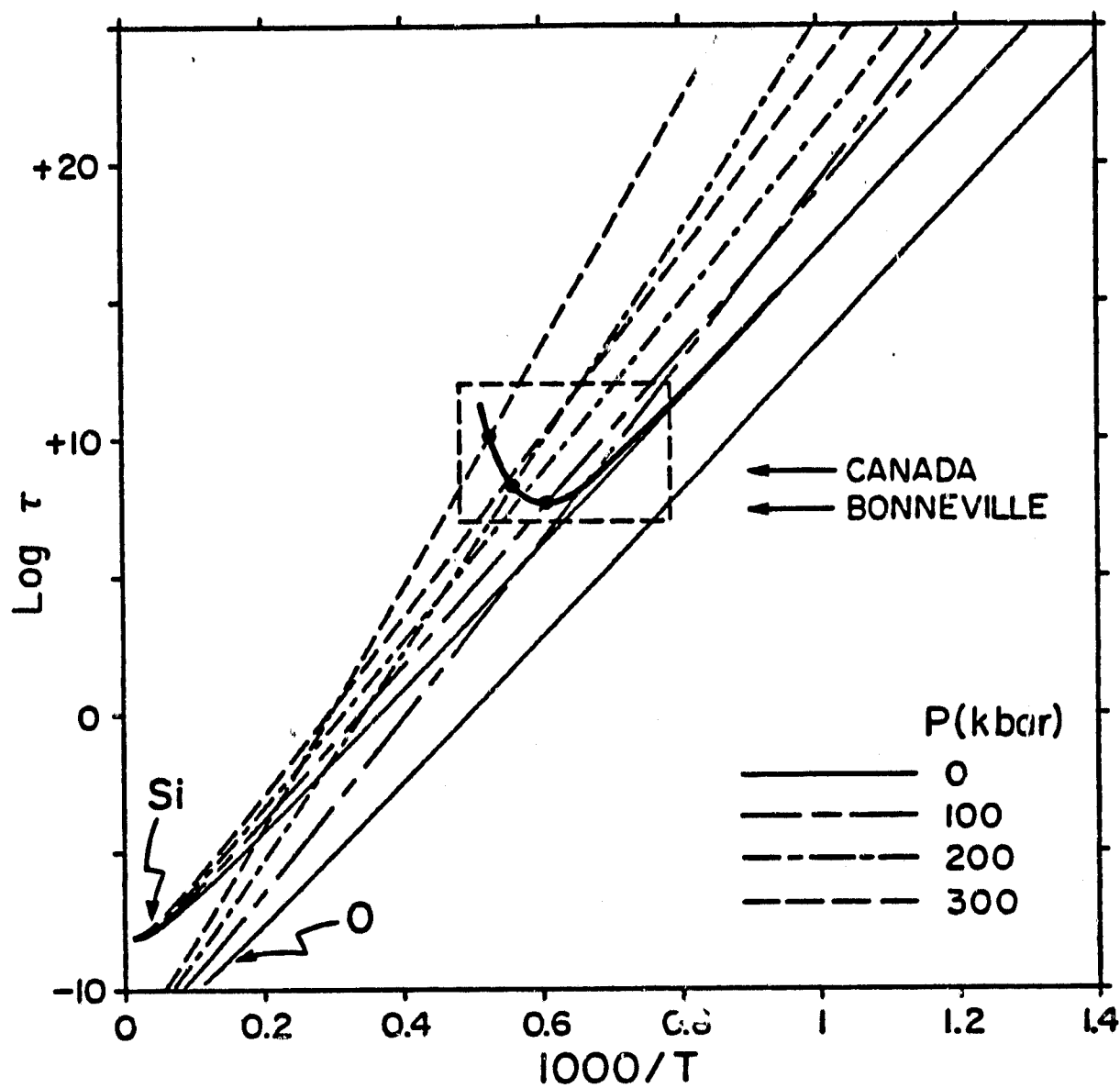


Fig. 9

$T, ^\circ K = \begin{cases} \cdots \cdots \cdots 1730.00 \\ \text{---} \text{---} \text{---} 1700.00 \\ \cdots \cdots \cdots 1670.00 \\ \text{---} \text{---} \text{---} 1640.00 \\ \text{---} \text{---} \text{---} 1500.00 \end{cases}$

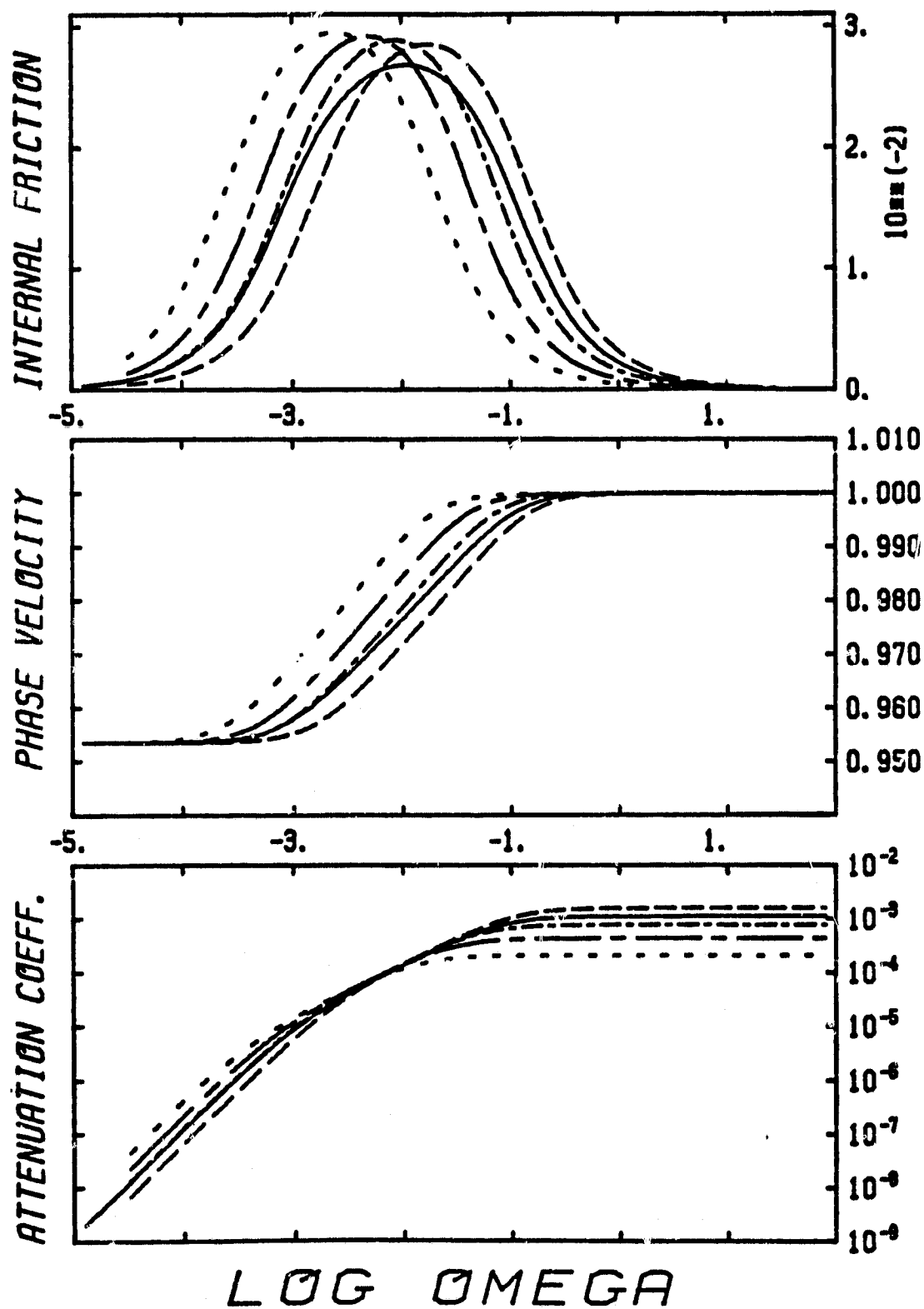


Fig. 10

$$\Omega = \begin{cases} \text{---} & 0.010 & 10^1 \\ \text{---} & 0.100 & 10^1 \\ \text{---} & 1.000 & 10^1 \end{cases}$$

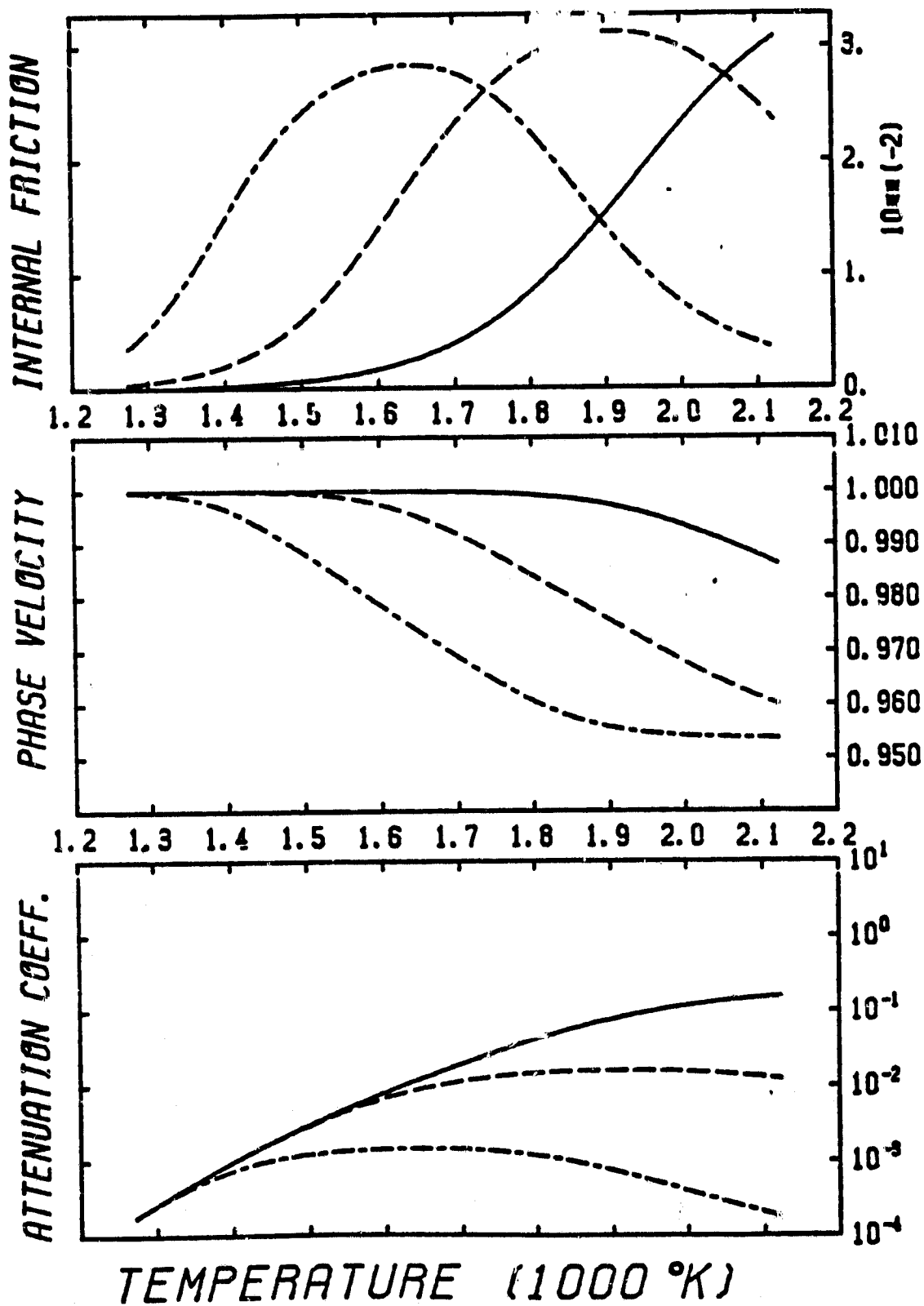


Fig 11

APPENDIX IV

A GLOBAL GEOCHEMICAL MODEL
FOR THE EVOLUTION OF THE MANTLE

Don L. Anderson

Proceedings of W.G.5 Symposium, "Geophysical-Geochemical Evolution of the Earth," (in press).

**A GLOBAL GEOCHEMICAL MODEL
FOR THE EVOLUTION OF THE MANTLE**

Don L. Anderson

**Seismological Laboratory
California Institute of Technology
Pasadena, California 91125**

ABSTRACT

The basalt, eclogite, and harzburgite that are the differentiation products of the Earth appear to be trapped in the upper mantle above the 670 km seismic discontinuity. It is proposed that the upper mantle transition region, 220 to 670 km, is composed of eclogite which has been derived from primitive mantle by about 20% partial melting and that this is the source and sink of oceanic crust. The remainder of the upper mantle is garnet peridotite which is the source of continental basalts and hotspot magmas. This region is enriched in incompatible elements by hydrous and CO₂ rich metasomatic fluids which have depleted the underlying layers in the L.I.L. elements and L.R.E.E. The volatiles make this a low-velocity, high attenuation, low viscosity region. The eclogite layer is internally heated and it controls the convection pattern in the upper mantle. Material can only escape from this layer by melting. The insulating effect of thick continental lithosphere leads to partial melting in both the peridotite and eclogite layers. Hotspots and ridges mark the former locations of continents. Most of the basaltic fraction of the oceanic lithosphere returns to the eclogite layer.

Plate tectonics is intermittent. The continental thermal anomaly at a depth of 150-220 km triggers kimberlite and carbonatite activity, alkali and flood basalt volcanism, vertical tectonics and continental breakup. Hot spots remain active after the continents leave and build the oceanic islands. Mantle plumes rise from a depth of about 220 km. Midocean ridge basalts rise from the depleted layer below this depth. Material from this layer can also be displaced upwards by subducted oceanic lithosphere to form back-arc basins.

INTRODUCTION

Although convection plays an important role in plate tectonics and heat transport in the Earth it has not succeeded in homogenizing the mantle. Magmas are still being produced from mantle reservoirs which have remained separate for the order of 1 to 2×10^9 years (e.g., De Paolo, 1979; Sun and Hansen, 1975). Oceanic lithosphere is continuously returned to the mantle but the difference in element ratios in the reservoirs, e.g., Rb/Sr, U/Pb, Th/Pb and Sm/Nd, persists. If the depth of earthquakes in subduction zones can be used as a guide, oceanic lithosphere is presently being delivered to the region of the mantle between about 220 km and 670 km. The isotopic data can be satisfied if this is also the source region for mid-ocean ridge basalts (MORB). This leaves the upper mantle or the lower mantle as the source region for continental flood basalts (CFB), hotspot magmas and ocean island basalts (OIB). The upper mantle low-velocity zone (LVZ), or asthenosphere, is the more likely source region since temperatures there are closest to the melting point.

Ocean floor basalts have comparatively uniform and low $^{87}\text{Sr}/^{86}\text{Sr}$, $^{206}\text{Pb}/^{204}\text{Pb}$, and $^{144}\text{Nd}/^{143}\text{Nd}$ ratios whereas continental magmas and basalts from ocean islands not associated with island arcs have less uniform and higher ratios (De Paolo and Wasserburg, 1979). The latter magmas are also enriched in volatiles and the incompatible large-ion lithophile (LIL) elements (White and Schilling, 1978; Frey et al., 1978). The study of isotopes has introduced the time constraint that reservoirs with different element ratios -- Rb/Sr, U/Pb, Th/Pb, and Sm/Nd -- have existed for the order of 1 to 2 b.y. The source region for MORB has been providing uniform composition lavas for long periods of time.

It must therefore be immense in size and global in nature (Schilling, 1975). The reservoir for continental and ocean island magmas also appears to be relatively uniform and global although its products are often mixed with varying amounts of MORB before it is sampled.

There are two competing petrological viewpoints regarding the nature of the source regions. The common view is that all basalts represent various degrees of partial melting of a garnet peridotite. The alternative position is that some basalts represent extensive melting of a deep eclogite source. Both eclogite and garnet peridotite inclusions are common in kimberlite pipes. The eclogite inclusions, although not rare, represent only about 20% of the total. This suggests that eclogite is either a less abundant component of the mantle or it occurs deeper than the garnet peridotite, as befits its higher density. Neither of the two types of fragments can represent primitive mantle (Allsop et al., 1969). They must therefore be a result of a previous differentiation event. The eclogite minerals are depleted in the trace elements which are enriched in peridotite nodules, the plume source region and the continental crust. It is therefore desirable to test the hypothesis that eclogite, peridotite and continental crust are the principle products of mantle differentiation and that xenoliths in kimberlites may be samples from the mantle source regions. If true, this would have considerable impact on our ability to model the composition and evolution of the mantle.

CHEMICAL STRATIFICATION OF THE MANTLE

The mantle is also heterogeneous in its seismic properties. It has not been clear, however, if or how the seismological and geochemical heterogeneities are related. The largest lateral variations in seismic

velocities occur in the outer 200-250 km of the Earth and are related to such surface tectonic features as shields, trenches, rises, and volcanic belts. The mantle is also inhomogeneous radially with the lithosphere, asthenosphere, and transition zone being the main subdivisions of the upper mantle.

A chemically layered upper mantle could provide distinct and isolated reservoirs and is more suitable in many ways than models involving isolated blobs or regional inhomogeneities (Hofmann et al., 1978). It has been proposed that the low-velocity zone is the depleted reservoir and the source of mid-ocean ridge basalts (Schilling, 1973). Plume basalts, i.e., magmas from the L.I.L. enriched reservoir, have been attributed to deeper sources. If the LVZ is enriched in volatiles, as proposed by Anderson and Sammis (1970) on geophysical grounds, then this explanation is untenable. Frey et al. (1978) have discussed other objections to this model. They argue that volatiles should have enriched the upper layers of the mantle.

On the basis of seismic velocities and seismicity patterns, Anderson (1979c) proposed that there were chemical discontinuities in the mantle at 220 and 670 km. The former is the base of the LVZ and near the maximum depth of earthquakes in continental collision zones and regions of subduction of young, <50 Ma, oceanic lithosphere. The latter is a sharp seismic discontinuity and is near the maximum depth of earthquakes. Only old oceanic lithosphere penetrates this deep. The seismic velocities between 220 and 670 km are consistent with eclogite.

The continental lithosphere extends no deeper than about 180 km (Anderson, 1979c). It may terminate at the boundary between granular and sheared lherzolite nodules, ~150 km (Boyd and Nixon, 1975). We

will assume that the sheared nodules are representative of the mantle below the lithosphere and above the Lehmann discontinuity at 220 km. The shallower granular nodules have apparently been subjected to basalt extraction since they contain less CaO and Al_2O_3 than the sheared variety. They may be an important, perhaps major, component of the continental lithosphere. Both varieties of nodules are enriched in the L.I.L. elements compared to oceanic crust, the MORB source region and the minerals of eclogite inclusions. The fertile peridotite presumably rises to shallower depths under the oceans, of the order of 80 km. Thus, the average thickness of the fertile peridotite layer is about 120 km. Volumetrically, this is an adequate source region for continental and hotspot magmas but not for the more voluminous MORB.

We suggest that differentiation of the Earth leads to two layers in the upper mantle, a thick basalt crust over residual peridotite. As the Earth cools the base of the original crust transforms to eclogite which sinks through the upper mantle. The present upper mantle is peridotite overlying a thick (450 km) eclogite section. Partial melting in the eclogite section allows material to escape and to melt extensively upon ascent. This is proposed as the source of oceanic crust.

The basalt and eclogite portions of the oceanic lithosphere return to the eclogite layer by subduction. The fertile peridotite layer of the upper mantle can partially melt and provide basalts when the upward convection of mantle heat is prevented by the insulation of continental lithosphere. Thus, both reservoirs are global and underlie both oceans and continents. It appears that the MORB source region can also provide magma to back-arc basins, perhaps when material is displaced by the descending slab.

THE ECLOGITE SOURCE REGION

Pipe eclogites have a strong resemblance to oceanic tholeiites in both the major and trace elements. The Rb/K and other ratios in biminerallitic eclogite closely resemble the corresponding ratios in abyssal tholeiite basalts. The similarities are even more pronounced if the eclogites are compared with the average composition of the oceanic crust.

The first column of Table 1 gives a composition which is representative of oceanic tholeiites. More likely estimates of the composition of the primary magma are the total composition of the oceanic crust (column 2) and basaltic komatiites (column 3). These compositions are remarkably similar and have appreciably more MgO and less Al_2O_3 and Na_2O than tholeiites which are considered to be the last crystallizing liquid from a more primary magma. The biminerallitic eclogites in kimberlite (columns 4, 5 and 8) are virtually identical to these estimates of the average composition of the oceanic crust. Trace element comparisons between kimberlite eclogites and abyssal tholeiites are given in Table 2. Again, the correspondence is remarkable.

It appears that material similar to eclogite inclusions in kimberlites is a suitable parent for the oceanic crust. The inclusions themselves may represent cumulates from mantle diapirs that were trapped in the continental lithosphere. Diapirs rising from such great depth would melt extensively if their ascent were unimpeded by the continent.

THE GARNET-PERIDOTITE LAYER

The K, Rb, and Sr contents of some kimberlite garnet peridotite inclusions are given in Table 2. Also given are estimates of CFB and

of the "plume" source. Note the agreement between tholeiites and eclogites and between peridotites and the inferred plume source region. Another way to estimate the trace element content of a partial melt from peridotite is to assume that the difference in composition between fertile and barren peridotite is due to basalt removal. The trace element content of the resulting liquid is given in Table 3 and compared with continental and oceanic basalts. The peridotite compositions are from Rhodes and Dawson (1975) and it is assumed that the basalts represent 20% melting. These are extremely fresh peridotite xenoliths from the Lashame tuff-cone in northern Tanzania that have apparently come from a depth of ~150 km. They are chemically and mineralogically similar to peridotite inclusions from kimberlites except that they appear to be relatively less contaminated. The $^{87}\text{Sr}/^{86}\text{Sr}$ ratios of these samples are about 0.705. The inferred melt is much higher in K, Rb, and Sr than oceanic tholeiites, a characteristic of continental basalts. The K/Rb and Rb/Sr ratios are also much different than abyssal basalts. Fertile garnet peridotite therefore seems a suitable source material for continental flood basalts but not for MORB. It also has the characteristics inferred for the "plume" source region (White and Schilling, 1978). This part of the mantle has probably been subjected to metasomatic enrichment of the incompatible trace elements (Lloyd and Bailey, 1975). Such enrichment has also been proposed for the source region of continental (Boettcher and O'Neil, 1979) and plume basalts (White et al., 1979). The fact that enriched xenoliths are extensively sampled by kimberlites argues for the shallowness of the plume reservoir.

Mid-ocean ridge basalts generally have $^{87}\text{Sr}/^{86}\text{Sr}$ ratios between about 0.702 and 0.704 while continental basalts are usually greater than

0.704 and range up to 0.710 (Carter et al., 1973; De Paolo, 1979).

Basalts from oceanic islands are intermediate in value and may represent mixtures. The data on kimberlite xenoliths is sparse and equivocal (Allsop et al., 1969; Barrett, 1975; Simazu, 1975). Pipe peridotites have $^{87}\text{Sr}/^{86}\text{Sr}$ values of 0.7060-0.7075 and other characteristics appropriate for the source region of continental basalts. Eclogite xenoliths may have been brought into the continental lithosphere by deeper diapirs and evolved for some time in an environment different from PEL prior to pipe eruption. Whole rock measurements on eclogite xenoliths from S. Africa generally have high $^{87}\text{Sr}/^{86}\text{Sr}$ ratios (0.704-0.711). Allsop et al. (1969) estimated the ratio in "ideal" biminerally eclogite as 0.702. A sample from Tanzania has a value of 0.7004; discrete diopside nodules give 0.7029-0.704 (Barrett, 1975).

LOCATION OF THE TWO SOURCE REGIONS

As discussed earlier, at least part of the oceanic lithosphere seems to be returned to depths between 220 and 670 km. The mantle discontinuities at these depths are sharp and they are associated with changes in seismicity, as if they were acting as barriers to slab penetration. This could be due to density jumps caused by changes in mantle chemistry. The isotopic data, although useful in finger printing the source regions and giving age control does not provide information about major element chemistry or intrinsic density. This is where the kimberlite inclusions become useful.

Eclogite is appreciably denser than garnet peridotite and should therefore occur deeper in a gravitationally stable mantle. I have suggested that the Lehmann discontinuity at 220 km is the boundary between garnet peridotite and eclogite, and the discontinuity at 670 km is the

boundary between eclogite in the garnetite assemblage and peridotite in the ilmenite plus spinel assemblage (Anderson, 1979b). The eclogite layer is perched (PEL) in the upper mantle and forms the transition region. In a convecting system composed of two superposed layers there is a thermal boundary layer, i.e., region of high thermal gradient, on each side of the interface. This is where temperatures are most likely to approach or exceed the solidus and where diapirs would originate. There is also a thermal boundary layer associated with the lithosphere-asthenosphere boundary. Temperatures at 670 km and below are likely to be well removed from the melting point.

Differentiation of a silicate planet results in two distinct products, basalt and residual peridotite. The basalt, resulting from low pressure, high temperature partial melting of primordial mantle possibly resembling peridotitic komatiite, would be originally concentrated in a thick layer at the surface. Subsequent cooling, primarily by convection, brings upper mantle temperatures into the stability field of eclogite which is denser than residual mantle. This leads to a massive overturning of the outer layers of the planet, subduction of the eclogite protoplate and destruction of the early geological record. This may explain the rarity of crustal rocks older than 3.8 Ga.

Given that planetary differentiation concentrates basalt in the outer layers and that the Earth has generated and subducted massive amounts of oceanic lithosphere what is the likely distribution of basaltic material in the interior? To answer this I have estimated the density as a function of depth for basalt and peridotite (Anderson, 1979a). Basalt below about 50 km converts to eclogite which is denser than normal mantle even after olivine has converted to spinel. Pyroxene

and garnet react at higher pressures to form a garnet solid solution. Normal mantle also undergoes a series of phase changes but remains less dense than garnetite until ilmenite and perovskite structures become stable below 670 km. The eclogite cannot sink below this level. The addition of Al_2O_3 to CaSiO_3 and $(\text{Mg}, \text{Fe})\text{SiO}_3$ expands the stability field of garnet and increases the pressure required for transformation to such dense lower mantle phases as perovskite and ilmenite. This means that eclogite cannot sink into the lower mantle. Whole mantle convection, which may have been possible prior to the establishment of the eclogite layer and the chemical discontinuities in the upper mantle, would be replaced by separate convection systems in the lower mantle, the eclogite layer and the upper mantle above 220 km.

The oceanic part of the plate tectonic cycle in this scheme is very simple (Figure 1). Heating of the eclogite layer causes partial melting and the rise of eclogitic diapirs. The latent heat for complete melting is provided by adiabatic decompression. Oceanic crust forms from this eclogite liquid. MORB forms the surface veneer and represents the latest freezing fraction. Subduction causes the crust to reinvert to eclogite and it sinks back to the PEL. The harzburgite part of the lithosphere remains in the upper mantle. The continuous recycling and remelting of the material in the oceanic crust depletes it in the LIL and, in particular, the LREE.

PRIMITIVE MANTLE

The isotopic data indicates that the two source regions are the results of an early differentiation event. If we accept the 220 and 670 km discontinuities as its boundaries, the eclogite layer represents about 20% of the mass of the mantle. By assuming that the whole mantle

was involved in this early differentiation we can obtain a spectrum of estimates of primitive mantle composition. Several of these are given in Table 4.

There are other approaches that have been used for estimating primitive bulk Earth chemistry. Ganapathy and Anders (1974) have provided a cosmochemical mixing estimate which is also given in Table 4. There is surprisingly good agreement between these estimates and the resulting compositions are distinct from any modern rock type. Peridotite komatiites are widespread in early (>3.5 Ga) Precambrian terrains. Viljoen and Viljoen (1969) propose that these approximate the composition of primitive mantle. Indeed, these have Mg/Si ratios in the range of whole Earth estimates. They may represent primitive mantle that has left some garnet in the source region. I propose that a material similar to those in Table 4 was the parent from which the current mantle reservoirs were derived. These reservoirs are a shallow peridotitic layer and a deeper eclogite layer. In this scheme pyrolite would not represent primitive mantle but mantle which has already been depleted in a basaltic component.

It has long been recognized that the source region of MORB is depleted in LIL elements compared to alkali basalts, continental flood basalts, and hot-spot magmas. One would expect, however, that the original primary differentiation would enrich the basalt/eclogite fraction relative to the residual peridotite. Whole rock analyses of pipe eclogite indeed show such enrichment. The major phases, omphacite and garnet are, however, depleted and the enrichment occurs in the intergranular material (Allsop et al., 1969). The intergranular material LIL content is similar to that of the continental crust (Table 2). The eclogite layer may have become depleted and the peridotite layer enriched

by the upward transport of fluids as discussed by Frey et al. (1978), Boettcher et al. (1979) and Mysen (1979).

Tatsumoto (1978) and Hedge (1978) proposed a model, based on lead and strontium isotopes that is similar to the present result, i.e., the LVL ("asthenosphere") is undepleted or enriched and supplies "hot-spot" magmas; the underlying mantle ("mesosphere") is depleted and provides abyssal tholeiites. This is the opposite of Schilling's (1973) model. Continental and hotspot related magmas represent a wide range of partial melting, from about 4% to 25% (Frey et al., 1978; White et al., 1979). This suggests that they come from a wide range of (shallow) depths. MORB's are invariably tholeiitic, indicating extensive (>25%) melting and a consistently deep origin.

The incompatible trace elements in both source regions are enriched relative to recent estimates of bulk Earth composition (Ganapathy and Anders, 1974). For example, if the lower mantle is identical in composition to the peridotitic upper mantle and if the silicate portion of the planet is 21% eclogite and 0.5% continental crust then the major elements are in agreement with bulk Earth estimates such as Ganapathy and Anders (1974) but such elements as K, Rb, and Sr are about a factor of 2-1/2 higher. This can be accounted for if the mantle below 670 km has transferred its incompatible trace elements to the crust and upper mantle. This presumably occurred during the early differentiation of the Earth and accompanied basalt extraction from primitive mantle. The calculated Rb/Sr ratio of the continental crust plus upper mantle (peridotite plus eclogite) is 0.028. This is also the value inferred for the bulk Earth (Ganapathy and Anders, 1974; DePaolo and Wasserburg, 1976).

This plus the complementary nature of the two source regions suggests that the material above 670 km may exhibit bulk Earth patterns of the LIL elements, and have a 2-3 times enrichment. The lower mantle is extremely depleted in the LIL elements.

EVOLUTION OF THE MANTLE

The evolution of the Earth's mantle according to the present scheme is shown in Figure 2. The primitive mantle has roughly the composition given by a 1:4 mix of eclogite and garnet peridotite. Early differentiation processes lead to the development of a thick enriched basalt crust and a residual peridotite mantle. As the outer layer cools it converts to eclogite which settles through the upper mantle and becomes perched near 670 km by a phase boundary in the peridotite mantle. Incompatible trace elements are removed into the continental crust and the upper mantle garnet peridotite regions by metasomatic fluids. The eclogite layer therefore becomes depleted in those components which are concentrated in the overlying layers including the continental crust.

The highest temperatures in the mantle, relative to melting temperatures, are in the thermal boundary layer near the top of the PEL, ~220 km depth. This is where the density contrast between eclogite

and peridotite can be overcome by partial melting and where eclogite diapirs originate. Peridotite diapirs originate from the top of the thermal boundary layer. Their shallower depth and the broad melting interval of peridotite leads to relatively small amounts of partial melting, a requirement of alkali basalt petrology (Frey et al., 1978). This is a persuasive but overlooked argument for a shallow location of the plume source region relative to the source region for tholeiites.

Continental and alkali basalts are usually emplaced at greater elevations than the oceanic tholeiitic basalts. This is sometimes taken as evidence that the MORB source region is shallower than the plume source region. Alternatively, the alkali basalts are emplaced at higher elevations because they are intrinsically less dense than tholeiites.

The parameters of the thermal boundary layer depend on the thermal properties, viscosity and heat flow at the interface. The thickness is calculated to be about 20 km and the temperature rise is 300-600°C. This is comparable to the near surface gradient and brings the average temperature close to the melting point of mantle silicates at 220 km. The thermal perturbation by a stationary continent, or a large continent moving slowly, causes a further temperature rise and may be the trigger that initiates partial melting.

Depleted peridotite, the refractory product of partial melting of the garnet peridotite layer, is lighter than any other component of the mantle and becomes part of the continental lithosphere and the suboceanic harzburgite layer. The lower mantle need not be involved at all in the current magmatic cycle.

MANTLE METASOMATISM AND THE REDISTRIBUTION OF TRACE ELEMENTS

Calculation of the partitioning of the rare Earth elements among the various regions indicated in Figure 2 for a dry planet give results which are contrary to observations (Schilling, personal communication). In particular the eclogite layer being the result of partial melting of primitive mantle should be LREE enriched even after removal of the continental crust. The peridotite layer should be depleted relative to primitive mantle and be LREE deficient. This suggests that there has been upward transport of a LREE phase which serves to deplete the PEL and enrich the overlying layers, including the peridotite plume source and the continental lithosphere. An H_2O -rich vapor phase strongly concentrates the REE and, in particular, the LREE (Mysen, 1979). Evidence that the mantle has experienced such metasomatism prior to the transport of samples to the Earth's surface by kimberlites has been provided by Ridley and Dawson (1975), Erlank and Shimazu (1977) and summarized by Mysen (1979). Parallel evidence from alkali basalts is given by Boettcher and O'Neil (1979). Carbonatites, kimberlites, "depleted" granular peridotites, alkali basalts and the interstitial phase in eclogite xenoliths all show extreme LREE enrichment. The source region of MORB on the other hand is LREE depleted. The degree of LREE enrichment in a water-rich fluid increases with garnet content (Mysen, 1979). These observations all suggest that a vapor or fluid phase removes the REE from the eclogite layer and deposits them in the peridotite layer and the continental lithosphere. The other LIL elements also show a complimentary pattern between MORB and plume basalts.

Since the enrichment of REE in general, and LREE in particular, in the fluid increases rapidly with pressure as well as garnet content, we expect an upward increase in LREE enrichment in the rocks as we proceed

from the eclogite to the fertile peridotite to the "depleted" peridotite (continental lithosphere) and finally to the crustal layers. Mass balance calculations suggest that the continental crust is not the only repository of LREE enriched material. The remainder we propose is in the continental lithosphere and the LVZ. This is supported by the evidence from material which has been sampled from these regions. The depleted nature of the MORB source region is an argument that it lies below the REE enriched regions, i.e., below the depth of generation of kimberlites and alkali basalts and the xenoliths they contain.

PLATE TECTONICS

A major source of mantle heat flow is the Perched Eclogite Layer (PEL). With tholeiitic concentrations it would provide $0.7 \mu\text{cal}/\text{cm}^2\text{sec}$, about $1/2$ of the global average surface heat flow. The scale length of convection in the PEL will be of the order of the layer thickness, ~ 450 km. Convection in the overlying peridotite layer would be driven by this non-uniform heating from below and would have a similar or smaller scale length and be characterized by narrow ascending plumes. The high thermal gradient in the boundary layer leads to a large decrease in viscosity at the interface and the two convecting systems may be thermally coupled rather than coupled by viscous drag forces. That is, cold descending regions would occur in close proximity in the two layers. A descending slab, for example, may trigger detachment of the cold boundary layer in the PEL. This is shown schematically in Figure 3. Seismic waves will see a continuous cold region with high velocities. There will also be other regions of cold descending plumes in the PEL which are not directly related to slabs. Likewise, there may be regions

of rising currents in both the PEL and the overlying layer, which do not express themselves in surface features such as mid-ocean ridges. The convective pattern, however, may be evident in detailed analyses of topography, gravity and seismicity.

Earthquakes do not extend below about 250 km at most convergent plate boundaries. In other regions there is a gap in the seismic zone between about 250 and 500 km. Even where the zone is continuous it is usually contorted near 250-350 km. In many cases the deeper zone is more-or-less spatially continuous with the upper zone but in Chile, Peru and New Zealand the two zones appear to be displaced. This is suggestive of the type of two-layered convection considered here.

There are several ways to estimate the lateral extent of the convection cells. We assume that convection in the eclogite layer controls convection in the thinner and shallower peridotite layer. Thiessen et al. (1979) suggested that the distribution of high spots in Africa reflects the underlying convection pattern. By comparison with laboratory data they inferred a vertical extent of convection of about 500 km, slightly greater than the thickness of the eclogite layer. They proposed that this pattern could only be observed through a stationary continent.

Jordan (1978) showed that terrain, crustal thickness, and Bouguer gravity anomalies have correlation distances of the order of 550 km, remarkably similar to African highspot distances. This again suggests a scale length of convection comparable to the thickness of the transition layer.

Menard (1973) attributed depth anomalies in the eastern Pacific and the bobbing motion of drifting islands to convection cells in the upper mantle of half-wavelength 250-500 km. The depth anomalies, having amplitudes of ± 300 meters can be explained by temperature

differences in a 200 km thick layer of about 200°C. The depth anomalies seem to be fixed relative to hot spots. Menard believes that motion of plates over these bumps explain many aspects of vertical tectonics. The "bumpy" asthenosphere envisaged by Menard is a natural consequence of the convection pattern proposed here.

The pattern of convection in the PEL is probably fairly complicated. The migration of trenches and continents may change the locations of the descending plumes in an individual cell or groups of cells in the PEL but it seems likely that the cells themselves cannot move far relative to one another. This provides a rationale for a fixed hot-spot reference frame and a mechanism for allowing the surface expression of a hot spot to wander on the order of 5°. The proposed upper mantle convection pattern is shown schematically in Figure 4.

HOT SPOTS AND PLUMES

Morgan (1972) suggested that island and sea-mount chains are produced by plate motion over convective plumes extending from near the core-mantle interface to the base of the lithosphere. Anderson (1975) proposed that plumes came from a distinctly different source region than midocean ridge basalts and that kimberlites, carbonatites and continental flood basalts were all related to hot-spot or plume activity. I suggested that plumes were a result of a thermal perturbation due either to continental insulation or a diapir rising from the deep mantle. In either case the plume source region differed in chemistry from mantle providing abyssal tholeiites and was the source region for distinctive ocean island magmas and undersaturated continental magmas. It was proposed that this source region was rich in Ti, Ba, Sr, Y, La, Zr, Nb, Rb, CO₂, P₂O₅, H₂O, etc., compared to "normal" mantle (the source

region of MORB). These characteristics have since been found to be typical of plume chemistry (Unni and Schilling, 1978; Schilling et al., 1976; Bonatti et al., 1977; White and Schilling, 1978).

Although I initially favored a deep mantle origin for plumes it now appears that they originate above the 220 km mantle discontinuity in a region of the mantle that has been enriched in incompatible components by metasomatic processes that have depleted the source region of MORB.

Since hot spot activity is restricted both in space and time we need a thermal anomaly to initiate partial melting in the peridotite layer. One possibility is thermal blanketing by the thick conductive continental lithosphere (Anderson, 1975). A large stationary continent may thereby cause its own break-up and a subsequent period of rapid plate motion. The temperature anomaly and partial melt zone remains after the continent leaves and it becomes an oceanic hot spot. Hot spots will have a finite lifetime which appears to be at least 200 Ma after the continent starts to move off.

With a mantle heat flow of $0.7 \mu\text{cal}/\text{cm}^2\text{sec}$ there are 2×10^9 cal/cm^2 delivered to the base of subcontinental lithosphere in 10^8 years. Even if only 20% of this is trapped this is enough to heat a 50 km thick section of mantle by 200°C and to melt it to the extent of 20%. Continental blanketing therefore seems to be an adequate mechanism for turning on melting spots below the continental lithosphere.

The hot spot tracks in the Atlantic and Indian Oceans can be traced back to continental interiors. The timing of Mesozoic and Cenozoic continental flood basalts in North and South America, Africa, Europe and Siberia is appropriate for their location over hot spots when they formed (Morgan, 1979). If our hypothesis concerning the origin of

hot spots under stationary continents is correct then we would expect that a continent would have been over Hawaii some 200 m.y. ago. The Hawaiian-Emperor seamount chain disappears into the Aleutian Trench so we cannot trace it beyond about 70 m.y. By backing up the Pacific plate we can infer that some of these continental fragments may have been incorporated into northwestern North America. The 210 m.y. old flood basalts from central Alaska to Northern Oregon, so-called Wrangallia (Jones et al., 1977), originated near the equator ($\sim 15^\circ$) and subsequently moved north to become attached to North America. Greenstones in central Japan were formed near the equator in the late Paleozoic (Hattori and Hirooka, 1979). Other fragments are elsewhere around the Pacific Margin (Nur and Ben-Avraham, 1979).

In the present scheme it is the thermal perturbation caused by the deep (~ 150 km) continental lithosphere that is responsible for the onset of hotspot activity. The hotspots generate kimberlites, carbonatites, alkali basalts, and lead to continental breakup. There follows a period of rapid continental drift and seafloor spreading. Continental igneous activity wanes as the continents drift off their hotspots but ridge and ocean island volcanism increase. In this scenario hotspots play an important, perhaps dominant, role in breaking up and driving the plates. At the end of an interval of rapid spreading they would tend to be centrally located in the oceans, much as they are today. An important force in plate tectonics may be the "hotspot fleeing force". The thermal perturbation by continents may also control locations of mid-ocean ridges (Nur and Ben-Avraham, 1979).

HOT SPOT PROPULSION

Elder (1976) has considered the propulsion of continents by a horizontal temperature gradient. In the absence of resisting forces at plate boundaries the velocity is

$$u = \alpha g \Delta T h^3 / 3 \nu \ell$$

where α is the coefficient of thermal expansion ($3 \times 10^{-5}/K$), g is acceleration due to gravity (10^3 cm/sec^2), ΔT is the temperature anomaly (200K), h is the layer thickness (100 km), ν is the viscosity (10^{20} P) and ℓ is the horizontal scale of continent (1000 km). The assigned values are just for the purpose of obtaining an order of magnitude estimate for u which turns out to be about 6 cm/yr.

Periods of extensive continental magmatism are correlated on a global basis and seem to last of the order of 0.3 to 0.4 Ga (Windley, 1977). They are separated by periods on the order of 0.7 to 1.0 Ga. Periods of rapid plate motion, or at least of rapid apparent polar wander, last for about 30-60 Ma (Gordon et al., 1979). At a velocity of 10 cm/yr. this would lead to total displacements of 3000 to 6000 km which are of continental and inter-continental distances. The continents, on the average, then would come to rest far from their own or other continents' hot spots. The gestation period for forming a hot spot appears to be 200 to 400 Ma and the lifetime estimated from the duration of continental magmatism and the duration of the subsequent hot spot track may be as much as 500 Ma. Since convection is more efficient through the oceanic mantle we expect that hotspots will start to dissipate as soon as their continents move off and that regions of high heat flow in the oceans would mark the previous locations of stationery or slowly moving continents.

Reconstruction of the continents indicate that most of the Atlantic and Indian ocean hotspots were beneath continents from about 100 to >350 m.y. ago. The present African hotspots were apparently beneath Europe at the earlier time.

SUMMARY AND DISCUSSION

Isotopic evidence indicates that there are at least two source regions of basaltic magma in the mantle which have remained separate for the order of 1 to 2 Ga. The sub-continental and hotspot source region is enriched in incompatible components compared to the source region for midocean ridge basalts. Eclogite and garnet peridotite xenoliths in kimberlite pipes seem to have the appropriate characteristics to provide mid-ocean ridge basalts, and continental basalts respectively. The eclogite layer, the source of mid-ocean ridge basalts, is denser, and therefore deeper than the enriched layer. Melting in both layers may result from the thermal insulation provided by the thick continental lithosphere.

The latent heat for extensive melting of eclogite diapirs is available if rapid ascent of 160 km or greater is possible (Yoder, 1976). This is less likely under thick continental lithosphere than in the oceanic asthenosphere. Therefore, oceanic tholeiites occur in the oceans and eclogite xenoliths occur under continents. The temperature rise required for the initiation of garnet peridotite diapirs may require a long period of continental insulation. Therefore, hotspots start under continents and lead directly to uplift and breakup and provide the initial driving force for continental drift.

It is possible that continental insulation is also required to initiate melting in the eclogite layer. The difference in geometric style between ridges and hotspots would then reflect the difference

in convection in the eclogite and peridotite layers; rising sheets in the internally heated eclogite layer and rising plumes in the overlying peridotite layer.

One would expect the basalts formed in the primary differentiation of the earth to be LREE enriched and enriched in the incompatible elements. Present MORB is coming from a source region which has been depleted in these elements. Continental and hotspot magmas are enriched in H_2O , CO_2 , P, Cl, F, Rb, Sr, Ba, Ti, etc. Ultramafic mantle xenoliths are also enriched in these components, even those which have been depleted in a basaltic component. The minerals in eclogite xenoliths are low in the incompatible elements but the intergranular material is enriched in a material having abundances similar to the continental crust. We suggest that LIL elements were removed from the MORB reservoir not only by extraction of the continental crust but also by removal of a fluid or vapor phase which has enriched the continental lithosphere and the upper mantle peridotite layer.

A schematic continental geotherm with a thermal boundary layer is shown in Figure 5. The ascent path of an eclogite diapir is also shown. Yoder (1976) has estimated that eclogite must rise about 160 km from its source region in order to completely melt if the heat of melting is obtained by adiabatic rise. For a 220 km deep source region complete melting would be achieved at 60 km. Note that completely molten eclogite, i.e., basaltic magma, can be delivered to the surface without melting dry garnet peridotite. With the geotherm shown, wet peridotite diapirs can rise from the thermal boundary layer but they will be only partially molten even after ascent to the surface because of the broad melting interval. Extensively molten peridotitic diapirs are not possible today because of their high liquidus temperature and their relatively shallow origin. This suggests that komatiites

could only form when peridotite diapirs could rise from depths greater than some 300 km, i.e., prior to the establishment of the thick eclogite layer. Only such deep diapirs could extensively melt (>60%) before they reach the surface. This assumes that the geotherm approaches the adiabat only at greater depths.

The gradual heating associated with continental insulation will mobilize mantle fluids before extensive melting occurs. Therefore, a metasomatic precursor and a redistribution of LIL can be expected prior to continental magmatism. Alkali basalt activity can also be expected to precede and accompany tholeiitic eruption from the deeper levels.

We have suggested that a thermal perturbation may be required to initiate the rise of diapirs from the MORB source region. Tholeiitic volcanism is also associated with back-arc spreading. This suggests that subduction can also trigger the rise of diapirs from the MORB source. They will not have been preheated to the extent of normal MORB magmas and may be more volatile rich. The spatial relationships of marginal basin and island arc volcanics, relative to the Benioff zone, suggest that the latter come from shallower depths than the back-arc tholeiites. Since island arcs are generally less than about 150 km above the Benioff zone (Ringwood, 1975) this suggests that marginal basin basalts come from somewhat deeper, consistent with our interpretation of the location of the MORB source region.

Acknowledgements

This work was supported by National Aeronautics and Space Administration Grant NSG-7610. I would like to thank G. J. Wasserburg, L. T. Silver, E. Stolper and F. Richter for helpful discussions. P. Wyllie, J.-G. Schilling, G. Ernst, R. Oxburgh and E. Stolper reviewed a preliminary draft and made helpful suggestions. Contribution No. 3296, Division of Geological and Planetary Sciences, California Institute of Technology, Pasadena, California 91125.

REFERENCES

- Akaogi, M., and S. Akimoto, Pyroxene-garnet solid solution, Phys. Earth Planet. Int., 15, 90-106, 1977.
- Allsop, H. L., L. O. Nicolaysen, and D. Hahn-Weinheimer, Rb/K ratios and Sr-isotopic compositions of minerals in eclogite and peridotitic rocks, Earth Planet. Sci. Lett., 5, 231, 1969.
- Anderson, D. L., Chemical plumes in the mantle, Geol. Soc. Amer. Bull., 86, 1593-1600, 1975.
- Anderson, D. L., The upper mantle transition region; eclogite?, Geophys. Res. Lett., 6, 433, 1979.
- Anderson, D. L., Chemical stratification of the mantle, J. Geophys. Res., 84, 6297-6298, 1979.
- Anderson, D. L., Deep structure of continents, J. Geophys. Res., in press, 1979c.
- Anderson, D. L., and C. Sammis, Partial melting in the upper mantle, Phys. Earth Planet. Int., 3, 41-50, 1970.
- Barrett, D. R., The genesis of kimberlites and associated rocks: strontium isotopic evidence, Physics and Chemistry of the Earth, 9, 637-654, 1975.
- Boettcher, A. L., and J. R. O'Neil, Stable isotope, chemical, and petrographic studies of high-pressure amphiboles and micas; evidence for metasomatism in the mantle source regions of alkali basalts and kimberlites, Am. J. Sci., in press, 1979.
- Bonatti, E., C. G. A. Harrison, D. Fisher, J. Hannorez, and J-G. Schilling, Easter volcanic chain (southeast Pacific): A mantle hot line, J. Geophys. Res., 82, 2457-2478, 1977.

- Boyd, R. R., and P. H. Nixon, Origins of the ultramafic nodules from some kimberlites of Northern Lesotho and the Monastery Mine, South Africa, Phys. and Chem. of the Earth, 9, 431-454, Pergamon Press, 1975.
- Carmichael, I. S. E., F. J. Turner, and J. Verhoogen, Igneous Petrology, 739 pp, McGraw-Hill, New York, 1974.
- Carter, S. R., N. Evensen, P. Hamilton, and R. K. O'Nions, Continental volcanics derived from enriched and depleted source regions: Nd- and Sr-isotope evidence, Earth Planet. Sci. Lett., 37, 401-408, 1978.
- DePaolo, D. J., Implications of correlated Nd and Sr isotopic variations for the chemical evolution of the crust and mantle, Earth Planet. Sci. Lett., 43, 201-211, 1979.
- DePaolo, D. J., and G. J. Wasserburg, Inferences about magma sources and mantle structure from variations of $^{143}\text{Nb}/^{144}\text{Nb}$, Geophys. Res. Lett., 3, 743-746, 1976.
- DePaolo, D. J., and G. J. Wasserburg, Neodymium isotopes in flood basalts from the Siberian platform and inferences about their mantle sources, Proc. Natl. Acad. Sci., 76, 3056-3060, 1979.
- Elder, J., The Bowels of the Earth, 222 pp., Oxford Press, 1976.
- Elthon, D., High magnesia liquids as the parental magma for ocean floor basalts, Nature, 278, 514-518, 1979.
- Engel, A. E., and C. G. Engel, Composition of basalts from the Mid-Atlantic ridge, Science, 144, 1330-1333, 1964.

- Erlank, A. J., and N. Shimazu, Strontium and strontium isotope distributions in some kimberlite nodules and minerals, Ext. Abs. Second Int. Kimberlite Conf., Santa Fe, New Mexico, 1977.
- Frey, F., D. Green, and S. Roy, Integrated models of basalt petrogenesis: A study of quartz tholeiites to olivine melilitites from southeastern Australia utilizing geochemical and experimental petrological data, J. Petrol., 19, 463-513, 1978.
- Ganapathy, R., and E. Anders, Bulk compositions of the Moon and Earth estimated from meteorites, Proc. Lunar Sci. Conf., 5th, 1181-1206, 1974.
- Gansser, A., V. J. Dietrich, and W. E. Cameron, Paleogene komatiites from Gorgona Island, Nature, 278, 545-546, 1979.
- Gordon, R., M. McWilliams and A. Cox, Pre-Tertiary velocities of the continents: A lower bound from paleomagnetic data, J. Geophys. Res., 84, 5480-5486, 1979.
- Green, D. P. and A. E. Ringwood, The genesis of basaltic magmas, Contr. Mineral. Petrol., 15, 103-190, 1967.
- Hattori, I., and K. Hirooka, Paleomagnetic results from Permian greenstones in central Japan and their geological significance, Tectonophysics, 57, 211-236, 1979.
- Hedge, C. E., Strontium isotopes in basalts from the Pacific Ocean basin, Earth Planet. Sci. Lett., 38, 88-94, 1978.
- Hofmann, A. W., W. M. White, and D. J. Whitford, Geochemical constraints on mantle models: The base for a layered mantle, Carnegie Inst. Wash. Yearbook, 77, 548-562, 1978.
- Ito, K., and G. C. Kennedy, The composition of liquids formed by partial melting of eclogites at high temperatures and pressures, J. Geol., 82, 383-392, 1974.

- Jacobsen, S. G., and G. J. Wasserburg, Nd and Sr isotopic study of the Bay of Islands ophiolite complex and the evolution of the source of mid-ocean ridge basalts, *J. Geophys. Res.*, in press, 1979.
- Jones, D. L., N. J. Silberling, and J. Hillhouse, Wrangellia -- A displaced terrane in northwestern North America, *Can. J. Earth Sci.*, 14, 2565-2592, 1977.
- Jordan, S., Statistical model for gravity- topography and density contrasts in the Earth, *J. Geophys. Res.*, 83, 1816-1824, 1978.
- Kay, R., N. J. Hubbard, and P. W. Gast, Chemical characteristics and origins of oceanic ridge volcanic rocks, *J. Geophys. Res.*, 75, 1585-1613, 1970.
- Lloyd, F. E. and D. Bailey, Light element metasomatism of the continental mantle: The evidence and the consequences, *Physics and Chemistry of the Earth*, 9, 389-416, 1975.
- Menard, H. W., Depth anomalies and the bobbing motion of drifting islands, *J. Geophys. Res.*, 78, 5128, 1973.
- Morgan, W. J., Plate motions and deep mantle convection, *Geol. Soc. Amer. Memoir*, 132, 7-22, 1972.
- Morgan, W. J., Hotspot tracks and the opening of the Atlantic and Indian oceans, in *The Sea*, in press, 1979.
- Mysen, B., Trace element partitioning between garnet peridotite minerals and water-rich vapor: Experimental data from 5 to 30 kbar, *Am. Mineral.*, 64, 274-287, 1979.
- Nesbitt, R. W., Skeletal crystal forms in the ultramafic rocks of the Yilgarn Block, Western Australia; evidence for an Archaean ultramafic liquid, *Geol. Soc. Australia Spec. Pub.*, 3, 331-350, 1972.
- Nixon, P. H. (ed.), Lesotho kimberlites, Lesotho National Development Corp., Maseru, Lesotho, 1973.

- Nur, A. and Z. Ben-Avraham, Speculations on mountain building and the lost Pacifica continent, *J. Phys. Earth*, 26, Suppl., 521-537.
- O'Hara, M., M. J. Saunders, and E. L. P. Mercy, Garnet-peridotite, primary ultrabasic magma and eclogite: Interpretation of upper mantle processes in kimberlite, *Phys. Chem. of the Earth*, 9, Pergamon Press, 571-604, 1975.
- Rhodes, J. M. and J. B. Dawson, Major and trace element chemistry of peridotite inclusions from the Lashine Volcano, Tanzania, *Phys. and Chem. of the Earth*, 9, Pergamon Press, 545-558.
- Ridley, W. I. and J. B. Dawson, Lithophile trace element data bearing on the origin of peridotite xenoliths, Ankaramite and Carbonatite from Lashaine Volcano, N. Tanzania, *Phys. and Chem. of the Earth*, 9, 559-570, 1975.
- Ringwood, A. E., Composition and Petrology of the Earth's Mantle, McGraw-Hill, New York, 1975.
- Schilling, J. G., Iceland mantle plume: geochemical evidence along Reykjanes Ridge, *Nature*, 242, 565-579, 1973.
- Schilling, J. G., Azores mantle blob: rare-earth evidence, *Earth Planet. Sci. Lett.*, 25, 103-115, 1975.
- Schilling, J. G., Rare earth, Fe, and Ti variations along the Galapagos spreading center, and their relationship to the Galapagos mantle plume, *Nature*, 261, 108-113, 1976.
- Shimizu, N., Geochemistry of ultramafic inclusions from Salt Lake Crater, Hawaii and from southern Africa kimberlites, *Phys. and Chem. of the Earth*, 9, 655-670, 1975.

- Sun, S. and G. N. Hanson, Evolution of the mantle; geochemical evidence from alkali basalt, *Geology*, 3, 297-302, 1975.
- Sun, S. S. and G. N. Hanson, Origin of Ross Island basanitoids and limitations upon the heterogeneity of mantle sources for alkali basalts and nephelonites, *Contrib. Mineral. Petrol.*, 52, 77-106, 1975.
- Tatsumoto, M., Isotopic composition of lead in oceanic basalt and its implication to mantle evolution, *Earth Planet. Sci. Lett.*, 38, 63-87, 1978.
- Thiessen, R., K. Burke, and W. S. F. Kidd, African hotspots and their relation to the underlying mantle, *Geology*, 7, 263-266, 1979.
- Unni, C. K. and J. G. Schilling, Cl and Br degassing by volcanism along the Reykjanes Ridge and Iceland, *Nature*, 272, 19-23, 1978.
- Viljoen, R. P. and M. J. Viljoen, Evidence for the composition of the primitive mantle and its products of partial melting, *Spec. Publ. Geol. Soc. S. Africa*, 2, 275-295, 1969.
- White, W. M., M. Tapia and J.-G. Schilling, The petrology and geochemistry of the Azores Islands, *Contrib. Mineral. Petrol.*, 69, 201-213, 1979.
- White, W. M., and J. G. Schilling, The nature and origin of geochemical variations in Mid-Atlantic ridge basalts from the central North Atlantic, *Geochim. Cosmochim. Acta*, 42, 5101-1516, 1978.
- Windley, B., The Evolving Continents, Wiley, London, 385 pp., 1977.
- Wyllie, P. J., *The Dynamic Earth*, Wiley and Sons, Inc., New York, 416 pp., 1971.
- Yoder, H. S., Jr., Generation of basaltic magma, *Natl. Acad. Sci.*, Washington, D.C., 265 pp., 1976.

Table 1
POSSIBLE COMPOSITIONS OF THE TRANSITION ZONE ECLOGITE LAYER

	<u>(1)</u>	<u>(2)</u>	<u>(3)</u>	<u>(4)</u>	<u>(5)</u>	<u>(6)</u>	<u>(7)</u>	<u>(8)</u>
SiO ₂	50.3	47.8	46.2	45.7	49.5	46.6	45.5	47.2 ± 2.4
TiO ₂	1.2	0.6	0.7	0.4	0.5	0.8	1.9	0.6 ± 0.3
Al ₂ O ₃	16.5	12.1	12.6	17.9	8.5	13.7	12.4	13.9 ± 4.5
FeO	8.5	9.0	11.4	11.2	8.8	9.1	9.5	11.0 ± 3.6
MnO	0.1	0.1	0.2	0.2	0.2	0.2	0.2	0.2 ± 0.1
MgO	8.3	17.8	16.6	11.9	16.2	16.1	18.8	14.3 ± 3.0
CaO	12.3	11.2	10.5	7.4	10.6	11.8	9.7	10.1 ± 2.2
Na ₂ O	2.6	1.3	1.2	2.0	1.7	1.3	1.6	1.6 ± 1.1
K ₂ O	0.2	0.03	0.02	0.4	1.1	0.02	0.1	0.5 ± 0.4

- (1) Oceanic tholeiite (Kay et al, 1970, Engel and Engel, 1964)
- (2) Oceanic crust, calculated from ophiolite section (Elthon, 1979)
- (3) Basaltic "komatiite", Gorgona Island (Gansser et al, 1979)
- (4) } Mantle eclogites (Nixon, 1973)
- (5) }
- (6) Possible eclogite extract in fractionation of primary magma in upper mantle (O'Hara et al, 1975)
- (7) Picrite (Ringwood, 1975)
- (8) Average biminerallitic eclogite in kimberlite (Ito and Kennedy, 1974)

Table 2

ESTIMATES OF LITHOPHILE ELEMENT CONCENTRATIONS
(ppm) IN BULK EARTH, THE ECLOGITE AND PERIDOTITE
SOURCE REGIONS AND VARIOUS PRODUCTS OF THESE
SOURCE REGIONS

	K	Rb	Sr	Rb/Sr	U	Ref.
Abyssal tholeiite	732	0.75	92	0.008	0.16	(1)
Kimberlite eclogite	820	0.7	95	0.007	0.17	(2)
Kimberlite peridotite	617	3.4	55	0.061		(2)
Kimberlite peridotite	483	2.0	59	0.035		(2)
"Plume" source	>468	2.5	60	0.042		(1)
Continental flood basalts	6400	17	320	0.053	0.3	(3,4)
Ocean island basalts	3160	5.3	231	0.023		(1)
Continental crust	15 000	33	370	0.089	0.7	(3)
Intergranular material in eclogites	16 000	48	550	0.087		(2)

TABLE 2

(LEGEND)

- (1) White and Schilling (1978)
- (2) Allsop et al (1969)
- (3) Jacobsen and Wasserburg (1979)
- (4) Carmichael et al (1974)

Table 3

TRACE ELEMENTS IN INFERRED MID-OCEAN RIDGE BASALTS,
ECLOGITE XENOLITHS, PARTIAL MELT OF "FERTILE" GARNET PERIDOTITE
AND CONTINENTAL FLOOD BASALTS

	<u>Oceanic</u>			<u>Continental</u>		
	(1)	(2)	(3)	(4)	(5)	(6)
K	820	732	700	2000-3600	4000	6400
Rb	0.7	0.75	1.1	11-20	20	17
Sr	95	92	134	30-500	400	320
K/Rb	1170	976	640	100-300	400	376
Rb/Sr	0.01	0.008	0.01	0.04-0.3	0.005	0.053

- (1) "Ideal" eclogite xenolith (Allsop et al, 1969). Potential source region for oceanic tholeiites.
- (2) Oceanic tholeiite (White and Schilling, 1978)
- (3) Oceanic tholeiite (Table 1)
- (4) Inferred partial melt (20%) product from fertile garnet peridotite xenoliths with sterile peridotite xenoliths as residual (Rhodes and Dawson, 1975)
- (5) Karoo basalts (Carmichael et al, 1974)
- (6) Continental flood basalts (Jacobsen and Wasserburg, 1979)

Table 4

INCLUSIONS IN KIMBERLITES AND ESTIMATES
OF PRIMITIVE MANTLE COMPOSITION

	Xenoliths		Mantle Compositions				
	(1)	(2)	(3)	(4)	(5)	(6)	(7)
SiO ₂	47.2	47.3	47.3	47.3	48.0	46.6	44.8
TiO ₂	0.6	0.05	0.2	0.2	0.3	0.3	0.2
Al ₂ O ₃	13.9	1.6	4.1	5.3	5.2	3.0	5.3
FeO	11.0	5.8	6.8	7.4	7.9	10.4	10.3
MgO	14.3	43.8	37.9	35.0	34.3	34.2	34.3
CaO	10.1	1.0	2.8	3.7	4.2	4.8	4.4
Na ₂ O	1.0	0.2	0.5	0.6	0.3	0.2	0.4
K ₂ O	0.5	0.2	0.2	0.3	0.2	0.03	0.03

- (1) Average eclogite nodules (Ito and Kennedy, 1974)
- (2) Average garnet lherzolite in kimberlite (O'Hara et al, 1975)
- (3) 20% eclogite, 80% garnet lherzolite.
- (4) 30% eclogite, 70% garnet lherzolite.
- (5) Primitive mantle (Ganapathy and Anders, 1974)
- (6) Average peridotitic komatiite, S. Africa (Viljoen and Viljoen, 1969)
- (7) Peridotite with quench texture, W. Australia (Nesbitt, 1972)

FIGURE CAPTIONS

- Figure 1. Schematic of the primary plate tectonic cycle with the transition zone eclogite layer serving as the source and sink of the oceanic lithosphere. The harzburgite portion of the lithosphere remains in the upper mantle.
- Figure 2. Flow chart of mantle differentiation. The primitive differentiation results in basalt and peridotite. Partial melting of the basalt layer concentrates the LIL elements into the continental crust.
- Figure 3. Schematic illustration of isotherms for convection in a stratified system showing boundary layer detachment. The locations of descending plumes in the lower layer will be controlled by the locations of the cold isotherms in the upper layer. Material penetrating into the lower layer may initiate diapiric uprise from this region.
- Figure 4. Illustration of flow in superposed convecting layers. The lower layer is internally heated and is characterized by broad upwellings. The upper layer is mainly heated from below and is characterized by narrow ascending plumes.

Figure 5. Geotherm in a chemically stratified mantle showing the thermal boundary layer and the path of ascent of an eclogite diapir that starts to melt at about 250 km. Temperatures at the top of the eclogite layer must appreciably exceed the solidus before the diapir has sufficient buoyancy to rise through the peridotite layer. It may heat further if its upward escape is prevented by an overlying continental lithosphere. Extrusion temperatures and depth of complete melting may therefore be greater than shown here. Dry melting curves are from Wyllie (1971) and Yoder (1976).

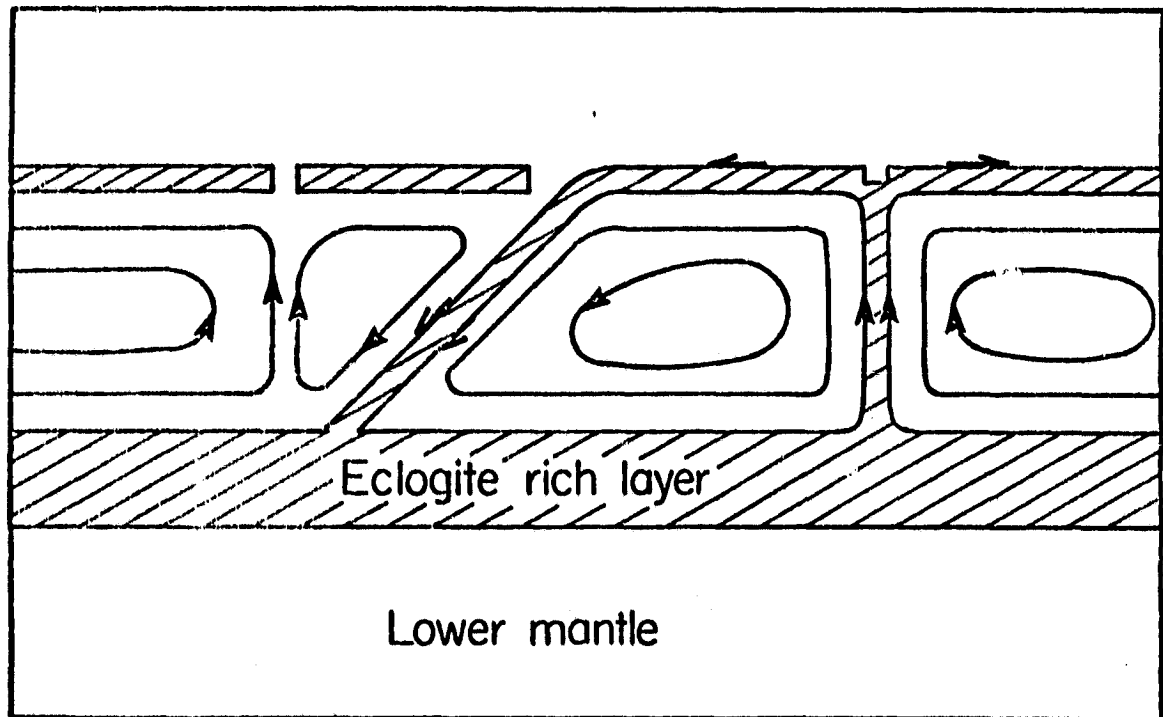


Fig. 1

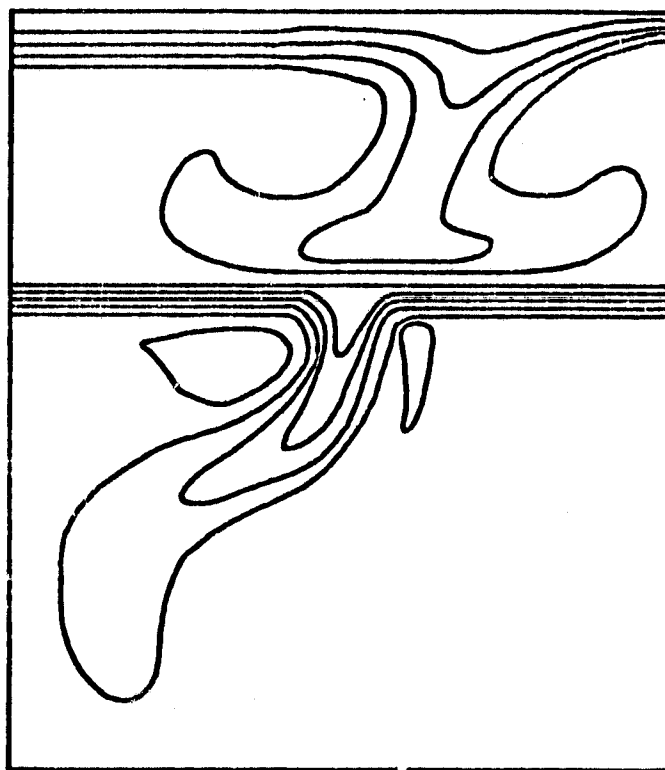


Fig. 3

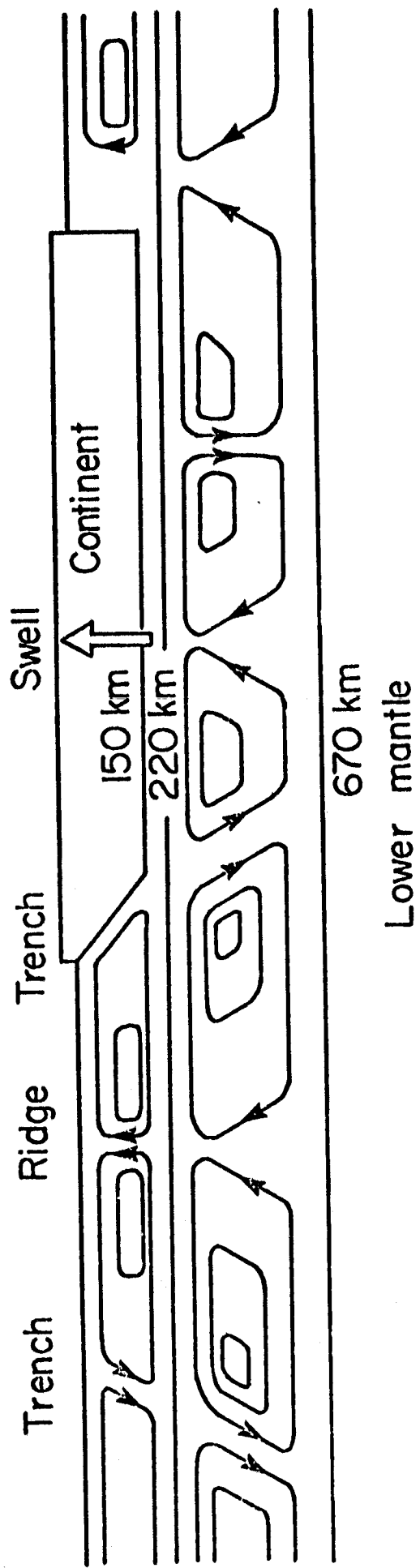


Fig. 4

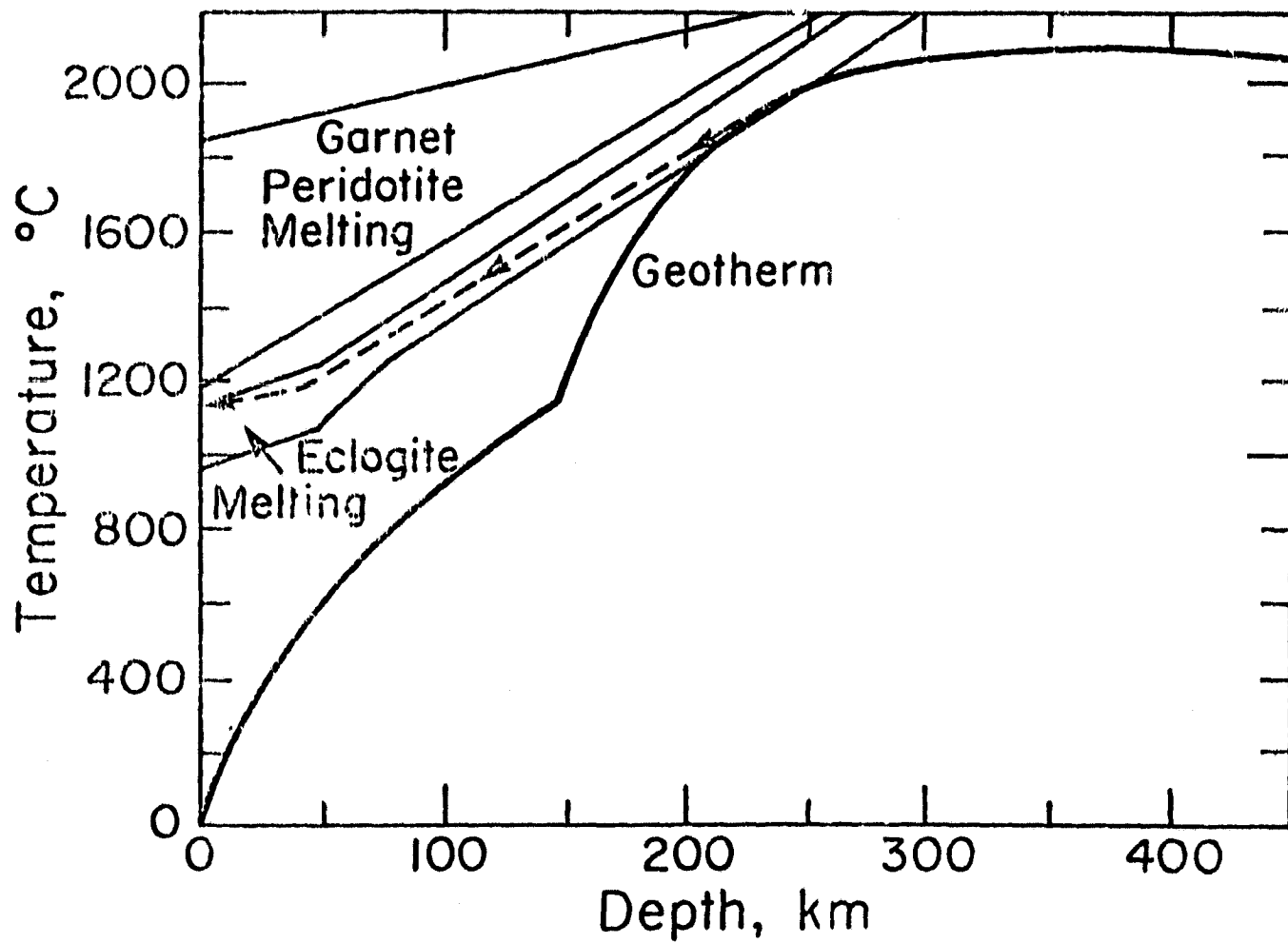


Fig. 5

APPENDIX V

PLATE TECTONICS ON VENUS

Don L. Anderson

Geophysical Research Letters, submitted.

Revision:
Sept. 22, 1980

PLATE TECTONICS ON VENUS

Don L. Anderson

Seismological Laboratory, California Institute of Technology,
Pasadena, California 91125

Abstract

The high surface temperature of Venus implies a permanently buoyant lithosphere and a thick basaltic crust. Terrestrial style tectonics with deep subduction and crustal recycling is not possible. Overthickened basaltic crust partially melts instead of converting to eclogite. Because mantle magmas do not have convenient access to the surface the ^{40}Ar abundance in the atmosphere should be low. Venus provides an analog to Archean tectonics on the Earth.

Introduction

The surface temperature of Venus is about 450 K warmer than the surface of the Earth. This affects the buoyancy, thermal expansion, thermal conductivity and, hence, the thermal evolution and ultimate fate of the lithosphere. The pressure in the upper mantle of Venus is at least 12% less than at equivalent depths in the Earth's upper mantle. Thus, the depth of melting, the locations of upper mantle phase changes and the viscosity of the upper mantle will be different for the two planets. The buoyancy and thermal properties of the lithosphere control the style of plate tectonics and the associated time and length scales.

Most discussions of the comparative tectonics between Earth and Venus address only the differences in viscosity.

The oceanic lithosphere of the Earth cools as it ages and it eventually becomes denser than the underlying mantle. This instability develops after about 40 m.y. (Oxburgh and Parmentier, 1977). Once cooling reaches a depth of 50 km the garnet pyroxenite or eclogite transformations may make a substantial contribution to the negative buoyancy of the lithosphere. Continents and oceanic plateaus resist subduction because of their thick low-density crusts. The fate of the terrestrial lithosphere, therefore, depends on both chemistry and temperature. The purpose of this paper is to investigate the implications for Venus tectonics of its high surface temperature. We will conclude that the surface thermal boundary layer on Venus is permanently buoyant and that the reversible part of mantle convection occurs below about 100 km.

The terms lithosphere and thermal boundary layer will be used for the cold outer layer of a planet. Neither term is strictly correct since the former has a strength connotation and the density of the latter is usually assumed to depend on temperature alone. The thickness of the mechanical or rheological lithosphere depends on temperature and, possibly, composition and is proportional to the thickness of the thermal lithosphere that is discussed here.

Lithospheric cooling

The average temperature of the oceanic lithosphere decreases about 660°C as it ages. The thickness of the conductively cooled thermal

boundary layer increases at a rate controlled by the thermal conductivity and the difference between the surface and interior temperatures. Since the crustal and harzburgite portions of the boundary layer are both less dense than the underlying mantle a gravitational instability can only occur after the conductive cooling penetrates for a sufficient distance, ~30 km, into the denser upper mantle portion of the boundary layer. In some petrological models the lower lithosphere is pyroxenitic. Upon cooling, plagioclase and spinel pyroxenite convert to garnet pyroxenite or eclogite with a substantial increase in density. These phase changes also require cooling to depths in excess of 30 kilometers.

The equilibrium thickness, δ , of a conductive boundary layer is

$$\delta = K\Delta T/\dot{Q} \quad (1)$$

where K is the thermal conductivity, $\Delta T/\delta$ is the average thermal gradient and \dot{Q} is the mantle heat flow. For K of 7×10^{-3} cal/cm sec°C, ΔT of 1300°C and \dot{Q} of $0.6 \mu\text{cal/cm}^2\text{sec}$, values appropriate for the terrestrial oceanic lithosphere, δ is about 150 km. For a lithosphere composed of 6 km of basalt, 24 km of harzburgite and a lower lithosphere composed of undepleted mantle, the equilibrium boundary layer for $\Delta T = 1300^\circ\text{C}$ is 1% denser than underlying mantle and therefore gravitationally unstable. Phase changes in the lower lithosphere may contribute further to the negative buoyancy.

For a given mantle temperature and heat flow the equilibrium thickness of the boundary layer on Venus is reduced by two effects; K

is about 30% lower at the higher temperature (Schatz and Simmons, 1972) and ΔT is reduced by 460°C. This reduces δ on Venus to 42 km and its density, assuming similarity with oceanic lithosphere, is 2% lighter than the underlying mantle. This is a result of the smaller amount of cooling, the higher proportion of basalt and harzburgite in the boundary layer and the lack of significant cooling where it is most required, i.e. the lower lithosphere. Furthermore, phase transformations in the lower lithosphere cannot contribute at high temperature and low pressure. Basalt has about one-half the thermal conductivity of ultramafic rocks. This reduces the thickness of the boundary layer to about 27 km if it is mainly basaltic.

The buoyancy of the Venus lithosphere, even for a relatively thin crust, is greater than the buoyancy of young oceanic lithosphere on Earth. Since a thicker crust for Venus is probable, it is certain that the surface thermal boundary layer for Venus is permanently buoyant and stable against subduction.

The temperature gradient in the conductive layer can be written

$$dT/dz = (1/K)(\dot{Q}_s - Az) \quad (2)$$

where \dot{Q}_s is the surface heat flow and A is the heat production rate in the layer. With basaltic conductivities and radioactivities ($A \sim 10^{-14}$ cal/cm³ sec) the temperature and thermal gradient at 20 km are 950°C and 23°C/km respectively and the solidus of dry basalt will be exceeded at depths shallower than 40 km. Eclogite is not stable in the mantle of Venus at depths shallower than about 100 km (Anderson, 1980).

Since crust cannot subduct and the garnet-rich assemblages are well below the boundary layer, all partial melt products of mantle differentiation that make their way into the outer 100 km or so will remain there. The crust is therefore likely to be thicker than either the oceanic crust or the average crustal thickness on Earth. It may be thicker than either the mechanical lithosphere or the thermal boundary layer. Crust which is overthickened by compression, buckling, thrusting, or collision will melt at its base. The resulting plutonism will further increase the density contrast between crust and mantle and increase the radioactivity and incompatible trace element content of the parts of the crust so affected.

The characteristic time for thickening of the boundary layer is

$$\tau = (\rho C_p / 4 K) \delta^2 \quad (3)$$

which for $\rho = 3.5 \text{ g/cm}^3$, $C_p = 0.25 \text{ cal/g}^\circ\text{C}$ and $\delta = 150 \text{ km}$ is $\sim 200 \text{ m.y.}$ for the Earth. For Venus the characteristic time is 20 m.y. or less.

Therefore, Venus has a thick, low-density and permanently buoyant crust-lithosphere that very quickly reaches thermal equilibrium. Upper mantle temperatures are high, resulting in low viscosities.

The basalt-eclogite transformation will occur below about 100 km. The driving mechanism for mantle convection may therefore be partly chemical. Basaltic melt rising in an upcurrent will freeze as eclogite if it remains below about 100 km, and provide the negative buoyancy required for overturn. The 670 km discontinuity which halts eclogite subduction on Earth (Anderson, 1979a,c) will occur at about 800 km in

Venus giving a convecting layer about 700 km thick. This should generate topographic and gravity anomalies of about 1400 km wavelength.

Equation (1) suggests that plate tectonics in the Archean on Earth may have been similar to present day tectonics on Venus. The small δ in early Earth history was primarily due to the high \dot{Q} , from radioactive decay, which was at least three times larger 4×10^9 years ago. The thermal boundary layer thickens as \dot{Q} decreases until eventually it becomes unstable and overturns, destroying the early geological record and setting the stage for the present style of tectonics (Anderson, 1979a,b, 1980). This overturn event would allow much of the accumulated ^{40}Ar in the upper mantle to escape and the subsequent steady-state ridge/trench style of tectonics allows continuous outgassing of the terrestrial mantle.

Early Evolution of Earth and Venus

The initial evolution of Earth and Venus were likely quite similar. The high accretional energies would result in partial melting of the mantle and upward transport of a picritic melt. Crystallization of this upper mantle melt layer, or magma ocean, yields a thin plagioclase-rich crust and a deep eclogite cumulate layer. An olivine-orthopyroxene cumulate layer may form at intermediate depths. This kind of scenario is well documented for the Moon except that pressures are too low for extensive eclogite fractionation. Eclogite fractionation removes Al_2O_3 from the melt and reduces the thickness of an early anorthositic crust. Eclogite cumulates sink no deeper than 670 km on Earth because of the intervention of the ilmenite and perovskite phase changes in a

peridotitic mantle (Anderson, 1979c). An eclogite cumulate layer will be deeper and smaller in Venus because of the effect of temperature and pressure on the phase boundaries and the limited stability field of eclogite in the upper mantle. Nevertheless, the early tectonics, geochemical differentiation and outgassing of the two planets were likely to have been similar.

If the outer layer becomes unstable as the planet cools, the situation changes. Subducted slabs affect both the flow and thermal regime of the upper mantle. The sinking of the cold boundary layer deep into the upper mantle drags cold isotherms to depth and allows hot replacement material to rise at ridges. This leads to relatively large lateral and vertical temperature differences in the upper mantle and rapid convection in which the surface boundary layer participates.

The mantle of the Earth contains approximately 15-20% of a basaltic component. If the mantle were well differentiated this would give a crustal layer 350-450 km in thickness. Only the top 50 km would be buoyant, because of the eclogite transformation, but this is still more than 4 times the present average crustal thickness. The lunar and Martian crusts are much closer to being the appropriate thickness for a well differentiated planet in spite of the fact that accretional heating must have been less for these bodies. The difference, of course, is due to the continuous removal of basaltic crust from the surface implying a long-term storage reservoir at depth. The size of this reservoir has been estimated to represent about 20% of the mantle (Anderson, 1980).

Samples thought to be representative of the upper mantle are depleted in Al_2O_3 , CaO and SiO_2 compared to cosmochemical estimates of

mantle composition. They are also depleted in trace elements which are retained by the eclogite minerals, garnet and clinopyroxene. The degree of depletion implies an eclogite layer about 450 km thick which is probably deeper than 200 km.

The ^{40}Ar abundance for Venus is about an order of magnitude less than for the Earth (Pollack and Black, 1979). This suggests that late outgassing has been less efficient for Venus than for the Earth in spite of the higher surface and upper mantle temperatures. This is easily understood with the present model. On Venus, mantle melts and their volatiles mainly have access to the surface through relatively transient rifts. Because of the conservation of near surface material these rifts can only form when the crust compresses or thickens somewhere else on the planet. The amount of early outgassing on the two planets may have been similar but Venus did not experience the early lithospheric overturn event or the outgassing associated with continuous crustal renewal at ridge axes.

Conclusions

The high surface temperature of Venus has several important tectonic implications. The most significant is the small amount of cooling that the lithosphere experiences before it reaches thermal equilibrium. This increases its buoyancy and long-term stability at the surface when compared with the terrestrial oceanic lithosphere. Since crust cannot be recycled into the mantle the thickness of the basaltic crust on Venus is much greater than on Earth. The combination of a thick crust and high temperatures decreases the thermal conductivity of

the lithosphere. This means that for a given mantle heat flow the temperature gradient in the lithosphere is greater than would be the case for a cold lithosphere with a thin crust. This leads to high upper mantle temperatures, low viscosities and the possibility of partial melting at relatively shallow depths.

Acknowledgements

This research was supported by the National Aeronautics and Space Administration, Grant No. NGL05-002-069 and the Earth Sciences Section of the National Science Foundation, Grant No. EAR77-14675. Contribution no.3504, Division of Geological and Planetary Sciences, California Institute of Technology, Pasadena, california 91125.

References

- Anderson, Don L., Tectonics and composition of Venus, *Geophys. Res. Lett.*, 7, 101-102, 1980.
- Anderson, Don L., The upper mantle transition region; eclogite?, *Geophys. Res. Lett.*, 6, 433-436, 1979a.
- Anderson, Don L., The deep structure of continents, *J. Geophys. Res.*, 84, 7555-7560, 1979b.
- Anderson, Don L., Chemical stratification of the mantle, *J. Geophys. Res.*, 84, 6297-6298, 1979c.
- Oxburgh, E. R. and E. M. Parmentier, Compositional and density stratification in oceanic lithosphere - causes and consequences, *J. Geol. Soc. Lond.*, 135, 343-555, 1977.
- Pollack, J. B. and D. C. Black, Implications of the gas compositional measurements of Pioneer Venus for the origin of planetary atmospheres, *Science*, 205, 56-59, 1979.
- Schatz, J. F. and G. Simmons, Thermal conductivity of earth materials at high temperatures, *J. Geophys. Res.*, 77, 6966-6983, 1972.

APPENDIX VI

HOTSPOTS, BASALTS AND THE EVOLUTION OF THE MANTLE

Don L. Anderson

Science, submitted.

Hotspots, Basalts and the Evolution of the Mantle

Don L. Anderson

Seismological Laboratory

California Institute of Technology

Pasadena, California 91125

Revised: July 23, 1980

Abstract

Trace element concentration patterns of continental and ocean island basalts and of mid-ocean ridge basalts are complementary. The relative sizes of the source regions for these fundamentally different basalt types can be estimated from the trace element enrichment/depletion patterns. Their combined volume occupies most of the mantle above the 670 km discontinuity. The separate source regions are the result of early mantle differentiation and crystal fractionation from the resulting melt. The MORB source evolved from an eclogite cumulate which lost its late stage enriched fluids at various times to the shallower mantle and continental crust. The MORB source is primarily garnet and clinopyroxene, while the continental and ocean island basalt source is a garnet peridotite that has experienced secondary enrichment. These relationships are consistent with the evolution of a terrestrial magma ocean.

Introduction

Hotspots, or plumes, have not yet been fitted satisfactorily into either the tectonic or geochemical framework for the evolution of the mantle. From the point of view of mantle processes and the chemical evolution of the mantle the alkali volcanism associated with hotspots is a very important process even if the abundance of such rocks is small compared to the volume of abyssal tholeiites (1). The processes of creation and subduction of oceanic crust and lithosphere clearly account for most of the mass transport into and out of the upper mantle and the study of mid-ocean ridge basalts (MORB) has placed important constraints on the part of the mantle that is providing these magmas. Trace element and isotopic considerations show, however, that the source region for MORB cannot be representative of the average composition of the mantle nor can it have existed as a separate entity with its present characteristics for the full age of the Earth. The composition, location and volume of this source region, which we designate MORBS, are still uncertain. It appears to be very large, homogeneous, global in extent, and to be the result of a previous differentiation or fractionation process that depleted it, relative to other source regions, of most of the incompatible elements. On the other hand, it is clearly not lacking in a basaltic component. The continental crust is complementary to MORB in both trace elements and isotopic ratios (2,3). Formation of the continents has presumably been at least partially responsible for the depletion of the so-called oceanic mantle. If the continental crust is the only enriched reservoir, then mass balance

calculations indicate that only about 30% of the mantle has been processed, the rest remaining undifferentiated and primordial (3,4). A large primitive reservoir would be difficult to reconcile with other evidence regarding the early thermal evolution of planetary interiors. There is, however, evidence for an additional enriched reservoir in the mantle. Magmas from continental interiors, rift zones, oceanic islands, anomalous ridge segments and island arcs, mantle xenoliths from kimberlites and alkali basalts, and kimberlites themselves, all indicate the presence of a mantle reservoir with trace element concentrations that are also complementary to trace element concentrations in MORB. This reservoir apparently is also global and can provide magmas to a variety of tectonic environments including all types of plate boundaries as well as plate interiors. These magmas, of which alkali basalts are one example, are not nearly as voluminous as MORB but they indicate the presence of an enriched region or layer which may be substantial compared to the continental crust. We shall designate this as the hotspot or plume reservoir, or simply PLUME (5), and assume that it is the source of alkali basalts, nephelinites, melilitites, basanites, kimberlites and continental tholeiites which it provides by varying degrees of partial melting (6,7). One of the diagnostic signatures of these basalts is the rare-Earth element (REE) pattern which implies a source enriched by about 10 in LREE and 3 in the HREE, relative to chondrites (6,7,8).

PLUME basalts also have high ratios of Rb/Sr, Rb/K, Ba/K, Nd/Sm, Ba/Nd, Ba/Sr, Nb/Zr, $^{87}\text{Sr}/^{86}\text{Sr}$, and $^{144}\text{Nd}/^{143}\text{Nd}$, and high concentrations

of H_2O , CO_2 , Ti, K, Rb, Sr, Ba, La, Nd, Th, and U relative to MORBS. These characteristics are shared by continental and ocean island basalts and are also evident, albeit diluted, in back-arc basins, island arcs, and transitional or anomalous ridge tholeiites. Other characteristics that may be common but which have been studied in only a few hotspot locations are high abundances of Cl, F, Br and the primordial rare gases (9). The process that led to the enrichment of PLUME will have depleted other, presumably deeper, regions of the mantle. The absolute and relative sizes of these enriched and depleted reservoirs bear directly on the problem of the evolution of the mantle and, in particular, on the question of whether there is a large primitive reservoir in the mantle.

Basalt source regions

The continental crust is extremely enriched in the incompatible trace and minor elements. Continental tholeiites, basanites, nephelenites, alkali basalts, kimberlites and basalts from oceanic islands are also enriched. The complement to the depleted mid-ocean ridge source region may, therefore, be much more voluminous than just the continental crust. The trace element and isotopic affinities of these rocks, regardless of their tectonic setting, suggests that they are all derived from a similar source region. This reservoir, PLUME, has previously been referred to as continental mantle, the enriched source region or primitive mantle. Its location is uncertain but it appears to be a global layer. Proposals for its location include the uppermost (6,10) and lowermost (11) mantle. In trace element ratios

such as Ba/Nd, Nd/Sm, Ba/Sr, Ba/K and Rb/K there is a progressive increase from ocean island and island arc basalts, basalts from anomalous ridge segments, continental tholeiites, alkali basalts to kimberlites. Mid-ocean ridge basalts have much lower ratios and tholeiites from back-arc basins are generally slightly higher than MORB. Trace element concentrations vary systematically through the compositional spectrum olivine melilitite, olivine nephelinite, basanite, alkali basalt, and olivine tholeiite and can be explained by varying degrees of partial melting ranging from 4 to 25% from a common source region which is enriched in the strongly incompatible elements (Ba, Sr, Th, U, LREE) by 10x chondritic and in the moderately incompatible elements (Ti, Zr, Hf, Y, HREE) by a factor of about 3 (6-8). Mid-ocean ridge basalts are derived from a very different source which is depleted in the large-ion lithophile (LIL) elements. The complementary nature of the two source regions is possibly due to the migration from the MORB source region of a melt or fluid with incompatible element concentrations similar to those of kimberlite. This fluid depletes the MORB source region and enriches the complementary mantle reservoir. The upper mantle low-velocity zone (LVZ) is a likely repository of these volatile and trace element enriched fluids and, therefore, a possible source region for the enriched magmas which are characteristic of the plume or hotspot source. Kimberlites come from depths as great as 220 km, consistent with an origin near the bottom of the LVZ. The xenoliths in kimberlites and alkali basalts represent mantle fragments from various shallower depths and also generally exhibit enrichment of the type inferred for the plume

source region. There is now a wealth of evidence for uppermantle metasomatism (12, 30) and enrichment events at various times. The source of the enriching fluid has not been much discussed.

The complementary nature of continental and oceanic tholeiites is illustrated in the center part of Figure 1. Alkali basalts, nephelinites, melilitites and basanites have similar but more enriched patterns than continental flood basalts, consistent with their derivation from the same source region by smaller degrees of partial melting. Continental and abyssal tholeiites exhibit reflection symmetry about a line corresponding to a 6 to 7 fold enrichment over average mantle concentrations.

Continental and ocean island basalts are relatively depleted in those elements that are retained by garnet and clinopyroxene. The reverse is the case for abyssal tholeiites. Since garnet and cpx are reduced or eliminated during the large amounts of partial melting usually inferred for the formation of tholeiites (6), the inverse ga-cpx pattern of plume basalts must be related to a prior history involving eclogite fractionation or invasion of PLUME by a fluid that was in equilibrium with a ga-cpx assemblage.

The origin of island arc basalts is still controversial but they have PLUME affinities in such trace element ratios as Rb/K, Rb/Sr, Ba/K, Ba/Sr and Ba/Nd. These ratios are closer to ocean island basalts, alkali basalts and continental flood basalts than they are to mid-ocean

ridge basalts. Back-arc basin basalts are intermediate to MORB and hotspot magmas, suggesting a mixture from a deeper MORB source and an overlying enriched source region. Ocean island tholeiites also appear to be mixtures both in trace element and isotopic ratios (2). The fact that both MORB and basalts with continental affinities are available at ridge environments, island arcs, oceanic islands and well developed continental rifts suggests a compositionally stratified mantle. The order of appearance of these basalt types is consistent with the shallower layer being enriched in the incompatible trace elements. In a stratified mantle the deeper layer should be denser and, therefore, more garnet rich. The ratio of concentrations in MORB to those in continental tholeiites indicates that the MORB source region, although depleted in most of the incompatible trace elements, has selectively retained those that are most comfortable in the garnet and clinopyroxene lattices. This suggests that MORBS is an eclogite or garnet pyroxenite cumulate.

The composition and volumes of the two source regions

The concentrations of some key incompatible trace elements in various magma types, normalized to average mantle concentrations, are shown in Figure 1. Relative to the average mantle, continental tholeiites, alkali basalts, kimberlites and the continental crust are all most enriched in K, Rb, Ba, La and U. These are the elements that are most discriminated against by the major mantle minerals, olivine, orthopyroxene, clinopyroxene and garnet, i.e., they have the lowest

mineral/melt partition coefficients. The other elements are also strongly rejected by olivine and orthopyroxene, having partition coefficients of less than 0.03 for these minerals (6). On the other hand, garnet and clinopyroxene have partition coefficients greater than about 0.1 for Y, Nd, Sm, Sr, and Yb. These are the least enriched elements in the magmas with continental and ocean island affinities and the most enriched in MORB. It appears that garnet and clinopyroxene are abundant minerals in the MORB source region, and that the fluid which enriched PLUME was previously in equilibrium with a ga-cpx rich reservoir.

The high concentration of Y and Yb in MORB relative to other elements and relative to concentrations in basalts from PLUME, the enriched source region, is particularly significant. These elements have mineral/melt partition coefficients greater than unity for garnet. Mass balance calculations suggest that most of the terrestrial inventory of Y and Yb may be in MORBS. This can only be accomplished if garnet is a dominant phase and if most or all of the mantle has experienced differentiation. Partial melting of primitive mantle concentrates Y and Yb into the melt; crystallization of this melt at moderate pressure would concentrate these elements into an eclogite cumulate.

The relative volumes of the two source regions can be inferred from Figure 1 if it is assumed that they, plus the continental crust, give an undifferentiated terrestrial pattern for the very incompatible elements. Using 0.56% for the mass of continental crust relative to the mantle (3)

we compute that the mass of MORB must exceed the tholeiitic fraction of PLUME by a factor of 12 to 15. Continental tholeiites represent about 20% melting of a peridotitic source region (6) and MORB must be mixed with at least 15% olivine to recover the composition of its parent magma (13,14). The residual crystals in both cases are assumed to be depleted because of their very low partition coefficients (6,8). The MORB source region is, therefore, at least 2.8 to 3.5 times the mass of PLUME and the enrichment of the combined source regions, relative to primitive mantle, is about 3.3 to 3.8. Note that MORB is depleted only in a relative sense. Compared to average mantle abundances it is enriched. This suggests that MORBS plus PLUME are complementary to the remainder of the mantle from which they have presumably been removed by partial melting. The enrichment factor implies whole mantle differentiation and a residual mantle about 2-1/2 times the size of the combined reservoirs.

By assuming that the very incompatible elements have been entirely fractionated into the two source regions it is possible to estimate their total mass. For example, if La is depleted in the lower mantle the combined source regions represent 26 to 30% of the mantle. This corresponds to a thickness of 560 to 640 km in the upper mantle, or a region extending upwards from the 670 km discontinuity to a depth of 27 to 110 km. If we take the transition region, 220-670 km, to be the depleted source region (20), then PLUME is 130-160 km thick, about the average thickness of the low-velocity zone (LVZ).

A similar calculation for the other strongly incompatible elements

(K, Rb, Ba, U) gives a range of 21-38% for MORBS plus PLUME. These are upper bounds since it has been assumed that the whole mantle has been processed and depleted. This, however, is a good approximation if olivine and orthopyroxene are the main residual phases. It is significant that the above estimates of the relative and absolute sizes of the principal mantle reservoirs correspond to the main subdivisions of the upper mantle, the LVZ and the transition region. The 670 km depth corresponds to a major seismic discontinuity and the maximum depth of earthquakes.

Other elements can be used to estimate the sizes of the individual reservoirs. The partition coefficients of Yb and Y are such that they strongly prefer the garnet structure (15). Both are enriched in MORB relative to PLUME, suggesting a higher portion of garnet in the former. If the entire mantle complement of Y and Yb reside in MORBS, then this would represent 14-17% of the mantle or an upper mantle equivalent thickness of 300 to 364 km. Sc is partitioned into garnet and clinopyroxene by a factor of 8 relative to olivine and orthopyroxene. Using this ratio of enrichment for the MORB source relative to the rest of the mantle it would constitute 26% of the mantle.

K, Rb, Ba, La and U have the highest relative concentrations in PLUME. These are the elements with the lowest partition coefficients for the major mantle minerals and those that are most likely to be concentrated into PLUME by melts or metasomatic fluids. The PLUME abundances of these elements can account for the entire mantle inventory

if PLUME is 9 to 19% of the mantle.

Using the above estimates of the relative sizes of the two source regions and Ganapathy and Anders (37) values for terrestrial abundances, we can now estimate the total abundances of the trace elements in the various reservoirs. The continental crust contains more than 26% of the mantle plus crust inventory of K, Rb, and Ba and less than 8% of Sr, Y, Zr, Nb, Sm, Yb, and Hf. The "depleted" MORB source contains more than 50% of the Earth's inventory of Y, Zr, Nd, Sm, Yb, Hf and Th and more than 20% of Nb, La and U. The PLUME source region, although generating highly enriched magmas contains only about 10 to 20% of the Earth's K, Rb, Sr, Nd, Sm, Yb, Th, and U. It is the primary repository for Ba and La and has small total abundances of Y, Zr, Nb, and Hf (less than 7%). The crust and the two upper mantle reservoirs account for about 75% of the heat production from K, Th, and U. Therefore, only 25% of the Earth's heat flow comes from the lower mantle. About 40% is due to MORBS. The continental crust and PLUME each contribute about 18%.

This distribution of heat sources affects the style of convection in the two reservoirs. Assuming PLUME to be the shallower reservoir it is primarily heated from below and will therefore be characterized by narrow ascending plumes. MORBS is primarily heated from within and will be characterized by broader ascending regions and narrow descending jets or "slabs".

The mineralogy of the two source regions

Assuming that the two source regions are related, an apparent partition coefficient can be determined by forming the ratio of the concentrations in MORB to those in continental tholeiites (CFB). This is shown in Figure 2 along with mineral/melt partition coefficients for garnet, clinopyroxene, orthopyroxene and olivine. Tholeiites are used in this comparison since they presumably are products of large degrees of partial melting. They will, therefore, have the trace element pattern of their source and a relatively uniform enrichment. The ratio of the concentrations in the two reservoirs can be explained if the MORB source is composed mainly of garnet and clinopyroxene and PLUME has been enriched with fluids that were in equilibrium with this layer and therefore depleted in such elements as Zr, Nb, Y, Yb, and Hf.

MORB is enriched with respect to continental tholeiites in Y and Zr and only slightly depleted in Hf and Yb. Both MORB and continental tholeiites represent rather large degrees of partial melting of their respective source region. A garnet peridotite would be expected to lose most of its garnet and clinopyroxene under these circumstances. The above results indicate that primary garnet must be a minor mineral in PLUME but a major component of the MORB source. MORB is depleted in the most incompatible elements, such as K, Rb, Ba, and U but not as much as would be expected if it were composed entirely of residual crystals. This suggests that MORBS evolved from a melt, presumably the result of an early differentiation event, and consists of a mixture of melt with

excess garnet which has settled into it during crystallization, i.e. it is an orthocumulate. The upper part of the mantle would consist of lighter, cumulate and residual, crystals and late stage fluids which impart an inverse garnet signature to this region.

This sequence of events, based on trace elements, is precisely what O'Hara et al. (14) proposed on the basis of petrological and major element considerations. They concluded that the parent magma for ocean island tholeiites had experienced a previous history of eclogite extraction. The remaining magma evolved to ocean island tholeiite by olivine fractionation. On the basis of major element (20) and trace element chemistry, I suggest that the eclogite cumulates constitute the source region for mid-ocean ridge basalts. The parent magma from which both MORBS and PLUME evolved by crystal fractionation would be picritic, the result of extensive partial melting of a primitive garnet peridotite mantle. Similar considerations have led to the concept of a magma ocean on the moon (41). Because of the higher pressures in the Earth's mantle a deep eclogite cumulate is the analog of the floating plagioclase cumulate that forms the lunar highland crust.

In order to see if this holds up quantitatively for the trace elements we investigate the following model. The primitive mantle is split into two reservoirs by 15% partial melting and melt extraction to the surface. The melt fraction reservoir is enriched by about a factor of 6 in the incompatible elements but, because of the low partition coefficients, has nearly primitive ratios of Rb/Sr and Sm/Nd.

Crystallization of the melt yields an eclogite cumulate layer which is modelled as a 50:50 mix of garnet and melt, proportions appropriate for an orthocumulate. Part of the final 5% melt fraction, a melt that is in equilibrium with eclogite, is removed to deplete the cumulate layer and enrich the overlying mantle. The mixing ratios were adjusted so that the former can yield MORB by 15% olivine fractionation and the latter can yield CFB by 20% partial melting (38).

Results of this model are shown as solid points in Figure 2. They are consistent with MORB being the result of nearly complete melting of a source region which represents high pressure cumulates from the melt fraction of the primary differentiation, i.e. eclogite or garnet pyroxenite.

Prior to providing depleted MORB this region lost its late stage fluids or, alternatively, crystallized completely and then lost its early melt fraction on a subsequent reheating cycle. PLUME was enriched by upward migration of this fluid. Thus, two stages of differentiation and fractionation are required in order to concentrate the LIL in the two upper mantle reservoirs. Isotopically, the MORB source evolves as nearly primitive mantle until it transfers its incompatible elements to PLUME. It subsequently evolves as a depleted reservoir. Basalts from PLUME will have time-integrated depleted, enriched or "primitive" isotopic ratios, depending on when the enrichment occurred.

Locations of the two source regions

There is variety of evidence that suggests that the plume source region is shallow. Anomalous low seismic velocities can be traced to a depth of about 250 km under Yellowstone but deeper velocities appear to be normal (17). The variable and small amounts of partial melting required to generate melilitites, nephelinites, basanites and alkali basalts (6) from a common source region are consistent with diapirs rising from various shallow depths. Tholeiites are the result of larger degrees of melting, consistent with adiabatic ascent from deeper levels. The xenoliths entrained in kimberlites and alkali basalts are volatile and trace element rich and these are samples from the upper 200 km of the mantle (12). Intuitively, we expect that volatiles will migrate upward and be trapped by the cold upper mantle. Volatile and LIL enriched magmas occur not only under continents but also at island arcs where the downgoing slab perturbs the upper mantle. Plume type basalts occur in continental rifts. These rifts evolve to oceanic ridges, with isolated oceanic island hotspots, when the rifting has led to the formation of an ocean basin.

There are also some suggestive geometric constraints. The volume of the low-velocity zone (LVZ) is adequate to provide the plume basalts but not the voluminous MORB (10). The preferred mode of convection in a region with a high temperature gradient and a rapidly varying viscosity takes the form of hexagonal cells with upwelling centers (18). This seems to be consistent with hotspot patterns (19) and the small areal

extent of hotspots. In more homogeneous regions of the mantle, where the temperature gradient is smaller and the viscosity more uniform, linear rolls are a possible mode of heat transport. Linear ridge systems and the uniformity of oceanic tholeiites therefore suggest a deeper source, one that is below the large vertical and lateral variations that occur in the upper 200 km. The sink of oceanic lithosphere, judging from the depth distribution of earthquakes, appears to be between 200 km and 670 km. The distinctive isotopic and trace element signature of MORBS can be maintained if it is also between these depths. Upper mantle temperatures are closest to the melting point between about 150 and 250 km depth and this is therefore the depth range where it is most likely for diapirs to originate.

It is difficult to estimate the depth at which partial melting first occurs. Seismic data from several hotspots give low velocities down to at least 150 km (17,21). Eruption temperatures of 1300°C and large degrees of partial melting require initiation of melting below 150-200 km (22). There is some evidence for crystal fractionation in melts as deep as 280 km (23). Mantle fragments brought up by alkali basalts and kimberlites do not, in general, have the trace element pattern required for the source region of MORB. Therefore, PLUME magmas may originate from shallow depths but MORBS must be deeper than 200 km. In a gravitationally stratified mantle one would expect the deeper layer to be denser and therefore rich in garnet. The inability of young buoyant lithosphere to subduct below about 220 km suggests a density increase at this depth and this may be the boundary between the two

source regions (20). Taking all evidence into account it appears that PLUME may be coincident with the LVZ and diapirs rising from the transition region supply the magmas that evolve to MORE.

A terrestrial magma ocean

The complementary LIL element patterns of the major terrestrial magma types is reminiscent of lunar data which has led to the widely accepted concept of crystal fractionation and cumulate formation in a magma ocean or vast lava lakes (41). The various source regions are attributed to cumulate and residual fluid layers that resulted from crystallization of a ~300 km thick magma ocean that, in turn, was derived from very early melting of at least half of the moon. If a body as small as the moon experienced such extensive differentiation and fractionation, then the Earth should have as well. The amount of partial melting required, ~15%, to explain the enrichment of the upper mantle reservoirs on Earth, is, in fact, relatively modest. Although the energy of accretion of the Earth is much greater than that of the moon, the greater size of the Earth results in high Rayleigh number convection and rapid increase of the melting curve with depth. This plus the latent heat buffer and the high melting temperature of olivine may prevent more extensive melting on a global scale. A 15% melt implies a magma ocean ~400 km deep. The pressures in the Earth are greater than on the moon. Early eclogite fractionation at depth therefore preempts the extensive plagioclase fractionation that resulted in the early lunar anorthositic crust.

Crystallization of a magma ocean will proceed from the base because of the relative slopes of the adiabat and the liquidus. The near liquidus phases at depths greater than 60 km are garnet and clinopyroxene (14, 16) and they will form an eclogite or garnet pyroxenite cumulate layer. Although there is a seismic discontinuity in the mantle near 400 km, eclogite is denser than residual garnet peridotite to depths of 670 km (20). These cumulates will therefore sink to this depth, displacing residual mantle upwards. The shallower part of the mantle will therefore consist of olivine and pyroxene cumulates and residual fluid from the magma ocean and displaced residual lower mantle. The top of the eclogite layer could be as shallow as 220 km (20) or as deep as 370 km based on considerations of this paper. The mantle discontinuity near 400 km, which is usually attributed to the olivine-spinel phase change could therefore be either a chemical discontinuity or could represent the completion of the garnet pyroxenite (eclogite) to garnetite (garnet solid-solution) phase change (42).

Isotopic ratios of the two source regions

The study of Sr and Nd isotopes places important time constraints on the evolution of mantle reservoirs (24-26). The continental crust and the depleted reservoir have mean ages of 1.5 b.y. (3). Kimberlites and continental flood basalts, although enriched in LIL, have been attributed to a primitive reservoir (2, 3, 24, 27). This interpretation is not required by the data as we show later. Some mantle samples have been derived from ancient enriched reservoirs (28). Other samples come

from reservoirs which apparently have been enriched only recently (28,29).

Consider a primitive mantle that partially melts and separates into two reservoirs, as before, by upward removal of the melt. The lower mantle consists of residual crystals and is therefore depleted in the incompatible elements. The melt fractionates into a deep eclogite cumulate layer and a shallow olivine-orthopyroxene cumulate layer. A 5% melt fraction is transferred from the deeper to the shallower layer at various times (40). The Nd and Sr isotopic ratios for the two reservoirs are shown in Figure 3. The central horizontal scale gives the ages of the depletion and enrichment events. The theoretical $\epsilon_{\text{Nd}} - \epsilon_{\text{Sr}}$ correlation lines agree with the data and indicate that the mid-ocean ridge basalt source region was depleted at times between 1.5 and 2.5×10^9 years ago. A redistribution of LIL makes it possible to satisfy the mantle isotopic data even if the primary differentiation occurred early in the history of the Earth. Thus, the trace element, petrological and thermal constraints on the evolution of the mantle and the various reservoirs are not contradicted by the isotopic data. The type of model investigated here is similar to previous ideas of mantle metasomatism and trace element redistribution (30).

Implications for mantle evolution

Isotopic studies indicate that the two major mantle reservoirs have been isolated for more than 1 or 2 b.y. (2,3). The evidence presented

here from trace elements, and previously from major element and seismic considerations (20), suggest that the mantle is chemically stratified and that the various regions of the mantle are complementary products of terrestrial differentiation. The present emphasis has been on magmas from these reservoirs but similar conclusions result from the study of solid fragments from the mantle (14, 20). O'Hara et al. (14) pointed out that the restricted number of phases found in biminerally eclogites from kimberlites indicate that they are either crystal accumulates or crystalline residue developed in contact with a liquid. This is exactly the situation inferred from the trace element patterns for the source region of abyssal tholeiites. Eclogite and garnet peridotite xenoliths from kimberlites may represent samples from MORBS and PLUME, respectively. They give satisfactory average mantle compositions for the major oxides when combined in the portions indicated by the trace elements (20).

Although whole mantle convection, in the conventional sense, is precluded in a chemically stratified mantle, transfer of material into and out of the various reservoirs is possible because of the large volume change associated with partial melting and phase changes, e.g., basalt-eclogite. The oceanic part of the plate tectonic cycle may be summarized as follows. Partial melting in the eclogite layer allows diapirs to rise to the base of the oceanic lithosphere. Nearly complete melting occurs during adiabatic ascent. This is possible because of the proximity, in temperature, of the liquidus and the solidus in eclogite. Peridotite diapirs can only partially melt because of their high

liquid. The resulting melt fractionates in near surface magma chambers to form tholeiitic melts which are light enough to rise to the surface. The pyroxenite residue forms the lower oceanic lithosphere. As the lithosphere cools and thickens the lower part transforms to garnet pyroxenite or eclogite which is denser than the underlying mantle. The oceanic lithosphere becomes gravitationally unstable and it returns to its source region which lies between about 220 or deeper and 670 km depth. Partial melting in the shallow enriched peridotite layer generates continental and ocean island basalts and a harzburgite residue, both of which are lighter than their source region. These PLUME products remain in the crust and upper mantle. Some volatiles are returned to PLUME by subducted sediments and hydrothermally altered oceanic crust. The high temperature gradient in the thermal boundary layer at the PLUME-MORB interface brings temperatures there close to the melting point (20). When mature oceanic lithosphere passes over a hotspot it is quite likely that the lower pyroxenite part will contribute xenoliths to the alkalic magmas and, by remelting, contribute to the trace element and isotopic signatures of ocean island basalts. The evolution of the mantle is shown schematically in Figure 4.

It has generally been assumed that basalts of all kinds represent partial melts of peridotites. Mantle compositions based on this premise have much lower abundances of SiO_2 , Al_2O_3 , and CaO than models based on cosmochemical considerations. The evidence used to construct the petrological models is obtained from the upper 200 km of the mantle and the models are therefore strictly only valid for the uppermost mantle.

A thick eclogite layer serves to increase the abundances of the above components and can reconcile the cosmochemical and petrological interpretations. The possibility of an eclogite layer in the upper mantle was also discussed by Press (43).

The idea that eclogite may be the source for oceanic basalts is an old one (31) but has not been in favor in recent years. The main objection is that limited partial melting of eclogite does not generate a tholeiite. Extensive or complete melting is required and this has been thought to be unlikely.

However, eclogite has an extremely small melting interval (about 60°C) compared to peridotite (16, 32). Since diapirs cannot rise out of an eclogite layer into a less dense peridotite layer until they are already extensively molten, it requires only a small additional temperature rise, relative to the liquidus, to complete the melting. This can be accomplished in a rising diapir. It is still unknown why melting initiates in the first place. One possibility is insulation by the thick continental lithosphere.

Hotspots and ridges in the Atlantic and Indian oceans were beneath continental lithosphere prior to 200 m.y. ago. A large number of hotspots are presently under the relatively stationary continent of Africa. This suggests that continental insulation, which prevents mantle heat from being efficiently removed to the surface, may be the cause of the partial melting that ultimately results in ridge and

hotspot volcanism. The thick, 150 km, continental lithosphere (20) prevents diapiric uprise and extensive melting may be possible until the continent rifts and rapid spreading and heat removal can take place. It is not so obvious that this explanation holds for the ridges and hotspots in the Pacific. The thick crust under the oceanic plateaus in the central Pacific or a thick oceanic lithosphere, due to a period of slow spreading, could also serve to insulate the mantle, raise temperatures and cause extensive in-situ melting prior to diapiric ascent. Parts of the Pacific rim continents such as Alaska, Mexico, Central America and S.E. Asia may also have been located in the the central Pacific prior to 200 m.y. ago. Once initiated, the rise of upper mantle diapirs should be rapid (33), possibly rapid enough to avoid crystal fractionation en route.

Conclusions

Garnet and possibly clinopyroxene control the complementary trace element patterns of MORB and plume basalts. I suggest that the source region for MORB was formed from an eclogite cumulate layer resulting from crystallization of the picritic melt fraction of the original differentiation of the Earth. The plume source is enriched in those elements that would be concentrated in a melt that was removed from a garnet rich region. This fluid, the result of an early partial melt or a late stage fluid from crystallizing eclogite in the MORB source, infiltrated the shallow mantle plume source at various times. This gives plume basalts an inverse garnet trace element signature relative

to MORB. The MORB and plume source regions together make up about 25-30% of the mantle. This requires that most, if not all, of the mantle has been processed to obtain the observed enrichment. There is no need to invoke a large primitive reservoir in the mantle or deep, lower mantle plume sources. On the contrary, the plume source region appears to be shallow and may be coincident with the LVZ. The upper mantle transition region, 220-670 km, represents about 21% of the mantle and the LVZ is about one-third as large. This is about the ratio of the sizes of the two upper mantle reservoirs which is required to satisfy the trace element data. The MORB source is probably an eclogite cumulate while the plume source is probably garnet peridotite. Crystallization of a magma ocean would give this kind of upper mantle stratigraphy. Nd and Sr isotopic data indicates that the depletion of that part of the MORB source region being sampled today occurred over the interval 1.5 to 2.5×10^9 years ago. The fluid involved in the depletion/enrichment events, and in the formation of the continental crust, appears to be a partial melt or late stage residual fluid from an eclogite cumulate layer. The lower mantle is residual peridotite and, although it may be convecting, it no longer communicates with the shallower reservoirs.

References and Notes

1. P. W. Gast, Geochem. Cosmochim. Acta 32, 1057 (1973).
2. D. J. DePaolo, G. J. Wasserburg, Geophys. Res. Lett. 3 249 (1976), Proc. National Acad. Sci. 76, 3056 (1979).
3. S. Jacobsen, G. J. Wasserburg, J. Geophys. Res. 84, 7411 (1979).
4. C. J. Allegre, D. Othman, M. Polve, P. Richard, Phys. Earth Planetary Interiors, 19, 293 (1979).
5. For those who insist on acronyms PLUME may be considered an abbreviation for Principal Layer of Upper Mantle Enrichment. Others may wish simply to consider this an English word with French, Latin and German antecedents as discussed in D. L. Anderson, Geol. Soc. Am. Bull. 86, 1593 (1975).
6. F. A. Frey, D. H. Green, S. D. Roy, J. Petrol. 19, 463 (1978).
7. S. S. Sun, G. N. Hanson, Contrib. Mineral Petrol 52, 77 (1975), Earth Planet. Sci. Lett., 35, 429 (1977).
8. W. M. White, J. G. Schilling, Geochem. Cosmochim. Acta 42, 1501 (1978).
9. H. Craig, J. E. Lupton, Earth Planet. Sci. Lett. 31, 369 (1976); C. K. Unni, J. G. Schilling, Nature 272, 19 (1978); E. C. Rowe, J. G. Schilling, Trans. Am. Geophys. Un. 59, 409 (1978)
10. M. Tatsumoto, Earth Planet. Sci. Lett. 38, 63 (1978); C. E. Hedge, Earth Planet. Sci. Lett. 38, 88, (1978).

11. W. J. Morgan, Nature 230, 42 (1971).
12. F. E. Lloyd, D. K. Bailey in L. H. Ahrens et al. (eds.).
 Physics and Chemistry of the Earth, 9, N. Y., Pergamon Press,
 389 (1975), N. Shimizu, loc. cit., 655, N. Shimizu, Earth
Planet. Sci. Lett. 25, 26 (1975), R. K. O'Nions, P. J.
 Hamilton, N. M. Evernsen, Earth Planet. Sci. Lett. 34, 13
 (1977); F. A. Frey, M. Prinz, Earth Planet. Sci. Lett. 38,
 129 (1978).
13. E. A. Duncan, D. H. Green, Geology 8, 22 (1980)
14. M. J. O'Hara, M. J. Saunders, E. L. P. Mercy, in Ahrens
et al. (eds.), Physics and Chemistry of the Earth, 9,
 N. Y. Pergamon Press, 571 (1975).
15. A. J. Irving, Geochem. Cosmochim. Acta 42, 743 (1978).
16. K. Ito, G. C. Kennedy, J. Geol. 82, 383 (1974).
17. H. M. Iyer, Tectonophysics 56, 165, (1979).
 D. M. Hadley, G. S. Stewart, J. E. Ebel, Science 193, 1237, (1976).
18. F. H. Busse, Phys. Earth Planet. Interiors 19, 149 (1979).
19. R. Thiessen, K. Burke, W. S. F. Kidd, Geology 7, 263 (1979).
20. Don L. Anderson, Geophys. Res. Lett. 84, 7555 (1979); J. Geophys.
Res. 84, 6297 (1979); A Global Geochemical Model for the
 Evolution of the Mantle, J. Geophys. Res. in press, 1980.
21. K. Aki, A. Christoffersson, E. S. Husebye, J. Geophys. Res.
82 277 (1977).
22. H. W. Green II, Y. Gueguen, Nature 249, 617 (1974).
 R. G. Cawthorn, Earth Planet. Sci. Lett. 23, 113 (1975);
- 23 D. R. Clarke, D. A. Carswell, Earth Planet. Sci. Lett 34,

- 30 (1977).
24. G. J. Wasserburg, D. J. DePaolo, Proc. National Acad. Sci. 76, 3594 (1979); D. J. DePaolo, Earth Planet. Sci. Lett. 43, 201 (1979).
 25. R. K. O'Nions, P. J. Hamilton, N. M. Eversen, Earth Planet. Sci. Lett. 34, 13 (1977).
 26. C. J. Allegre, J. F. Minster, Earth Planet. Sci. Lett. 38, 1 (1978).
 27. A. R. Basu, M. Tatsumoto, Science 205, 398 (1979).
 28. M. Menzies, V. R. Murthy, Nature, 281, 289 (1979); 283, 634 (1980); Earth Planet. Sci. Lett. 37, 401 (1978).
 29. S. R. Carter, N. M. Eversen, P. J. Hamilton, R. K. O'Nions, Nature 281, 289 (1979); Earth Planet. Sci. Lett. 37, 401 (1978).
 30. A. Basu, V. R. Murthy, Geology 5, 365 (1977); S. S. Sun, G. N. Hanson, Geology 3, 297 (1975); A. L. Boettcher, J. O'Neil, R. Windom, D. Stewart, H. Wilshire, Proc. Second Kimberlite Conference, Santa Fe, New Mexico, extended abstracts (1977); M. Menzies, V. R. Murthy, Earth Planet. Sci. Lett. 46, 323 (1980); V. R. Murthy, Earth Planet. Sci. Lett. 46 323, (1980); V. R. Murthy, Earth Planet. Sci. Lett. 46 323 (1980).
 31. L. R. Fermor, Rec. Geol. Surv. India 43 Pt. 1, 41 (1913)
 32. H. S. Yoder, Jr. Generation of Basaltic Magma, Nat. Acad. Sci. Washington, D. C. 265 pp. (1976).
 33. H. R. Shaw, J. Petrol. 10, 510 (1969).
 34. S. R. Taylor, in M. W. McElhinny (ed.), The Earth: It's Origin,

Structure and Evolution, Academic Press, New York, 597 pp. (1979), p. 353-376.

35. J. A. Philpotts, C. C. Schnetzler, H. H. Thomas, Geochem. Cosmochim. Acta 36, 1131 (1972); H. W. Fesq, E. J. Kable, J. J. Gurney, in L. H. Ahrens et al. (eds.) Phys. Chem. Earth, v. 9, N. Y. Pergamon Press, 687 (1975), E. J. Kable, H. W. Fesq, J. J. Gurney, loc. cit., 709.
36. R. W. ~~W. W.~~ J. Hubbard, Earth Planet Sci. Lett. 38, 95 (1978).
37. R. Ganapathy, E. Anders, Proc. 5th Lunar Sci. Conf. 1181 (1974).
38. The two source regions (MORBs and PLUME) are constructed as follows. For primitive mantle (PM) we use the Ganapathy-Anders (37) values and extract 15% melt (ME). The LIL concentrations in ME and residual mantle (RM) are calculated using partition coefficients appropriate for a peridotitic residue (3, 6). The eclogite cumulate (EC) is a 50:50 mix of garnet and equilibrium intercumulus fluid (EIF). To obtain the depleted LIL pattern for MORBS half of the final 5% melt (LSM) is removed. Partition coefficients for an eclogite residue are used at this stage. LSM is the enriching or metasomatic fluid for PLUME which is composed of 10% LSM and 90% RM. Thus, PM evolves to ME and RM by partial melting; ME evolves to EC and a silica-undersaturated fluid by eclogite fractionation. EC minus LSM yields MORBS.

RM plus LSM yields PLUME.

39. ϵ_{Nd} and ϵ_{Sr} are the $^{143}\text{Nd}/^{144}\text{Nd}$ and $^{87}\text{Sr}/^{86}\text{Sr}$ ratios expressed as the fractional deviation in parts of 10^4 from those in a primitive, undifferentiated reference reservoir (2). Thus, $\epsilon_{\text{Nd}} = 0$ implies a primordial mantle with the following qualifications. Small degrees of partial melting fractionate Rb/Sr and Sm/Nd in both the melt and the residual crystals and they subsequently evolve as enriched and depleted reservoirs, respectively. For large degrees of partial melting, $> 15\%$, the melt has near primitive ratios of Rb/Sr and Sm/Nd. Even large amounts of olivine and orthopyroxene fractionation from such a melt do not much affect these ratios. Garnet and clinopyroxene orthocumulates, i.e., nearly equal proportions of crystals and melt, also give nearly unfractionated ratios. These results follow from the small mineral/melt partition coefficients and the complementary concentrations in garnet and its intercumulus fluid.
40. The following model gives the observed $\epsilon_{\text{Nd}} - \epsilon_{\text{Sr}}$ correlation. As before, 15% melt is extracted from the primitive reservoir. The proto-MORB cumulate is 60% melt, 40% garnet. This is slightly different than the ratios used in the previous calculation since we are now requiring a fit for only Rb, Sr, Sm and Nd. For present purposes this difference is not significant. The depletion of this reservoir is modelled by extracting 5% melt at various times. This melt extract is used to form the continental crust and to enrich, or metasomatise, PLUME. The enriched upper mantle reservoir is modelled as 4% melt extract from the eclogite

cumulate, 21% of the original melt and 75% of the depleted residue of the original differentiation. The enrichment event occurs at various times.

41. M. J. O'Hara, G. M. Biggar, S. Richardson, C. Ford, B. Jamieson, Proc Apollo 11 Lunar Sci. Conf., 1, 695, 1970; J. V. Smith, A. T. Anderson, R. C. Newton, E. Olsen, P. J. Wyllie, J. Geol., 78, 381, 1970; J. A. Wood, J. Dickey, Jr., U. Marvin, Science, 167, 602, 1970; H. Wakita, R. Schmitt, Science, 170, 969, 1970; Don L. Anderson, Phys. Earth Planet. Interiors, 6, 116, 1972; Nature, 239, 263, 1972; S. R. Taylor, Proc. Lunar Planet. Sci. Conf. 9th, 15, 1978.
42. M. Akaogi, S. Akimoto, Phys. Earth Planet. Interiors, 15, 90, 1977.
43. F. Press, Science, 160, 1218, 1968.
44. This research was supported by NASA Grant No. NGL05-002-069.
 I would like to thank E. Stolper, A. E. Ringwood, P. Wyllie, A. Boettcher, G. J. Wasserburg, C. Allegre, S. Jacobson, L. Silver, H. Taylor, and D. Green for helpful conversations. R. Oxburgh, J. G. Schilling, P. Wyllie and G. Ernst reviewed earlier versions of the manuscript. Art Boettcher kindly provided a most useful preprint co-authored with J. O'Neil, and made some important suggestions. I thank an anonymous reviewer for his editorial comments. Contribution Number 3432, Division of Geological and Planetary Sciences, California Institute of Technology, Pasadena, California 91125.

Figure Captions

Figure 1. Normalized trace element concentrations in the continental crust (dots), continental basalts and mid-ocean ridge basalts (2, 6, 8, 34, 35). All concentrations are normalized to terrestrial values of Ganapathy and Anders (37), recalculated to mantle equivalents. The lower curves for continental tholeiites and MORB are normalized to mantle concentrations after removal of the continental crust, as are the curves for alkali basalts and kimberlites. The complementary nature of MORB and the other magma types is evident. The continental crust is not the only "enriched" reservoir.

Figure 2. Crystal/liquid partition coefficients for garnet, clinopyroxene, orthopyroxene and olivine (6). Heavy line is ratio of concentrations in primitive mid-ocean ridge basalts (36) and continental tholeiites (2, 6). This indicates that MORB results from melting of a garnet and clinopyroxene rich source region and that the continental tholeiite (CFB) source region has experienced eclogite extraction. The points are for a model (38) in which the proto-MORB source region is an eclogite orthocumulate from the initial melt fraction of primitive mantle differentiation. The continental and ocean island basalt, or plume, source region is depleted residue enriched by a late stage melt from the proto-MORB cumulate layer.

Figure 3. Present $\epsilon_{nd} - \epsilon_{sr}$ values (39) for an eclogite cumulate (solid line) which has been depleted at various times by removal of a melt fraction (40). This melt fraction enriches the complimentary reservoir (dashed line). Data from references 2, 24, 25, 29, and 30.

Figure 4. A model for the evolution of the mantle. Primitive mantle (1) is partially molten either during accretion or by subsequent whole mantle convection which brings the entire mantle across the solidus at shallow depths. LIL elements are concentrated in the melt. The deep magma ocean (2) fractionates into a thin plagioclase-rich surface layer and deeper olivine-rich and garnet-rich cumulate layers (3). Late stage melts in the eclogite cumulate are removed (4) to form the continental crust (c.c.), enrich the peridotite layer and deplete MORBS, the source region of oceanic crust (o.c.) and lower oceanic lithosphere. Partial melting of PLUME (5) generates continental flood basalts (CFB), ocean island basalts (OIB) and other enriched magmas, leaving a depleted residue (harzburgite) that stays in the upper mantle.

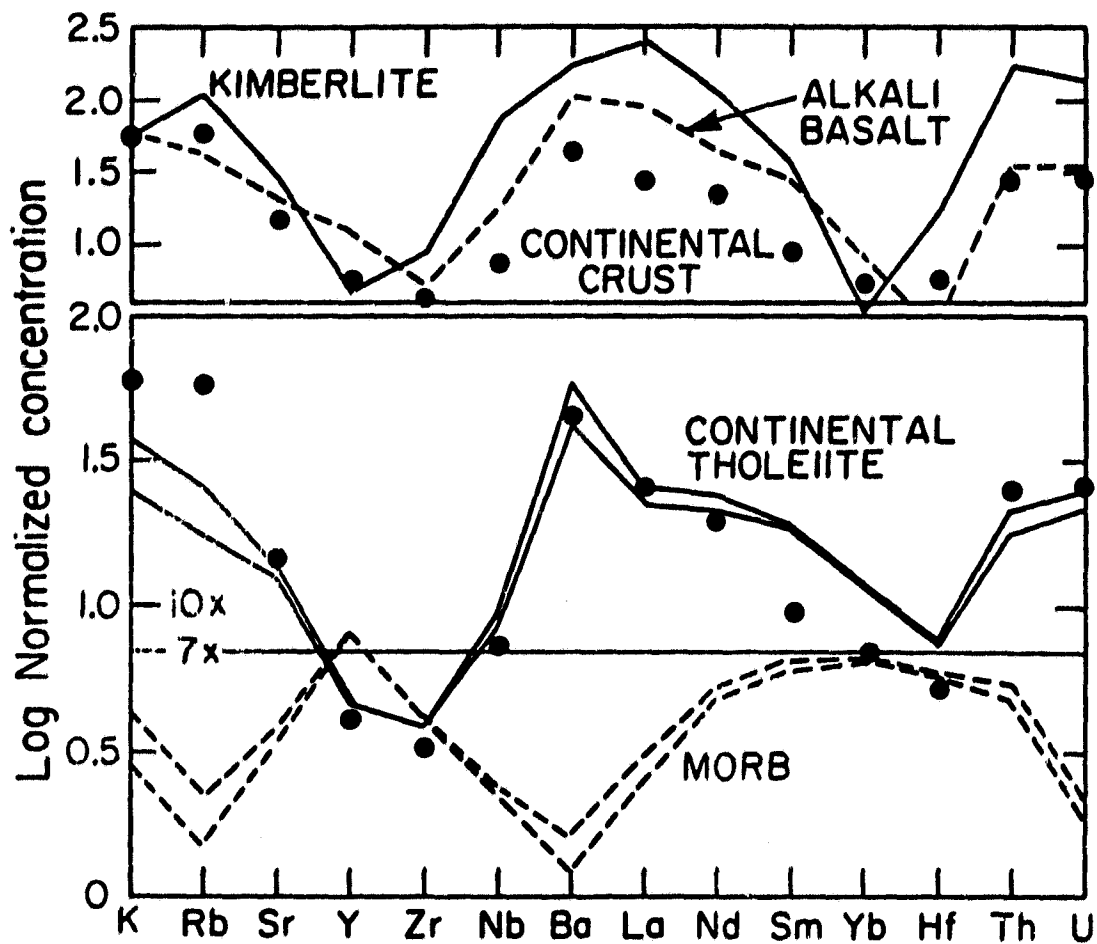


Fig. 1

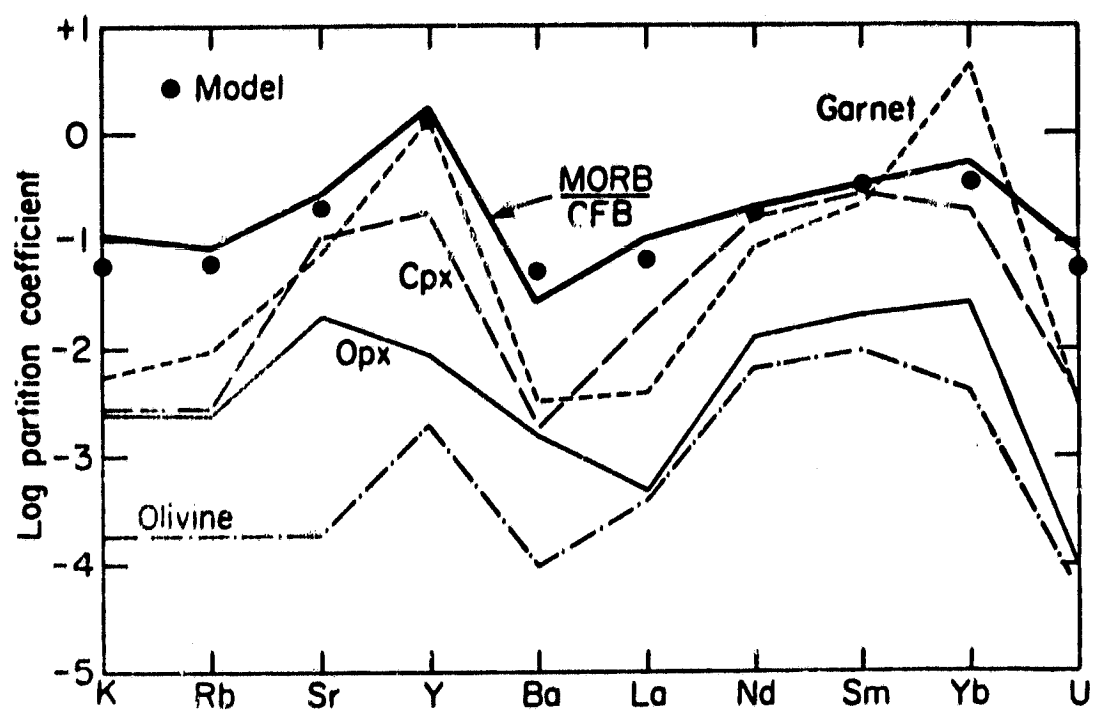


Fig. 2

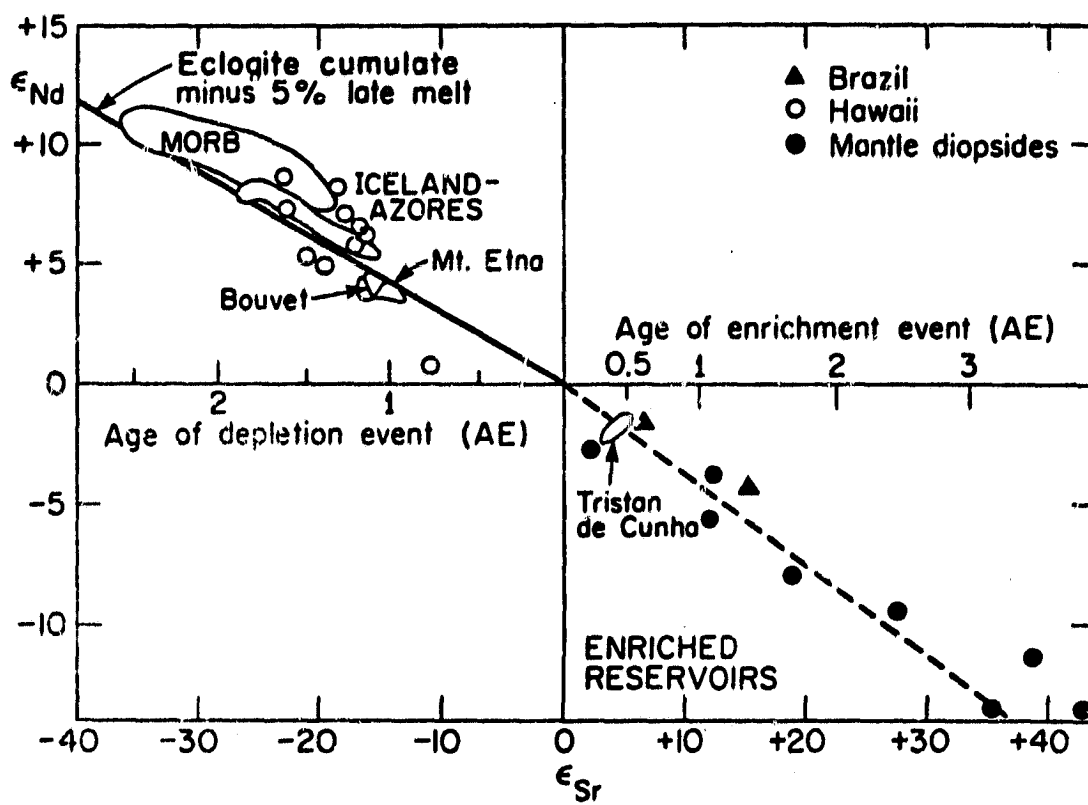
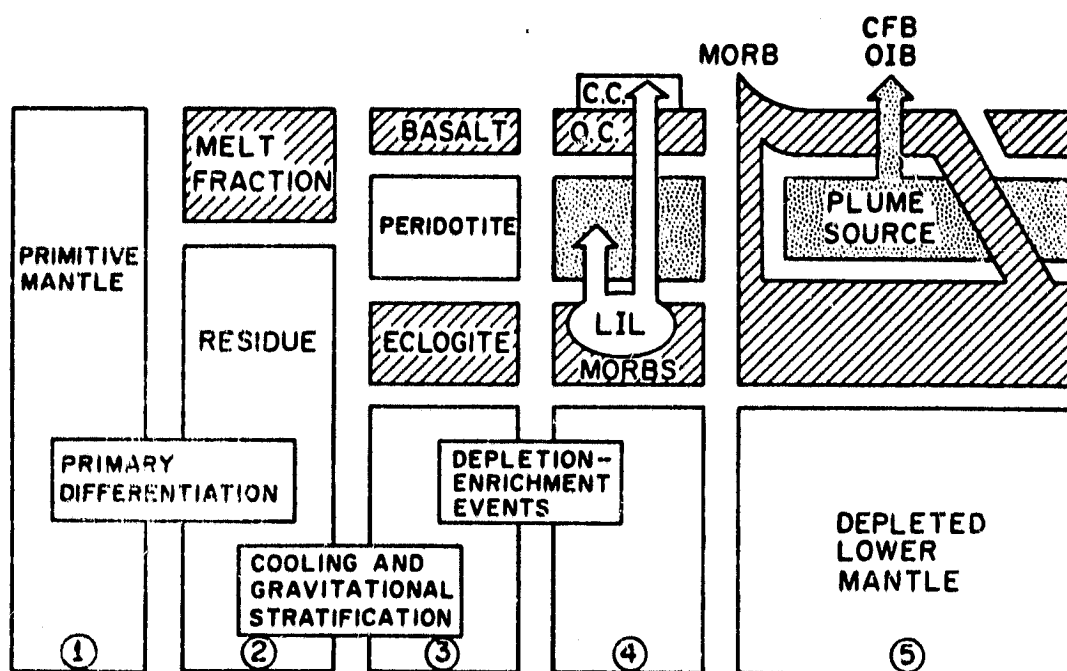


Fig. 3



ORIGINAL PAGE IS
OF POOR QUALITY

Fig. 4

APPENDIX VII

THE EARLY EVOLUTION OF THE MANTLE

Don L. Anderson

Episodes, Vol. 1980, No. 3, 1980.

THE EARLY EVOLUTION OF THE MANTLE

by

Don L. Anderson

Seismological Laboratory

California Institute of Technology

Pasadena, California 91125

Although the mantle of the Earth appears quite rigid on the time scales of seismic waves and solid Earth tides it behaves as a fluid for longer term processes such as postglacial rebound, plate tectonics and removal of heat from the deep interior. The mantle is convecting and will convect until all the original heat and heat sources are removed. Although convection itself is not questioned, geophysicists are currently debating whether the mantle is convecting as a whole or is divided into layers which are convecting separately. A major driving force for convection is thermal buoyancy although the plates and subducting slabs also affect motions in the mantle. Material deep in the mantle warms up either due to its own radioactivity or due to heat brought to it from below. As it heats up, it becomes buoyant and rises. Similarly, hot material brought to the surface cools off and becomes denser. In a homogeneous planet the cold surface material eventually sinks back into the interior. However, thermal buoyancy is only part of the story. In a chemically stratified or differentiated planet, convection will be confined to the individual layers if thermal expansion and contraction cannot overcome the intrinsic density differences between layers. Density differences due to chemistry, phase changes and partial melting are also important in mantle convection. For example, by partial melting a mantle diapir can become much more buoyant than

it could by thermal expansion alone and it can therefore rise to higher levels in the mantle. On the other hand, if a large volume of basaltic melt forms below about 50 km depth it will freeze as eclogite, which is denser than normal mantle, and it will therefore eventually sink. If the Earth had never experienced partial melting or differentiation it would be reasonable to suppose that the mantle is convecting as a whole. Such a mantle would be chemically homogeneous, and would not be very interesting.

The two mantle source regions

There is now abundant geophysical, petrological and geochemical data that points toward a chemically inhomogeneous mantle. Mid-ocean ridge basalts come from a region of the mantle that is depleted in most of the large-ion incompatible elements such as Rb, Sr, Ba, U and the rare-Earth elements. These elements are not retained effectively by the major mantle minerals, olivine, garnet and pyroxenes. They therefore become concentrated in melts. Abyssal tholeiites, however, originate as melts or partial melts and this means that their source region is depleted in these elements. The part of the mantle that is providing these voluminous magmas must therefore have originated as a crystal cumulate or have experienced a prior episode of partial melting and melt extraction.

Alkali basalts, on the other hand, whether found on continents or on oceanic islands, are enriched in volatiles and the incompatible elements. The enrichment is not uniform but is complementary to the depletion found in ocean floor basalts. That is to say these basalts are most enriched in the elements that are most depleted in MORB (Mid-ocean Ridge Basalts), and vice versa. The trace element patterns of continental and ocean island basalts

are also complementary to garnet. For example these magmas are particularly enriched in K, Rb, Ba, Th, U and the light rare-Earth elements and are relatively depleted in Y, Zr and the heavy REE, the elements favored by garnet. This suggests that garnet has either been left behind or was previously removed from the source region of the enriched magmas. Since some of these magmas, particularly the continental tholeiites, represent large degrees of partial melting, it is unlikely that garnet is still a residual phase. Olivine and orthopyroxene are the probable main residual phases and these are essentially free of the large-ion incompatible elements. It appears, therefore, that the mantle source region for the enriched basalt types, such as nephelinites, melilitites, basanites, alkali basalts, continental flood basalts and kimberlites, had previously experienced an episode of garnet or eclogite removal. The continental crust has a similar enrichment pattern and probably came from the same reservoir.

The MORB characteristics can be explained if the "depleted" reservoir is eclogitic since these basalts are enriched in those elements which are concentrated in garnet and, to a lesser extent, clinopyroxene. The important role of eclogite removal and crystal fractionation has been emphasized by O'Hara (1968) and O'Hara and Yoder (1967).

A terrestrial magma ocean

A similar complementarity among lunar basalts has led to the concept of a crystallizing magma ocean (Wood, 1975; Smith et al, 1970; and Anderson, 1973). The thick anorthositic highland crust is thought to represent light plagioclase-rich cumulates and the other basalt types have been attributed to remelting of denser and deeper olivine-pyroxene rich

cumulates. The complementarity of the various reservoirs is controlled by plagioclase separation. If the moon was extensively molten early in its early history then the Earth and the other terrestrial planets should have been as well. On a large body, however, garnet crystallization is important. Garnet settling is the terrestrial analog of plagioclase floatation. A thin plagioclase-rich crust will form in the surface chill layer of a terrestrial magma ocean but much of the Al_2O_3 will be removed from the magma by garnet fractionation before temperatures in the bulk of the ocean are low enough for plagioclase formation.

A thick eclogite cumulate layer will therefore form at depth in an Earth-sized planet. Crystallization of a magma ocean will lead to a stratified mantle and the source regions will bear the imprint of garnet or garnet extraction. A deep garnet-rich cumulate layer would be an appropriate source region for MORB. A possible mantle stratigraphy resulting from crystallization of a terrestrial magma ocean is shown in Figure 1.

How does a magma ocean form and what will be its composition? The energy of accretion of the Earth is sufficient to vaporize most of the mantle. Much of the energy of accretion is radiated away but most of the mantle was probably raised above the solidus during accretion. Differentiation, including segregation of the core, would be occurring while the Earth was being assembled. Silicate melts remain at the surface and the residual crystals settle to the interior. The proto-Earth would therefore be concentrating Al_2O_3 , CaO, U, Th, Ba, Sr, etc. in the upper mantle while it was growing. The concentration of incompatible elements in the upper mantle can be explained if the whole mantle experienced about 15% partial melting (Anderson, 1980).

Even if one could assemble a cold and homogeneous Earth-size body it would experience whole mantle convection that would bring most or all of the mantle through the upper mantle melting zone. Separation of melt and solid would ensue, just as is happening at ridges today.

The higher abundances of the radioactive elements in the past means that the cold conductive surface layer was thinner and that the deep mantle adiabatic gradient extended closer to the surface. The upper mantle melting zone was therefore broader in the Precambrian and melting was more extensive. The requirement that the larger amount of heat be removed results in a thin conductive thermal boundary layer with a high temperature gradient. If a significant fraction of this layer is basaltic then it will be buoyant and will be unable to subduct. Subduction only occurs today because part of the lithosphere is composed of material denser than basalt and because cooling occurs over a rather large depth extent. Areas having thick crusts, such as continents, oceanic plateaus and aseismic oceanic ridges resist subduction. Early Precambrian plate tectonics was likely quite different in style than modern plate tectonics. It would be dominated by collisional tectonics, shallow underthrusting and remelting of overthickened crust. As the outer layer cools the lower basaltic parts eventually convert to eclogite and a massive overturning would result. This presumably erases the early geological record and sets the stage for the current style of plate tectonics which involves deep subduction and continuous regeneration of ocean lithospheres.

The Earth is unique among the terrestrial planets in having plate tectonics and, probably, in having a very thin crust. These phenomena are related since oceanic crust is continuously being returned to the mantle. In principle, the Earth could support a basaltic crust about 50 km thick.

At this depth basalt transforms to eclogite. A widespread eclogite layer, however, is unstable and would sink into the mantle. This transformation occurs at much greater depths in Mars and the Moon, because of the lower pressures, and in Venus, because of the higher surface and upper mantle temperatures. Therefore, thick and permanently buoyant crusts are expected on these planets. An equivalent quantity of material is presumably buried somewhere in the Earth's mantle. Where is it, how big is it and how long has it been there?

The last question is the easiest to answer with presently available data. Isotopes tell us that the various source regions of the mantle have been isolated for at least 10^9 and possibly more than 3×10^9 years (Patterson and Tatsumoto, 1964; Tatsumoto, 1978; De Paolo and Wasserburg, 1979; Jacobsen and Wasserburg, 1979). This is much longer than the $\sim 10^8$ year average age of the oceanic crust. The isolation of these reservoirs may have been a result of the initial differentiation of the mantle. The size of the depleted reservoir is about 20% of the mantle, which is equivalent to a 450 km thick layer in the upper mantle (Anderson, 1980).

In most subduction areas of the world earthquakes occur as deep as 220 km. In a few places, particularly where the oceanic lithosphere is old, earthquakes occur as deep as 670 km, the depth of a major seismic discontinuity in the mantle. Therefore, oceanic lithosphere appears to be disposed of between these depths. This is the transition region of the mantle.

I have shown elsewhere (Anderson, 1979a,b) that eclogite is denser than garnet peridotite to a depth of 670 km. Below this depth normal low aluminum mantle minerals transform to ilmenite and perovskite polymorphs. These are denser than garnet, the main mineral of eclogite at these depths,

and they will form a floor to subducting crust or a garnet cumulate layer forming in a crystallizing magma ocean. It appears that the 670 km discontinuity is not only a phase boundary, separating garnet from ilmenite/perovskite, but is also a chemical boundary, separating eclogitic from ultrabasic rocks.

The lower mantle is presumably the crystalline residue remaining after extraction of a basaltic, probably picritic, melt. This melt, the result of early mantle differentiation, fractionates into eclogitic and peridotitic cumulate layers, both of which currently reside in the upper mantle. Because of the phase change boundary the differentiation of the Earth is irreversible. Mixing of the upper mantle reservoirs is inefficient because of the large density contrast between eclogite and garnet peridotite. Normally, the two upper mantle reservoirs convect separately because of this density stratification. However, if the eclogite layer partially melts it becomes less dense than the overlying mantle. Partially molten diapirs can then rise out of the eclogite layer and melt completely during adiabatic ascent. This is possible because of the small melting interval of eclogite. The diapirs then provide picritic melts to near surface magma chambers where they fractionate to form midocean ridge tholeiites and, possibly, a pyroxenitic lower lithosphere. The latter evolves to garnet pyroxenite as the lithosphere thickens and cools. This is denser than normal mantle peridotite and the oceanic lithosphere eventually becomes unstable and sinks back to its source region.

The alternative point of view is that ocean floor tholeiites are primary magmas, unaffected by crystal fractionation, which are formed by partial melting of garnet peridotite, or pyrolite, leaving behind a thick depleted harzburgite layer. Since basalt and harzburgite are both buoyant

in normal mantle, a large amount of cooling is required in order to overcome this chemical stabilization. A thick layer of depleted peridotite in the upper mantle is one consequence of this model.

Hotspots and plumes

The other major reservoir in the mantle provides magmas for the oceanic islands and the alkalic provinces on continents. Continental flood basalts apparently come from this same reservoir. Current sites of this kind of igneous activity are called plumes or hotspots (Wilson, 1963; Morgan, 1971). In many respects these basalts are complementary to midocean tholeiites and appear to come from an enriched source region. What is the size and location of this reservoir?

Although it is usually assumed that plumes originate deep in the mantle, there is a variety of evidence that indicates they come from a shallower reservoir than MORB. The limited areal extent of hotspots suggests that they are caused by narrow upwellings in the mantle. This is typical behavior of fluids heated from below and is consistent with an upper mantle location. Uniform fluids which are heated from within exhibit broad, often roll-like, upwellings. This pattern is more appropriate for oceanic ridges. Internal heating of a deep upper mantle layer would generate internal rolls and plume-like convection in the overlying layer. Kimberlites and their entrained xenoliths are enriched in volatiles and the incompatible elements and these come from the upper 250 km or so of the mantle. Xenoliths brought to the surface in alkali basalt flows also apparently originate in the shallow mantle. The nature of the enrichment in continental and ocean island basalts is such that their source region could be the upper mantle low-velocity zone.

Partial melting in the upper mantle can explain the low seismic velocities and high electrical conductivity in the low-velocity zone. Partial melting is consistent with estimates of upper mantle temperatures if this region is volatile rich.

The appearance of enriched magmas at developing continental rifts, island arcs, and back-arc basins also suggests a shallow source origin. Trace element patterns indicate that the enriched reservoir is much smaller than the depleted reservoir, perhaps only one-third as large. Plume basalts represent varying degrees of partial melting. This is consistent with a small and variable depth of origin. Deep diapirs, brought adiabatically to the surface, would exhibit a large and more uniform degree of partial melting. This property is more typical of MORB than the hotspot magmas.

Theoretical calculations indicate that the Earth is getting rid of its heat at about the same rate as it is generating it by radioactive decay. Convection is an efficient transmitter of heat and the main bottleneck is the cold layer at the surface that must transmit heat by conduction. There are also conductive boundary layers at each chemical interface in the Earth. Because of the temperature dependence of viscosity, these boundary layers adjust their thickness to accommodate changes in heat flow and temperature. The current heat flow through the surface of the Earth is probably within 30% of the current rate of heat production. Below about 250 km the temperature gradient is probably near adiabatic. In addition to the near surface thermal boundary layer, sometimes referred to as the thermal lithosphere, there is also a region of high thermal gradient across the lithosphere-asthenosphere boundary which is thought to be at about 150 km under shields (Anderson, 1979c). Pressure increases the melting point of mantle silicates so rapidly that

melting is unlikely to occur in a convecting mantle at depths below about 250 km. Solid material brought adiabatically from depth, however, will intersect the melting curve in the upper mantle. Thus, upper mantle melting is a natural consequence of mantle convection and the relative slopes of the adiabat and the solidus. The presence of volatiles also decreases the solidus in the upper 150 km of the mantle. Water and CO_2 are locked in mineral phases at greater depths and the melting point is not much affected.

There is another way in which excess temperatures can be generated in the upper mantle. The thin lithosphere under oceans allows a balance between the rate at which heat is convected into the upper mantle and the rate at which it can be conducted to the surface. The lithosphere is much thicker under shields and the geothermal gradient is relatively low. This means that the mantle heat flow cannot be rapidly removed through a thick continent. A stationery continent will, therefore, heat up at its base and hotspots can be generated in the mantle beneath large continental masses that are stationery or slowly moving. These self-generated hotspots weaken and uplift the continent and are probably responsible for continental breakup and dispersal.

It is instructive to plot the locations of present day hotspots in the Atlantic and Indian oceans relative to the locations of continents prior to the breakup of Gondwana. Figure 2 shows such a display. The currently active hotspots in this hemisphere are in a part of the mantle that was insulated by a super continent from before 350 to 200 my ago, i.e., for more than 150 my prior to breakup and dispersal. The hotspot grouping in the center of the map is currently under Africa and those under North America are currently along the mid-Atlantic ridge. Two hundred million years ago the Eiffel plume was under northern Europe, Iceland and Jan Mayan were under

Siberia and St. Helena, Tristan and Bouvet were under South America. In many cases continental uplift, alkaline basalt provinces, continental flood basalt and kimberlite activity can be associated directly with a hotspot track. I suggest, therefore, that continental insulation is responsible for melting anomalies in the mantle. These melting anomalies, in turn, lead to uplift, intraplate magmatism and the breakup of large continental masses. Melting in the shallow peridotite layer gives enriched continental and ocean island magmas and melting in the deeper eclogite layer provides the depleted magmas which emerge at well developed ridges.

Similar mantle insulation is provided by anomalously thick oceanic crust such as the high standing oceanic plateaus in the western Pacific. These plateaus may have been responsible for turning on the central Pacific hotspots.

On keeping an open mind

It is appropriate at the start of the joint IUGG, IUGS and ICSU program on the Lithosphere to review our assumptions and working hypotheses. Geological, geophysical and geochemical data are subject to multiple interpretations, and models derived by workers in one discipline are often contradictory to those derived by those working in a different field. It is often the case, however, that the data are not contradictory, only the models.

For example, the following assumptions are commonly made:

- 1) The majority of the mantle is relatively homogeneous in composition and primitive (pyrolite);
- 2) Basalts of all types represent varying degrees of partial melting of garnet peridotite or pyrolite.

3) Oceanic tholeiites are primary liquids formed by partial melting and the upper oceanic mantle is the depleted residue.

4) The oceanic lithosphere subducts as a result of cooling and thermal contraction.

5) The seismic discontinuities in the mantle represent phase changes in an olivine-rich mantle rather than chemical boundaries.

6) The large sizes of the rigid plates and the separation of ridges implies large convection cells having dimensions that correspond to the depth of the mantle.

7) The lower mantle is primitive and provides the material for hotspots, oceanic islands and continental flood basalts.

8) The enormous quantities of oceanic crust that have been generated by sea-floor spreading have sunk to the core-mantle boundary.

Many of these assumptions have recently been called into question. I suggest that alternatives to each of the above assumptions are viable and they must be considered as we strive toward a coherent theory of the evolution of the mantle and plate tectonics. The evidence for early melting and differentiation of small solar system objects make it difficult to understand how the Earth could have remained primitive, homogeneous and undifferentiated. The processes of crystal fractionation and gravitational stratification are important in the Moon and in terrestrial magma chambers and were also probably involved in the early evolution of the mantle. Petrological models for the mantle are strongly influenced by samples from the upper mantle which, in many cases, are clearly residual after melt removal, or crystal cumulates. Thus, there is a strong bias toward an olivine rich mantle. Even primitive appearing specimens are samples from the upper mantle and do not necessarily represent

C-4

the average composition of the whole mantle. When the large quantities of subducted oceanic crust are taken into account, the average mantle becomes more CaO , Al_2O_3 , TiO_2 and SiO_2 rich and closer to cosmochemical estimates of mantle composition. Workers who propose the existence of a large primitive, undifferentiated reservoir in the mantle overlook the fact that elements such as Rb, Sr, Sm and Nd are so strongly concentrated into melts that by the time one melts ~20% of primitive mantle the melt has essentially "primitive" ratios of Rb/Sr, Sm/Nd and their isotopes. The ratios stay nearly primitive even after large amounts of olivine and orthopyroxene fractionation. Garnet and clinopyroxene fractionate these elements but orthocumulates composed of these minerals and equilibrium interstitial fluids give nearly primitive ratios. The "primitive reservoir" theories assume that the continental crust is the only enriched reservoir that is complementary to the depleted MORB reservoir. In the "differentiated mantle" theory outlined in this essay the source region of continental and ocean island basalts is the enriched complement of the depleted reservoir. Isotopic studies of more hotspot locations and mantle xenoliths should resolve these two models.

The study of the oceanic and continental lithospheres is of central importance in unraveling the evolution of the mantle. In the fractional crystallization model the lower oceanic lithosphere is pyroxenitic rather than harzburgite or pyrolite. The spinel to garnet pyroxenite phase change would be the main cause of instability of old lithosphere. "Eclogite" xenoliths found in Hawaii may be samples of this lower lithosphere. Study of the lithosphere under shields may shed light on early mantle processes and the development of the continental crust. Shields exhibit long term stability in spite of the fact that they are cold. This may result from chemical buoyancy.

It is possible that chemical effects, i.e., partial melting and phase changes, may be as important in driving the terrestrial engine as thermal convection.

The evolution of a primitive mantle into two upper mantle reservoirs and a depleted lower mantle is shown in Figure 3. The formation of hotspot magmas by partial melting of garnet peridotite in the upper mantle probably follows conventional views of petrogenesis. Trace elements indicate that this region has experienced eclogite extraction and enrichment in the incompatible elements. Diapirs from the eclogite cumulate layer are presumed to evolve to mid-ocean ridge tholeiites. The long term isolation of the two major source regions strongly supports the concepts of chemical stratification in the mantle and chemical driving forces, i.e., partial melting and phase changes in the lithosphere, in addition to thermal buoyancy.

REFERENCES

- Anderson, D. L., 1973, The composition and origin of the Moon: Earth and Planetary Science Letters, v. 18, p. 301-316.
- Anderson, D. L., 1979a, The upper mantle transition region; eclogite?: Geophysical Research Letters, v. 6, p. 433-436.
- Anderson, D. L., 1979b, Chemical stratification of the mantle: Journal of Geophysical Research, v. 84, p. 6297-6298.
- Anderson, D. L., 1979c, The deep structure of continents: Journal of Geophysical Research, v. 84, p. 7555-7560.
- Anderson, D. L., 1980, Hotspots, basalts and the evolution of the mantle: Science (in press).
- DePaolo, D. J. and Wasserburg, G. J., 1979, Nd isotopes in flood basalts from the Siberian platform and inferences about their mantle sources: Proceedings of the National Academy of Science: v. 76, p. 3056-3060.
- Jacobsen, S. and Wasserburg, G. J., 1979, The mean age of mantle and crustal reservoirs: Journal of Geophysical Research, v. 84, p. 7411-7427.
- Morgan, W. J., 1971, Convection plumes in the lower mantle: Nature, v. 230, p. 42-43.
- O'Hara, M., 1968, The bearing of phase equilibria studies in synthetic and natural systems on the origin and basic and ultrabasic rocks: Earth-Science Reviews, v. 4, p. 69-133.

O'Hara, M. and Yoder, H. S., Jr., 1967, Formation and fractionation of basic magmas at high pressure: *Scottish Journal of Geology*, v. 3, p. 67-117.

Patterson, C. C. and Tatsumoto, M., 1964, The significance of lead isotopes in detrital feldspar with respect to the chemical differentiation of the Earth's mantle: *Geochimica et Cosmochimica Acta*, v. 28, p. 1-22.

Smith, J. V., Anderson, A. T., Newton, R. C., Olsen, E. J., Wyllie, P. J., Crewe, A. V., Issacson, M. S. and Johnston, D., 1970, Petrologic history of the Moon inferred from petrography, mineralogy and petrogenesis of Apollo 11 rocks: *Proceedings of the Apollo 11 Lunar Science Conference*, p. 897-925.

Tatsumoto, M., 1978, Isotopic composition of lead in oceanic basalt and its implication to mantle evolution: *Earth and Planetary Science Letters*, v. 38, p. 63-87,

Wilson, J. T., 1963, Continental drift: *Scientific American*, v. 28, p. 86-100.

Wood, J. A., 1975, Lunar petrogenesis in a well-stirred magma ocean, *Proceedings Lunar Science Conference 6th*, p. 1087-1102.

About the author: Director of the Caltech Seismological Laboratory and Professor of Geophysics at the California Institute of Technology in Pasadena, Dr. Don L. Anderson's research interests include the structure, composition and evolution of the mantle and the terrestrial planets. He was Principal Investigator of the Viking seismic experiment on Mars. He is an Editor of Physics of the Earth and Planetary Interiors. He is also working on the physics of attenuation of seismic waves and rheology of the mantle.

Contribution No. 3499, Division of Geological and Planetary Sciences, California Institute of Technology, Pasadena, CA 91125. This research was supported by National Aeronautics and Space Administration Contract NSG-7610 and the Earth Science Section National Science Foundation Grant No. EAR77-14675.

FIGURE CAPTIONS

Figure 1 Schematic illustration of the sequence of layers in a crystallizing terrestrial magma ocean. The magma ocean is the result of partial melting of a primitive garnet peridotite mantle. This melt, probably picritic, collects in the upper mantle. A garnet-rich cumulate layer forms at the base of the molten layer leaving behind an Al_2O_3 and SiO_2 -poor liquid. Shallower cumulate layers consist of olivine, orthopyroxene and interstitial melt. Olivine and orthopyroxene react with the fluid to form clinopyroxene and garnet if they settle below about 100 km. These cumulate layers evolve to the two major reservoirs which are being sampled today. The lower mantle is depleted peridotite, the residue after about 15% melt removal. The upper boundary of the lower mantle is controlled by phase changes in peridotite. Because of the broad stability field of garnet, eclogite cannot sink below 670 km. The 670 km discontinuity is, therefore, a chemical and phase boundary.

Figure 2 The location of the continents at about 350 my ago. Also shown are the hotspots in this hemisphere, most of which are currently in the Atlantic and Indian oceans and under the continent of Africa. The continents move slowly north for the next 150 my and then break up and disperse to their present locations. The majority of present day hotspots were beneath Gondaland for a long period of time prior to 200 my ago. They may have been formed by continental insulation.

Figure 3 Evolution of primitive mantle into a chemically stratified mantle with separate isolated upper mantle reservoirs. Melt is removed from primitive mantle, probably during accretion, and concentrated at the surface. As the Earth cools, the melt fractionates into a deep eclogite cumulate layer and a shallow peridotite layer. The eclogite cumulate becomes depleted in large-ion lithophile elements (LILE) which enrich the overlying peridotite layer. Diapirs from the eclogite source region evolve to mid-ocean tholeiites by near surface crystal fractionation. The enriched peridotite source region provides, by varying degrees of partial melting, kimberlites, melilitites, nephelinites, alkali basalts and continental tholeiites. Depleted peridotites are the residue of hotspot magmatism. These are less dense than fertile peridotites and therefore occur in the uppermost mantle. The oceanic lithosphere, at least the Al_2O_3 -rich portions, return to the eclogite layer.

Dominant
Mineralogy

Petrology

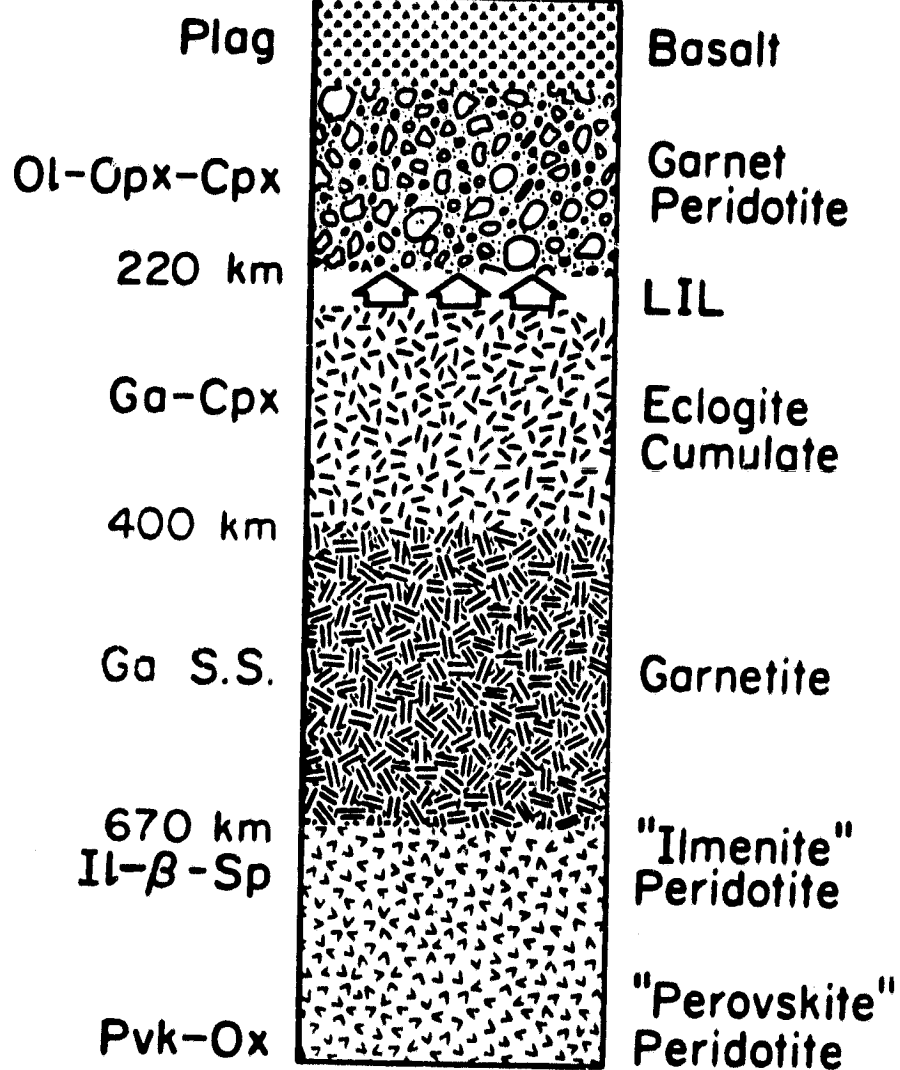


Fig. 1

ORIGINAL PAGE IS
OF POOR QUALITY

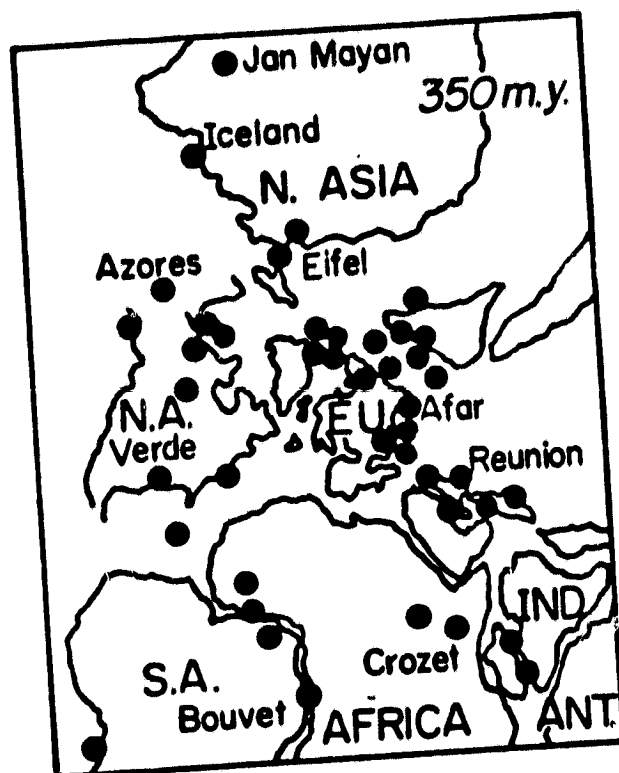


Fig. 2

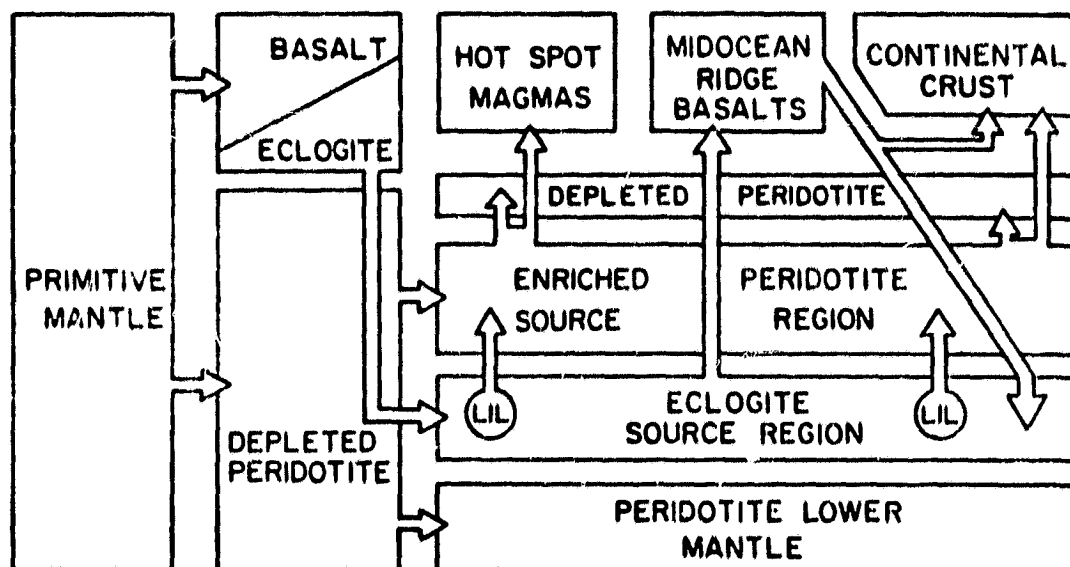


Fig. 3